UNIVERSITÀ DEGLI STUDI DI PALERMO
Dottorato in Ingegneria dell'Innovazione tecnologica
Dipartimento di Ingegneria
Settore Scientifico Disciplinare (ING-IND/26)

DEVELOPMENT AND MODELING OF MEMBRANE PROCESSES FOR THE REGENERATION OF ACID PICKLING SOLUTIONS

IL DOTTORE
ING. ROSA GUECCIA

IL COORDINATORE
PROF. SALVATORE GAGLIO

IL TUTOR
PROF. ING. GIORGIO MICALE

EVENTUALE CO TUTOR
PROF. ING. ANDREA CIPOLLINA
ING. SERENA RANDAZZO

CICLO XXXIII
ANNO CONSEGUIMENTO TITOLO 2021

TABLE OF CONTENTS

ABSTRACT

The doctoral thesis focuses on a novel integrated process for the recovery and valorisation of acid and metal salts present in the waste solutions of the pickling process. The proposed process is based on the integration of two innovative membrane technologies, the Diffusion Dialysis and the Membrane Distillation, coupled with a reactive precipitation section. This hybrid process allows the recovery and the enhancement of waste solutions, as well as optimal operating conditions for the continuous pickling process, thus improving its efficiency.

Hydrochloric acid recovery was assessed through a detailed study on the Diffusion Dialysis process by implementing a wide experimental campaign using artificial solutions produced in laboratory, in order to understand and characterize the system. A mathematical model was developed with time and space distributed-parameters structure for the effective simulation of steady state and transient batch operations, thus providing an operative tool for the design and optimization of DD units.

Selective separation of metal salts was reached by precipitating ferric hydroxide and maintaining ammonium and zinc chlorides in solution, which can be used as fluxing solution in the galvanizing process itself, thus implementing the typical Circular Economy concept.

The feasibility of the proposed process is demonstrated through the use of a purposely developed process simulator able to predict steady state operation of the integrated process and to perform sensitivity analysis for the identification of the best operating conditions of the system.

An experimental campaign was carried out with a demonstrator unit, jointly designed and constructed by Fraunhofer ISE (Freiburg, Germany), eventually installed in the real industrial environment of Tecnozinco s.r.l hot-dip galvanizing plant in Carini, Sicily. The campaign assessed the integration performance of the different units and the process reliability, resulting in a minimization of spent pickling solution disposal and in high quality recovered compounds.

An engineering economic analysis was carried out in order to assess the economic feasibility of the proposed process.

The economic model was implemented in the gPROMS simulation platform and was used to conduct an optimization analysis, defining the optimal operational and design conditions for which the process is more profitable and performing. The process simulator was also used to provide a scale-up of the demonstrator plant. The results have shown that the process has a good potential for industrial implementation, thanks to the economic and environmental benefits.

INTRODUCTION

Traditional business models have mostly implemented a “take-make-consume-dispose” linear model. This old-fashioned approach is based on the assumption that unlimited natural resources are available, easy to exploit and cheap to dispose of. Unfortunately, the incessantly growing demand and the depletion of resources have caused environmental degradation, thus boosted research and efforts toward a circular economy approach implementation [1].

The industrial sector is responsible for a large amount of wastes generation. In particular, the metal process and coating industry consumes a large amount of different process fluids like acids, bases and salts leading to contaminated waste water streams, which need disposal causing high costs and significant environmental impact. These wastewater streams contain valuable dissolved metals salts, acids. The spent pickling solution (SPS) discharge has a dramatic impact in the industry economics as well as in the ecological footprint. In the EU alone, up to 380.000 m^3/year of SPS is produced [2][3]. This leads to a high ecologic and economic burden and significant room for improvement has been recently identified [4].

The environmental impact and costs of their disposal can be minimized by the recovery and recycling of valuable substances. Waste water treatment systems addressing closed loop process design for the metal processing industry will increase its ecological and economic impact significantly [5]–[7]. Circular economy systems maintain the added value in products for as long as possible, while the generation of wastes is avoided or reduced.

This thesis is focused on the evaluation of potential routes of valorisation of wastes from the hydrometallurgical and metallurgical industries, especially of the acidic liquid wastes. The main objective of this thesis is the development, modeling and demonstration of an innovative integrated hybrid technology for the treatment and recovery of acidic pickling waste solution. By combination and integration of existing but highly innovative technologies, valuable resources such as metals and process fluids will furthermore be recovered, thus reducing raw material consumption, closing process chain loops and leading to the effective implementation of European directives and policies [8]. Additionally, utilizing waste heat

widely available in metal processing as driving force for the treatment and recovery process, will be a fundamental aspect in optimizing the production efficiency in an already energy intensive industry.

The proposed system envisages the integration of different technologies such as:

1. *Diffusion Dialysis* (DD) membrane separation process, aiming for the recovery of acid directly from the waste solution thanks to a concentration difference between two solutions, separated by an anionic exchange membrane. It is a novel but commercially available technology, however, it has not yet been utilized in a hybrid version such as proposed in the present work.
2. *Membrane Distillation* (MD) membrane thermally driven process for the concentration of the recovered acid and production of low concentrated acidic water. Membrane distillation is not yet commercially available for these applications but has been validated in an environment relevant to the thesis goals.
3. *Reactive precipitation* performed in a *continuous stirred tank reactor* (CSTR), for the selectively metals separation and products valorisation. The choice of type of reagents and suitable operating conditions will lead to a production of valuable products and by-products.

Furthermore, the system allows the strategy of continuously regenerating acid solutions when they still have a good pickling capacity. Continuous treatment of an aliquot of the solution, by recovering acid, removing the excess of metals and refilling with fresh acid, leads to an extension of the pickling bath lifetime. The non-variable and optimal conditions enhance the pickling efficacy, thus decreasing the process time and increasing the treatment capacity. Moreover, no further waste effluent is generated and small on-site plants could be installed and operated, thus solving the problem of transportation of dangerous waste acid solutions, along with the relevant environmental issue.

Finally, the modular and flexible system design will offer high applicability to the specific requirements of an industry consisting of companies with a wide variety of production capacities and sizes.

This thesis work is in line with the objectivises of the ReWaCEM European project (Resource recovery from industrial wastewater by cutting edge membrane technologies) (http://www.rewacem.eu/), which aims to minimize the environmental impact and disposal

costs of such effluents through the recovery and recycling of substances with high added value.

The process feasibility will be demonstrated gradually, starting from (i) experimental findings in laboratory scale of the different processes, (ii) developing a mathematical model for the process characterization and prediction, both for the single unit operation and for the integrated system performance, (iii) testing and evaluating the integration of the technology in real conditions and into the production process chain; (iiii) concluding with demonstrating technical and economic performance and implemented strategy for upscaling and manufacturing of the final product to bring the new technology to the relevant market.

The present PhD thesis has been organised in order to cover the main aspects of the integrated process and describe the above-mentioned objectives. Particularly, it is divided in 8 chapters, which are briefly described in the following.

Chapter 1 introduces the concept of pickling process and spent pickling solution (*SPS*) and related treatment recovery strategies, describing the concept and analysing the state of the art of the technology. Therefore, this chapter establishes the motivation of this thesis, presenting the main existing problems and giving meaning to the proposed treatment process that will be the relevant topic of the following chapters.

Section I - Experimental and Modeling activities at laboratory scale

Firstly, the operational feasibility on a laboratory scale of two of the stand-alone main technologies involved in the process is tackled. In particular, *Chapter 2* presents an overview of the *diffusion dialysis* process, describing the technological fundamentals, experimental tests and the rigorous developed mathematical model. *Chapter 3* reports experimental and strategies applied for the metals separation in the *reactive precipitation* unit.

Section II - From lab to pilot

The feasibility of the proposed process is shown through the development and use of a process simulator of the integrated system, which is presented in *Chapter 4*. The detailed integrated process flow diagram description, the hierarchical model implemented and the sensitivity analysis on the influence of operating variables are reported as well. It is therefore possible to make the leap from the laboratory studies to the demonstrator scale through the model design

tool. Thus, *Chapter 5* and *Chapter 6* are dedicated to the pilot system description, integration, assembly, commissioning and operations.

Section III - Process Optimization and Profitability Analysis

Finally, the process economy feasibility is addressed in *Chapter 7*, which is focused on the economic consideration and profitability assessment of the proposed technology. Economic upscaling considerations are implemented in order to consider the full integration of the process in the industrial environment.

Chapter 8 presents the optimization problem formulation and provides different optimized scenarios aiming to investigate the best operating and design conditions along with explore the possible weaknesses of the technology.

1. TREATMENT PROCESSES OF SPENT PICKLING SOLUTIONS

Chapter Outline

1.1 **Hot-dip galvanization and pickling process overview**

Hot-dip zinc galvanizing is one of the leading technologies used worldwide for steel rustproofing. The hot-dip galvanization process, like all industrial operations, consists of a series of consecutive steps, which begin with the pre-treatment operations of the products, then involve the specific operations of the treatment and end up with the processes upstream, before sales or commercial distribution. In hot-dip galvanization iron work pieces are immersed in a bath of molten zinc, enabling the zinc to alloys with the metal. This form of surface finishing is mainly used to prevent rusting. A schematic representation of the galvanizing process is shown in Figure 1-1. The various stages of the process are reported in chronological order and will be briefly presented in the same paragraph.

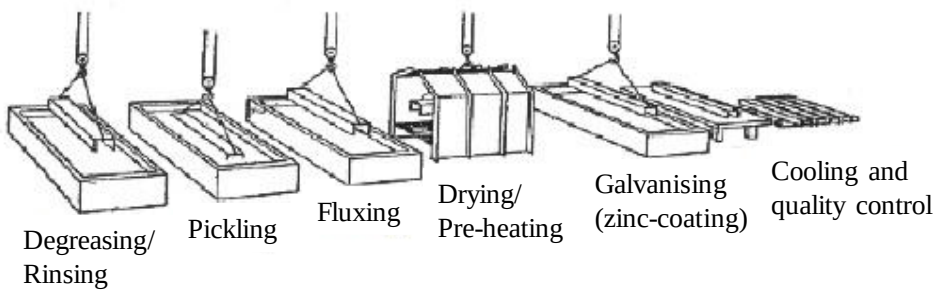

Figure 1-1 Schematic representation of all the steps of a galvanizing process.

Following the pathway shown, the manufactured steel is first degreased in a bath under the emulsifying action of surfactants, namely non-ionic surfactants, for oil removal, to remove oily residues and dirt from the metals surface. To avoid contamination of the following pickling baths the work piece is next rinsing.

The pickling process consists of a series of surface reactions of chemical attack [9], for iron oxides removal and degradation. During the pickling process the efficiency of the pickling liquid decreases due to the accumulation in the bath of metal salts, the consumption of active acid and the constant input of rinse water from the previous process (which is about 2.5 l per ton of processed material).

Fluxing protects the metal from corrosion before it is exposed to molten zinc. The fluxing components are zinc chloride $ZnCl_2$ and ammonium chloride NH_4Cl salts. The first one has

the function of protecting the product during the time that elapses between extraction and immersion in the molten zinc; the second one catalyses the galvanizing reaction.

Before galvanizing the piece is preheated and dried inside ovens (T = 130 °C), in such way a homogeneous salt film is created which prevents thermal shock during immersion in the molten zinc, which is at 400 °C. The zinc atoms penetrate into the steel structure and vice versa, establishing chemical bonds with the surface layer of the products. The zinc present on the surface, reacting with humid air, forms a protective patina consisting of zinc oxide. This patina protects the underlying iron from oxidation.

After removing the work piece from the zinc bath, it is left to cool. Post-treatment includes removal of zinc nibs and resulting defects from the mounting framework, as well as quality checks.

1.1.1 *Kinetics of the pickling process*

Main product of pickling reactions is ferrous chloride $FeCl_2$. In the work of Jatuphaksamphan et al. [10] the following reactions have been identified:

$$FeO + 2HCl \rightarrow FeCl_2 + H_2O \quad \text{1-1}$$

$$Fe_2O_3 + Fe + 6HCl \rightarrow 3FeCl_2 + 3H_2O \quad \text{1-2}$$

$$Fe_3O_4 + Fe + 8HCl \rightarrow 4FeCl_2 + 4H_2O \quad \text{1-3}$$

Clearly, the knowledge about the relationships existing between reaction rate, structure of the oxide layers and the main process variables, are of fundamental importance at an industrial level, as they allow to control and optimize the pickling process and therefore to increase its productivity.

According to the fact that pickling reactions are surface reactions, the reaction kinetics depends both on parameters related to metal element features and on characteristics of the pickling bath. To the first group belong:

- Type of steel worked;
- Structure;
- Area / Volume ratio;
- Thickness of the oxide layer, which depends on the chemical-physical conditions in which it was formed.

On the other hand, from the group of parameters relating to the pickling bath:

• Chemical composition of the pickling solutions;

• Bath temperature.

The reaction kinetics were described in the work of Gines et al. [9]. This experimental study indicates the dependence of the dissolution rate of the work piece oxidized layer on the chemical composition of the pickling bath and operating temperature, as well.

Another important contribution to the kinetic study of the pickling process is provided by the work of Jatuphaksamphan et al. [10]. Also in this last work, it is concluded that both the temperature and the initial concentration of HCl play a decisive role in the pickling reactions rate, showing kinetic constants values for different operating conditions. Both works provides kinetic equations taking into account the different investigate parameters.

It should be emphasized, however, that the pickling process strongly depends on the metal structure. Metallic elements can also have rather complex structures and therefore the kinetic data obtained from laboratory tests must be considered only for estimates and to determine the qualitative trends of the dissolution kinetics as a function of the main process variables. Therefore, these studies remain only useful on a laboratory scale.

On industrial level, the Kleingarn curve [11] is employed as practical guide for the optimal operating conditions choice in the galvanizing industry. According to Kleingarn, optimal pickling conditions given by acid and iron concentration combination can be identified.

As for the dissolution kinetics, it is observed that a higher concentration of hydrochloric acid facilitates the pickling process. Furthermore, ferrous chloride acts as a catalyzing chemical species that facilitates the kinetics of the pickling process. However, the excessive presence of dissolved salts in solution determines the increase in pickling time [12] which therefore represents an undesirable operating condition. The combination of all these factors leads to the identification of a link between the concentration of free acid and that of the iron present in solution, as reported in Figure 1-2. Under optimal operating conditions, the time required for the dissolution of the oxide layers present in the product is minimal and therefore the efficiency of the pickling bath is maximized [12]. Hence, the importance of continuously controlling acid and iron composition in the bath in order to optimise the pickling process.

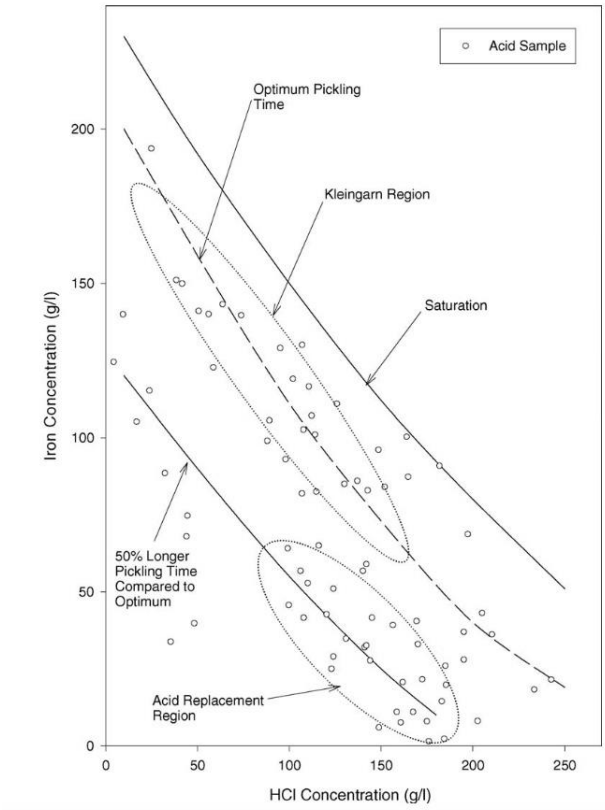

Figure 1-2 Kleingarn Curve[11].

1.1.2 *Spent pickling solutions*

Reached the limit operating conditions dictated by the experience of the plant operators, the pickling bath must be regenerated as the acid and iron concentrations reached are no longer optimal and therefore the process is not efficient. Currently, pickling baths are stressed until the acid concentration decreases by 75-85% and the metals concentration reaches the highest solubility threshold.

In common industrial practice, the regeneration of the bath is typically carried out by making "cuts" in the pickling tanks. The solutions are partly removed from the bath, and eliminated. The same quantity removed must be replaced by an equal amount of water and fresh acid solution in order to restore the initial optimal operating concentrations.

Although the management of the pickling process is undoubtedly more efficient using the Kleingarn Curve, the exhausted solutions coming from the tank cuts remain to be disposed of. These spent pickling solution (SPS) has to be disposed and treated in centralized plants, often located hundreds or thousands kilometers away from the factory, thus representing a serious environmental and economic burden for the pickling company [13]. SPS discharge has a dramatic impact in the industry economics as well as in the ecological footprint.

The specific waste composition relies on the plant and the pickling strategy adopted. Typical composition ranges of the SPS are reported in Figure 1-3, for different acid pickling application. While in Table 1-1 concentration values are referred to the particular case of a hot-dip galvanizing plant situated in the south of Italy (Tecnozinco SrL, Carini, Italy), which deals with hydrochloric acid pickling process. The lowest acid concentration and the highest metals concentrations are referred to the composition of pickling bath at the end of its life.

Acid type	Acid conc., g/dm^3	Zn, g/dm^3	Fe, g/dm^3	Other
H_2SO_4	150	–	70	–
	92	–	78	–
HCl	237	~80	90–96 Fe(II), or 84 Fe(II), 8.3 Fe(III)	6.4 M Cl^-, less than 400 ppm of Mn, Pb, Al, Cr, Ni, Cd, Cu, Co
	150	–	50	–
	101	–	8.9 Fe(III)	–
	90	80	30 Fe(II)	6 M Cl^-
	85	25	160 (158 Fe(II), 2 Fe(III))	Traces of Cd
	80	4.65	88.5 (incl. 1.6 Fe(II))	–
	~70	34	204	0.04 g/dm^3 Cr
	~40	110	88.5	7.7 M Cl^-
	33	12	106 Fe(II)	–
	20–60	–	80–110 Fe(II)	–
	18	26	140	0.09 g/dm^3 Pb, 0.08 g/dm^3 Ni, 0.03 g/dm^3 Cu, 0.09 g/dm^3 Al
	~10	70	92	–
	30	20	120	–
Mixed acids				
HNO_3	180–200		28–30 (max. 35)	10–15 g/dm^3 Cr(III), 5–10 g/dm^3 Ni(II)
HF	40–45			
	120–150	–	30–45 Fe(III)	5–10 g/dm^3 Cr(III), 3–5 g/dm^3 Ni(II)
	15–30			
	125	–	40	–
	30			

Figure 1-3 Compositions of real effluents [14].

Table 1-1. Acid and metals concentration ranges of a pickling solution (data provided from Tecnozinco SrL, Carini, Italy).

Component	Unit	Mean
Free acidity (HCl)	g/l	150-20
Fe	g/l	50-150
Zn	g/l	1-20

Zinc in solution is mainly coming from the zinc-plated tools, which release some zinc ions when immersed in the pickling baths.

In addition, all solutions contain surfactants, corrosion inhibitors and stabilizers that are added to improve the effectiveness of the pickling. The concentration ranges of acids and iron ions are very wide, which makes it difficult to select a universal method for regenerating solutions [15]. Thus, the complexity of treating solutions from a pickling bath is related to the fact that these are mixtures of numerous inorganic and organic compounds.

1.2 **Recovery systems for acid pickling solutions: Literature review**

According to the EPA (Environmental Protection Agency) regulation accepted both in Europe and in the United States, the concentration of metals and acids in wastewater must be strictly controlled and limited. The "Spent pickle liquor generated by steel finishing operations" is identified as hazardous waste for its toxic and corrosive nature (listed with K062 identification code) [16]. European and national standards provide for an admissible content of metals and chloride ions in waste, after neutralization, equal to: 2 mg dm^{-3} of Zn, 10 mg dm^{-3} of Fe, 1 g dm^{-3} of Cl^- ions and a pH value including between 6 and 9 [17].

Apart from the severe environmental and economic issues, the non-stable pickling conditions (due to the continuous consumption of acid and increase in metals concentration) and the shutdown procedures for baths composition adjustments and cleanings/replacements can importantly affect the normal operation of the pickling process.

The IPPC (Integrated Pollution Prevention and Control) policy pushes for the adoption of innovative integrated and eco-friendly systems for recovery of acids and metals compounds, by applying the circular economy concept, with the goal of contemporarily reducing the environmental impact and making the production steps more efficient.

Disposal of the spent pickling solution strongly affects the hot-dip galvanizing industries environmental footprint and costs. Thereby, a cleaner pickling process could be one of the most beneficial steps to achieve a sustainable development of hot-dip galvanizing industry [4]. In fact, for instance, by their holistic approach adopted to assess hot-dip galvanizing process sustainability, Hernandez-Betancur et al. found that pickling stage is critical and it is not expected to be improved without a significant modification of the process [18]. The

remarkable importance of this step in hot-dip galvanizing industry have significantly boosted the interest of researchers and technologists.

Some researchers studied strategies to apply the zero emission/discharge concept to improve pickling process by identifying optimisation options, yet maintaining conventional equipment [19]. Others focused on the pickling rate optimization by using an optimal iron/hydrochloric acid concentration ratio in the pickling tank aiming at the minimization of waste acid [20].

A different and likely more effective approach is to recover waste acid solutions by means of auxiliary technologies. This topic has been widely addressed over the years and numerous solutions have been suggested in literature. The main treatment technologies are reported in the following paragraphs where their main advantages and disadvantages are indicated.

1.2.1 *Thermal energy consuming processes*

As far as the regeneration of HCl is concerned, the *spray roasting* (the so-called "Ruthner process") and the fluidized bed processes (the so-called KCH technology) are applied at the industrial scale in many plants in the world [17][21][22].

The *spray roasting* method, as described by M. Ruthner [23], is a technique that consists in regenerating the exhausted solution by a process that involves the conversion of the aqueous solution containing iron chlorides into acid and iron oxide. Thus, the spent pickle liquor is thermally decomposed by means of Eq. 1-4 (pyrohydrolysis reaction):

$$4FeCl_2 + 4H_2O + O_2 = 8HCl + 2Fe_2O_3 - 55\frac{kJ}{mol} \qquad 1\text{-}4$$

The core technology is a vertical metal reactor internally covered with refractory material, in which there is a combustion area in the lower part. The acid crosses the reactor from top to bottom, in counter-current with the hot fumes, evaporates (on average around 450 ° C) and, at the same time, there is the formation of iron oxide granules. Subsequently the acid gas is cooled and condensed, then recycled to the pickling bath, while the oxides formed are continuously removed and can be reused in steel mills. A typical process flow diagram of the process is presented in Figure 1-4.

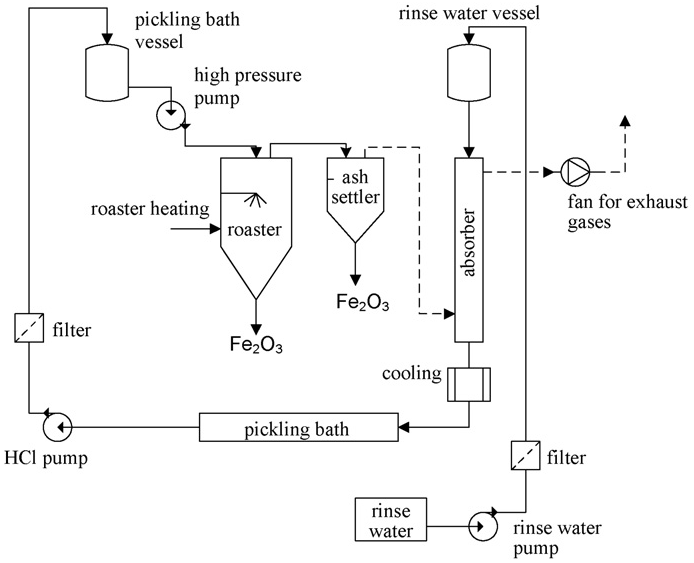

Figure 1-4 Typical PDF of a regeneration plant using Spray Roasting [14].

However, the engineering complexity and the harsh operating conditions (high temperature and corrosive gases) of this technology makes its application suitable only for large-scale metallurgical plants [24]. The main drawbacks are that it is a very energy intensive technology [15], [20] and it suffers for the presence of zinc in solution, due to the formation of low melting compounds at the high process working temperature [25], as well as for the high consumption of process water involved in the chemical reaction of pyrohydrolysis.
Nevertheless, the pyrohydrolysis process is one of the few systems that allow the almost complete regeneration (over 99%) of pickling acids and allows also to recover the iron oxide (according to Eq. 1-4) valuable product [26].

In the *fluidized bed* acid regeneration process, the principle of operation is similar as it is for all roasting processes, but with some variation in equipment used and for the working temperature achieved (fluid bed temperature over 800 °C).

Thermal decomposition is also a conventional method for treatment of acidic waste, which sprays the waste acids including metal ion into a furnace heated from 600 ◦C to 1000◦C [27]. Acid is recovered by absorbing the gases products of the decomposition. Many drawbacks are detected: loss of huge amount of energy during the thermal decomposition, High maintenance cost due to the severe damage of the apparatus by acidic gases.

1.2.2 *Reagent consuming processes*

The oldest and most straightforward way to deal with spent pickling solution is the *neutralization and precipitation* technology. An application of the above mentioned technology is reported by Armco Steel Corporation [28].

This process is a simple engineering system but, on the other hand, it consumes a high amount of chemical reagents. Furthermore, the main feature of the process is the neutralization of the free acidity of the solution. Therefore, there is no acid recovery from the exhausted solution. Thus, this strategy is not anymore considered a BAT technology [29].

The *evaporation* process is a technique that is mostly used for the regeneration of solutions of nitric and hydrofluoric acids [30] [31]. The SPS is treated with another acid, typically H_2SO_4 at 80 °C and in vacuum conditions, in order to cause the dislocation of the positive ions complexed to the chlorides in solution, with the cations possessed by the added acid. The recovered acids are then condensed and reused, while the heavy metal sulphates are neutralized with lime and disposed of as hazardous waste. This technique allows an acid recovery greater than 90% and therefore is a process that has high efficiency. The biggest problem of this technology is the high initial investment cost and the equally high operating costs.

Solvent extraction utilizes the different solubility properties of a component present in a mixture in the solvent used. This technique has been studied for the recovery of metals present in pickling waste. It is one of the few techniques available for the selective recovery of zinc component [32]–[34]. Generally, different kind of organic solvents for the selectivity extraction of metal components and acid are used. Furthermore, acid solutions have to be employed too for the subsequent solvent-metals separation step (stripping step).

The main drawbacks of the process are the partially loss of solvent, thus generating waste water streams containing organic solvent, the consumption of several reactants, the increasing cost with the metals concentration, as well as a complex engineering system. However, the method provides high efficiency recovery, high flexibility and the generation of valuable products that can be recycled and / or sold [14].

An industrial example is provided by Kawasaki Steel Corporation for the recovery of exhausted solutions coming from the pickling lines of stainless steel with nitric and hydrofluoric acids [35] (see Figure 1-5).

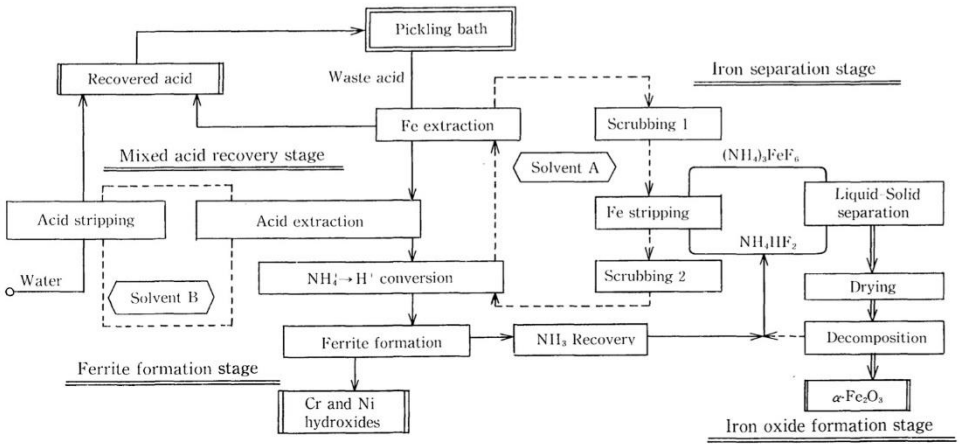

Figure 1-5 Flow sheet of the process of the Kawasaki Steel Corporation company for the recovery of the exhausted pickling by solvent extraction [35].

1.2.3 *Ion exchange processes*

The *ion exchange resins* process is a separation technique for the removal of metals present in pickling spent liquor. These are strongly basic resins [36] capable of separating Fe ions from both Zn ions and HCl. In the separation of the two metal salts, the formation of stable anionic complexes (mainly $ZnCl^{3-}$and $ZnCl^{2-}$), due to the simultaneous presence of chloride ions and zinc ions in solution, play a fundamental role, an aspect that is a main drawback for other regeneration techniques. However, the solutions of zinc chloride and recovered acid are highly diluted and must undergo a further concentration step before they can be reused [27]. The method is severely limited by the zinc and iron concentrations. The investment costs also increase as the concentration of Zn present increases, as greater volumes of resin are required.

The *Acid Retardation* process is a variant of the ion exchange process discussed above. Unlike traditional ion exchange, resins are not retained the heavy metal ions (iron and zinc) but the acid molecules [37].

1.2.4 *Integration of different technologies*

Interesting and more complex solutions for the selective recovery of the different valuable components dissolved in the spent pickling solution suggest the integration of different technologies, as the stand-alone application of individual processes often fails to recover all the possible valuable materials present in complex wastewaters.

Csicsovszki et al. [38] suggested the coupling of anion exchange resin bed step for the separation of Fe and Zn metals and an electrowinning process for the acid and iron separation through a cathodic iron deposition step. However, optimal performance is concentration dependent, thus not providing high flexibility to the process.

Roman et al. [39] have proposed selective membrane-based solvent extraction step to achieve the separation of cationic iron from a solution containing the acid together with anionic species of zinc followed by an electrodialysis (ED) step for acid permeation. However, the recovery of zinc is only possible by considering a furthermore process step (e.g. the electrodeposition), in addition the ED performance are strongly dependent on the specific characteristics of the application, quantitative results are case-dependent.

Studies on the combination of evaporation and crystallization are also present in literature [40], even though relevant application have not proved.

Machado et al. have presented two different integration scheme [41]: distillation combined with solvent extraction or crystallization. High acid recovery were achieved on a lab scale, but no efforts on the zinc recovery were implemented.

An hybrid membrane application is presented from Ortiz et al. [42] consisting of a liquid membrane step for the separation of an iron chloride highly concentrated raffinate and a mixture of HCl and zinc chlorides in the stripping solution coupled with Diffusion or Donnan dialysis process.

Of interest, all these integration technologies foresee the application of at least a membrane process step, thus highlighting the increasing predisposition to use cleaner and more innovative technologies. Therefore, these deserve a separate and more detailed description provided in 1.3 paragraph.

1.3 **Membrane processes for the valorisation of acidic liquid wastes**

In recent years, membrane processes have been used in many fields (medicine, food industry, desalination, etc.), replacing largely traditional separation methods. Membrane technologies have great potential for integrated applications in industrial processes. The affirmation of these processes is related to their advantages: temperatures close to the environment temperatures; no need for chemical additives; a compact and modular design (easy scale-up and scale-down of the processes); large and well-defined contact areas for separation; the ability to selectively transfer specific components and the production of low pollutants and reusable waste [43]. Nevertheless, their actual applicability strongly depends on high-performing membranes availability and cost.

A membrane separation process is driven by a force which activates the flux through the membrane of only some components of the mixture feed, thus obtaining a permeate (product) and a concentrated or retentate (waste). The primary role of a membrane is therefore to act as a selective barrier, which can allow the passage of some components of the mixture while retaining others. The driving force of the process can be a difference in pressure, concentration, electrical potential or temperature.

Among many existing membrane processes, two processes, which are attracting increasing interest, were deeply studied and investigated in this work: the *Diffusion Dialysis* (DD) and the *Membrane Distillation* (MD).

1.3.1 *Diffusion Dialysis*

Diffusion Dialysis (DD) is an *Ionic Exchange Membrane* (*IEM*) process driven by the chemical potential difference between two salt solutions. A DD unit consists of repetitive units called *cell pairs*. Each cell pair consists of an anion exchange membrane (*AEM*) and two compartments, i.e. a diffusate and a concentrate compartment. All the compartments are alternately fed with the two feed streams, thus generating a concentration gradient across all the membranes.

A schematic representation of the DD unit is reported in Figure 1-6.

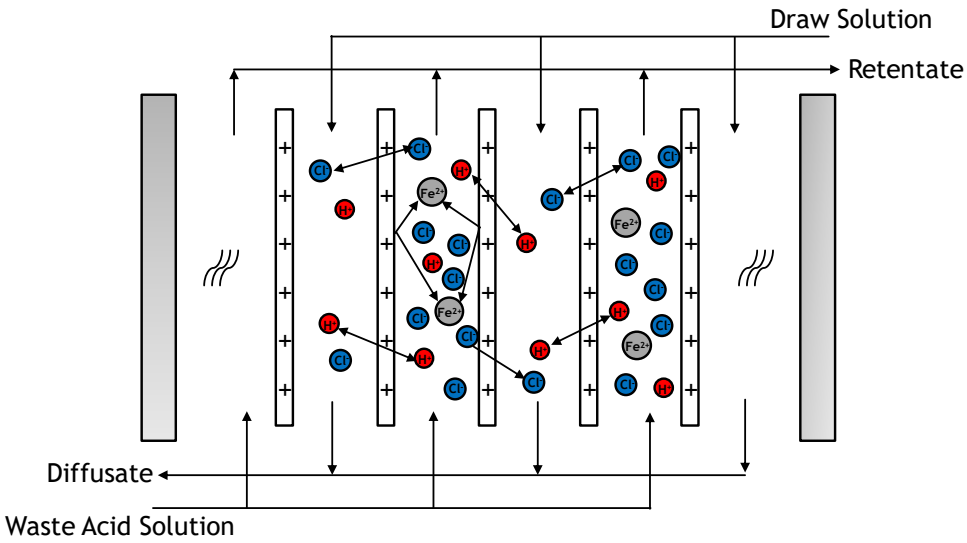

Figure 1-6 Schematic representation of a DD unit.

DD unit configuration consists of net spacers interposed between the membranes to generate the feed channels, maintaining fixed channel dimensions and promoting fluid dynamics. Common spacers are made by two arrays of polymeric wires either extruded (overlapped) or woven, with circular cross section, though other geometries have been devised too. Novel stack configurations adopt profiled membrane without the use of any spacer. In fact, in the case of profiled membrane, the surface contains "*membrane's reliefs*" acting as the traditional spacers.

The standard geometry adopted in DD unit is plate-and-frame. Membranes and spacers are piled up between two end plates. The sealing between each compartment is provided by the use of rubbery gaskets. Co-current, counter-current and cross-flow arrangements can be used in DD units. In general, the counter-current arrangement gives higher driving force and then co-current but it might cause larger pressure difference between the two feed solutions, which may result in leakages and membrane deformations. A schematic representation of the unit is reported in Figure 1-7 for a counter-current configuration.

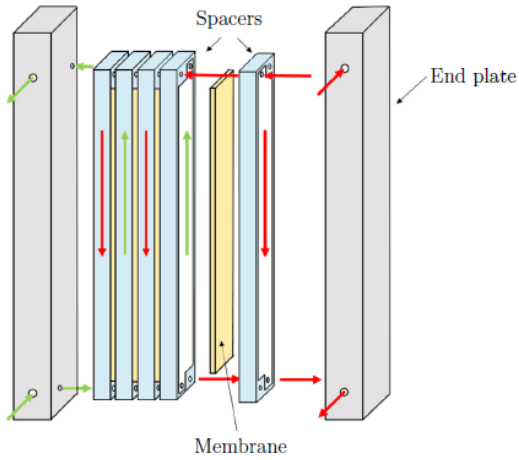

Figure 1-7 Schematic representation of a DD stack elements in a counter-current configuration.

Diffusion dialysis is a simple membrane separation technique, which can be successfully used for the treatment of waste acid solutions containing very high concentrations of metal ions. Plenty of studies are available in literature for the single DD unit application as pickling waste treatment process [44]–[46]. It represents a fascinating technology in the recovery of the acid from steel treatment processes waste [47].

Compared to some conventional processes, this technology demonstrates a significant superiority in terms of [48]–[51]:

- Greater efficiency in the purification of wastewater;
- Low energy consumption;
- Low installation and operating costs; stable, reliable and easy operation;
- Modularity and flexibility;
- No environmental pollution

As regards the first aspect, it has been shown that through the DD process it is possible to recover most of the free acid present in the waste solution, for all the different application. In Table 1-2, acid recovery and metals leakages value collected from scientific literature are reported.

Table 1-2 Collection of selected findings regarding acid recovery and metals leakages with DD technology.

Composition	Acid Recovery	Metals Leakages	Reference
Acid: H_2SO_4 Metals: Cu, Fe, Al	65-85%	Cu: <5% Fe: 15% Al: <8%	[49], [52]–[55]
Acid: HNO_3+HF Metals: Fe, Ti	HNO_3: >100% HF: 60-70%	Fe: <20% Ti: <15%	[46], [49], [56], [57]
Acid: HCl Metals: Fe, Zn	70-90%	Fe: 10-25% Zn: 50-70%	[58][51][49]

For the H_2SO_4 acid recovery shows a strongly influenced with the acid concentration, and contrarily to the other acid trends, it decreases when acid concentration increases.

For the HF–HNO_3 system, the Fe–F complex formation gave the unusual result of a HNO_3 recovery exceeding 100%, albeit lower HF recovery are observed.

Under selected operating conditions HCl recovery can reach values of 90% acid recovery. Main metals in the feed waste were rejected effectively by the diffusion dialysis membrane, while Zn in HCl solution is leaked through the membrane in large measure [59], [60].

The DD process is one of the cheapest regeneration technologies, as it does not require energy costs (except for the handling of fluids) as it operates under normal operating conditions and because, during the process, the phases are not involved in phase change. The cost-effectiveness of the process is also expressed in the use of inexpensive materials for the modules, in particular polymeric material, which, in addition to low cost, have great chemical resistance against corrosive substances. This is a significant advantage over other conventional treatment systems, which use specific and particularly expensive metal alloys to resist corrosion. The systems can be easily integrated into existing plants.

A further advantage typical of membrane technologies is modularity [61]. This allows the implementation of treatment systems, which have the same basic technology and similar configuration, but which are suitable for specific requests for both small plants and large-scale industrial plants.

Surely, the unique and undisputed advantage in DD is the environmental aspect, being a highly non-polluting technology. DD is counted among the Best Available Techniques (BAT) technologies [29], [62]. The term "best available techniques" is defined in the European Directive 96/61/EC. By “techniques” we mean the technologies used and the way in which the plant is designed, built, maintained and the method by which its dismantling is envisaged; the term "available" includes the techniques that are developed on a larger scale that allows

their implementation in the industrial sector, under economic and advantageous operating conditions; "Best" means operating in the achievement of high levels of environmental protection

The main disadvantage of this technology, as already mentioned, is the impossibility of separating the Zn (II) from the acid, which is transported with it. In addition, since diffusion across membranes is a relatively slow process, a large membrane area is required to remove a significant amount of ions in solution.

1.3.2 *Membrane Distillation*

Membrane Distillation (MD) is a thermally driven separation process with various applications in water treatment, desalination or food industry [63]. A hydrophobic membrane separates the vapour from the aqueous solution at different temperature and composition [64]. MD is governed by the difference in temperature, and thus by the partial pressure difference, between the two sides of the membrane. The different partial pressures at the two membrane sides generate the driving force for the passage of vapour molecules through the microporous membrane and the permeate composition is a function of both the temperature and the composition of the feed [65]. Due to the liquids surface tension and the hydrophobic nature of the membrane, no liquid crosses the membrane despite its porousness and even though the pores have an average diameter of 0,1-0,5 μm and water molecules are 50-250 times smaller [66]. Interestingly, MD is characterized by low operational pressure requirement as well as low working temperatures. The process can be performed at a feed temperature considerably lower than its boiling point, thus allowing the utilization of waste heat or alternative thermal energy sources [65], [67], and boosting its applicability in remote areas and small scale production [64], [68]. The lower operating pressures involve lower equipment costs, greater process safety and reduce the stresses to which the membranes are subjected. For this reason, no particular mechanical characteristics of the membranes are required and their only function is that of maintaining the liquid / vapour interface.

Despite the demonstrated advantages, it has not yet been commercially successful. One of the main reason is the high energy consumption (typical thermal energy consumption ~100 kWh/m^3) [69] compared, for example, to reverse osmosis (RO) (mechanical energy consumption 2–4 kWh/m^3) [70]. Other reasons are related to the lack of commercially available high performance membranes and the low water flux. One of the main causes

responsible for low water flux is the temperature polarization phenomenon, while the concentration polarization has a negligible effect on the permeate flow rate reduction [71].

Membrane distillation can be used to concentrate hydrochloric acid solutions with metal salts dissolved [65], [72]. Metal salts components are non-volatile compounds hence massive rejection is achievable. Unfortunately, HCl is a volatile compound and, indeed, the liquid-vapour equilibrium is influenced from both the temperature and concentration of acid and salts in the feed [65], [73].

MD can be generally classified based on configuration into direct contact membrane distillation (DCMD), air gap membrane distillation (AGMD), sweeping gas MD and vacuum MD. The most studied configuration is the Direct Contact Membrane Distillation (DCMD), where the permeate is collected in a cold stream in direct contact with the membrane. This configuration is characterized by high driving force but also high heat losses.

The MD modules used in the technology proposed throughout this thesis has a conceptually modified design in order to suit the harsh conditions of the pickling wastewater. As this new module design resembles an AGMD module, the latter one was used as a basis to expand on the technical details of the design applied in this thesis.

An AGMD has three channels: condenser channel, evaporator channel and the gap channel. The channels are separated by membrane or polymer film as shown in Figure 1-8 (A). An impermeable film is placed between coolant and membrane, leaving an air gap for permeate. This gap is quite wide so the permeate does not have direct contact to the membrane. The released vapour crosses the gap and condenses on the cooled impermeable film. Advantage of this design is reduced heat loss by conduction since the air gap poses as thermal insulation. Also more volatile substances can be separated because of there is no contact between the liquid permeate and the membrane [74]. Drawback is additional resistance to mass transfer leading to decreased performance [75].

Taking into account the harsh environment created due to the acids, an additional feed gap is implemented in the just described AGMD technology. The acid feed loop is introduced in the gap channel (called as feed channel) instead of the former evaporator channel. One of the major advantages of this setup is that the heating and cooling loops have no contact with acids and thus the whole hydraulic cycle (pumps, heating and cooling exchangers, piping, sensors etc) does not need special acid resistant materials thus saving costs.

Feed gap air gap membrane distillation (FGAGMD) [76] is thus conceptualized from Solar Spring GmbH spin-off company of the Fraunhofer ISE (see concept design in Figure 1-8 (B)).

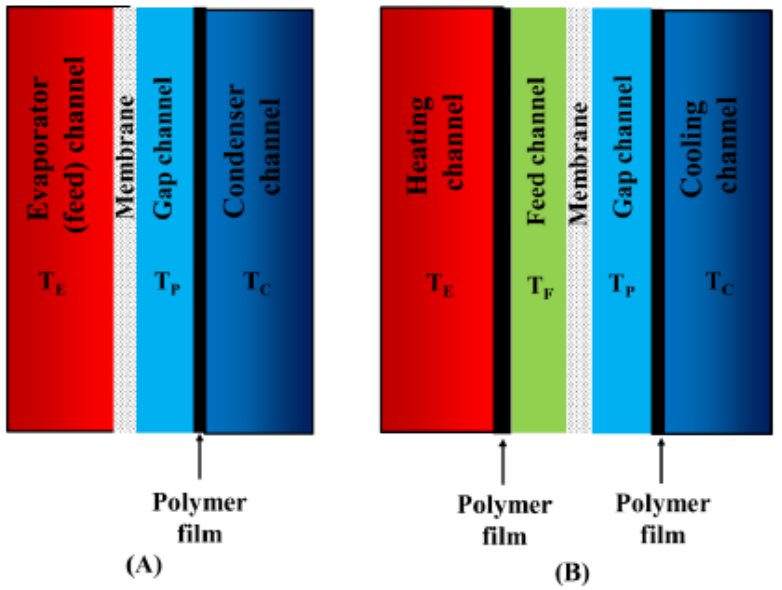

Figure 1-8 (A) – Concept for a standard AGMD module with three channels. (B) – Concept for the MD modules FGAFMD designed to treat acid wastewater.

A summary of the treatment processes discussed so far is presented in Table 1-3, highlighting the most relevant advantages and disadvantages.

Table 1-3 Methods of SPS regeneration.

Input for recovery	Method	Advantages	Disadvantages
Thermal energy	Spray roasting	-Effective method for large amounts of SPS -Acid regeneration (>99%) -Metal oxides recovery [26] -Applied in industry [17], [22]	-High consumption of fresh water and energy [15], [20] -Limited by Zn(II) concentration [25] -Complex installation -Suitable for large-scale applications [24] -Energy intensive (working temperature 600-1000 °C) [27] -High maintenance cost due to acidic gases
	Fluidized bed		
	Thermal decomposition	-Acid regeneration -Metal oxides recovery	
Reactants	Neutralization and Precipitation	-Simple engineering system [28] -Low operating costs	-No recovery of acid and metals -Large consumption of chemicals

Resins	Evaporation	-Acid regeneration (>90%)	-High investment and operating cost -High energy consumption -Consumption of additional acid -No metals recovery
	Solvent extraction	-High flexibility -Selectivity separation of metals [32]–[34]	-Organic impurities in the waste solutions -Consumption of additional acid -Complex system
	Ion exchange resins	-Selectivity separation of metals -Low operation cost	-Production of high volume of waste -High consumption of fresh water -Diluted products-requires further treatment
	Acid Retardation	-Simplicity, reliability[77]	-High consumption of fresh water -Diluted acid
Membrane	Diffusion Dialysis	-Low energy consumption [48]–[51] -Increases environmental liability [29], [62] -Modularity and flexibility [61] -Acid recovery >80%	-Metal leakage across the membrane [59], [60]
	Membrane Distillation	-Use of waste heat or alternative thermal energy [65], [67] -Recovery of water and acid -High concentration of metals	-Strong effect of feed composition on HCl recovery [65], [73]

1.4 **Motivation and goal of this work**

The metal process and coating industry consumes a large amount of different process fluids like acids, bases and salts leading to contaminated waste water streams. The spent solution discharge has a dramatic impact in the industry economics as well as in the ecological footprint.

Among the different treatment processes of spent pickling solution, this thesis focuses on the analysis of an hybrid membrane integrated system with a circular economy approach implementation.

Different theoretical and pratical studies have been carried so far, providing stand-alone applications which often fail to recover all the possible valuable materials present in complex wastewaters. For the most of the works reported in the literature focused on techonoligies integration no process feasibility has been reported in literature.

The main objective of this thesis is to provide a proof of valorisation of the industrial wastes thorugh the proposed techonology, demonstrating the feasability in the industrial environment at a pilot scale which is able to reduce the waste water disposal issue and guarantee continuous optimal conditions in the relevant industrial processes. To this aim, both modeling and experimental activities have been carried-out. In particular:

(i) Modeling activities focused on the development of modeling tools validated against experimental results, in order to predict the performance of single unit (e.g. *Diffusion Dialysis* unit) and of the overall integrated process.

(ii) Ad hoc experimental campaigns were carried out to characterise the behaviour of the different techonologies, membrane properties but also the operability of lab-scale units.

(iii) All the knowledge gained has made possible the design, construction and testing a prototype unit in the industrial environment, demonstrating the feasibility of the process.

(iv) Techno-economic profitability of the fully integration of the hybrid system in the hot-dip galvanizing process chain was assessed.

(v) An optimization analysis tool was applied to investigate the impact of operating and design variables and to investage critical issues of the proposed technology.

SECTION 1: EXPERIMENTAL AND MODELING ACTIVITIES AT LABORATORY SCALE

ABSTRACT

An intense experimental campaign aiming to show the feasibility of valorising the waste pickling components, e.g. acid and metals, and minimize the environmental impact caused by the waste solution production is discussed in this first section.

In particular, diffusion dialysis (DD) can be used to separate acids and heavy metals from pickling waters, while reactive precipitation which has been performed in continuous stirred tank reactor (CSTR), is employed to selectively separate the two main metals (iron and zinc), thus promoting the circular use of such materials.

Hydrochloric acid recovery from pickling solutions was studied by employing a laboratory scale unit operating in batch and a continuous large-scale unit, both equipped with Fumasep anionic exchange membranes.

The effect of main operating parameters such as HCl concentration (0.1-3 M) and the presence of Fe and Zn (up to 150 and 10 g/l, respectively) was investigated to simulate the system operation with real industrial streams. The variation of HCl, Fe, Zn and water flux was identified. Results obtained show that zinc and iron concentration affect the HCl recovery in opposite ways. Iron chlorides enhance acid recovery, while zinc chlorides considerably tend to diffuse through the membrane because of negatively charged chloro-complexes formation and slightly reduce the acid diffusion.

A comprehensive multi-components mathematical model was developed and validated with experimental data. The model has a time and space distributed-parameters structure allowing to effectively simulate steady-state and transient batch operations, thus providing an operative tool for the design and optimization of DD units. As a result, a good comparison between model simulations and experiments was achieved in both configurations.

Selectively separation of Fe and Zn was reached by implementing a strategy of precipitating $Fe(OH)_3$ as solid 99% purity product, and keeping in a liquid phase a fluxing reusable solution (composed by $ZnCl_2$ and NH_4Cl) which is a by-product for the galvanizing industry itself. Best operating condition, in term of concentration, excess ratio of reactants, and operational mode were chosen following experimental investigations.

2. DIFFUSION DIALYSIS

Chapter Outline

Part of this chapter has been published in:

Experimental investigation and modeling of diffusion dialysis for HCl recovery from waste pickling solution" R. Gueccia, S. Randazzo, D. Chillura Martino, A. Cipollina, G. Micale, Journal of Environmental Management 235 (2019) 202–212;
doi: 10.1016/j.jenvman.2019.01.028

Diffusion Dialysis for Separation of Hydrochloric Acid, Iron and Zinc Ions from Highly Concentrated Pickling Solutions" Rosa Gueccia, Alba Ruiz Aguirre, Serena Randazzo, Andrea Cipollina, Giorgio Micale, Membranes 2020, 10, 129
doi:10.3390/membranes10060129

2.1 **Literature overview**

Diffusion dialysis (DD) is becoming popular thanks to the recent important advances in ion exchange membranes (IEMs) [78]. These are usually classified by their function of separation media as cation exchange membranes (CEM), which contain negative fixed charges and have a selective permeability for cations, and as anion-exchange membranes (AEM), which contain positive fixed charges and have a selective permeability for anions.

AEMs have brought much attention for acid recovery with DD process as their positive fixed charges promote the transport of the strong acids in ionized form (e.g. HSO^{4-}, Cl^{-}, NO^{3}) [79]. Due to the positive fixed charges present in the membrane, the transport of counter-ions (chlorides) is facilitated, whereas co-ions (iron cations, for instance) are rejected because of the electrostatic repulsion. However, also H^{+} ions can diffuse through the anionic membrane, despite their positive charge, thanks to their little size and through the tunneling mechanism [48], [51], [80]. Therefore, the acid recovery and separation from salts occur.

The majority of AEMs are usually synthesized from polymers as polysulfone (PSU), polystyrene (PS), and brominated poly (2,6-dimethyl 1,4-phenylene oxide) (BPPO) ([81][82]). Some commercially available AEMs have been evaluated in DD process to acid recover, such as the Selemion ([83]–[85]), Neosepta ([47], [57], [85]–[88]), DF-120B ([55], [89], [90]). Very few researchers studied the performances of Fumasep membranes [42], [91].

Research efforts have been devoted also to analyze how the acid concentration and the presence of metal salts can affect HCl recovery in DD. Palatý and Žáková have carried out studies on the application of DD for acid recovery under different acid feed compositions [[52], [57], [92]–[99]). In their works, they characterised the transport of species across an AEM (Neosepta-AFN) and studied how speciation affected the transport of acids and metals. They have worked with different kinds of acids and electrolytes, such as H_2SO_4 and its mixture with $CuSO_4$ or $ZnSO_4$, HCl with $FeCl_3$ or $NiCl_2$, HNO_3, H_3PO_4 and HF.

As concern the hydrochloric application, they have studied systems containing HCl [86], [92], [93], [98], HCl-$FeCl_3$ [86], HCl-$FeCl_2$[96] and HCl-$ZnCl_2$[59]. The addition of chloride (e.g. $FeCl_3$ and $FeCl_2$) promotes the transport of HCl across the AEM, reaching higher concentrations in the water compartment than in the feed side, as also stated from other researchers [49], [51], [100]. In fact, chloride ions permeability is affected by the metal chloride involved in the process. Iron salt enhances HCl diffusion through the membrane due to the so-called "salt effect", because of the supply of Cl^{-} ions. However, even an iron leakage

occurs and these phenomena increases as the iron ion concentration increases. Their effect on the diffusive permeability and the acid recovery have been quantitatively analysed.

The acid and iron salt diffusive permeability of the membrane is highly related to the mobility of all ionic species. Several researchers developed theoretical models to characterize transport phenomena in DD. Some important parameters, especially the permeability (P), have been defined and determined, both for the acid and the iron chloride transport, by carrying out experiments in batch [58], [96], [101], [102] and in continuous [58], [98], [101] systems. Interestingly, only few researchers used very high concentrations of iron ions as in an industrial pickling waste (up to 150 g/l), when the leakage of cations through the anionic exchange membrane can be considerable [51].

On the other side, the co-existence of Zn^{2+} cations and Cl^- anions in the pickling solution, leads to formation of negative chloro-complexes, which can considerably leak through the AEM, such as $[ZnCl_3]^-$ and $[ZnCl_4]^{2-}$ [103]. Several studies on inorganic acids coupled with a the single zinc metal salt are present in the literature [59], [100]. Despite the loss of membrane permselectivity and transport properties in the presence of Zn ions have been addressed by different authors [60], [104], concluding that HCl-$ZnCl_2$ mixture separation exhibits low efficiency due to the strong attraction of Zn towards chlorides ions, the recovery of hydrochloric acid from waste acidic metal brines having real industrial composition in terms of Zn and Fe ions has not been investigate in detail. An experimental campaign aiming at the investigation of the effects of metal species on the recovery of inorganic acids was presented by Suk Jung Oh et al. [49], even though no modeling efforts were made to better characterize the system.

Another important parameter, the water flux through the membrane, was also observed and poorly discussed only in a few cases [49], [51], [101].

For the sake of clarity, a summary of the membranes used in the diffusion dialysis process according to the SPS types is reported in Table 2-1. Recovery and metals leakage values for the studies performed in continuous system are reported as well. In the case of batch conditions, permeability and concentration profiles were investigated and main values are reported in Table 2-6 in paragraph 2.4.4.

Table 2-1 Spent pickling solution types and membranes applied in diffusion dialysis process for acid and metal recovery.

SPS type	Membrane	Recovery (R)/ Metals leakage (Leak)	Ref
HCl	Neosepta AFN	-	[86], [93], [98]
	Fumasep FAD	-	[91]
H_3PO_4	Neosepta AFN	-	[98]
H_2SO_4	Neosepta AFN	-	[95]
	Fumasep FAD	-	[91]
HNO_3, HF	Fumasep FAD	-	[91]
H_2SO_4, H_3PO_4	Neosepta AFN	-	[47]
H_2SO_4, $Al_2(SO_4)_3$	Selemion DMV	R <80% $Leak_{Al}$ 30%	[84]
H_2SO_4, $CuSO_4$, $Al_2(SO_4)_3$	DF120	R 60-70% $Leak_{Cu}$ <15% $Leak_{Al}$ <8%	[89]
Real waste acid sol. (mainly H_2SO_4, $FeSO_4$, $NiSO_4$)	Selemion DSV	R 80% $Leak_{Ni}$ 1% $Leak_{Fe}$ 4%	[83]
Acid leaching sol. (mainly H_2SO_4, $VOSO_4$, $FeSO_4$)	DF120-III	R 70-84% $Leak_V$ 4.5-5% $Leak_{Fe}$ 2.5-6%	[55], [90]
H_2SO_4, $CuSO_4$	Neosepta AFN	R >90% $Leak_{Cu}$ <3.5%	[52], [99], [105]
	Fumasep FAD	R >90% $Leak_{Cu}$ 5%	[105]
H_2SO_4, $ZnSO_4$	Neosepta AFN	-	[88]
HNO_3, $Fe(NO_3)_3$	Neosepta AFN	$Leak_{Fe}$ <3%	[57]
HCl, NaCl	Neosepta AFN	R >95%	[87], [92]
HCl, $NiCl_2$	Neosepta AFN	$Leak_{Ni}$ <3%	[97]
HCl, $FeCl_2$	Neosepta AFN	-	[96]
	DF120	R <80% $Leak_{Fe}$ <20%	[51]
HCl, $FeCl_3$	Neosepta AFN	-	[86]
HCl, $ZnCl_2$	Neosepta AFN	-	[59]
HCl, $FeCl_2$, $ZnCl_2$	DF120	R 88% $Leak_{Fe}$ 11-23% $Leak_{Zn}$ 60%	[51]
HCl, Zn, Cu, Fe; Ni, Cr	Neosepta AFN	R >85% $Leak_{Zn}$ 70% $Leak_{Cu}$ 30% $Leak_{Fe}$ 10% $Leak_{Ni}$ 5% $Leak_{Cr}$ 5%	[49]
H_2SO_4, Zn, Cu, Fe; Ni	Neosepta AFN	R <70% $Leak_{Zn, Cu, Fe, Ni}$ <2.5%	[49]

HNO_3, HF, Cu, Ni, Fe; Cr	Neosepta AFN	R_{HNO_3} 100% R_{HF} <65% $Leak_{Cu, Ni}$ 20% $Leak_{Fe}$ 10% $Leak_{Cr}$ 7%	[49]

In this study, two DD modules equipped with Fumasep FAD-PET-75 anionic exchange membranes were used for assessing the separation of hydrochloric acid from highly concentrated zinc and iron solutions. A single-cell plate and frame laboratory-scale DD unit (10x10 cm^2) operating in a batch configuration and a large pilot-scale DD unit (10x80 cm^2) operating in continuous mode were tested. A mathematical model, with a time and space distributed-parameters architecture [106], was developed and validated, providing an effective tool for the prediction of all the main process phenomena, from acid and iron and zinc ions fluxes to the water flux and the simulation of continuous or transitory operation. The model was thoroughly validated with experimental data for the two configurations, highlighting its ability to well predict the observed experimental trends.

2.2 **Experimental**

2.2.1 *Materials*

The solutions for diffusion dialysis experiments were prepared in laboratory from 37% HCl solution, $FeCl_2$ tetrahydrate (Carlo Erba reagents, purity ≥ 99%), $ZnCl_2$ (Carlo Erba, ≥ 99%) and deionized water. Na_2CO_3 (Carlo Erba reagents, purity ≥ 99.5%) was used for HCl titration. The retentate solutions, precisely concentrated feed solutions, consisted of HCl solutions at 0.1 to 3 M, when only acid behaviour is analysed. Multi-component solutions were prepared by adding Fe ions with a concentration ranging from 50 to 150 g/l, Zn ions concentration from 5 to 20 g/l and HCl concentration from 70 to 100 g/l. The concentration ranges were opportunely chosen in order to make the laboratory artificial solutions comparable with the real industrial ones.

Deionized water was used as diffusate solution for the tests aiming to investigate either the permeability of the acid or the combined effect of acid and metal salts. Differently, for the tests carried out to explore the isolated iron and zinc diffusive behaviour through the

membrane, 0.1 M HCl was used either in the retentate and diffusate solutions, in order to thus reducing acid and water fluxes thorough the membrane.

The membrane adopted is a Fumasep membrane (type FAD-PET-75, by Fumatech GmbH, https://www.fumatech.com/EN/Onlineshop/Products%2bof%2bHydrocarbon%2bpolymers/index.html) and the main characteristics are reported in Table 2-2.

Table 2-2 Properties of Fumasep FAD-PET-75 type anion exchange membrane.

Item	Unit	Specifications
thickness (dry)	µm	70-80
electric resistance [a)]	Ω cm²	< 1
selectivity [b)]	%	> 90
stability	pH	< 9
ion exchange capacity	meq/g	> 1.5
specific conductance [c)]	mS/cm	> 13
weight per unit area	mg/cm²	9-12
proton (H^+) transfer rate [d]	µmol/min/cm²	> 1500
Young's modulus [e)]	MPa	> 1000
tensile strength [e)]	MPa	> 40
elongation at break [e)]	%	> 15
bubble point test in water at T = 25 °C	bar	> 3

[a)] in Cl^- form in 0.5 M NaCl at T = 25°C, measured in standard measuring cell (through-plane)
[b)] determined from membrane potential measurement in a concentration cell 0.1/0.5 M KCl at T = 25°C
[c)] determined in Cl^- form in 0.5 NaCl at T =30°C
[d)] determined from pH potential measurement in a concentration cell 0.5 M HCl/0.5 M KCl at T = 25°C
[e)] determined by stress-strain measurement at T = 25°C and 50 % r.h., according to DIN EN 527-1

2.2.2 *Diffusion dialysis set-up and experimental procedures: lab scale*

The diffusion dialysis module has a plate and frame configuration, consisting of two Plexiglas plates (20x20x2 cm³) equipped with inlet-outlet manifolds, two spacers (thickness 270 µm) and an anion-exchange membrane (active area 10x10 cm²) interposed between the

two spacers. Retentate and diffusate solutions are circulated from/to in the same tanks and they are circulated through the DD module by two peristaltic pumps, thus realizing a batch operation mode. Figure 2-1 illustrates the laboratory DD experimental set-up.

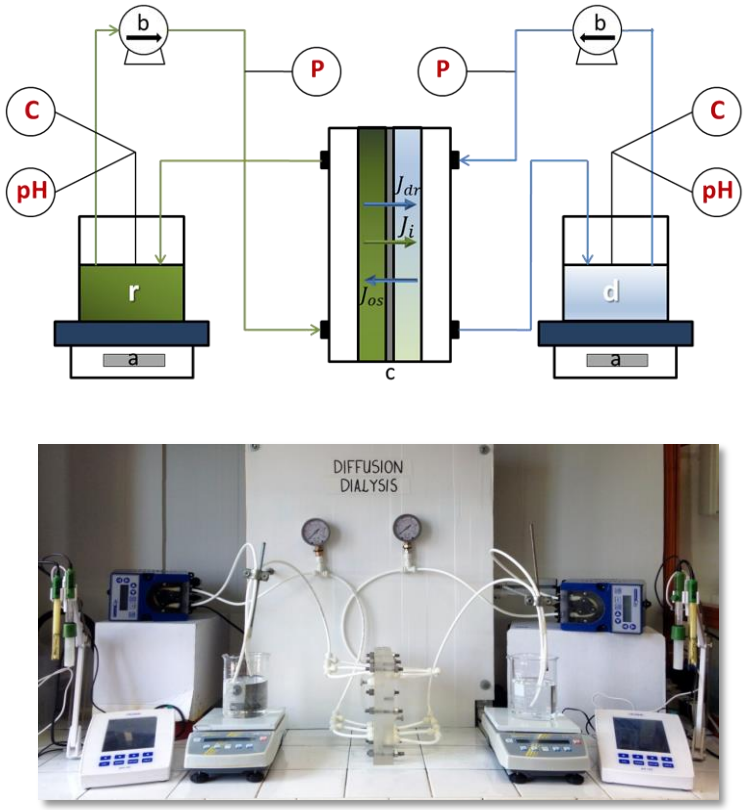

Figure 2-1 Schematic representation of the experimental set-up: (a) scales, (b) pumps, (c) DD module, (P) pressure gauges, (r) retentate tank, (d) diffusate tank. The arrows denote the osmotic flux (J_{os}), the drag flux (J_{dr}) and the i-component flux (J_i) across the membrane (on top); picture of the real DD laboratory experimental set-up (on the bottom).

After the module assembly, a leakage test was performed by recirculating deionized water for 60 minutes and observing any internal or external leakage. Before each experiment, the apparatus was fully fed with an acidic solution (with an acid concentration equal to the average of the two feed solutions) in order to condition the membrane for 120 minutes. During experiments, pH and conductivity in the recirculation tanks were measured by digital multi parameter pH/conductivity-meter (Hanna Instruments) and several samples were withdrawn to measure acid and iron concentration, the first one after 1 h, the others every two hours. At

the output of each pump, a pressure gauge was connected to the circuit, in order to monitor the pressure drops inside the stack.

Error bars were obtained and shown in all the reported graphs by repeating each experiment at least two times.

Batch tests were run at ambient temperature (20-25 °C), by recirculating a set flow rate of 48 ml/min, corresponding to a channel linear velocity of 3 cm/s. Weight variations of the retentate and diffusate tanks were used for water flux determination. By measuring volume (or total weight) and concentration variations, it is possible to characterize the system performances in terms of *i*-species fluxes (J_i), batch acid recovery ($RR_{HCl,t}$) and metal salt leakage ($Leakage_{Me,t}$) by means of simple transport and mass balance equations:

$$J_i = -\frac{\Delta\left(V_r c_{i,r}\right)}{A_m \Delta t} = -\frac{V_r|_t}{A_m}\left(\frac{c_{i,r}\big|_{t+\Delta t} - c_{i,r}\big|_t}{\Delta t}\right) - \frac{c_{i,r}\big|_t}{A_m}\left(\frac{V_r|_{t+\Delta t} - V_r|_t}{\Delta t}\right) \quad 2\text{-}1$$

$$RR_{HCl,t} = \frac{V_d c_{HCl,d}\big|_{t+\Delta t} - V_d c_{HCl,d}\big|_t}{V_r^{in} c_{HCl,r}^{in}} \quad 2\text{-}2$$

$$Leakage_{Me,t} = \frac{V_d c_{Me,d}\big|_{t+\Delta t} - V_d c_{Me,d}\big|_t}{V_r^{in} c_{Me,r}^{in}} \quad 2\text{-}3$$

with *V* being the tank volume, c_i the bulk concentration of the *i*-component, A_m the membrane area, *t* the operation time. Subscripts *r* and *d* state for retentate and diffusate, respectively, subscripts *Me* state for metal salt (i.e. $FeCl_2$ and $ZnCl_2$) while *t* denotes a variable being function of time.

Moreover, the acid recovery efficiency (η_{HCl}) parameter takes into consideration the ratio between actual and theoretical maximum acid recovery(RR_{HCl}^{max}):

$$\eta_{HCl}(\%) = \frac{RR_{HCl,t}}{RR_{HCl}^{max}} x100 \quad 2\text{-}4$$

More specifically the theoretical maximum recovery is defined as the highest acid recovery obtainable in equilibrium condition, which means 50% of the total initial acid amount when same volume for the retentate and diffusate tanks are considered.

2.2.3 *Diffusion dialysis set-up and experimental procedures: large scale*

The experimental set-ups for the continuous operating configurations have similar characteristics to the previous one. A plate and frame DD unit composed of 18 Fumasep FAD anionic exchange membranes (80 cm length, 10 cm width and 270 µm thickness) and 19 spacers with integrated gasket, thus leading to 9 feed and 10 diffusate channels. Feed and deionized water solutions were fed to the DD unit in one-path countercurrent configuration, and they were drained out in the retentate and diffusate buffers, respectively.

Samples were collected in line at the outlet of the retentate and diffusate circuits. Steady state conditions were assessed by monitoring the acid, iron and zinc concentration every 10 minutes in the samples. In all tests, steady state conditions were achieved after less than 20 minutes of operation (corresponding to about 5 times the residence time of solutions in the compartments).

A scheme of the continuous set-up is presented in Figure 2-2 along with a picture of the large DD module.

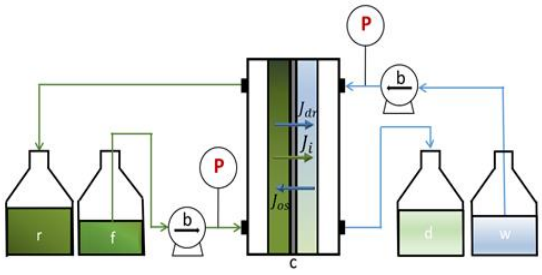

Figure 2-2 Schematic representation of the continuous experimental systems. (a) balances, (b) peristaltic pumps, (c) Diffusion Dialysis units, (r) retentate buffer, (d) diffusate buffer, (f) feed tank, (w) deionized water tank, (P) pressure meter. The arrows have the same meaning of Figure 2-1 (on the left); picture of the real DD large laboratory experimental set-up (on the right).

A flow rate of 48 ml/min was adopted for the tests performed with the large-scale unit in continuous operating mode, corresponding to a channel linear velocity of 3 mm/s, typical industrial value for accomplishing a suitable components transport across the membrane. For this configuration, the main two considered parameters, acid recovery ratio (RR_{HCl}) and iron and zinc leakage through the membrane ($Leakage_{Me}$) were evaluated in terms of flow rates as follow:

$$RR_{HCl}\ (\%) = \frac{F_d c_{HCl,d} - F_w c_{HCl,w}}{F_f c_{HCl,f}} x100 \qquad 2\text{-}5$$

$$Leakage_{Me}(\%) = \frac{F_d c_{Me,d} - F_w c_{Me,w}}{F_f c_{Me,f}} x100 \qquad 2\text{-}6$$

where *F* is the volumetric flow rate. Subscripts *f* and *w* state for feed and water, respectively.

2.2.4 *Analysis*

The acid concentration was detected by titration with Na_2CO_3 solutions.

Iron ions concentration was revealed by spectrophotometry (spectrophotometer Beckham DU 800), by adding 1,10-phenanthroline. Water samples were characterized at a wave length of 510 nm.

Zn detection was performed by atomic absorption (Shimadzu mod. AA6200).

2.3 **Results and Discussion**

2.3.1 *Effect of HCl concentration on acid permeability*

The flux of acid at different initial concentrations was studied in order to determine the membrane acid permeability. Several experiments were carried out with HCl at 0.1, 0.5, 1, 2 and 3 M at room temperature using deionized water as draw solution. In Figure 2-3, time variations of HCl concentration are reported in the retentate and diffusate tanks.

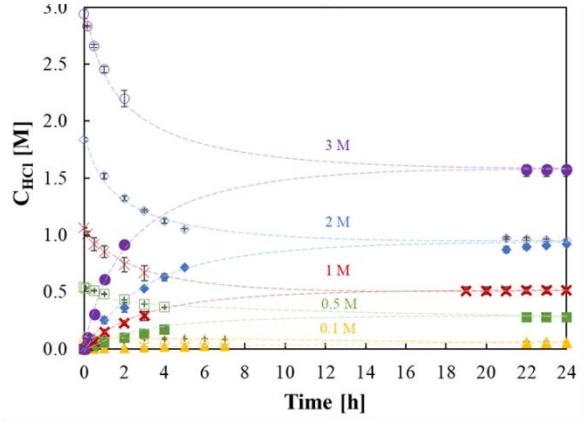

Figure 2-3. HCl concentrationvs. time in the retentate (empty symbols) and in the diffusate (solid symbols). Initial HCl concentrations in the retentate: 0.1M (△), 0.5M (□), 1M (X), 2M (◊) and 3M (○). Flow rate: 48 ml/min. Retentate: HCl solution. Diffusate: deionized water.

Such variation can be ascribed to the presence of a diffusive acid flux through the membrane from the retentate to the permeate channel. This is reported in Figure 2-4, where the flux of HCl is plotted versus the time; it quickly decreases when the acid concentration increases.

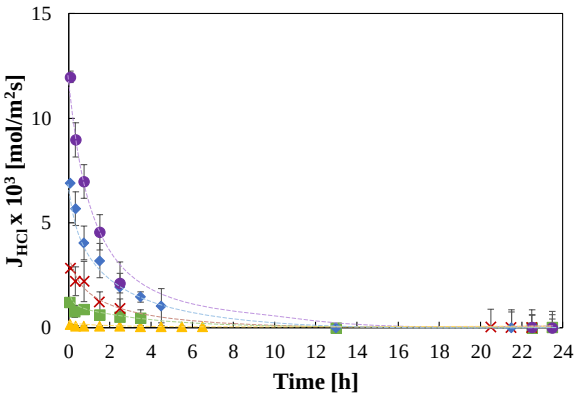

Figure 2-4 HCl flux vs. time in the retentate (empty symbols) and in the diffusate (solid symbols). Initial HCl concentrations in the retentate: 0.1M (△), 0.5M (□), 1M (X), 2M (◊) and 3M (○). Flow rate: 48 ml/min. Retentate: HCl solution. Diffusate: deionized water.

In fact, according to the Fick's law, which relates the diffusive flux to the concentration gradient across the membrane, this flux decreases significantly along time due to the reduction in the concentration driving force, as also observed by Jung Oh et al. [49]. Moreover, also the

permeability value is influenced by acid concentration (see section 5). In all these cases, a recovery efficiency of almost 100% is reached after 24 hours of operation (see section 0).

The influence of HCl concentration on the water flux through the membrane was also investigated (Figure 2-5). An appreciable decrease of diffusate volume was detected only for the lowest HCl concentration investigated (0.1 M), justified by the presence of the osmotic flux from dilute to concentrate channel. Conversely, at higher concentrations (0.5–3 M), the diffusate volume increases. This can be attributed to the drag flux, i.e. flux of water molecules associated to the acid transported from the retentate to the diffusate. The drag flux direction is opposite to the osmotic flux (see Figure 2-1) and it prevails when acid concentrations are above a threshold limit of about 0.5 M. In fact, above this threshold the significant flux of acid leads to an important drag flux of water molecules, as already reported by some authors for the case of higher acid concentrations [49], [101].

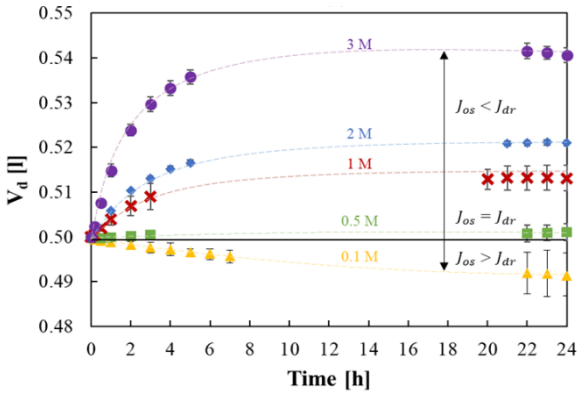

Figure 2-5 Diffusate volume vs. time in the retentate (empty symbols) and in the diffusate (solid symbols). Initial HCl concentrations in the retentate: 0.1M (△), 0.5M (□), 1M (X), 2M (◊) and 3M (○). Flow rate: 48 ml/min. Retentate: HCl solution. Diffusate: deionized water.

2.3.2 *Fe passage and its effect on HCl recovery*

To evaluate the iron passage through the membrane, two solutions at the same HCl content (0.1 M) were used in the two channels in order to always keep an acidic pH. $FeCl_2$ was added in the retentate at different concentrations (namely 50, 100 and 150 g/l of Fe ions). The experiments were performed with a flow rate of 48 ml/min in both the channels, at room

temperature. As reported in Figure 2-6, a leakage from 2 to 12 g/l was detected after 7 hours increasing as the iron concentration increases.

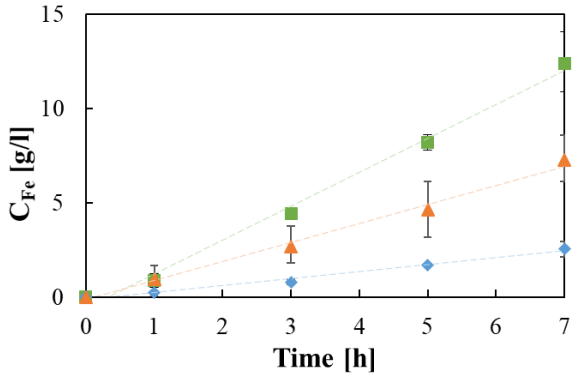

Figure 2-6 Fe concentration vs. time in the diffusate. Initial Fe concentrations: 50 (♦), 100 (▲) and 150 (■) g/l. Initial acid concentration:2M. Flow rate: 48 ml/min. Retentate: HCl and $FeCl_2$ solution. Diffusate: deionized water.

The effect of $FeCl_2$ concentration on the HCl recovery was also studied. As shown in Figure 2-7, for an initial iron concentration of 100 g/l, the acid recovery in the presence of iron in solution was higher compared to the one revealed in the absence of Fe.

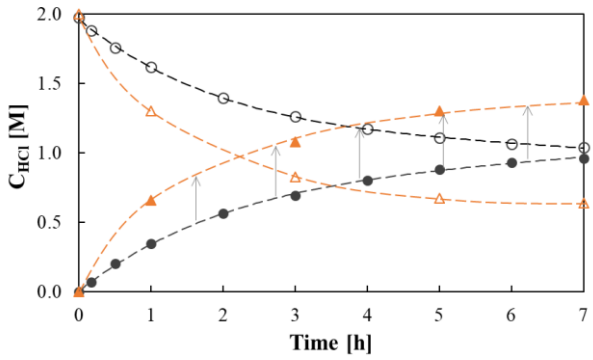

Figure 2-7 Time variation of HCl concentration in the diffusate (solid symbols) and retentate (empty symbols). Initial Fe concentrations in retentate: 0 g/l (○) and 100 g/l (△). Initial acid concentration: 2M. Flow rate: 48 ml/min. Retentate: HCl and $FeCl_2$ solution. Diffusate: deionized water.

In fact, the acid concentration in the diffusate is higher than the one in the retentate (a cross can be observed in the figure), differently from the case without iron salt, when the

maximum value of acid recovery is 50%. This is imputed to the salt effect, i.e. the addition of salt with the same anion of the acid causes an additional driving force for the diffusion of chlorides [48], [51], [101]. Thus, in order to establish the electroneutrality of the system, higher diffusion of protons occurs.

Moreover, it was observed that the HCl recovery increases by increasing $FeCl_2$ concentration, keeping the initial HCl concentration at a constant value (2 M). Of course, even though the acid permeation increases, also the Fe leakage through the membrane increases, causing a loss of membrane efficiency in co-ions rejection. The two performance parameters, acid recovery and iron leakage, increase from 50 to 75% and 7%, respectively, by increasing initial Fe ions concentration from 50 to 150 g/l, as shown in Figure 2-8, which results in an acid recovery efficiency of 150%.

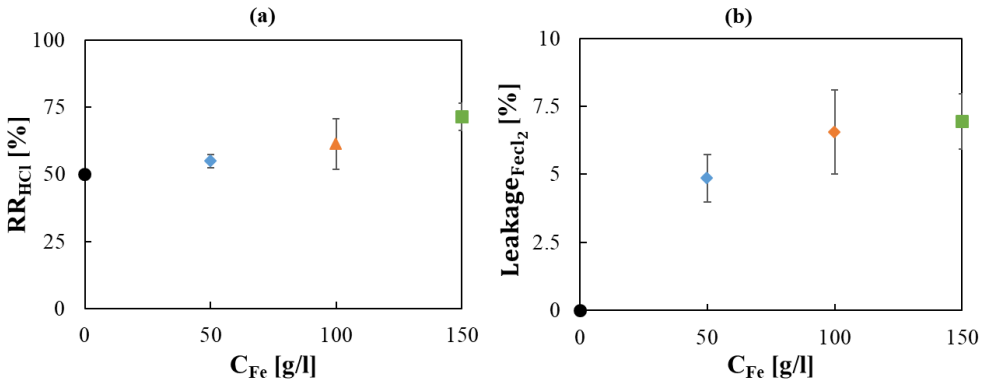

Figure 2-8 (a) HCl Recovery Ratio and (b) $FeCl_2$ leakage percentage vs. initial Fe concentration in the retentate: 0 (●), 50 (♦), 100 (▲) and 150 (■) g/l. Initial acid concentration: 2M. Flow rate: 48 ml/min. Retentate: HCl and $FeCl_2$ solution. Diffusate: deionized water.

Concerning the water flux, diffusate volume profiles are reported in Figure 2-9. As shown, the drag flux initially prevails, and then a net water flux from the diffusate to the retentate was observed, thus indicating an overall prevalent osmotic flux. A critical time, t*, can be identified when drag and osmotic fluxes are equivalent. As expected, t* decreases when increasing $FeCl_2$ concentration, due to the stronger effect of salts in determining the osmotic pressure increase in the retentate.

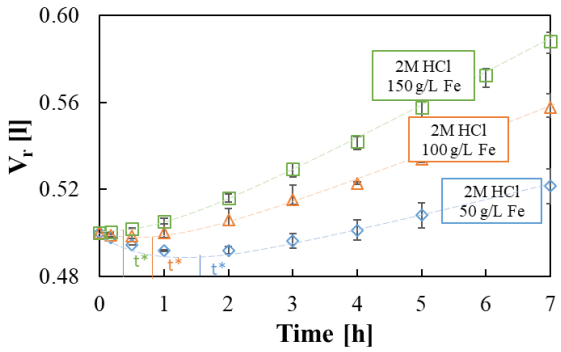

Figure 2-9 Retentate volume vs. time. Initial Fe concentrations: 50 (◊), 100 (△) and 150 (□) g/l. Initial acid concentration: 2M. Flow rate: 48 ml/min. Retentate: HCl and $FeCl_2$ solution. Diffusate: deionized water.

2.3.3 *Characterization of Zn transport behaviour*

Likewise, experimental campaign with HCl and Zn was carried out through two different sets of tests in the batch experimental set-up. In the first one, an equal acid concentration of 0.1M in the retentate and diffusate channels was used, while Zn ions were added in the retentate solution in two concentrations, 10 and 20 g/l, in order to isolate the behaviour of zinc transport, from the retentate to the diffusate, across the membrane. Conversely, in the second set, HCl 2 M and different Zn ions concentrations (5, 10 and 20 g/l of Zn^{2+} ions) in the retentate and deionized water as inlet diffusate stream were used. The main outcome obtained from the comparison between these experiments is a strong influence of HCl concentration on Zn membrane permeability. As reported in Figure 2-10(a), Zn concentration increase is expressed in Zn leakage growth through the membrane from 7 to 11%, when HCl concentration is comparable in the two compartments, as clearly the Zn transport driving force increases with concentration. Higher leakages and a counter trend were observed when feed acid concentration is 2 M, as a leakage reduction from 41 to 34% is reported. This can be explained considering that the common Cl^- ion from the acid molecule in solution promotes zinc tendency to form negatively charged chloro-complexes, which are more permeable through the anionic membrane, hence explaining the higher leakage values. Our results are in agreement with those published by other authors [59], where the transport properties of a Neosepta- AFN anion-exchange membrane in contact with aqueous solutions containing zinc chloride at different acid and zinc concentrations were investigated.

Following the same reasoning, Zn leakage decreasing trend with metal concentration increase is due to the reduced relative possibility of chloro-complexes formation, since the initial acid concentration is invariable.

HCl recovery is influenced, consequentially, as demonstrated in Figure 2-10(b), showing how the acid recovery with zinc in solution is lower than the value documented without the zinc metal in solution, with an asymptotic tendency to a value slightly lower than 40 %.

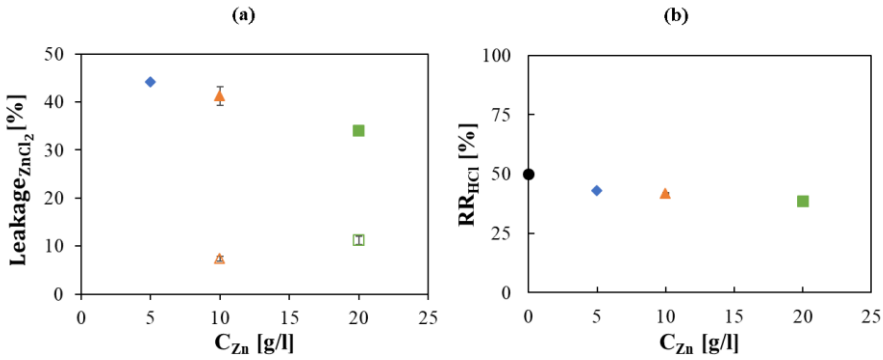

Figure 2-10 (a) $ZnCl_2$ leakage percentage and (b) HCl Recovery Ratio vs. initial Zn concentration in the retentate: 0 (●) 5 (♦), 10 (▲) and 20 g/l (■). Initial acid concentration: 0.1 M (empty symbols) and 2 M (solid symbols). Solutions flow rate fixed at 48 ml/min. Feed solution: HCl + $ZnCl_2$. Inlet diffusate:0.1 M HCl solution (empty symbols) and deionized water (solid symbol). Batch experimental-set-up.

Thus, an acid recovery efficiency η_{HCl} lower than 100% was observed for all the tests, contrarily to the case of HCl-$FeCl_2$ mixture [96] as presented in the previous paragraph and published in my work [106]. Indeed, Luo et al. [102] demonstrated that the Cl^- permeability coefficient for the HCl-$ZnCl_2$ system is the lowest among all the other investigated systems, which is in agreement with the above finding.

Figure 2-11 shows the volume variation in the feed tank against the test duration, which is due to the net water flux through the membrane.

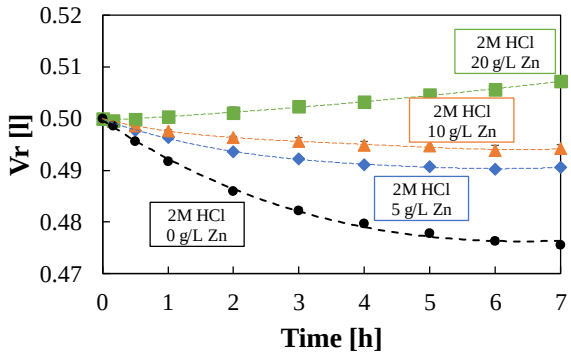

Figure 2-11 Trend over time of the retentate tank volume. Initial Zn conc.: 0 (●) 5 (♦), 10 (▲) and 20 g/l (■). Initial HCl concentration: 2 M. Solutions flow rate fixed at 48 ml/min. Feed solution: HCl + $ZnCl_2$. Inlet diffusate: deionized water. Batch experimental-set-up.

Concentration difference between the two channels generates an osmotic pressure resulting in water passage from the diluted to the concentrated compartment. However, an opposite water flux is realized as result of the water molecules dragging for hydration of the acid and metals molecules.

A reversal trend within the examined concentration range is observed: the feed volume is reduced over the time at lower zinc concentrations (0, 5 and 10 g/l), resulting in a prevailing drag flux, whereas an opposite behavior characterizes the volume variation at the higher concentration (20 g/l), where the osmotic pressure is enhanced due to the higher salt concentration difference between the feed and the retentate compartment.

2.3.4 *HCl, Fe and Zn test: mutual effects*

The combined effects of the main ions present in a pickling solution were considered in order to better predict the behavior in a real environment. Artificial solutions with Fe, Zn and HCl in the range of typical industrial pickling solutions were prepared and tested in laboratory. In this respect, four different tests were carried out by changing the concentration of a single metal, alternatively, and keeping the HCl concentration to 2 M. In particular, the iron concentration was varied from 100 to 150 g/l, while the zinc concentration from 5 to 10 g/l.

Experimental results for the test with initial Fe and Zn concentrations of 100 and 10 g/l, respectively, were considered as reference case to describe and characterize all the phenomena

involved in HCl, Fe and Zn mixtures in comparison with the solutions of HCl coupled with a single salt. Concentration profiles for HCl, Fe and Zn are reported versus time in Figure 2-12.

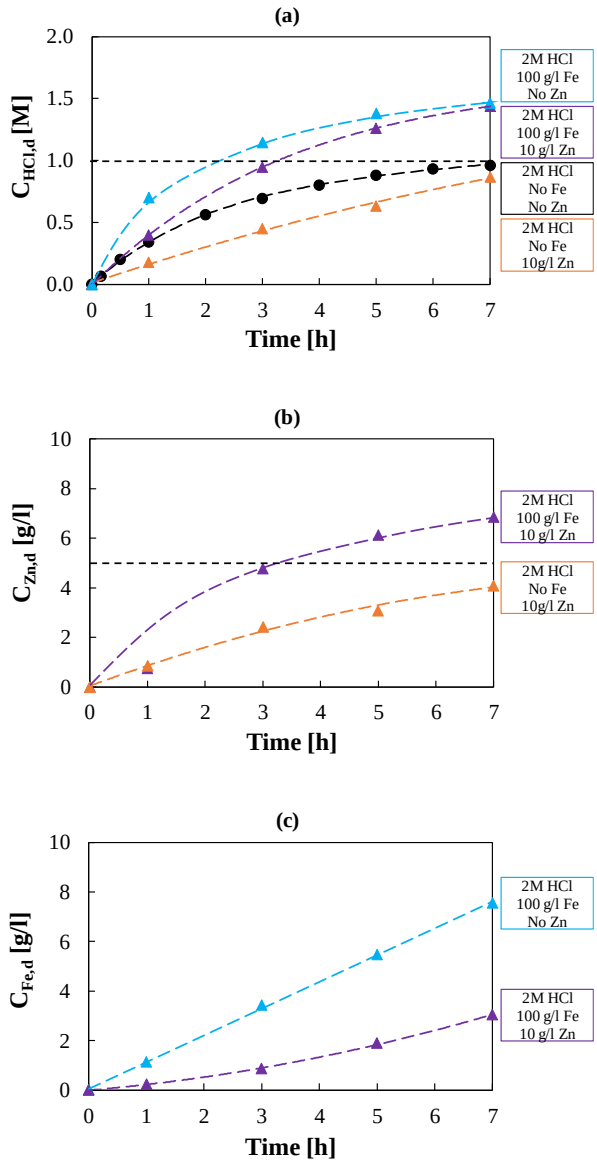

Figure 2-12 Temporal trend of HCl concentration (a), Zinc concentration (b) and Iron concentration (c) in the diffusate. Initial Zn concentrations: 0 (●,▲) and 10 (▲,▲) g/l. Initial Fe conc.: 0 (●,▲); 100 (▲,▲) g/l. Initial acid conc.: 2 M. Solutions flow rate fixed at 48 ml/min. Feed solution: HCl + $FeCl_2$ + $ZnCl_2$. Inlet diffusate: deionized water. Batch experimental-set-up.

As reported in Figure 2-12 (a), HCl flux was reduced by the presence of Zn caused by the competitive flux of the negative Zinc-chloro complexes, as already mentioned. Nevertheless, in the tests with Fe, the considerable amount of iron chlorides in solution causes a supplementary driving force for the diffusion of acid molecules (salt effect), resulting in acid recovery efficiencies over 100% and, in more detail, 116% and 125% for the test with the three components and the HCl+Fe test, respectively. This result shows the crucial behavior of iron salt to achieve high acid recoveries. The effect of iron chloride on Zn permeation can be reasonably expected: it supplies additional chlorides ions for the zinc chloro-complexes formation, resulting in higher flux through the membrane. Indeed, the zinc concentration in the diffusate is much higher when iron is also present in the feed solution (Figure 2-12 (b)).

On the other side, the leakage of iron through the membrane undergoes an important decrease due to the competitive passage of Zn, as shown in Figure 2-12 (c).

2.3.5 *Long scale DD*

Similar considerations can be derived for tests run with the continuous dialyzer. Continuous operation tests were performed with different feed composition in order to validate the reproducibility of all the effects described for the batch tests. In Table 2-3 all the test performed with the continuous dialyzer are reported.

Results obtained are in agreement with previously presented effects.

Table 2-3. Summary of tests performed with the continuous dialyzer. Flow rate refers to both diffusate and dialysate. Concentration values reported indicate the initial feed concentration for the different species. Diffusate solution consists of deionized water.

№ test identification	№ of repetitions	Flow rate ml/min	$C_{HCl,f}$ g/l	$C_{Fe,f}$ g/l	$C_{Zn,f}$ g/l
1	1	48	73	-	-
2	3		100	-	-
3	1		100	117	-
4	3		100	117	8

Worth noting that for better assessing results reliability, the tests n. 2 and 4 were repeated 3 times and the experimental error has been estimated and reported in Table 2-4.

Table 2-4 reports the value of the main performance parameters for all the continuous operation tests.

Table 2-4 Acid recovery and salt leakages for continuous operation tests. Values between brackets indicate the standard deviation.

№ test identification	RR_{HCl} (%)	$Leakage_{FeCl_2}$(%)	$Leakage_{ZnCl_2}$(%)
1	76	-	-
2	80 (± 1.8%)	-	-
3	87	35	-
4	79 (± 6.0%)	30 (± 7.8%)	60 (± 7.7%)

The test n.4, with 100 g/l HCl, 117 g/l of Fe and 8 g/l of Zn in the feed stream and deionized water as diffusate stream, the most relevant one as it covers all phenomena under investigation, is commented in details. The particular composition chosen for the feed solution is the designed operating composition at which the pickling bath would efficiently work in view of the continuous regeneration.

Concerning the acid recovery, despite the reduction of acid flux due to the competitive presence of zinc, the acid recovery settles around a relatively high value of 79%. A similar acid recovery was reported in Oh et al. [49], although in their study the investigated iron and zinc concentration range was considerably lower (5-30 g/l and 2-3 g/l, respectively), and the acid concentration higher (up to 180 g/l). This confirms the crucial importance of the iron ions in the recovery efficiency, as a comparable acid recovery rate was gained at lower HCl and higher Zn concentrations. The iron leakage through the membrane (about 30%) is slightly lower than the tests n.3 (with only HCl and $FeCl_2$), but much lower compared to the zinc one (60%). However, it reaches significantly higher values than in batch operations, likely due to the higher residence time of solutions in feed and diffusate compartments. The membrane, as expected, is highly permeable to zinc. The high initial concentration in HCl and $FeCl_2$ is expressed in high concentration of Cl^- ions, which are available for the zinc chloro-complex formation. However, the initial amount of zinc is much lower than the iron one, thus the concentration in the diffusate stream can be acceptable in the view of reusing it as recovered pickling solution. Indeed, the concentration of iron in the diffusate stream reaches values up

to 65 g/l while the zinc concentration is about 9 g/l. Concentration values for the test n.4 are reported in the next section (see Figure 2-21).

2.4 **Multi-Metals mathematical model**

This section describes the semi-empirical mathematical model for the *DD* process developed, validated and used in this PhD thesis. The model is able to to simulate the Diffusion Dialysis process under steady state and transitory functioning when feeding acid solutions with multi-metal ions mixtures. The DD process model, implemented in Excel® describes all the main phenomena involved in the process.

The DD model has a 1-dimensional distributed parameters spatial discretization along the channel length dimension with steady-state spatial differential mass balance equations, thus providing information on how concentrations vary along the channel and allowing the simulation of co- and counter-current system configurations (section 2.4.1).

The outputs of the DD model, namely concentrations and flow rates of both streams, are used as inputs in a dynamic model for the entire test-rig. The dynamic model consists of time-differential equations with a time discretization in order to simulate the time-dependent variation of ions concentrations and volumes in the solutions buffers, when the system is operated in batch (section 2.4.2).

Overall, the model can be considered with a 2D structure, 1 spatial and 1 time parameters distribution.

An algorithm for the numerical implementation of the spatial-time dependent model is reported, showing how the two different model sections are linked together.

The model has been adapted also to simulate the larger DD unit, by wider discretization along the channel length and accounting for the *n* number of feed/diffusate channels in one unit.

2.4.1 *1-dimensional spatial differential model equations*

Figure 2-13 shows the sketch of a counter-current module of length z_{ch} and membrane area A_m.

Since the concentration of the i-component in I is higher than in II, a mass transport from I to II occurs. Thus, the concentration of the i-component in the retentate side decreases and, conversely, in the diffusate side it increases along the flow direction.

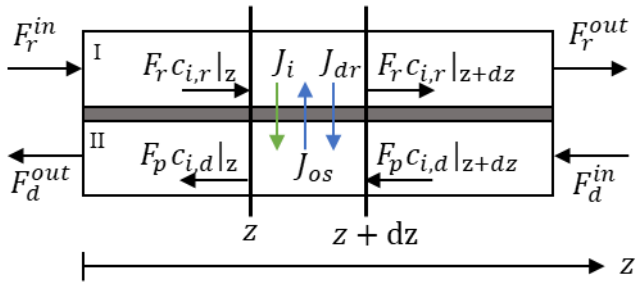

Figure 2-13 Schematic representation of the discretized domain of the DD unit, indicating the main variables.

Assuming steady-state conditions and considering diffusion and convection mass transport, the variation of concentration along z in the two channels can be derived from the mass balance on the differential volume between *z* and *z+dz* (only the equations for the retentate are reported to not be repetitive):

$$F_r c_{i_r}\big|_z = F_r c_{i_r}\big|_{z+dz} + J_i dA_m \qquad 2\text{-}7$$

$$dA_m = dz W_{ch} \qquad 2\text{-}8$$

$$\frac{dF_r c_{i_r}}{dz} = -J_i W_{ch} \qquad 2\text{-}9$$

$$\frac{dF_r}{dz} = \sum_i \frac{dF_r c_{i_r}}{dz} \frac{MM_i}{\rho_r} \qquad 2\text{-}10$$

where c_{i_r} is the bulk concentration of the *i*-component in the retentate side; F_r is the volumetric flow rate [l/s] in the retentate channel; J_i is the flux of the *i*-component through the membrane; dA_m is the differential membrane area; W_{ch} is the channel width; MM_i and ρ_r are molecular weight and density of the retentate solution, respectively.

The boundary conditions for the two feeds are:

$$z = 0 \qquad c_{i,r} = c_{i,r}^{in} \qquad 2\text{-}11$$

$$z = Z_{ch} \qquad c_{i,d} = c_{i,d}^{in} \qquad 2\text{-}12$$

The flux of the i-component is controlled by resistances in series i.e. from the bulk of retentate to the membrane interface (Eq. 2-13), across the membrane (Eq. 2-14) and from the membrane interface at the diffusate side to the bulk of the diffusate (Eq. 2-15):

$$J_i = k_{i,r}\left(c_{i,r} - c_{i,r}^{int}\right) \qquad 2\text{-}13$$

$$J_i = p_{i,m}\left(c_{i_r}^{m} - c_{i_d}^{m}\right) \qquad 2\text{-}14$$

$$J_i = k_{i,d}\left(c_{i,d}^{int} - c_{i,d}\right) \qquad 2\text{-}15$$

where $k_{i,r}$ and $k_{i,d}$ are the mass transport coefficients for the *i*-component in retentate and diffusate channels, respectively; $c_{i,r}$ and $c_{i,d}$ are the bulk concentrations in the retentate and diffusate solutions; $p_{i,m}$ is the membrane permeability of the *i*-component through the membrane; $c_{i_r}^{m}$ and $c_{i_d}^{m}$ are the retentate and diffusate membrane concentrations. Figure 2-14 shows the typical concentration profiles in the membrane and in the liquid films.

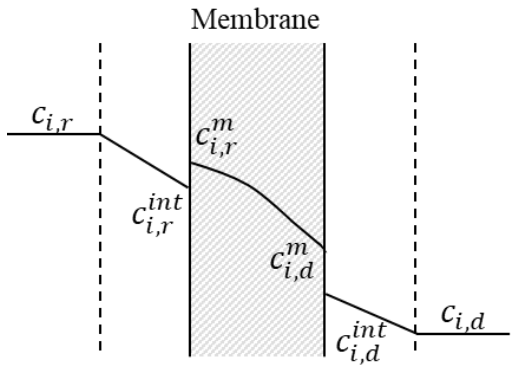

Figure 2-14 Concentration profiles in the membrane and liquid films.

Considering that between the concentrations at the interface and in the membrane there is an equilibrium relationship such as:

$$c_{i,r;d}^{int} = a c_{i,r;d}^{m} \quad 2\text{-}16$$

where $c_{i,r}^{int}$ and $c_{i,d}^{int}$ are the solution concentrations at the retentate and diffusate membrane interface, respectively; a is the absorption coefficient. It is possible to explain the two concentrations in the membrane in functions of the respective concentrations on the solution side. Thus, a single equation transport can be derived (Eq. 2-17), where an overall mass transfer coefficient of the i-component (U_i) can be used (Eq. 2-18) to express the flux as function of the bulk concentration.

$$J_i = U_i\left(c_{i,r} - c_{i,d}\right) \quad 2\text{-}17$$

$$U_i = \left(\frac{1}{k_{i,r}} + \frac{1}{P_i} + \frac{1}{k_{i,d}}\right)^{-1} \quad 2\text{-}18$$

The permeability coefficient (P_i) takes into account the absorption coefficient and the membrane permeability itself.

To determine the mass transport coefficients, correlation coming from CFD simulations designed for the Deukum woven spacer was used [107]. In particular, a Sherwood number in a laminar regime, in forced convection and for planar configuration was derived as:

$$Sh_r = \left(-1.48110^{-7} {Re_r}^5 + 3.73910^{-5} {Re_r}^4 - 0.003253 {Re_r}^3 + 0.1118 {Re_r}^2 + 0.1348 Re_r + 6.9536\right)\left(\frac{Sc_r}{600}\right)^{0.5} \quad 2\text{-}19$$

where Sh_r, Re_r and Sc_r are dimensionless numbers:

$$Sh_r = \frac{k_{i_r} D_{eq}}{\mathcal{D}} \qquad Re_r = \frac{\rho_r v_r D_{eq}}{\mu_r} \qquad Sc_r = \frac{\mu_r}{\rho_r \mathcal{D}_i} \quad 2\text{-}20$$

where v_r is the fluid linear velocity in the retentate channel, μ_r is dynamic viscosity of the fluid in the retentate channels, $\mathcal{D}_i$ is the mass diffusivity of the i-component and D_{eq} is the hydraulic diameter defined as:

$$D_{eq} = \frac{4t_{ch}w_{ch}}{2(t_{ch} + w_{ch})} \quad 2\text{-}21$$

where t_{ch} is channel thickness.

The physical and transport properties μ, $\mathcal{D}_i$ of the solutions were calculated using the *Aspen Plus*® software at the atmospheric temperature and pressure values equal to P = 1 atm and T = 25 ° C. While for the density calculation, Laliberté et al. equations [108] were implemented in the model.

The laminar hypothesis is always adhered as maximum Re values in both the DD stacks are below 30 and the Re transition value for membrane process in the presence of spacers is around 300/400 evaluated as follows [109]:

$$Re_{transition} = \frac{v\ \varepsilon_{spacer}\ 2t_{ch}}{\mu} \quad 2\text{-}22$$

where ε_{spacer} is the spacer porosity.

2.4.1.1 Acid and salt fluxes through the IEMs

The flux of HCl through the membrane is affected by the presence of $FeCl_2$ and $ZnCl_2$in solution. As reported by some authors [96], [101], the total acid flux (J_{HCl}^{tot}) can be considered as the sum of different terms, one dependent on the real acid concentration difference and the other ones related to the presence of metal salts. In particular, the iron in solution provides additional chlorides for the acid diffusion, thus a positive contribution appears. As concerns the zinc ion in solution, a detrimental effect on the acid flux is characterized by subtracting a quote to the acid flux (Eq. 2-23):

$$J_{HCl}^{tot} = U_{HCl}\left(c_{HCl,r} - c_{HCl,d}\right) + U_{HCl}^{FeCl_2}\left(c_{FeCl_2,r} - c_{FeCl_2,d}\right) - U_{HCl}^{ZnCl_2}\left(c_{ZnCl_2,r} - c_{ZnCl_2,d}\right) \quad 2\text{-}23$$

where J_{HCl}^{tot} is the hydrochloric acid flux through the membrane, U_{HCl} is the acid mass coefficient when only acid is present in solution, $U_{HCl}^{FeCl_2}$ and $U_{HCl}^{ZnCl_2}$ are the secondary overall mass transfer coefficients related to the presence of iron and zinc salts, respectively, and

$c_{i,r}$ and $c_{i,d}$ are the concentrations of acid and metal salts components in the retentate and diffusate solutions, respectively.

Likewise, the acid and iron salt enhances the zinc passage for the Cl^- common ion, thus aside from the zinc permeability (P_{ZnCl_2}) which counts for the zinc mass transfer coefficient (U_{ZnCl_2}), the further contributions to the Zn mass diffusion through the membranes ($U_{ZnCl_2}^{HCl}$) and ($U_{ZnCl_2}^{FeCl_2}$) have been added:

$$J_{ZnCl_2}^{tot} = U_{ZnCl_2}\left(c_{ZnCl_2,r} - c_{ZnCl_2,d}\right) + U_{ZnCl_2}^{HCl}\left(c_{HCl,r} - c_{HCl,d}\right) + U_{ZnCl_2}^{FeCl_2}\left(c_{FeCl_2,r} - c_{FeCl_2,d}\right) \quad 2\text{-}24$$

On the other hand, the iron flux is competitively reduced by the zinc flux when a second salt with common anion and with a higher tendency to form negative complexes is present in solution, and the rate of this reduction was experimentally estimated to be of 30% of the iron flux itself. Thus it is possible to derive the flux of $FeCl_2$ as a part of the Fe mass coefficient (U_{FeCl_2}):

$$J_{FeCl_2}^{tot} = 0.7U_{FeCl_2}\left(c_{FeCl_2,r} - c_{FeCl_2,d}\right) \quad 2\text{-}25$$

2.4.1.2 Water flux and ions speciation

Transport of water through the membrane also affects process performances. Water flux was considered in the model as the sum of the osmotic and drag fluxes, where the osmotic flux depends on the osmotic pressure driving force, while the drag flux is related to the total water molecules associated to ions transport (Eqs. 2-26,2-27,2-28).

$$J_w = J_{os} + J_{dr} \quad 2\text{-}26$$

$$J_{os} = P_{os}\pi \quad 2\text{-}27$$

$$J_{dr} = \sum_i \beta_i J_i \qquad 2\text{-}28$$

where J_w, J_{os} and J_{dr} are the total, osmotic and drag water fluxes, respectively, P_{os} is the osmotic permeability of the membrane and β_i is the hydration number of species *i*. Hydration numbers equal to 1 for protons, 6 for chlorides and 6 for the iron cations were considered [110].

Osmotic pressure evaluation was calculated by including in the model structure the Pitzer model equations. As a result, the osmotic pressure [111] has been evaluated as reported below:

$$\pi = \frac{RTM_{solv}\phi}{1000 v_{solv}} \cdot \sum (im)_i \qquad 2\text{-}29$$

where R is the ideal gases constant of, M_{Solv} is the molecular weight of the solvent, v_{solv} is the solvent molar volume, i is the Van´t Hoff coefficient of the i-component, m_i is the molal concentration of the i-component and π is the osmotic pressure. The osmotic coefficient (ϕ) was calculated according to Pitzer equations [112]. Hydrochloric acid, iron and zinc chlorides Pitzer parameters were extrapolated from the literature [113], [114].

In order to properly implement the above Eq. 2-29, dissociation reaction equilibria were studied. Dissociation reactions equilibria for the HCl+ $ZnCl_2$ and HCl+ $FeCl_2$ systems are reported in Table 2-5, where also the equilibrium dissociation constants are shown (source: PHREEQC software, https://www.usgs.gov/software/phreeqc-version-3).

Table 2-5 Dissociation reactions for the HCl+ $ZnCl_2$ and HCl+ $FeCl_2$ systems and relative equilibrium constants (source: PHREEQC software).

Dissociation reaction	$-\log K_{eq}$	**Equilibrium constant** K_{eq}
$ZnCl^+ \leftrightarrow Zn^{2+} + Cl^-$	0.43	$K_{eq,1} = 0.37$
$ZnCl_2 \leftrightarrow Zn^{2+} + 2Cl^-$	0.45	$K_{eq,2} = 0.35$
$ZnCl_3^- \leftrightarrow Zn^{2+} + 3Cl^-$	0.5	$K_{eq,3} = 0.32$
$ZnCl_4^{2-} \leftrightarrow Zn^{2+} + 4Cl^-$	0.2	$K_{eq,4} = 0.63$
$FeCl^+ \leftrightarrow Fe^{2+} + Cl^-$	0.43	$K_{eq,1} = 0.37$

Different species concentration for the HCl+ $ZnCl_2$ system were assessed from Eqs. 2-30 to 2-36:

$$[ZnCl^+] = \frac{[Zn^{2+}][Cl^-]}{K_{eq,1}} \frac{\Upsilon_{Zn^{2+}}\Upsilon_{Cl^-}}{\Upsilon_{ZnCl^+}} \quad 2\text{-}30$$

$$[ZnCl_2] = \frac{[Zn^{2+}][Cl^-]^2}{K_{eq,2}} \frac{\Upsilon_{Zn^{2+}}\Upsilon_{Cl^-}^2}{\Upsilon_{ZnCl_2}} \quad 2\text{-}31$$

$$[ZnCl_3^-] = \frac{[Zn^{2+}][Cl^-]^3}{K_{eq,3}} \frac{\Upsilon_{Zn^{2+}}\Upsilon_{Cl^-}^3}{\Upsilon_{ZnCl_3^-}} \quad 2\text{-}32$$

$$[ZnCl_4^{2-}] = \frac{[Zn^{2+}][Cl^-]^4}{K_{eq,4}} \frac{\Upsilon_{Zn^{2+}}\Upsilon_{Cl^-}^4}{\Upsilon_{ZnCl_4^{2-}}} \quad 2\text{-}33$$

$$[Zn]_{tot} = [ZnCl^+] + [ZnCl_2] + [ZnCl_3^-] + [ZnCl_4^{2-}] + [Zn^{2+}] \quad 2\text{-}34$$

$$[Zn^{2+}] = \frac{[Zn]_{tot}}{1 + [Cl^-]\Upsilon_{Zn^{2+}}\Upsilon_{Cl^-}(\frac{1}{K_{eq,1}}\frac{1}{\Upsilon_{ZnCl^+}} + \frac{[Cl^-]}{K_{eq,2}}\frac{\Upsilon_{Cl^-}}{\Upsilon_{ZnCl_2}} + \frac{[Cl^-]^2}{K_{eq,3}}\frac{\Upsilon_{Cl^-}^2}{\Upsilon_{ZnCl_3^-}} + \frac{[Cl^-]^3}{K_{eq,4}}\frac{\Upsilon_{Cl^-}^3}{\Upsilon_{ZnCl_4^{2-}}})} \quad 2\text{-}35$$

$$[Cl^-] = [H^+] + 2[Zn^{2+}] + [ZnCl^+] - [ZnCl_3^-] - 2[ZnCl_4^-] \quad 2\text{-}36$$

For the HCl+$FeCl_2$ system, Eqs. from 2-37 to 2-40 were considered for the dissociation species concentrations evaluation:

$$[FeCl^+] = \frac{[Fe^{2+}][Cl^-]}{K_{eq,1}} \frac{\Upsilon_{Fe^{2+}}\Upsilon_{Cl^-}}{\Upsilon_{FeCl^+}} \quad 2\text{-}37$$

$$[Fe]_{tot} = [FeCl^+] + [Fe^{2+}] \quad 2\text{-}38$$

$$[Fe^{2+}] = \frac{[Fe]_{tot}}{1 + \frac{[Cl^-]}{K_{eq,1}}\frac{\Upsilon_{Fe^{2+}}\Upsilon_{Cl^-}}{\Upsilon_{FeCl^+}}} \quad 2\text{-}39$$

$$[Cl^-] = [H^+] + 2[Fe^{2+}] + [FeCl^+] \quad 2\text{-}40$$

The ions activity coefficients reported in Eqs. from 2-30 to 2-40 were evaluated from Davies equation [115] which gives the mean activity coefficient of an electrolyte that dissociates into ions having charges z_1 as a function of ionic strength I:

$$-\log \Upsilon_{\pm} = 0.5042 z_1^2 \left(\frac{\sqrt{I}}{1+\sqrt{I}} - 0.3I \right) \quad 2\text{-}41$$

Specifically, for the HCl+$ZnCl_2$ system 2-42 and 2-43 were considered, while for the HCl+$FeCl_2$ system Eqs. 2-44 and 2-45 are reported:

$$\Upsilon_{\pm} \simeq \Upsilon_{Cl^-} \simeq \Upsilon_{ZnCl^+} \simeq \Upsilon_{ZnCl_3^-} \quad 2\text{-}42$$

$$\Upsilon_{2^{\pm}} \simeq \Upsilon_{Zn^{2+}} \simeq \Upsilon_{ZnCl_4^{2-}} \quad 2\text{-}43$$

$$\Upsilon_{\pm} \simeq \Upsilon_{Cl^-} \simeq \Upsilon_{FeCl^+} \quad 2\text{-}44$$

$$\Upsilon_{2^{\pm}} \simeq \Upsilon_{Fe^{2+}} \quad 2\text{-}45$$

The dissociation % species is defined as the ratio between the concentration of the different species in solution and the total metal concentration.

$$dissociation\ \%_{species} = \frac{[species]}{[Metal]_{tot}} x100 \quad 2\text{-}46$$

It is thus possible to evaluate the dissociation factor by multiply the different dissociation % species by the number of discrete ions obtained from the dissociation reactions of $ZnCl_2$ or $FeCl_2$ that produce the particular species:

$$ZnCl_{2_{dissociation\ factor}} = \frac{3[Zn^{2+}] + 2[ZnCl^+] + [ZnCl_2] + [ZnCl_3^-] + [ZnCl_4^{2-}]}{[Zn]_{tot}} \quad 2\text{-}47$$

$$FeCl_{2_{dissociation\ factor}} = \frac{3[Fe^{2+}] + 2[FeCl^+]}{[Fe]_{tot}} \quad 2\text{-}48$$

In particular, at the pH of the experiments (typically, pH < 1), for single iron chlorides solutions, iron is present as a mixture of Fe^{2+} (30 %) and $FeCl^{+}$ (70 %), while for single zinc chlorides solutions, the salt is present as a mixture of Zn^{2+} (15%), $ZnCl^{+}$ (14%), $ZnCl_{2aq}$ (15%), $ZnCl_3^{-}$ (30%), $ZnCl_4^{2-}$ (26%). Therefore, over 50% of zinc is present as negatively charged complex, thus strengthening the argument of high zinc leakage through the membrane.

The hydrochloric acid, for its strong acidic strength, is totally dissociated in water solution. Corresponding to this, the Van´t Hoff coefficient for HCl was 2, for $FeCl_2$ was 2.3 and for $ZnCl_2$ was 1.6.

2.4.2 *Time-dependent model equations*

In order to simulate the time-dependent variations of concentrations and volumes of the two tanks in the batch operation mode, the model also includes a dynamic part consisting of time-differential equations for the volume and concentration of the feed tanks (see Figure 2-15):

$$\frac{d\rho_r V_r}{dt} = \rho_r^{in} F_r^{in,Dyn} - \rho_r^{out} F_r^{out,Dyn} \qquad 2\text{-}49$$

$$\frac{dV_r c_{i,r}^{tank}}{dt} = F_r^{in,Dyn} c_{i,r}^{in,Dyn} - F_r^{out,Dyn} c_{i,r}^{out,Dyn} \qquad 2\text{-}50$$

where $F_r^{in,Dyn}$ and $F_r^{out,Dyn}$represent the inlet/outlet volumetric flow rates in the retentate tank, equal to the outlet/inlet retentate stream in the DD unit, respectively. In the same way, $c_{i,r}^{in,Dyn}$and $c_{i,r}^{out,Dyn}$ are the inlet/outlet concentrations in the retentate tank, equal to the outlet/inlet concentrations retentate stream in the DD unit, respectively, while $c_{i,r}^{tank}$ is the concentration of the *i*-component in the retentate tank. In all cases, perfect mixing is assumed in the tanks, thus:

$$c_{i,r}^{out,Dyn} = c_{i,r}^{tank} \qquad 2\text{-}51$$

Volume and concentration variations in the diffusate tank are calculated from the closure of mass balance equations.

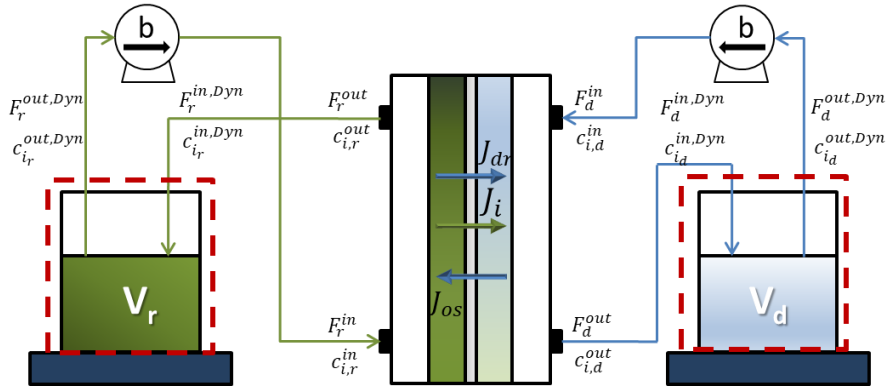

Figure 2-15 Schematics of the control volumes in the DD set-up for the dynamic section of the model.

2.4.3 *Numerical details*

As previously mentioned, the *DD* process model was implemented in *Excel*®, using the Euler's method to solve the mass balance equations. In this method, the numerical accuracy of the solution depends on the discretization length (Δz) and discretization time (Δt). Discretization length of 1 cm and discretization time of 50 s are small enough to get stable and accurate solutions. The overall concentration and volume profiles were determined by numerically implementing the model according to the algorithm shown in Figure 2-16.

Values of permeability were determined through a calibration procedure (presented in section 2.4.4) and are related to the acid concentration in the retentate solution.

The model has been adapted also to simulate the larger DD unit, by implemented only the first spatial dependency in steady-state operation and accounting for the *n* number of feed/diffusate channels in one unit. A wider discretization along the channel length (Δz=0.6 cm) has been considered.

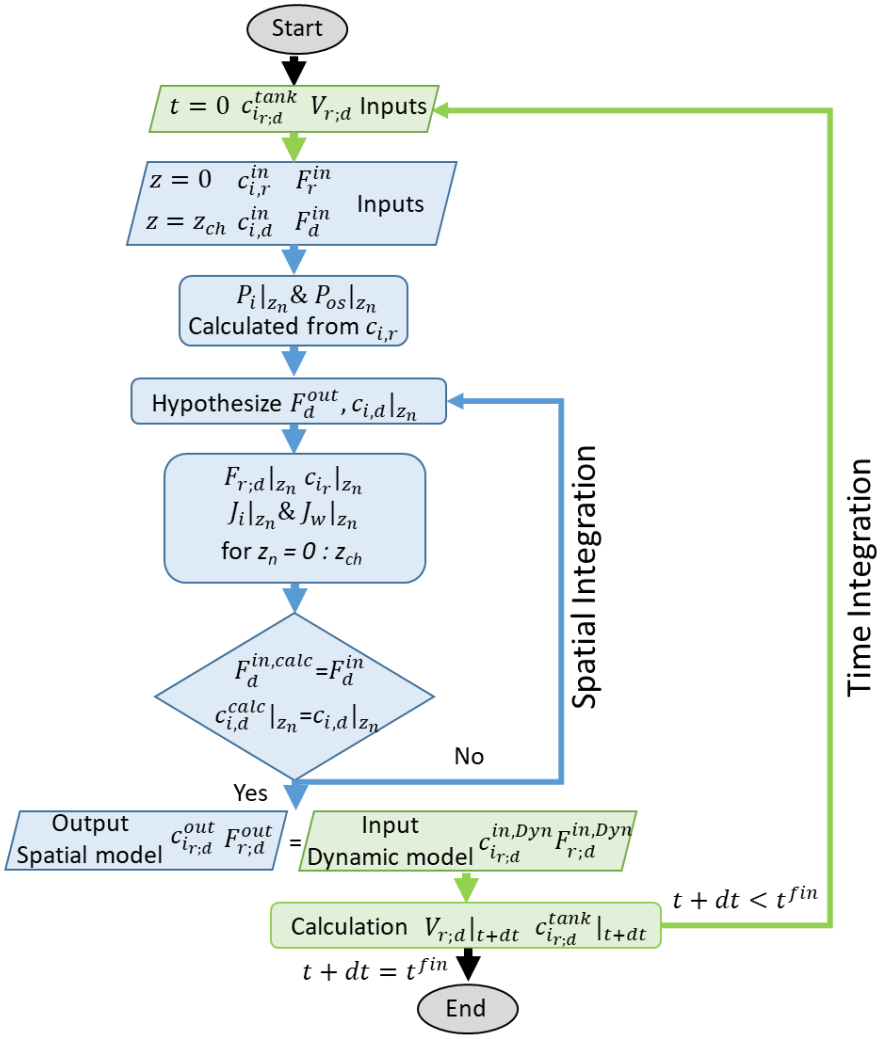

Figure 2-16 Algorithm for the numerical implementation of the spatial-time dependent in diffusion dialysis model.

2.4.4 *Model Calibration*

Calibration permeability values of the membrane with respect to the acid, salts and water diffusion have been related to the concentration of the acid and salts in the feed solution using experimental data.

Calibration procedure was carried out gradually, by considering at first hydrochloric acid solution, and adding one by one the metal salts.

As concern the HCl solution test, for each experiment a good fitting between experimental and model data was obtained by using linear correlations for the acid (P_{HCl}) and a quadratic correlation for the water (P_{os}) permeability as a function of the acid concentration in the retentate.

Therefore, all these trends were plotted in a graph (Figure 2-17) in order to obtain a unique correlation relating acid permeability values to the acid concentration in the retentate tank, as reported below:

$$P_{HCl} = 3.21 \cdot 10^{-7} c_{r,HCl}^3 - 1.93 \cdot 10^{-6} c_{r,HCl}^2 + 4.11 \cdot 10^{-6} c_{r,HCl} + 6.61 \cdot 10^{-7} \qquad 2\text{-}52$$

As previously mentioned in section 2.4.1.1, the diffusive permeability to the acid is strongly affected by the acid concentration.

In fact, as reported in Figure 2-17(a), it increases as HCl concentration increases in the whole range investigated.

In a similar way, osmotic permeability coefficients were obtained experimentally as a decreasing function of the acid concentration (Figure 2-17(b)) as:

$$P_{os} = 1.3 \cdot 10^{-7} c_{r,HCl}^2 - 9 \cdot 10^{-7} c_{r,HCl} + 8.1 \cdot 10^{-6} \qquad 2\text{-}53$$

Calibration of permeability coefficients was performed in order to consider also the presence of iron and zinc in solution, by identifying possible dependences with its concentration in the feed solution. In particular, all transport equations were re-adapted including correction terms, which account for the effect of co-ions present in solution promoting or hindering the passage of species as already phenomenological described in section 2.4.1.1.

Firstly, the model was applied to derive the Fe and Zn permeability (P_{FeCl_2} and P_{ZnCl_2}, respectively) through the membrane by considering the experimental data with HCl 0.1M in the two compartments. Then, the case of retentate solution composed by a mixture of HCl and $FeCl_2$ and HCl and $ZnCl_2$ were considered in order to find the mutual effect, as already described in Eq. 2-23.

$FeCl_2$ leakage permeability coefficient was calibrated by considering a constant value for each test. As shown in Figure 2-17(c), also $FeCl_2$ diffusive permeability increases as the salt concentration increases, though, as expected, permeability of the salt is 10 times lower than for the acid:

$$P_{FeCl_2} = 2.5 \cdot 10^{-8} c_{r,FeCl_2}^2 + 1.5 \cdot 10^{-7} c_{r,FeCl_2} + 3.9 \cdot 10^{-7} \quad 2\text{-}54$$

$$P_{ZnCl_2} = -2.7 \cdot 10^{-6} c_{r,ZnCl_2}^2 + 1.7 \cdot 10^{-6} c_{r,ZnCl_2} + 0.7 \cdot 10^{-8} \quad 2\text{-}55$$

In order to consider the salt effect, acid permeation in the presence of $FeCl_2$ was modelled. In this case, the $U_{HCl}^{FeCl_2}$ coefficient was also experimentally obtained, showing a linear dependence on the acid concentration:

$$U_{HCl}^{FeCl_2} = 2.0 \cdot 10^{-6} c_{r,HCl} + 3.5 \cdot 10^{-7} \quad 2\text{-}56$$

While the acid does not affect significantly the iron diffusion trough the membrane.

Differently, the additional zinc permeability related to the additional chloride provided from the hydrochloric acid ($U_{ZnCl_2}^{HCl}$) was calibrated. At the same time, the detrimental effect on the acid flux was characterized by a secondary correction factor($U_{HCl}^{ZnCl_2}$). In particular, the transport equations for HCl and Zn solutions are reported below:

$$U_{HCl}^{ZnCl_2} = 6.1 \cdot 10^{-5} c_{r,ZnCl_2}^2 - 8.5 \cdot 10^{-5} c_{r,ZnCl_2} + 2.8 \cdot 10^{-5} \quad 2\text{-}57$$

$$U_{ZnCl_2}^{HCl} = -1.7 \cdot 10^{-6} c_{r,ZnCl_2}^2 + 1.1 \cdot 10^{-6} c_{r,ZnCl_2} + 0.2 \cdot 10^{-7} \quad 2\text{-}58$$

where $U_{HCl}^{ZnCl_2}$ accounts for the HCl flux reduction related to the Zn presence; $U_{ZnCl_2}^{HCl}$ is the additional mass coefficient for the Zn passage due to the HCl concentration difference between the two compartments.

Although most trends shown in Figure 2-17 are almost linear, the choice of 2nd order correlations resulted in a more accurate fitting, thus being the final choice for the model.

The zinc diffusive permeability, as reported in Figure 2-17(d), increases as Zn concentration increases in the entire examined span. This value is 10 times lower than the acid permeability.

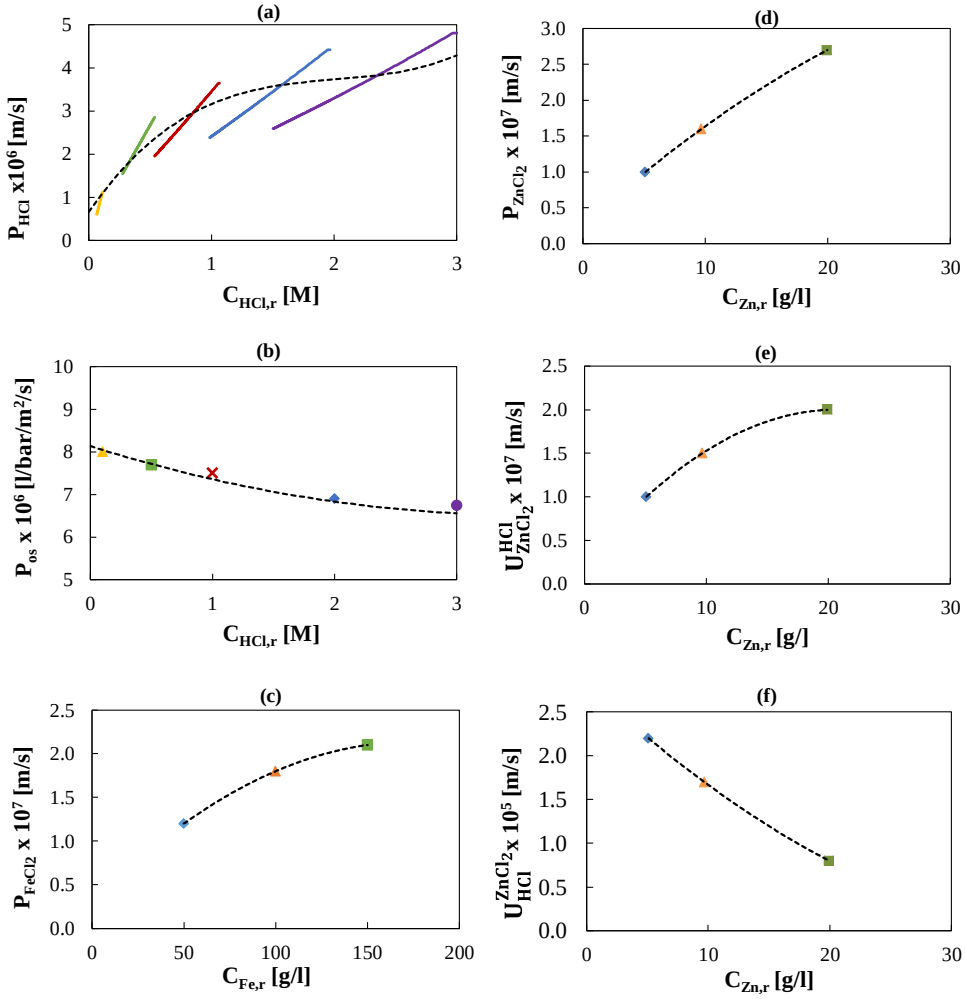

Figure 2-17 Linear correlations (continuous line), constant values and overall trend (dotted curve) of the acid diffusive permeability (a) and osmotic permeability (b) as a function of HCl concentration in the retentate; of the iron diffusive permeability as a function of Fe concentration in the retentate (c); of the zinc diffusive permeability (d), additional Zn mass coefficient (e) and additional HCl mass coefficient (f) as a function of Zn concentration in the retentate obtained from the model calibration.

Table 2-6 Comparison of diffusive permeability among different membranes.

Membrane AEM	Concentration Range	Operation Configuration	P_{HCl} ($10^{-6}\frac{m}{s}$)	P_{FeCl2} ($10^{-7}\frac{m}{s}$)	P_{ZnCl2} ($10^{-7}\frac{m}{s}$)	Ref
Fumasep FAD	0.1-3 M HCl 50-150 g/l Fe 5-20 g/l Zn	Batch recirculation/ Dialyzer Stack (3.1 mm/s)	1-4	1-2	1-2.7	This work
Fumasep FAD	0.2-2 M HCl	Two compartment stirred cells	3.7-13.4	-		[91]
Neosepta AFN	4 M HCl 5-30 g/l Fe 2-3 g/l Zn	Dialyzer Stack (0.8 mm/s)	2.1	0.14	5.7	[49]
DF-120	1.28 M HCl 12 g/l Fe	Two compartment stirred cells	3	1.4		[50]
PPO-SiO_2	1.28 M HCl 44g/l Fe	Two compartment stirred cells	1.5-3	0.7		[50]

2.4.5 *Model Validation*

The model was validated by comparison with all experimental trends observed. As examples, Figure 2-18 and Figure 2-19 report a comparison between predicted and experimental trends for some of the investigated cases.

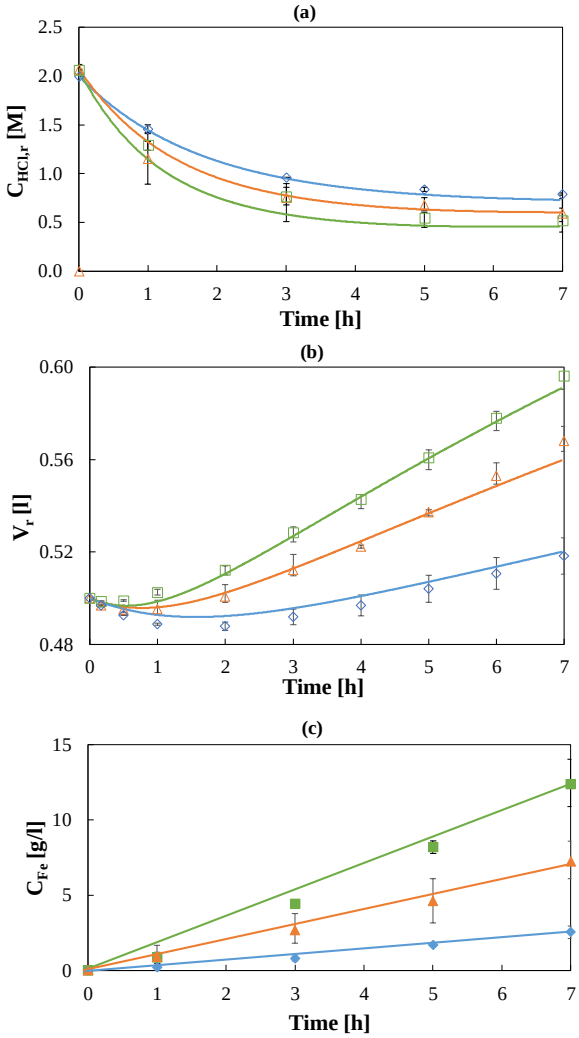

Figure 2-18 HCl concentration in retentate (a), retentate volume (b) and Fe concentration in diffusate (c) vs. time. Initial Fe concentrations: 50 (◊,♦), 100 (△, ▲) and 150 (□, ■) g/l. Initial acid concentrations: 2M. Flow rate: 48 ml/min. Retentate solution: deionized water, HCl, $FeCl_2$. Diffusate solution: deionized water. Theoretical curves (—) obtained by using the model.

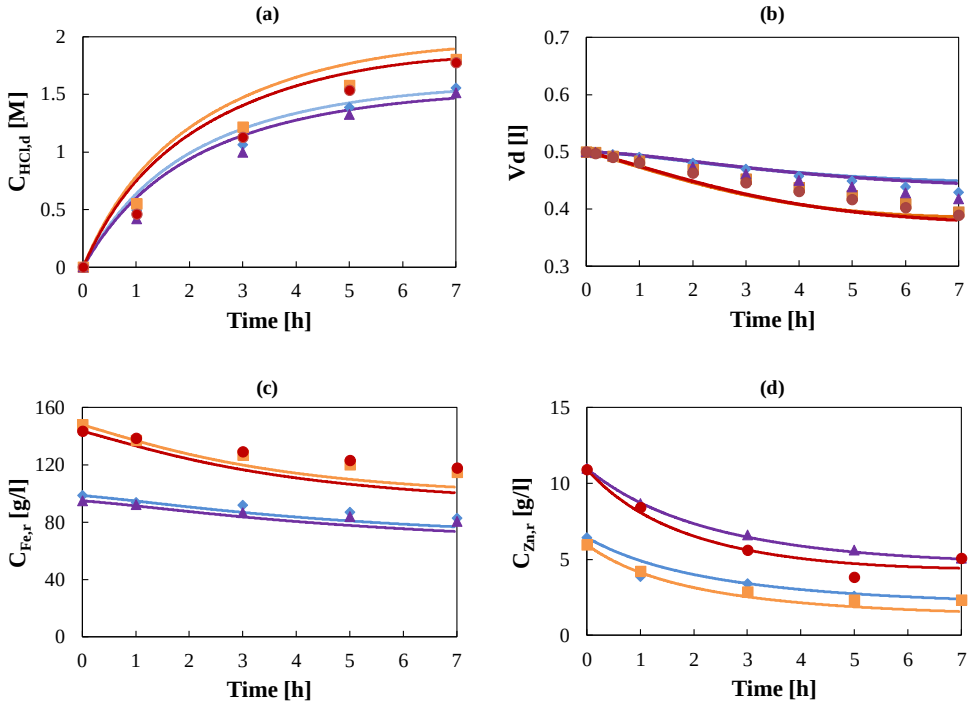

Figure 2-19 HCl concentration in diffusate (a), diffusate volume (b), Fe concentration in retentate (c) and Zn concentration in retentate (d) vs. time. Initial Zn concentrations: 5 (♦,■) and 10 (▲,●) g/l. Initial Fe concentrations: 100 (♦,▲) and 150 (■,●) g/l. Initial acid concentrations: 2 M. Flow rate: 48 ml/min. Feed: HCl, $FeCl_2$, $ZnCl_2$ solution. Diffusate IN: deionized water. Theoretical curves (—) obtained by using the model.

Instead, in Figure 2-20 a comparison of experimental data and model predictions is reported for all the investigated cases.

In all cases, a good agreement is shown between model and experiments.

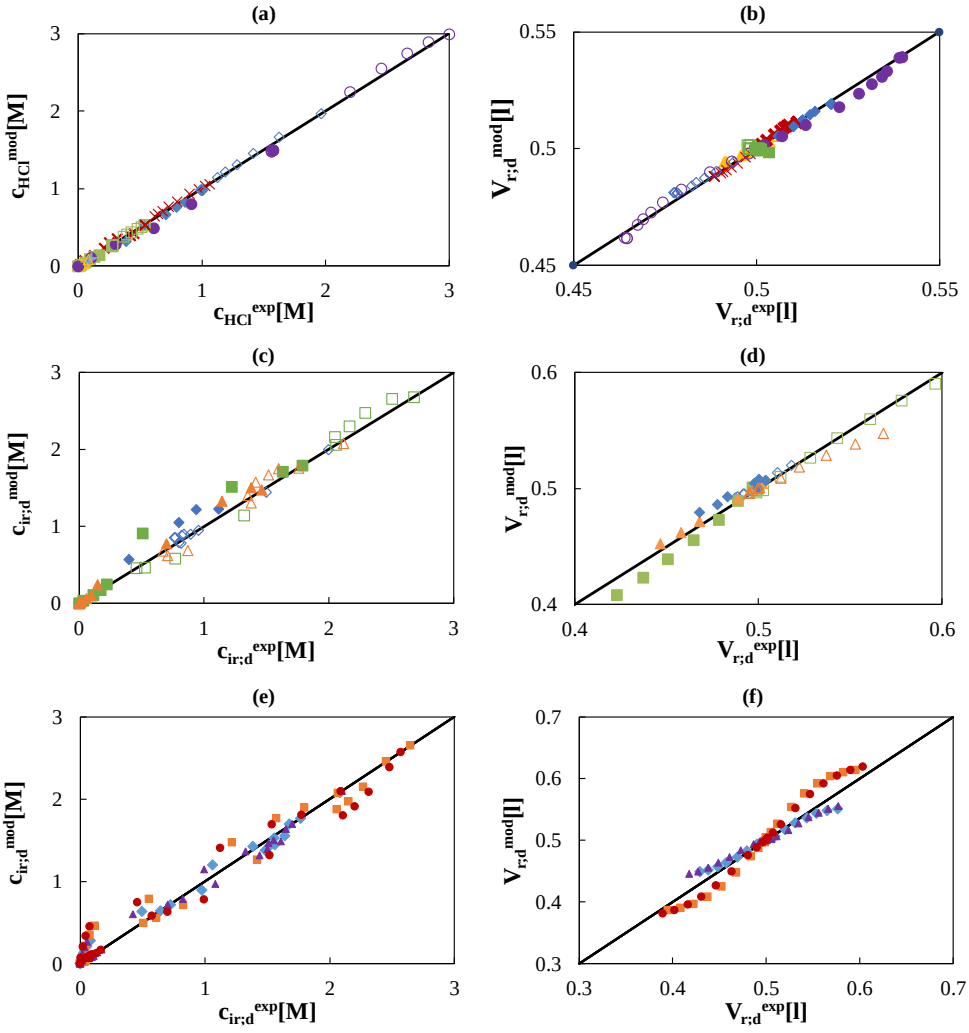

Figure 2-20 Parity plots of experimental (exp) and predicted (mod) values of concentration of species and tanks volumes in retentate and diffusate compartments. (a)&(b) tests with only HCl at 0.1M (▲), 0.5M (■), 1M (X), 2M (♦), 3M (●); (c)&(d) tests with initial HCl at 2M and Fe at 50 (♦), 100 (▲), 150 (■) g/l; (e)&(f) tests with initial HCl at 2 M and Zn at 5 (♦,■) and 10 (▲,●) g/l, and Fe at 100 (♦,▲) and 150 (■,●) g/l.

As a further validation of the proposed model, the correlations obtained were used to predict the operation of the large-scale unit. The predicted concentration and flow rates along the channel are shown in Figure 2-21, where they are compared with the inlet and outlet experimental measurements. Of interest, the acid diffusate concentration at the outlet of the unit is larger than the feed concentration thanks to the salt effect, though the osmotic flux,

reflecting in a reduction of the diffusate flow rate along the channel, restricts the RR below the 80%. Same behavior is observed for the Zn concentration profile, even though the initial low amount of the component let to have a low concentration in the recovered acid stream. A lower passage of iron is observed in agreement with the batch results. The discrepancy between the experimental data and the predicted values can be ascribed to the expected fluxes reduction when the net driven force approaches to values close to zero. The suggested correlations do not consider these phenomena and overestimate the fluxes in these ranges.

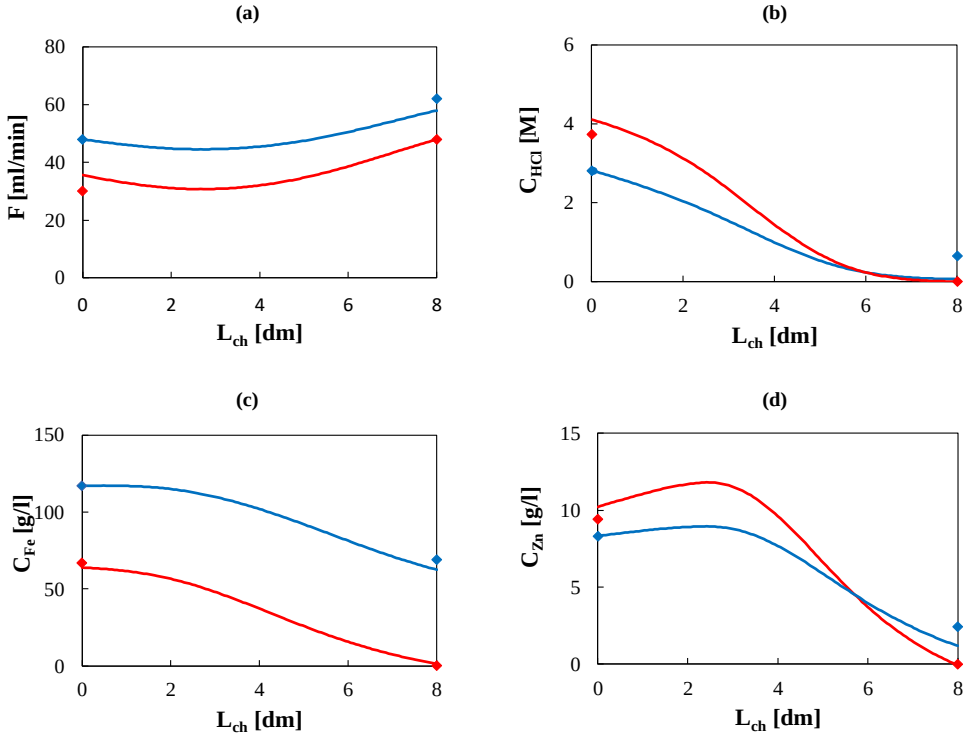

Figure 2-21 Flow rate (a), HCl concentration (b), Fe concentration (c) and Zn concentration (d) vs. channel length for retentate (blue) and diffusate (red) for the continuous test 4 named in Table 2-3. Theoretical curves (—) obtained by using the model. Experimental data (dots).

Finally, all the presented experimental data within the continuous configuration, previously reported in Table 2-4, are displayed against model prediction data in the form of parity plots in Figure 2-22.

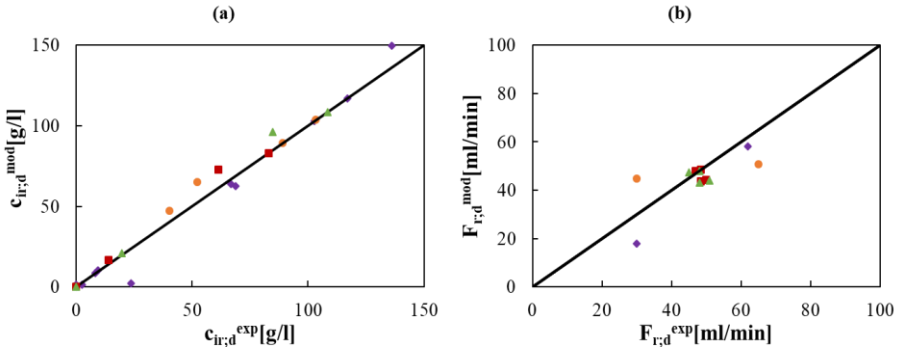

Figure 2-22 Parity plots of all experimental (exp) and predicted (mod) values of species concentration (a) and flow rates (b) in retentate and diffusate streams. Tests 1 (■) 2 (▲), 3 (●), and 4(♦), named in Table 2-3.

2.5 **Conclusions**

Hydrochloric acid recovery from highly concentrated iron and zinc chlorides solutions by diffusion dialysis (DD) was explored. Two different DD units (a laboratory- and a large-scale) were used for characterizing the behaviour of the system fed by artificial solution mimicking the real industrial solutions composition. Fumasep FAD membranes were studied for the first time with multicomponent metals solutions and their relevant concentrations.

The main effects of operating parameters were highlighted and presented as process performance variations.

Acid flux was significantly enhanced by both the higher acid concentration in the retentate due to a larger driving force and a higher value of acid diffusive permeability through the membrane.

Isolated influence of iron and zinc on the acid recovery was explored, which has conveyed to understand and characterize all the different phenomena observed for a multicomponent waste solution. Thus, deviation from the pure acid solution behaviour can be correlated to the two competitive phenomena: the enhancing iron effect, due to the additional driving force provided by the common anion, and the competitive zinc flux, caused by the presence of negative zinc-chloro complexes. As a result, in batch tests high acid recovery efficiency values were gained reaching acid recovery efficiency even over 100%, despite the batch

configuration adopted, thus denoting the fundamental and synergic influence of iron effect in the HCl recovery achievement.

Zinc leakage through the membrane firmly depends on the presence of both HCl and $FeCl_2$, which has led to an increase of the zinc leakage across the membrane, while for the iron leakage the highest leakage detected is lower than 10% in the most severe conditions.

A detailed analysis of osmotic and drag water flux in DD operation was also presented. For pure HCl tests at higher concentrations a net water flux opposite to the osmotic one was observed due to the presence of a drag flux, related to the water molecules associated to ions transported through the membrane. Conversely, in the presence of metal ions, the osmotic flux dominates at the higher metals concentration.

All such findings have been found entirely in agreement with the results obtained with the continuous large-scale unit. Despite the reduction of acid flux due to the presence of zinc, up to 80% of the free acid was recovered. Zinc leakage can be twice than the iron one. However, because of the lower zinc concentration, with respect to the other components, the concentration in the diffusate stream can be acceptable in the view of reusing it as recovered pickling solution. Therefore, it possible to claim that DD can be employed as SPS treatment process with high acid recovery.

The whole process was mathematically described within a time/space distributed-parameters model implemented and adopted as a process simulator, able to simulate both bath and continuous operations. The model was calibrated and fully validated using the available experimental data in the wide range of acid, iron and zinc concentration investigated (0.1-3 M, 50 – 150 g/l and 5-20 g/l respectively).

The study gives a deep knowledge of all the phenomena involved in the process allowing to characterize the behaviour of the solution and the single components in an extended range of composition, also providing a valid mathematical tool that can be applied for the elaboration of further routes for system optimization.

3. REACTIVE PRECIPITATION PROCESS

Chapter Outline

Part of this chapter has been submitted in:

"Metals recovery from waste pickling solutions by reactive precipitation" Serena Randazzo, Daniele La Corte, Rosa Gueccia, Andrea Cipollina, Giorgio Micale, submitted to Chemical engineering transaction journal.

3.1 **Reactive Precipitation overview**

The objective of the following experimental study is to verify whether, in the operating conditions of the process, it is possible to achieve the separation of heavy metals from the solution leaving the Diffusion dialysis. The purpose of this thesis is, in fact, to investigate a technological method that allows the enhancement of the metals present in the pickling waste, thus to accomplish the circular reuse of all the process streams and, at the same time, minimizing the environmental impact caused by the waste solution.

3.1.1 *Early studies: selectively precipitation*

The original idea was to selectively separate the two metals component in the form of metals hydroxide precipitate. Thus, NaOH solution was chosen as alkaline reagent for that purpose. The chemical reactions involved are:

$$H^+ + Cl^- + NaOH = H_2O + NaCl \quad (3\text{-}1)$$

$$FeCl_2 + 2NaOH = Fe(OH)_2 + 2NaCl \quad (3\text{-}2)$$

$$ZnCl_2 + 2NaOH = Zn(OH)_2 + 2NaCl \quad (3\text{-}3)$$

Since the solution is highly acidic, it is assumed that most of the iron present in the solution is Fe (II) and therefore the precipitation of ferrous hydroxide is considered. If we considered the Fe (III) presence, the involved chemical reaction is:

$$FeCl_3 + 3NaOH = Fe(OH)_3 + 3NaCl \quad (3\text{-}4)$$

In order to have a prevision of the pH values for the precipitation start point, the solubility equilibria of the iron and zinc hydroxides were studied by means of the values of the Kps solubility products[116] which are reported in Table 3-1.

Table 3-1 Kps values for iron and zinc hydroxides [116].

Compound	K_{ps}
$Fe(OH)_2$	$4.87 \cdot 10^{-17}$
$Fe(OH)_3$	$2.79 \cdot 10^{-39}$
$Zn(OH)_2$	$3 \cdot 10^{-17}$

3.1.1.1 Materials

Synthetic solutions were prepared in laboratory with concentration of the components reported in the following paragraph (see Table 3-2). As concerns HCl, $FeCl_2$ and $ZnCl_2$ components, same products reported in the Materials section 2.2.1 were used. Moreover, $FeCl_3$ hexahydrate (Carlo Erba reagents, purity ≥ 99%) and NaOH anhydrous pellets (Sigma Aldrich reagents, purity ≥ 98%) were selected.

The concentration of the caustic soda solution was chosen with reference to the moles of OH^- ions necessary for complete precipitation and for reaching pH 12. This estimate is made using equation (Eq. 3-5):

$$n°_{OH^-} = \left[(10^{-pH_{in}} - 10^{-12}) + \frac{2[Fe^{2+}] + 3[Fe^{3+}]}{MM_{Fe}} + \frac{2[Zn^{2+}]}{MM_{Zn}}\right] V \qquad 3\text{-}5$$

where $n°_{OH^-}$ is the number of moles of OH^- required for the test, pH_{in} is the initial pH of the solution, $[Fe^{2+}]$, $[Fe^{3+}]$ and $[Zn^{2+}]$ are respectively the concentration of iron (II), iron (III) and zinc (II) dissolved in solution, MM_{Fe} and MM_{Zn} are the atomic masses of iron and zinc and finally V is the volume of the solution.

3.1.1.2 Experimental set-up and procedure

The schematic representation of the experimental set-up used to carry out the reactive precipitation tests is shown in Figure 3-1. It is a semi-batch configuration.

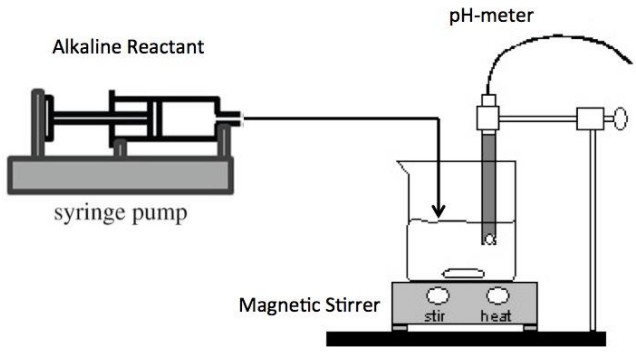

Figure 3-1 Experimental set-up of reactive precipitation tests.

The experimental setup features a 250 ml tank representing the precipitation reactor unit and a syringe pump (New Era Pump Systems, Inc.) that allows the introduction of alkaline reagent into the tank. A magnetic stirrer tool continuously stirs the tank. The mixing of the solution during the test avoids any local increases in pH that can affect the precipitation process. pH measures are detected every 15-30 seconds measured by digital multi parameter pH/conductivity-meter (Hanna Instruments). The test is considered concluded once a pH value greater than 12 is detected.

3.1.1.3 Experimental results

Iron (II) hydroxide precipitation curve was tested at first (Test 1). Operating conditions are summarized for all the investigated cases in Table 3-2.

Table 3-2 Initial operation conditions of Test 1, 2, 3 and 4.

Composition	Unit	Test 1	Test 2	Test 3	Test 4
pH_{in}	[-]	0.99	1.05	-0.01	-0.04
$[Fe^{2+}]_{in}$	[g/l]	20.2	-	-	
$[Fe^{3+}]_{in}$	[g/l]	-	-	20	20
$[Zn^{2+}]_{in}$	[g/l]	-	20		20
$[NaOH]_{mol}$	[M]	2	2	2	6
F_{NaOH}	[ml/min]	2	2	2	1.33

As shown in Figure 3-2(a), the pH trend presents a plateau between pH values of 7.1 and 7.8. In this pH range, lasting around 15 minutes, ferrous hydroxide precipitates from the solution. During the test, it is possible to identify the formation of the precipitated hydroxide flakes with a characteristic green colour. Once the precipitation phase is over, the pH suddenly rises again, settling at pH 12.5 after 23 minutes of testing.

The second main component in the pickling waste is the Zn (II), thus Test 2 was carried out to study the precipitation behaviour of the last one. The precipitation pH of zinc hydroxide is slightly lower than that shown for the ferrous hydroxide, and it is between pH 6 and 6.6 (Figure 3-2(b)). Around pH 7.5 the slope of the curve increases significantly and the pH value reaches 12.6 in lower time than 20 minutes.

Thus, the precipitation iron (III) was investigated (Test 3), in order to see if a separation between metals is still viable. Figure 3-2(c) shows a pH plateaux in the range between pH 1.85 and 2.2 was observed for the iron (III), therefore, the precipitation of ferric hydroxide occurs at a pH value significantly lower than that relating to iron (II).

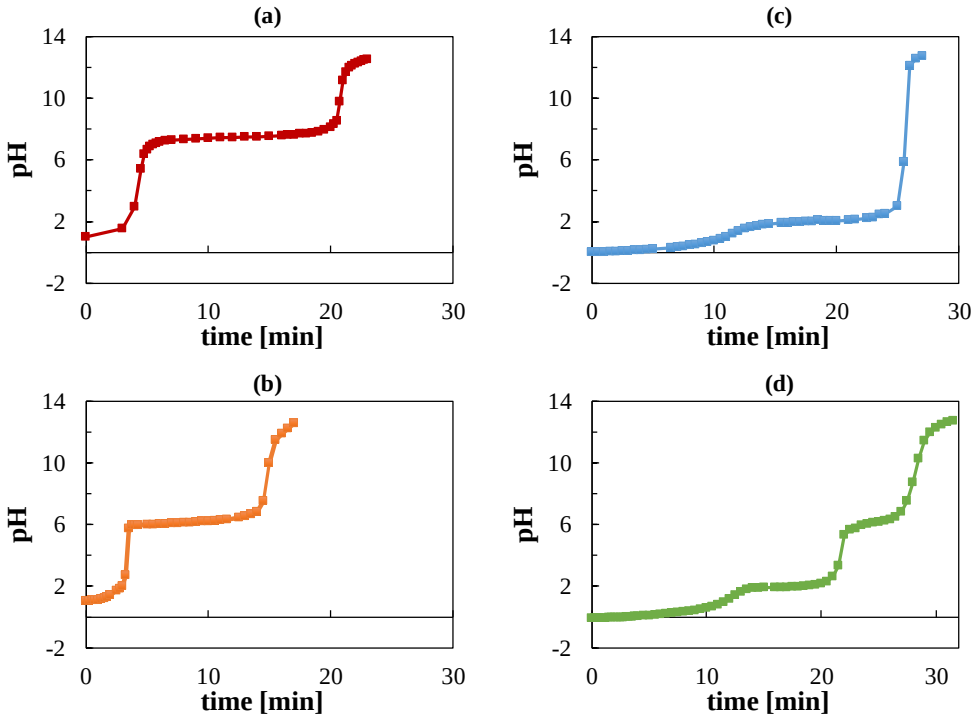

Figure 3-2 pH curve for the Fe (II) (Test 1) (a), Zn (II) (Test 2) (b), Fe (III) (Test 3) (c) components and the Fe (III) and Zn (II) solution (Test 4) (d).

At last, for this reason, the combined Fe (III) and Zn (II) precipitation trend is studied (Test 4) and graphically reported in Figure 3-2(d). It is possible to state that a selectively precipitation between this last two components is obtainable thanks to the marked difference between the precipitation pH plateaux.

In order to characterize the precipitation products purity, Test 4 was performed also by separating the two products. In particular, the experimental test was divided into two parts. The first part ends as soon as first plateaux of ferric hydroxide precipitation has overcome and pH starts to increase. At that point the test is stopped and the product thus obtained is filtered through a vacuum filtration (Buchner filter) in order to separate the iron hydroxide precipitate cake from the solution. The second part of the test was carried out with the collected solution, with the same experimental procedure. In this way, two hydroxide precipitate products were obtained as shown in Figure 3-3.

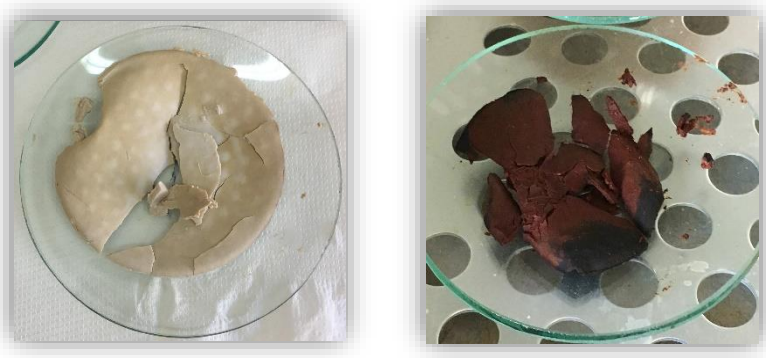

Figure 3-3 Zinc(II) (on the left) and Fe(III) (on the right) hydroxide cakes obtained after filtration step.

Metal hydroxide products purity was evaluated as follows:

$$Me(OH)_3\ purity(\%) = \frac{mass_{Me}^{analysis}}{mass_{Me}^{theor}} \times 100 \qquad 3\text{-}6$$

where $mass_{Me}^{analysis}$ is the fraction of Metals, detected in the solid sample (after filtration, washing, drying and dissolution in stoichiometric quantities plus 10% excess of HCl solution at 1 M) by spectrophotometric analysis for the iron and atomic absorption for the zinc;

$mass_{Me}^{theor}$ is the theoretical amount of metal in the sample, assuming that this contains only the particular metal hydroxide.

From the analysis results, it is observed that the presence of zinc in the iron hydroxide product is practically negligible, value below the measuring device tolerance, while the iron in the zinc hydroxide is 0.04%. However, even such low concentration could not be acceptable to make the product marketable, as only high purity Zn hydroxide is a valuable product, and even such small amount of iron contaminates the product (as also can be seen from the colour of the zinc hydroxide product in Figure 3-3).

3.2 **Adopted strategy**

Since in Tecnozinco case the iron in the waste acid solution is mainly present as iron(II), oxidizing of the solution (to perform the Fe^{2+} /Fe^{3+} oxidisation reaction) is necessary to avoid iron and zinc co-precipitation. Moreover, in order to overcome the Zn product purity issue, a different strategy was adopted.

Chemical reactants, specifically hydrogen peroxide and ammonium hydroxide (i.e. ammonia) solution, were selected for the precipitation process. A nearly pure iron hydroxide solid product, with a marketable value (e.g. fields of application are the painting industry or wastewater treatment plants [117]) is thus obtained. While, the choice of using ammonia hydroxide as alkaline reactant, though not being most cost-effective and environmental advantageous option, allows to generate a by-product stream consisting in a zinc/ammonium chloride solution ($ZnCl_2$ and NH_4Cl solution) which is suitable as fluxing solution to be used in the corresponding step of the hot-dip galvanizing production chain. This approach also overcomes the main limitation of traditional neutralisation with hydroxides (NaOH or $Ca(OH)_2$) consisting in the co-precipitation of different metals, thus preventing from the achievement of high purity precipitates [25], [27].

Thus, reaction that occurs in such conditions are reported below along with their standard enthalpy of reaction:

$HCl+NH_4OH=NH_4Cl+H_2O$	$\Delta H°_{298K}$=-41620 kcal/kmol	3-7
$FeCl_2+1/2H_2O_2+2NH_4OH=Fe(OH)_{3(s)}+2NH_4Cl$[118]	$\Delta H°_{298K}$=-12077 kcal/kmol	3-8

The selectivity of fractionated precipitation depends on the effectiveness of both the oxidation and of the precipitation processes, thus some parameters, such as the *Recovery Efficiency* and the *Fe(OH)$_3$ purity*, were used to assess the performance, as defined according to the following equations:

$$Recovery\ Efficiency\ (\%) = \frac{c_{Fe}^{in} - c_{Fe}^{sol}}{c_{Fe}^{in}} \times 100 \qquad 3\text{-}9$$

where c_{Fe}^{in} and c_{Fe}^{sol} represent the total Fe concentration in the inlet feed and in the sampled filtered solution, respectively.

$$Fe(OH)_3\ purity(\%) = \frac{mass_{Fe}}{mass_{Fe} + mass_{Zn}} \times 100 \qquad 3\text{-}10$$

where $mass_{Fe}$ and $mass_{Zn}$ are the (pondered) amounts of Fe and Zn detected in the solid sample, respectively.

The following paragraphs explain and show motivation and results that led to the choice of this strategy.

3.2.1 *PFR versus CSTR configuration*

First, the oxidation step was performed in order to characterize the process and the operating conditions. In this regards, oxidization was carried out in a Process Flow Reactor (PFR).

The PFR reactor (Plug Flow Reactor) is a continuous ideal reactor model. In the typical schematic of ideal reactors, the composition of the fluid is homogeneous in each section of the reactor, while it varies along its main development coordinate. Therefore, in this type of reactor, in the steady state, the reaction becomes an exclusive function of space and not of time.

In the particular case, the experimental set-up is made up of a main horizontal plastic tube (45 cm length, 8 mm and 5.33 external and internal diameter, respectively) with eight channels branch off, four are used for the oxidant inlet and the other ones for samples withdraw, each interposed between two adjacent inlets and at 10 cm distance from the next inlet point. A

schematic representation of the experimental test rig is shown in Figure 3-4 along with a picture of the PFR laboratory set-up:

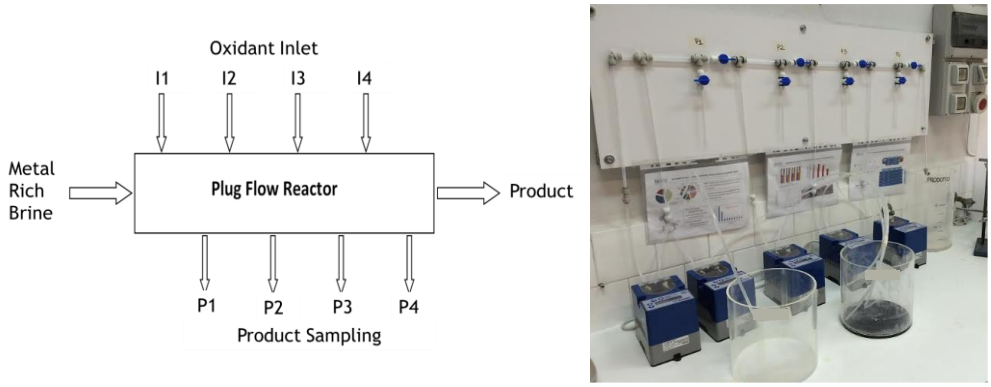

Figure 3-4 Schematic representation of the PFR reactor (on the left) and laboratory PFR experimental set-up picture (on the right).

Firstly, air was blown in the reactor to test the possibility of using air as oxidant, concluding that this option was not viable. So the hydrogen peroxide H_2O_2 was selected as oxidant for the Fe^{2+}/Fe^{3+}.

In Table 3-3 are reported *Recovery Efficiency* values obtained by performing oxidation test of an acidic solution (20 g/l HCl) contain 110 g/l Fe^{2+} in the PFR at different H_2O_2 concentrations (4.9 and 9.7 M) and by varying the "excess" flow rate ratio (ratio between the actual flow rate and the stoichiometric one). Results are reported for the four samples (P1, P2, P3 and P4 refers to Figure 3-4). Results show that the oxidation reaction occurs instantly, no further enhancement was obtained with the increasing space dimension. An improvement was detected for 4.9 M H_2O_2 solution by increasing the excess flow ratio; however, no one of the investigated test led to have a complete oxidation of Fe^{2+}/ Fe^{3+}. This result is achievable only with a concentrated H_2O_2 (30% w/w, or rather 9.7 M). For the first 3 samples the Fe^{2+} concentration was below the measureable value of the instrument, while only for the last sample a concentration of Fe^{2+} component was detected. To be even more confident, a flow rate ratio of 1.2 and a 30% w/w H_2O_2 oxidant solution were chosen as best operating conditions for the oxidation step.

Table 3-3 Results on an oxidation campaign conducted with different H_2O_2 concentration and flow rate ratio.

Operative conditions	**Results**				
Fe^{2+} 110 g/l, HCl 20 g/l, 2 cm/s	F_H_2O_2/F_stoich [-]	P1	P2	P3	P4
		Recovery Efficiency [%]			
H_2O_2 9.7 M	1.1	100	100	100	98.9
	1.2	96.5	96.0	95.6	96.0
	1.5	96.8	97.1	96.8	96.8
H_2O_2 4.9 M	2	98.8	-	98.8	-
	2.3	99.2	-	99.3	-
	2.7	99.4	-	99.4	-
	3.2	99.6	-	99.6	-

Same experimental test rig was adopted to perform precipitation step. As already mentioned in the introduction of this paragraph, the ammonia solution was selected as base reactant, in order to produce a by-product (NH_4Cl and $ZnCl_2$ fluxing solution) to be recycled directly in the galvanizing plant itself. Thus, the second set of experiments was performed by adding the alkaline reactant (5 M) to the acid solution (20 g/l HCl), assuming a complete oxidation of the Fe^{2+}, thus 110 g/l Fe^{3+} has been dissolved in solution, and with a Zn concentration of 10 g/l.

A second configuration was investigated too, specifically a Continuous Stirred Tank Reactor (CSTR), whose picture is reported in Figure 3-5. The tank capacity is 1 l, with an internal and external diameter of 8 and 9 cm, respectively, and a height of 26.6 cm. A marine propeller (diameter of 6 cm) was selected and designed to achieve the best mixing in the reactor.

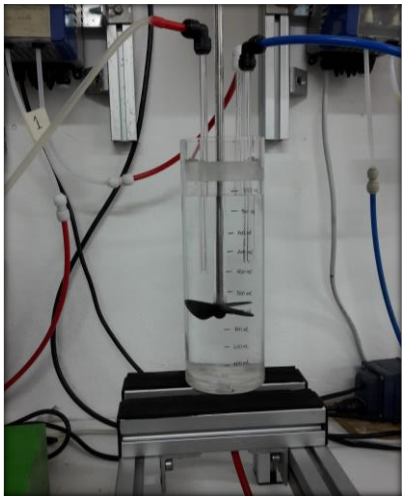

Figure 3-5 Laboratory CSTR pictures.

Table 3-4 reports the main outcomes of the laboratory tests performed with the two configurations. Purity of the final $Fe(OH)_3$ solid product was evaluated by detecting Fe and Zn contents. A very high value of 99 % was achieved with the CSTR, thus demonstrating the effectiveness of the process. Not least in importance, lower amount of Zn was lost with the liquid phase entrained by the solid product. In addition, lower filtration times and lower humidity were observed for the separation of solids produced by the CSTR, thanks to the better-controlled particles granulometry. Furthermore, the lower working concentration compare to that of the PFR, which results in lower reaction rates, is not crucial in this circumstance as the reactions, mainly the oxidization, are instantaneous reactions. All this, along with a safer and simpler operation of CSTR units, have let to the selection of this latter as best option.

Table 3-4 Main results of the precipitation step in the PFR and CSTR.

Fe^{3+} 110 g/l, Zn^{2+} 10 g/l, HCl 20 g/l	**PFR v=2 cm/s** NH_3 [5 M]	**CSTR V=0.5l** NH_3 [5 M]
Filtration	Long operation time	Less operation time
Fe in filtrate	< Minimum measurable value	< Minimum measurable value
Zn in filtrate (%)	55	72
Precipitate Purity (%)	98.5	99.1

At last, the two different steps were combined in a cooled CSTR configuration (Figure 3-6), to assess the feasibility of the process. Since the oxidation reaction is exothermic, and the high temperature effects the precipitate product [119], the CSTR previously described has been immerged in a cooling bath (ice and water bath) to keep the temperature at maximum 60°C, range of temperature that ensures no modification of the iron hydroxide structure. As visible from Figure 3-6, four peristaltic pumps were employed in this configuration, two for the reactants, oxidant and base, one for the feed (green solution) and one for the continuous draining of the CSTR.

Figure 3-6 Laboratory cooled CSTR experimental set-up pictures.

Two different tank capacity were tested: 400 and 1000 ml, which mimic the real conditions, in terms of residence time (27 and 67 minutes for the 400 and 1000 ml, respectively) and flow rate ratios, of a pilot reactor capacity of 10 and 25 l. NH_4OH commercial concentrated solution (28% w/w) was used, in order to handle with lower flow rates and to limit the dilution of the fluxing by-product.

With respect to the *Recovery Efficiency* parameter, very high values were obtained during the test for both configurations, namely always higher than 99.9 %. In particular, such low amounts of iron in solution were detected only in the first samples, while no iron was found in all other samples, thus indicating a 100 % recovery.

In Figure 3-7 values of key process parameters are reported as a function of the normalised reaction time. Fe^{2+} and Fe^{3+} concentrations were detected in the precipitate and results are presented in Figure 3-7(a). As shown, Fe^{3+} amount, compared to the total Fe, was very high since the beginning with values above 90 % for the 1000 ml capacity configuration, while an increasing trend, from 25% to 90%, is observed for the 400 ml configuration.

In addition, a better stability of the process was obtained for the1000 ml configuration, in fact results in term of pH and temperature values (Figure 3-7(b))) are stable and always below the values of 4 and 45 °C, respectively. Since we deal with NH_4OH solution and exothermic reactions, the safest configuration (1000 ml capacity) was adopted to in order to limit the risk of uncontrolled reactions with ammonia gas release.

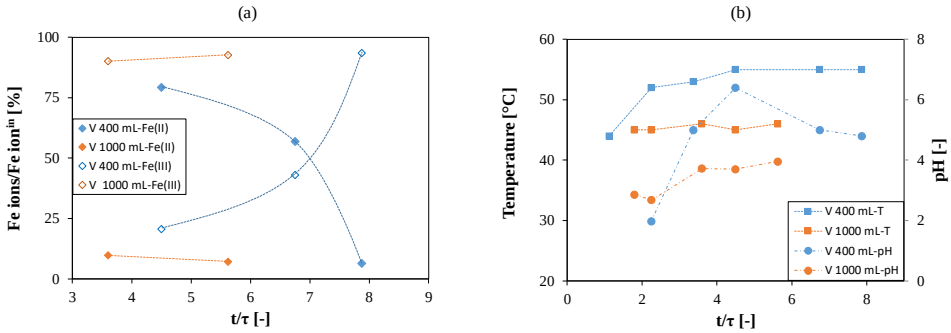

Figure 3-7 (a) Fe speciation, Fe^{2+} (solid) and Fe^{3+} (empty) rhombic symbol, in the precipitated and (b) pH (round symbol) and temperature (square symbol) values vs the normalized reaction time for the configurations with 400 ml (blue) and 1000 ml (orange) reactor capacities. Feed solution: 20 g/l HCl, 123 g/l Fe^{2+}, 10 g/l Zn; H_2O_2 30%wt and NH_3 28%wt. Feed, H_2O_2 and NH_4OH flow rate: 9, 2 and 4 ml/min.

The result of the absence of Fe in solution coupled with the very high values of Fe^{3+} (compared to Fe^{2+} and to Zn) in the solid implies a good efficiency of the overall process, where oxidation and precipitation reactions coexist, as the iron is continuously removed from the solution in the form of highly pure $Fe(OH)_3$ solid product.

3.2.2 *Cooling system design*

A cooling system with a capacity of 1.2 KW, derived from energy balance considering the two exothermic reaction reported in Eqs. 3-7 and 3-8 has to be designed in order to do not exceed the temperature of 40 °C in the reactor, set as the highest achievable temperature. For the cooling system design, three options were evaluated: (1) precipitation and oxidation occurs in a cooled CSTR; (2) reaction inside the CSTR and recycling stream for an outside cooling; (3) oxidation reaction occurs in an external heat exchanger and precipitation in the CSTR. The three different configuration are schematically represented in Figure 3-8.

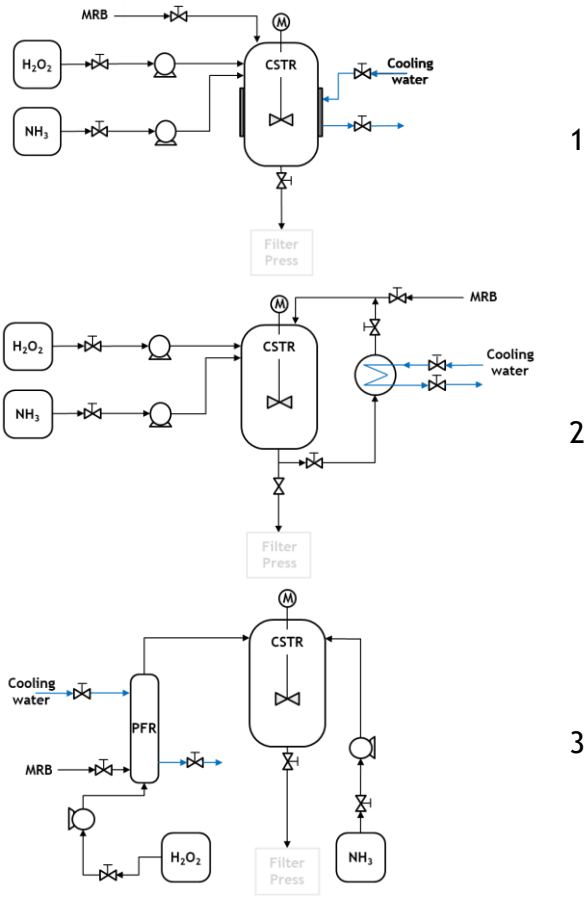

Figure 3-8 Schematic representation of the different cooling options: 1. Oxidation & Precipitation in a cooled CSTR; 2. Oxidation & Precipitation in a CSTR with external cooling in a heat exchanger; 3. Oxidation in a heat exchanger & Precipitation in a CSTR.

Advantages and disadvantages for the three different options are summarized in Table 3-5.

The first option was discarded, as it was not possible to reach suitable heat coefficient able to provide the required cooling, as reported in Table 3-6. While for the second and third option, a proper design of the heat exchanger can provide the cooling required. Option 2 with an external shell and tube heat exchanger was selected as best choice, it is reviled a more stable and compact option compared to the option 3, and a commercial and easy to design system.

Table 3-5 Advantages and disadvantages of the three different cooling options.

Option	Cooling type	Material	Advantages	Disadvantages
1. Oxidation & Precipitation in a cooled CSTR	Internal cooling coil	Plastic	-Easy design	-Coil surface fouling with consequent decrease of the heat exchange capacity
		Stainless Steel covered by PP		
	Jacketed reactor	Stainless steel with PP cover film	-Higher heat exchange coefficient	Impossibility to use level measurement system
		Glass	-Higher heat exchange coefficient	-Too expensive -Impossibility to use level measurement system
	Cooling coil dug in the reactor wall	Covered with PP film	-No deposition and fouling problem	-Low structural resistance -Possible leakage of cooling water inside of the tank
2. Oxidation & Precipitation in a CSTR with external cooling in a heat exchanger	Shell & tube (MRB in tube side)	Plastic	-Possibility to control T by controlling flow rate - Possibility to replace the tube for cleaning	-High risk of precipitation in the heat exchanger -Complexity of recycle
	Plate & frame		-Less fouling in respect to shell & tube -Fluid exposed to a much larger surface area	- Problem of mechanical strength -Complexity of recycle -No commercial plastic plate exchanger available
3. Oxidation in a heat exchanger & Precipitation in a CSTR	Heat exchanger	Plastic	-No cooling of CSTR -Oxidation in a heat exchanger	-Oxidation step with gas evolution too dangerous -Risk of precipitation in the heat exchanger

Table 3-6 Resulting heat coefficients for the option 1.

Option	Cooling type	Material	h [W/m^2/K]	Q [kW]
1. Oxidation & Precipitation in a cooled CSTR	Cooling coil	Plastic	170/230	0.5/0.7
		SS covered by PP	400/600	1 /1.5
	Jacketed reactor Spirally baffled	Stainless steel with PP cover film	250/500	0.7/1.5
		Glass	150/300	0.5/0.8
	Cooling coil dug in the reactor wall	Covered with PP film	350/400	0.7/0.8

3.3 **Conclusions**

Separation of heavy metals from the highly metals concentrated solution leaving the Diffusion dialysis module has been successfully achieved, so as making possible the implementation of a fully circular use of the process streams.

Early studies have demonstrated that Fe^{2+} and Zn^{2+} selectively separation is only possible by considering a Fe^{2+}/ Fe^{3+} oxidation step, since Fe^{2+} and Zn^{2+} present a very close pH precipitation plateau.

Hydrogen peroxide (30% w/w) and ammonium hydroxide (30% w/w) solutions were selected for the oxidation/precipitation process. The choice of using ammonia hydroxide as alkaline reactant, though not being most cost-effective and environmental advantageous option, allows generating a by-product stream consisting in a zinc/ammonium chloride solution ($ZnCl_2$ and NH_4Cl solution) to be re-used in the fluxing baths.

The highest performance in terms of reactor configuration and cooling system were selected as a result of the experimental campaign carried out in a laboratory scale. In particular, a continuous stirred tank reactor with an external shell and tube heat exchanger was selected as best choice, as it is reviled a more stable and compact option. All the evaluated process parameters showed that an efficient reactive precipitation process in terms of both process feasibility and precipitate purity could be obtained. In fact, no iron was detected in

the solution filtered from the slurry samples (Recovery Efficiency of 99.9 %) and a highly pure Fe(III) hydroxide product (99 % purity) was obtained.

Moreover, the laboratory experimental campaign laid the basis for the design of the pilot scale reactive precipitator.

SECTION 2: FROM LAB TO PILOT

ABSTRACT

A novel sustainable waste acid recovery process from pickling solutions, including diffusion dialysis (DD), where HCl is recovered, membrane distillation (MD), where HCl is concentrated, and reactive precipitation (CSTR), where metal ions are recovered in different forms, based on circular approach is proposed to tackle the variability of the pickling operating conditions and the costly and risky waste acid disposal issue. The strength of the proposed technology is shown through a development of a process simulator able to predict steady state operation of the integrated process and to perform sensitivity analysis aiming at the identification of best operating conditions at which the demonstrator will work. The simulator is a crucial tool for the design of the main process units.

Therefore, a demonstrator plant, jointly designed and constructed by Fraunhofer ISE (Freiburg, Germany), was integrated in the hot-dip galvanizing process.

Process reliability was proved through the operation of the demonstrator plant in the real industrial environment of the Tecnozinco SrL (Carini, Italy) hot-dip galvanizing plant, assessing the actual performances in fully reducing spent pickling solution disposal and in terms of recovered compounds quality. Tests were conducted firstly with artificial solutions and then with real waste liquors from the pickling plant. A high acid recovery (80%) can be achieved in the Diffusion Dialysis unit and quantitative metals separation was achieved, with iron hydroxide produced at 99% purity. The membrane distillation performances suffer when metal salts are present in large quantities due to the “salting out” effect resulting in reduced water vapor pressure, though, the use of available low-grade waste heat allows energy-sustainable operation of MD.

4. MATHEMATICAL MODELING OF THE INTEGRATED SYSTEM

Chapter Outline

Part of this chapter has been published in:

"Design of a novel membrane-integrated waste acid recovery process from pickling solution" A. Culcasi, R. Gueccia, S. Randazzo, A. Cipollina, G. Micale, Journal of Cleaner Production 236 (2019) 117623; doi: 10.1016/j.jclepro.2019.117623

4.1 Introduction

In the Chapter 4, common industrial practices, mainly for the pickling unit of the Tecnozinco hot-dip galvanizing plant, were studied in order to have a detailed description and characterization of the industrial process, for the purpose of develop a model as realistic and descriptive as possible of the real operating conditions. Starting from the model of the pickling bath and the determination of all the streams involved in that process, the integrated process model has been developed and built, by modeling two cutting-edge membrane technologies (i.e. diffusion dialysis and membrane distillation) and the precipitative reactor.

The so constructed model is a hierarchical model including all the sub-models of the plant, which have been thoroughly validated with original experimental information collected and presented in Chapters 2 and 3. The goal is to create a mathematical tool that gives predictive information on what may be the characteristics of the currents upstream and downstream of each process unit of the integrated system as the main operating conditions vary.

Moreover, a parametric analysis of the process was performed by evaluating the effect of the inlet stream (pickling solution) composition on the process performance figures of merit (e.g. recovery ratio, concentration ratio, etc.), refers to the specific Tecnozinco case study.

It is worth noting that the final aim of the present work will be to support the design, construction and operation of a pilot system, described in Chapter 5 and 6.

4.2 Tecnozinco case study

In this section, a focused on the Tecnozinco hot-dip galvanizing plant is conducted. Moreover, the proposed integrated process is described in detail.

As described in Section 0, steel pickling is typically performed by immersing the manufactured steel in hydrochloric acid (HCl) bath. The kinetic of pickling chemical reactions is strongly affected by the presence of acid molecules and the iron ions concentration. A specific relationship between the acid and the iron concentration for optimal pickling operation is reported in the literature [11] and known as the *Kleingarn Curve* (see Figure 1-2). In Figure 4-1, the optimal pickling line and the delimited pickling active region are reported, together with the composition of some representative samples from Tecnozinco pickling baths. Therefore,

controlling acid and iron concentrations within the tank increases pickling rate compared to replacing the entire spent acid bath with fresh acid.

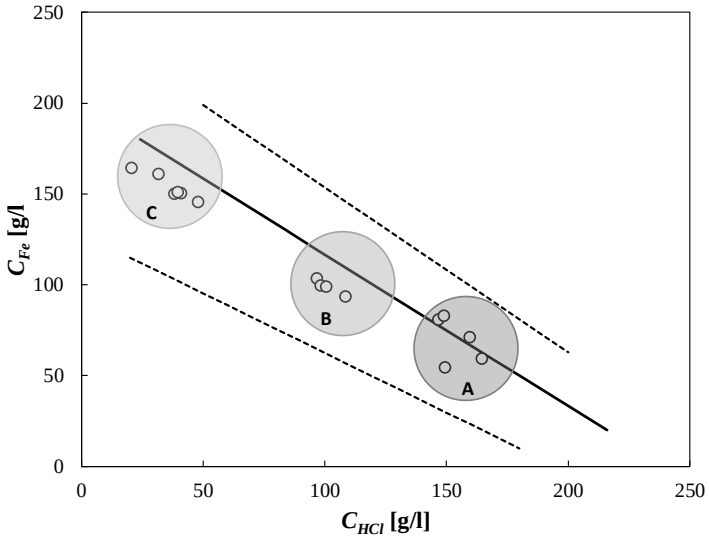

Figure 4-1 Graphical representation of the optimal pickling Kleingarn curve (continuous line) [11], with indication of minimum and maximum threshold lines for pickling operation (dashed lines). Empty circles represent the compositions of some real samples from Tecnozinco pickling baths.

Tecnozinco facility uses 7 pickling bathes containing in total more than 350 m³ of acid pickling solution. The site has a capacity of 20,000 tons per year of treated steel. The acid consumption is approximately 160-240 ton per year. Bathes can be grouped in three classes according to the "pickling power": highly effective pickling at higher acid concentration and lower iron concentration (HCl 125-170 g/l, Fe 40-100 g/l - area A in Figure 4-1), intermediate effective pickling at intermediate acid and iron concentrations (HCl 75-120 g/l, Fe 80-145 g/l - area B in Figure 4-1) and poorly effective pickling at lower acid concentration and higher iron concentration (HCl 15-60 g/l, Fe 135-195 g/l - area C in Figure 4-1). Based on periodical analysis of free acidity and iron content, the pickling solution composition is "adjusted" by spilling part of the solution and subsequent replenishing with water and HCl in order to remain close to the optimal condition curve.

Besides iron ions, also zinc is present in the pickling tanks of hot-dip galvanizing plants where goods and winches used for pieces handling are often covered with zinc. Therefore, the pickling process generates a waste acid stream of approximately 300 tons per year,

characterized by high concentrations of heavy metals, namely iron (150-180 g/l) and zinc (10-30 g/l).

4.2.1 *Integrated process description*

The proposed innovative process aims at integrating DD and MD processes with a reactive precipitation unit to keep HCl and iron concentrations in the pickling tank at the optimal values and to separate iron and zinc ions in a reactive precipitation unit producing two valuable by-product streams.

The Process Flow Diagram and relative streams characterization are shown in Figure 4-2.

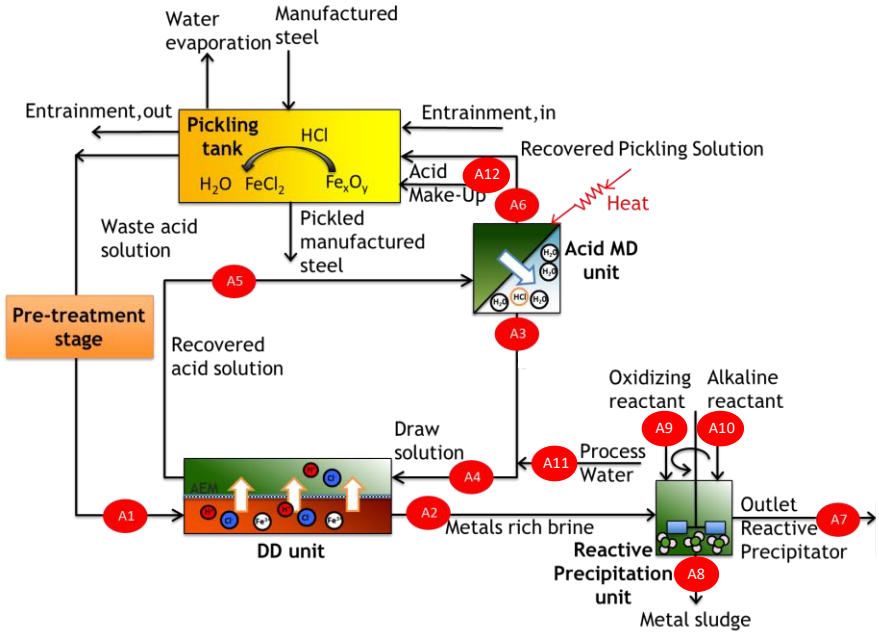

Figure 4-2 Process Flow Diagram (PFD) of the membrane-integrated process for HCl and metals recovery. Red circles identify all main process streams.

The outgoing stream from the pickling tank, named *Waste Acid solution (WAS)*, is pre-treated in order to remove particles, oil and surfactants. Then, it is fed to the Diffusion Dialysis unit (in the retentate side) where the recovery of acid occurs. Here, a high percentage of the acid (around 80%) is recovered from the waste solution thanks to the anionic exchange membrane, which allows the transport of chlorides driven by a concentration difference to the

diffusate compartment, while rejecting large cations in solution. Thanks to their small size and high mobility, H^+ ions can diffuse through the anionic membrane, by means of the so-called tunneling mechanism [48], [51]. Therefore, the acid is recovered in the diffusate side of the DD unit and separation from salts occurs. An ideal membrane should reject 100% of metal ions, in practice, real Anionic Exchange Membranes (AEMs) allow some iron and zinc ions to diffuse through them, reaching leakage percentage of 5-10% for iron and up to 50-60% for zinc [51], [106]. This latter can be actually explained due to the formation of negative Zn^{2+} complexes in solution as $ZnCl_3^-$ and $ZnCl_4^{2-}$, whose diffusion through AEMs is allowed.

The stream enriched in acid, named *Recovered Acid Solution (RAS)* is sent to the Membrane Distillation (MD) unit, where the acid is concentrated by evaporation/removal of water. In the MD unit, the microporous hydrophobic membrane separates two aqueous solutions at different temperature and composition: the *RAS*, enriched in acid, in the hot side and the *Permeate*, mainly distilled water, in the cold side. In fact, the membrane rejects liquid solution and permits vapour passage from the hot to the cold side. Thus, mainly water vapour passes and condenses directly in the *Permeate* stream within the cold compartment. As a drawback, also HCl can pass from the feed to the vapour phase and is transported through the membrane especially at high concentrations [65].

The *Permeate* stream from MD is blended with *Process Water (PW)*, used as a feed drawing solution to the DD unit (diffusate side), namely the *Draw Solution (DS)*. The stream exiting from MD feed channel, the concentrated *Recovered Pickling Solution (RPS)*, is finally sent to the pickling tank.

The other stream exiting from the DD unit in the retentate side, called *Metals Rich Brine (MRB)*, is a low acid ($0<pH<1$) stream enriched in iron and zinc chlorides. This stream is fed to the Reactive Precipitation unit where the acid is neutralized and iron hydroxide is produced by addition of ammonia solution. Moreover, a hydrogen peroxide stream is added since the iron in solution is mainly present in reduced form (Fe(II)). Here, oxidizing process is necessary to obtain a highly pure iron hydroxide precipitate, free of zinc. In fact, pH precipitation of zinc hydroxide is very similar to iron (II) hydroxide, but higher enough than that of iron (III) hydroxide to obtain the precipitation of only iron(III) at an operating pH range of 3-4. Consequently, a zinc chloride/ammonium chloride solution is produced from this stage, the *Outlet Reactive Precipitator* stream *(ORP)*. Moreover, iron hydroxide precipitates within the reactor and the resulting *Metal Sludge (MS)* can be treated in a filter press to recover iron hydroxide as a product.

In order to compensate the acid reacted in the pickling bath and that lost in the *MRB*, a *Make-Up (MU)* of fresh acid is needed in the pickling bath to maintain the optimal concentration.

The above-described integrated scheme is a nice example of a sustainable process integration and raw materials use, in which all process streams are recirculated in order to re-use a waste stream from a unit as a feed for another or, more in general, to re-use a produced stream elsewhere in the plant or commercializing it. Thus, an overall recovery of materials and minimization of waste streams can be successfully achieved. Moreover, for the pilot-scale unit installed at Tecnozinco, a recovery of waste heat, necessary for the MD operation, is also planned for enhancing the process sustainability.

4.3 **Modeling the integrated process**

A mathematical model able to simulate the integrated system operations was developed and implemented in Microsoft® Office Excel spreadsheets with Macros in Visual Basic language.

Hereinafter, model details are presented for each unit.

4.3.1 *Pickling unit*

The first step of the modeling activity was to fix parameters and operative conditions of the pickling process.

4.3.1.1 Data mining from Tecnozinco plant

In order to estimate the reaction rate of each chemical compound within the pickling tank, two possible options are possible: using kinetics data from literature or collecting information from available historical statistics of the company. In this work, the latter was selected as starting point using average data of the last 5 years. To this purpose, streams reported in Figure 4-3 were considered and the real data collected from Tecnozinco for a manufactured steel flow rate of 7410 ton/y (±14.7%), fixing a time frame of 1 year, are shown in Table 4-1, although data are quite variable within the different years, as revealed from standard deviation values evaluated for the 5 years' time span considered.

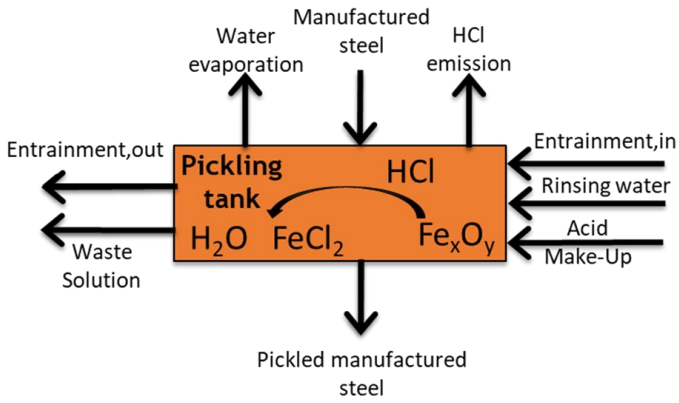

Figure 4-3 Scheme of the pickling process at Tecnozinco plant.

Table 4-1 Operational data on inlet/outlet streams under "traditional" operation of Tecnozinco plant.

	Acid Make-Up	Waste Solution	Rinsing water	Entrain. Inlet	Entrain. Outlet	HCl emission	Water evapor.
	173 (±29.5%) ton/y	247 (±35.5%) ton/y	48.1 (±54.6%) ton/y	2.5 l/ton	2.5 l/ton	0.33 ton/y	4.2 kg/ton
C_{HCl} [g/l]	400	8.50	16 g	0.00	97	-	-
ρ [g/l]	1,170	1,296	1,087	1,092	1,254	-	-

The chemical pickling reactions considered in the presence of corrosion inhibitors are Eqs. 1-2 and 1-3 reported in Section 0 and here presented again for the sake of clarity:

$$Fe_2O_3 + Fe + 6HCl = 3FeCl_2 + 3H_2O \quad 4\text{-}1$$

$$Fe_3O_4 + Fe + 8HCl = 4FeCl_2 + 4H_2O \quad 4\text{-}2$$

Reaction 4-1 accounts for the 20% and reaction 4-2 for the 80% of the overall acid consumption according to the average metal scale composition [120]. Depending on the HCl consumed per year (reported in Table 4-1), the reaction rate of the hydrochloric acid follows the expression:

$$K_{HCl} = \frac{10^3 \cdot \left(w_{y,HCl}^{MU} + w_{y,HCl}^{Rinsing} + w_{y,HCl}^{entr,in} - w_{y,HCl}^{entr,out} - w_{y,HCl}^{waste} - w_{y,HCl}^{gas}\right)}{w_{y,steel}} \quad 4\text{-}3$$

where $w_{y,HCl}^{MU}$, $w_{y,HCl}^{Rinsing}$, $w_{y,HCl}^{entr,in}$, $w_{y,HCl}^{entr,out}$, $w_{y,HCl}^{waste}$ and $w_{y,HCl}^{gas}$ are the make-up, the rinsing, the entrainment inlet, the entrainment outlet, the actual waste produced in Tecnozinco and the gaseous emission of HCl flow rate, respectively and $w_{y,steel}$ is the manufactured steel flow rate. The rate of consumed oxides and of released iron ions, water and chloride ions from the complexation reactions reported in Equations 4-1 and 4-2, can be quantified as follows:

$$K_{oxides} = 0.2 \cdot \frac{k_{HCl}\left(MM_{Fe_2O_3} + MM_{Fe}\right)}{6\, MM_{HCl}} + 0.8 \cdot \frac{k_{HCl}\left(MM_{Fe_3O_4} + MM_{Fe}\right)}{8\, MM_{HCl}} \quad 4\text{-}4$$

$$K_{Fe} = \frac{k_{HCl}\, MM_{Fe}}{2\, MM_{HCl}} \quad 4\text{-}5$$

$$K_{w} = \frac{k_{HCl}\, MM_{w}}{2\, MM_{HCl}} \quad 4\text{-}6$$

$$K_{Cl} = \frac{k_{HCl}\, MM_{Cl}}{MM_{HCl}} \quad 4\text{-}7$$

Estimated kinetic constants values are reported in Table 4-2.

Table 4-2 Kinetic constants values for the components involved in reactions 4-1 and 4-2.

Kinet constant kg/ton	Values	Description
K_{HCl}	7.6	HCl consumption per ton of steel manufactured
K_{oxides}	7.5	Oxides and iron consumption per ton of steel manufactured
K_{Fe}	5.8	Iron ions released per ton of steel manufactured
K_{w}	1.9	Water released per ton of steel manufactured
K_{Cl}	7.4	Chloride ions released per ton of steel manufactured

4.3.1.2 Pickling unit modeling

For the modeling of the pickling tank, the streams considered are shown in Figure 4-4: Manufactured Steel, Entrainment,in, Acid Make-Up and Recovered Pickling Solution as inlets, Waste Acid Solution, Entrainment,out, Water evaporation and Pickled Manufactured Steel as outlets.

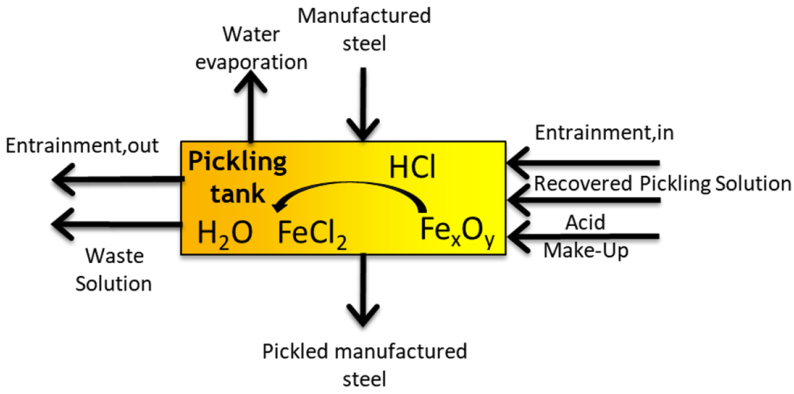

Figure 4-4 Pickling process scheme.

The pickling bath is modelled as a continuous stirred-tank reactor (CSTR) and the pickled manufactured steel is fixed equal to 290 kg per working hour. As a result, the volumetric flow rate coming from the pickling bath is calculated by Eq. 4-8:

$$F^{WAS} = \frac{10^{-3} \cdot K_{Fe} \cdot w_{steel} + w_{Fe}^{DD} + w_{Fe}^{entr,in} - w_{Fe}^{entr,out}}{10^{-3} \cdot C_{Fe}^{WAS}} \qquad 4\text{-}8$$

where F^{WAS} is the *Waste Acid Solution* volumetric flow rate, k_{Fe} is the iron release rate, w_{steel} is the pickled manufactured steel mass flow rate obtained dividing the yearly manufactured steel flow rate by the number of yearly working hours equal to 3650, w_{Fe}^{DD} is the iron mass flow rate arriving with the acid from the whole recovery process, $w_{Fe}^{entr,in}$ and $w_{Fe}^{entr,out}$ are the iron flow rates related to the streams *Entrainment,in* and *Entrainment,out* arriving from the degreasing and leaving to the rinsing tanks, respectively. C_{Fe}^{WAS} represents

the optimal iron concentration corresponding to the optimal HCl concentration of the pickling process, calculated from the Kleingarn Curve, as reported in Eq. 4-9:

$$C_{Fe} = -0.833 \cdot C_{HCl} + 200 \quad \text{4-9}$$

$w_{NH_4^+}^{MS} = w_{NH_4OH}^{alk} \cdot \alpha \cdot \frac{MA_{NH_4^+}}{MM_{NH_4OH}}$To evaluate the process streams mass density, the model developed by Lalibertè et al. was adopted [108]. According to this work, the specific volume of the mixture is evaluated by the relation:

$$v_{mix} = x_{w,H_2O} \cdot v_{H_2O} + \sum_i v_i = x_{w,H_2O} \cdot v_{H_2O} + \sum_i x_{w,i} v_{app,i} \quad \text{4-10}$$

where v_{mix} is the specific volume of the current, v_{H_2O} the specific volume of water and v_i that one of the *i*-th species in the mixture. The specific volume of the *i*-th species in the mixture is obtained by the product of the mass fraction of the i-th species $x_{w,i}$ and the electrolyte *i* specific volume i $v_{app,i}$.

The specific volume of water in the stream is evaluated according to the Kell correlation [121], while those relating to other species are calculated according to the relationship:

$$v_{app,i} = \frac{x_{w,i} + c_2 + c_3 T}{(c_0 x_{w,i} + c_1) e^{(0.000001(T+c_4)^2)}} \quad \text{4-11}$$

where c_0 and c_1 are empirical constants evaluated in g/l, c_2 is a dimensionless constant, c_3 is an experimental constant reported in 1/°C, c_4 an empirical constant evaluated in °C and T the temperature of the solution expressed in °C. Finally, the mass density of the mixture is obtained as follows:

$$\rho_{mix} = \frac{1}{x_{w,H_2O} \cdot v_{H_2O} + \sum_i x_{w,i} v_{app,i}} \quad \text{4-12}$$

Since the mass fraction of the *i*-th species is not known a priori, a trial calculation is necessary in which the density is updated at each subsequent calculation cycle until

convergence. The water flow rate in each flow stream is calculated by difference according to the relationship:

$$w_{water} = w_{tot} - \sum_i w_i \qquad 4\text{-}13$$

where w_{water} is the flow rate of water in the current considered, w_{tot} the total one and w_i that relative to the other species present in the mixture, all expressed in kg/h.

As the tank is considered as a CSTR, the *Waste Acid Solution* composition is constant during the process and it is equal to the composition inside the pickling tank.

The mass flow rate of the Acid *Make-Up* stream is calculated by the following equation:

$$w_{HCl}^{MU} = w_{HCl}^{MRB} + 10^{-3} \cdot k_{HCl} \cdot w_{steel} + w_{HCl}^{entr,out} \qquad 4\text{-}14$$

where w_{HCl}^{MU}, w_{HCl}^{MRB} and $w_{HCl}^{entr,out}$ are the hydrochloric acid mass flow rates of the *Make-Up, Metals Rich Brine* and *Entrainment,out* streams, respectively. The $k_{HCl} \cdot w_{steel}$ term concerns the HCl flow rate reacted in the pickling process.

To complete the estimation of the main streams of the integrated system, *Process Water* stream is evaluated by performing a global mass balance using the entire integrated system as control volume (Eq. 4-15).

$$w^{pw} = w^{MRB} + w^{entr,out} + w^{evap} - w^{MU} - 10^{-3} \cdot k_{oxides} \cdot w_{steel} - w^{entr,in} \qquad 4\text{-}15$$

where $w^{pw}, w^{MRB}, w^{entr,out}, w^{evap}, w^{MU}$ and $w^{entr,in}$ are the water mass flow rates in the *Process Water* incoming into the system, in the *Metals Rich Brine*, in the *Entrainment,out*, in the evaporation, in the *Make-Up* and in the *Entrainment,in* streams, respectively. The $k_{oxides} \cdot m_s$ term concerns the oxides mass flow rate inlet within the manufactured steel in the pickling tank.

4.3.2 *Diffusion Dialysis unit*

Concerning the Diffusion Dialysis unit, the streams considered for the integrated process simulation are: *Waste Acid Solution* and *Draw Solution* as inlets, *Recovered Acid Solution* and *Metals Rich Brine* as outlets (see Figure 4-5).

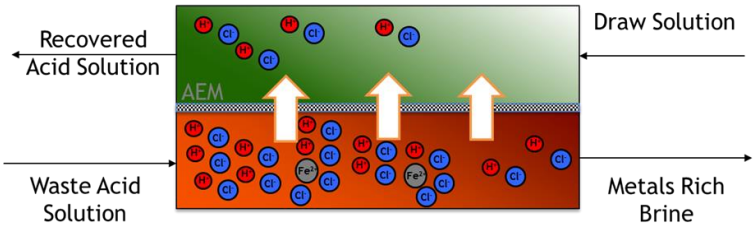

Figure 4-5 Diffusion dialysis process scheme.

The ratio between *WAS* and *DS* volumetric flow rates is assumed fixed to 1.

The equations used in this section were derived from the results obtained from the experimental investigation presented in Chapter 2, whose main findings have been published [106], [122].

The hydrochloric acid recovery was obtained by using Eq. 4-16, based on a lumped-parameters mathematical description of the DD unit:

$$w_{HCl}^{DD} = A_{DD} \cdot 3600 \cdot MM_{HCl} \Big(P_{HCl} \cdot \left(\overline{c_{r,HCl}} - \overline{c_{d,HCl}}\right) + U_{HCl}^{FeCl_2}\left(\overline{c_{r,FeCl_2}} - \overline{c_{d,FeCl_2}}\right) - U_{HCl}^{ZnCl_2}\left(\overline{c_{r,ZnCl_2}} - \overline{c_{d,ZnCl_2}}\right)\Big) \quad 4\text{-}16$$

where w_{HCl}^{DD} is the mass flow rate of hydrochloric acid passing from the retentate to the diffusate side of the DD unit, A_{DD} is the DD membrane area, MM_{HCl} is the HCl molar mass, P_{HCl} is the membrane permeability to hydrochloric acid and $U_{HCl}^{FeCl_2}, U_{HCl}^{ZnCl_2}$ are the secondary overall mass transfer coefficients taking in account the passage of acid due to the presence of the chlorides salts. $\overline{c_{r,HCl}}$ and $\overline{c_{d,HCl}}$ are the average concentrations of hydrochloric acid in the retentate and diffusate side respectively, $\overline{c_{r,FeCl_2}}, \overline{c_{d,FeCl_2}}$ and, $\overline{c_{r,ZnCl_2}}, \overline{c_{d,ZnCl_2}}$ are the average molar concentrations of iron and zinc in the retentate and in diffusate side, respectively. The

expressions for P_{HCl}, $U_{HCl}^{FeCl_2}$ and $U_{HCl}^{ZnCl_2}$ were derived experimentally and are reported in Section 2.4.4 Eqs. 2-52, 2-56 and 2-57, respectively.

Although the anionic exchange membrane theoretically rejects all iron cations, a small passage of iron chloride is observed. Therefore, salt diffusion through the AEM membrane was considered by Eq. 4-17.

$$w_{Fe}^{DD} = 0.7 \cdot A_{DD} \cdot 3600 \cdot MM_{HCl} \cdot P_{FeCl_2} \cdot \left(\overline{c_{r,FeCl_2}} - \overline{c_{d,FeCl_2}}\right) \qquad 4\text{-}17$$

where w_{Fe}^{DD} is the iron mass flow rate passing from the retentate to the diffusate side of the DD unit, P_{FeCl_2} is the membrane permeability to the $FeCl_2$. The expression for P_{FeCl_2} was derived experimentally and it is reported in Eq. 2-54 (Section 2.4.4).

Concerning the zinc passage, the following equation was adopted:

$$w_{Zn}^{DD} = A \cdot 3600 \cdot MM_{Zn}\Big(P_{ZnCl_2} \cdot \left(\overline{c_{r,ZnCl_2}} - \overline{c_{d,ZnCl_2}}\right) + U_{ZnCl_2}^{HCl}\left(\overline{c_{r,HCl}} - \overline{c_{d,HCl}}\right) + U_{ZnCl_2}^{FeCl_2}\left(\overline{c_{r,FeCl_2}} - \overline{c_{d,FeCl_2}}\right)\Big) \qquad 4\text{-}18$$

where w_{Zn}^{DD} is the zinc mass flow rate across the AEM, A is the membrane area, P_{ZnCl_2} is the membrane permeability to $ZnCl_2$, $U_{ZnCl_2}^{FeCl_2}$ and $U_{ZnCl_2}^{HCl}$ are the secondary overall mass transfer coefficients to take into account the passage of zinc due to the presence of the iron chlorides and the hydrochloric acid. P_{ZnCl_2}, $U_{ZnCl_2}^{HCl}$ and $U_{ZnCl_2}^{FeCl_2}$were derived from focused experiments carried out at the laboratory scale (Eqs. 2-55, **2-57**, 2-58).

For the water passage, two contributions are considered: the osmotic and the drag fluxes through the membrane, where the latter is related to the water solvation shell of transported acid. The osmotic flow rate w_{os} is calculated by Eq. 4-19:

$$w_{os} = 3600 \cdot P_{os} \cdot \Delta\pi \cdot MM_{H_2O} \qquad 4\text{-}19$$

where P_{os} is the water permeability, $\Delta\pi$ is the average osmotic pressure difference between the two solutions. The expression for P_{os} was derived experimentally (Eq. 2-53).

The osmotic pressure was derived following the Pitzer multi-ionic virial equations as described in Section 0.

The drag mass flow rate w_{drag} is calculated according to the following equation:

$$w_{drag} = \left(7 \cdot \frac{w_{HCl}^{DD}}{MM_{HCl}} + 18 \cdot \frac{w_{FeCl_2}^{DD}}{MM_{FeCl_2}} + 18 \frac{w_{ZnCl_2}^{DD}}{MM_{ZnCl_2}}\right) \cdot MM_{H_2O} \cdot 3600 \quad 4\text{-}20$$

where w_{HCl}^{DD}, $w_{FeCl_2}^{DD}$ and $w_{ZnCl_2}^{DD}$ are the HCl, $FeCl_2$ and $ZnCl_2$ mass flow rates passing through the DD membrane, MM_{HCl}, MM_{H_2O}, MM_{FeCl_2} and MM_{ZnCl_2} are the HCl, H_2O, $FeCl_2$ and $ZnCl_2$ molar masses.

The local ΔC driving force in terms of HCl concentration difference between retentate and diffusate streams in the DD unit is bound to be higher than 3 g/l. Finally, the overall mass balance and the generic i-component mass balance for the DD unit are reported in Eqs. 4-21 and 4-22:

$$w^{DS} + w^{WAS} = w^{MRB} + w^{RAS} \quad 4\text{-}21$$

$$w_i^{DS} + w_i^{WAS} = w_i^{MRB} + w_i^{RAS} \quad 4\text{-}22$$

where w^{DS}, w^{WAS}, w^{MRB} and w^{RAS} are the total mass flow rates of the *Draw Solution*, *Waste Acid Solution*, *Metals Rich Brine* and *Recovered Acid Solution* streams, while the subscript *i* indicates the i-component (e.g. $FeCl_2$, HCl, $ZnCl_2$). The main figure of merit to assess the Diffusion Dialysis performance is the Recovery Ratio of acid (RR), which is defined as follows:

$$RR\ (\%) = \frac{w_{HCl}^{RAS} - w_{HCl}^{DS}}{w_{HCl}^{WAS}} \cdot 100 \quad 4\text{-}23$$

where w_{HCl}^{RAS} , w_{HCl}^{DS} and w_{HCl}^{WAS} are the hydrochloric acid mass flow rate of the RAS, DS and WAS solutions, respectively.

4.3.3 *Membrane Distillation unit*

With regard to Membrane Distillation unit, the streams considered for the simulation are: *Recovered Acid Solution* as inlet, *Recovered Pickling Solution* and *Permeate* as outlets (see Figure 4-6).

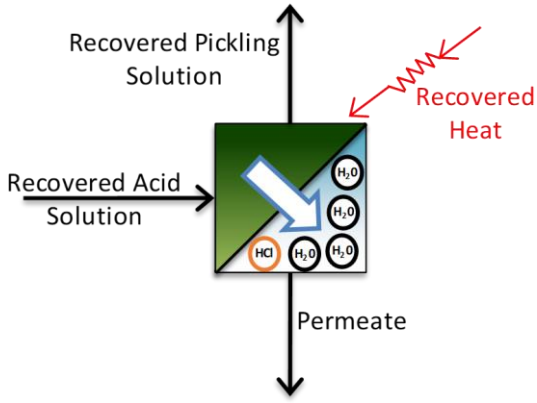

Figure 4-6 Membrane Distillation process scheme.

The fluxes of water and HCl in the vapour phase passed through the membrane are derived from simulations carried out by another research partner within the ReWaCEM consortium[66]. The values of J_i used in the model are extrapolated from simulations results carried out considering fixed temperature values at both the sides of the membrane. Specifically, in the range of the considered concentrations, and fixing average temperature to 75-65 °C, the fluxes are calculated to be: J_w=2.97-3.02 kg/m^2 h^1 and J_{HCl}= 0.08-0.12 kg/m^2 h^1, for HCl concentration entering with the *Recovered Acid Solution* varying from 75 to 111 g/l. The overall and for the i-component mass balances for the Membrane Distillation unit are reported in Eqs. 4-24 and 4-25:

$$w^{RAS} = w^{RPS} + w^{Perm} \quad 4\text{-}24$$

$$w_i^{RAS} = w_i^{RPS} + w_i^{Perm} \quad 4\text{-}25$$

where w^{RAS}, w^{RPS} and w^{Perm} are the total mass flow rates of the *Recovered Acid Solution*, *Recovered Pickling Solution* and *Membrane Distillation Permeate* streams.

The efficiency of the MD unit can be evaluated according to the Concentration Ratio parameter (CR) given by

$$CR = \frac{C_{HCl}^{RPS}}{C_{HCl}^{RAS}} \quad 4\text{-}26$$

which is the hydrochloric acid mass concentration ratio in the *Recovered Pickling Solution* C_{HCl}^{RPS} and in the *Recovered Acid Solution* C_{HCl}^{RAS}.

4.3.4 *Reactive Precipitation stage*

The streams of the Reactive Precipitation unit, as shown in Figure 4-7, are: *Metal Rich Brine* and *Oxidizing reactant* and *Alkaline reactant* streams as inlets, *Metal Sludge* and *Outlet Reactive Precipitator* stream as outlets.

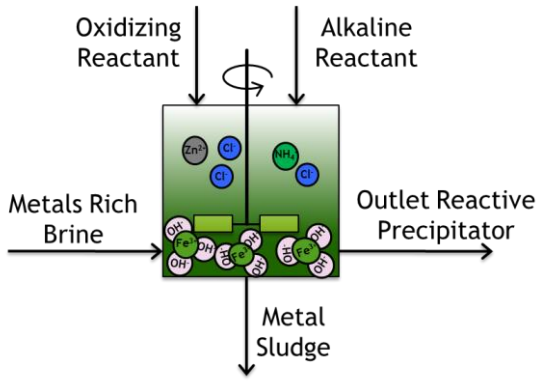

Figure 4-7 Reactive precipitator process scheme.

This unit is considered as a CSTR too. The neutralization (Eq 3-7), oxidation and precipitation (Eq. 3-8) reactions discussed in Section 3.2 are considered in the reactive precipitation process.

The hydrogen peroxide mass flow rate is calculated according to the following expression:

$$w_{H_2O_2}^{Ox} = \frac{w_{Fe}^{MRB} MM_{H_2O_2}}{2\, MM_{Fe}} \qquad 4\text{-}27$$

where $w_{H_2O_2}^{Ox}$ is the inlet H_2O_2 mass flow rate, w_{Fe}^{MRB} is the Fe mass flow rate in the *MRB*, $MM_{H_2O_2}$ and MM_{Fe} are the molar masses of H_2O_2 and Fe, respectively.

The mass flow rate of the alkaline reactant is computed using the relation:

$$w_{NH_4OH}^{alk} = \left[(10^{-pH_{in}} - 10^{-pH_{out}}) \cdot F^{MRB} + 2 \cdot \frac{C_{Fe}^{MRB} \cdot F^{MRB}}{MM_{Fe}}\right] \cdot 10^{-3} \cdot MM_{NH_4OH} \qquad 4\text{-}28$$

where $w_{NH_4OH}^{alk}$ is the NH_4OH mass flow rate in the alkaline reactant stream, pH_{in} and pH_{out} are the inlet and outlet pH of the solution, F^{MRB} is the *MRB* volumetric flow rate, C_{Fe}^{MRB} is the iron molar concentration, MM_{Fe} and MM_{NH_4OH} are the iron and NH_4OH molar masses, respectively.

Regarding the *Metal Sludge (MS)* calculations, the following equations are used:

$$w_{H_2O}^{MS} = \left[(10^{-pH_{in}} - 10^{-pH_{out}}) \cdot F^{MRB} \cdot 10^{-3} \cdot MM_{H_2O} + w_{H_2O}^{MRB} + w_{H_2O}^{alk} + w_{H_2O}^{Ox}\right]\alpha \quad 4\text{-}29$$

$$w_{HCl}^{MS} = [w_{HCl}^{MRB} - (10^{-pH_{in}} - 10^{-pH_{out}}) \cdot F^{MRB} \cdot 10^{-3} \cdot MM_{HCl}] \cdot \alpha \quad 4\text{-}30$$

$$w_{Cl}^{MS} = [w_{Cl}^{MRB} + (10^{-pH_{in}} - 10^{-pH_{out}}) \cdot F^{MRB} \cdot 10^{-3} \cdot MM_{Cl}] \cdot \alpha \quad 4\text{-}31$$

$$w_{NH_4}^{MS} = w_{NH_4OH}^{alk} \cdot \alpha \cdot \frac{MM_{NH_4}}{MM_{NH_4OH}} \quad 4\text{-}32$$

$$w_{OH}^{MS} = \frac{2 \cdot 10^{-3} \cdot C_{Fe}^{MRB} \cdot F^{MRB} \cdot MM_{OH}}{MM_{Fe}} + \frac{2 \cdot w_{H_2O_2}^{Ox} \cdot MM_{OH}}{MM_{H_2O_2}} \quad 4\text{-}33$$

where $w_{H_2O}^{MS}$, $w_{H_2O}^{MRB}$, $w_{H_2O}^{alk}$ and $w_{H_2O}^{Ox}$, w_{HCl}^{MS} and w_{HCl}^{MRB}, w_{Cl}^{MS} and w_{Cl}^{MRB}, $w_{NH_4}^{MS}$ and $w_{NH_4OH}^{alk}$, w_{OH}^{MS} and $w_{H_2O_2}^{Ox}$ are the mass flow rates of water, HCl, chloride ions, ammonium cations, ammonium hydroxide, hydroxyl ions and hydrogen peroxide in the Metal Sludge, Metals Rich Brine, Alkaline reactant and Oxidizing reactant streams; pH_{in} and pH_{out} are the inlet and outlet pH of the solution; F^{MRB} is the MRB volumetric flow rate; MM_{H_2O}, MM_{HCl}, MM_{Cl}, MM_{NH_4}, MM_{NH_4OH}, MM_{OH}, MM_{Fe} and $MM_{H_2O_2}$ are the molar masses and C_{Fe}^{MRB} is the iron concentration in Metals Rich Brine. α is a coefficient which represents the amount of the flow rate of solution trapped in the humid cake, expressed by the following equation:

$$\alpha = \frac{w_{sol}^{MS}}{w_{sol}^{MS} + w^{ORP}} \quad 4\text{-}34$$

in which w^{ORP} is the *Outlet Reactive Precipitator* stream mass flow rate and w_{sol}^{MS} is the mass flow rate of aqueous solution in the *Metal Sludge*. w_{sol}^{MS} is given by

$$w_{sol}^{MS} = w^{MS} - w_{prec}^{MS} \quad 4\text{-}35$$

where w_{prec}^{MS} is the iron hydroxide mass flow rate precipitated within the reactive precipitation unit. In this work, α was determined experimentally by precipitation and filtration tests and it was fixed equal to 0.35, resulting from experimental actives conducted for the reactive precipitator unit (Chapter 3).

Regarding the *Outlet Reactive Precipitator* stream, the pH is kept constant and equal to 4. The mass flow rates of each i-component (i.e. H_2O, HCl, Cl^-, NH_4^+) can be calculated by the following equation:

$$w_i^{ORP} = \frac{w_i^{MS}}{\alpha} \cdot (1 - \alpha) \qquad 4\text{-}36$$

4.3.5 *Numerical details*

All the equations presented in the previous paragraphs were solved using Microsoft® Office Excel spreadsheets with macros, according to the numerical algorithm shown in Figure 4-8. A summary table with all the equations implemented is also reported later in Section 8.2, Table 8-1. By selecting the C_{HCl}^{WAS} value and assuming a first guess value for RR and DD and MD membrane areas, the mass balance equations for the pickling, DD and MD units are solved. Computed results lead to the estimation of operating parameters, which should verify the constraints reported in the rhombic shapes. If not, DD and MD area and RR are adjusted to achieve this goal. When these conditions are fully satisfied, mass balances of Reactive Precipitation units are solved and the numerical procedure is completed.

Thus the outputs of the mathematical model calculations are: (i) the acid concentration of the waste solution to be treated, and consequently the iron one; (ii) the flowrate to be feed in the integrated system which ensures the closure of the mass balance equations in steady state conditions; (iii) the membrane areas of DD and MD unit.

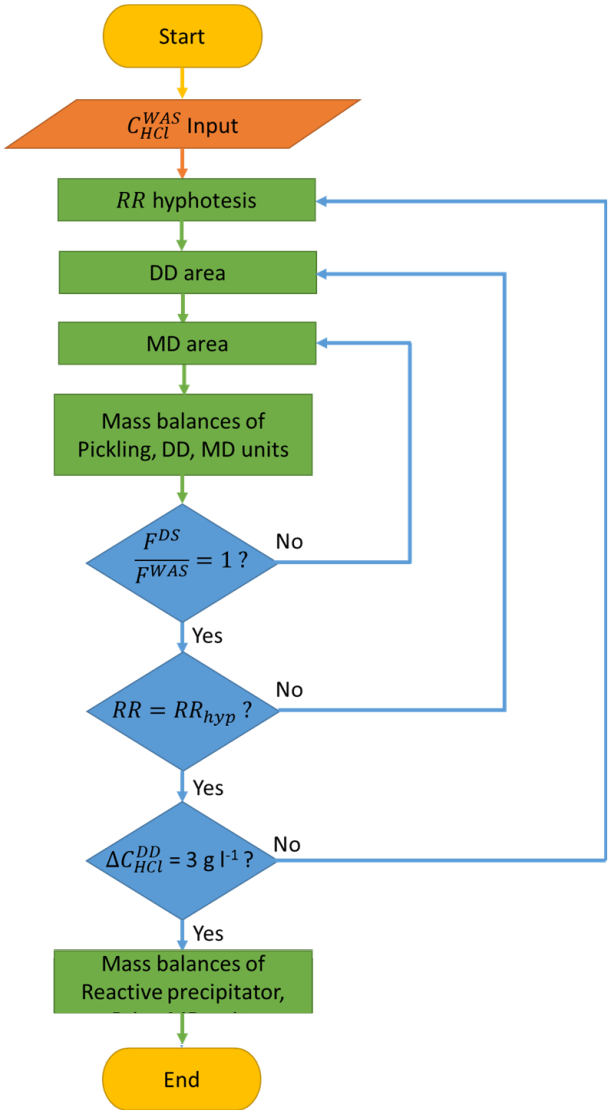

Figure 4-8 The implemented algorithm solved within Microsoft® Office Excel spreadsheets with macros.

4.4 **Results and discussion**

A parametric analysis of the process was performed by varying the main operating parameters in order to find the operating conditions for optimal process efficiency. In particular, three case studies were considered by fixing the HCl concentration in the pickling bath to 80, 100 and 120 g/l and imposing the corresponding iron concentration from the

Kleingarn curve. It is worth noting that values of evaporation flux and inlet/outlet entrainment rate in the pickling tank were considered constant (as reported in Table 4-1) for the three analysed scenarios.

As a reference case, the streams reported in the process flow diagram of Figure 4-2 were characterized considering the HCl concentration in the pickling bath equal to 100 g/l. The relevant streams properties are reported in Table 4-3.

Table 4-3 PFD streams characterization (see Figure 4-2) for $\boldsymbol{C_{HCl}^{WAS}}$=100 g/l.

Stream	w	F	C_{HCl}	$C_{Fe^{2+}}$	$C_{Zn^{2+}}$	C_{NH_4Cl}	C_{NH_4OH}	$C_{H_2O_2}$
	kg/h	l/h	g/l	g/l	g/l	g/l	g/l	g/l
A1	21.1	16.4	100	117	12.6	0.0	0.0	0.0
A2	19.3	16.0	14.4	102	4.77	0.0	0.0	0.0
A3	5.44	5.40	22.8	0.0	0.0	0.0	0.0	0.0
A4	16.4	16.4	7.5	0.0	0.0	0.0	0.0	0.0
A5	18.3	16.8	91.3	16.6	7.81	0.0	0.0	0.0
A6	12.9	11.4	124	24.4	11.5	0.0	0.0	0.0
A7	15.7	15.1	0.00252	0.0	3.30	154	0.0	0.0
A8	11.6*	-	-	-	-	-	-	-
A9	3.44	3.07	0.0	0.0	0.0	0.0	0.0	325
A10	4.63	5.20	0.0	0.0	0.0	0.0	525	0.0
A11	11.0	11.0	0.0	0.0	0.0	0.0	0.0	0.0
A12	7.32	6.26	400	0.0	0.0	0.0	0.0	0.0

*Metal sludge, after filtration, containing 29% iron(III) hydroxide and 71% of spent brine with up to 13% of $ZnCl_2$ and NH_4Cl salts).

Clearly, the variation of HCl and Fe concentration in the pickling bath affects flow rates, composition and performance parameters of the integrated system.

Figure 4-9 shows the volume flow rates of all considered streams. They strongly depend on the HCl concentration. In fact, as shown in Eq. 4-8, the *WAS* flow rate is inversely proportional to the iron concentration. Moreover, the iron and hydrochloric acid concentrations are interrelated by the Eq. 4-9 (the Kleingarn curve). Thus, the higher the hydrochloric acid concentration, the lower the iron concentrations. As a consequence, the increase of C_{HCl}^{WAS} leads to the rise of the WAS flow rate. Of course, the higher the WAS flow rate, the higher that of the other process streams.

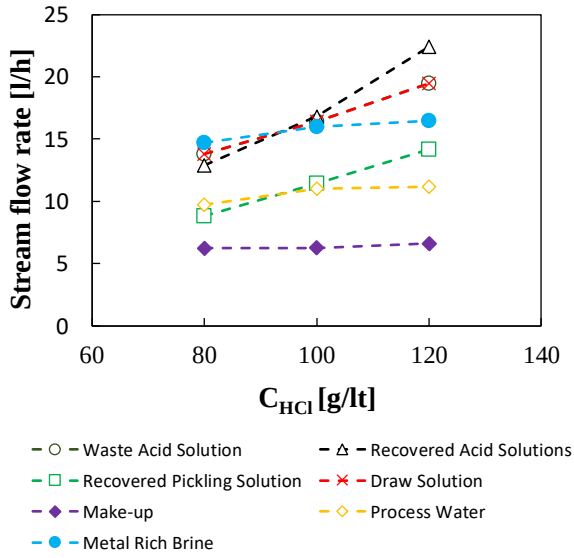

Figure 4-9 Streams flow rates as a function of C_{HCl}^{WAS}.

The HCl concentration in the *WAS* affects acid and iron concentrations of the other streams, such as *RPS*, *RAS* and *MRB*. In fact, as shown in Figure 4-10, increasing HCl concentration from 80 to 120 g/l leads to an increase of acid and a reduction of iron concentrations in the just mentioned streams.

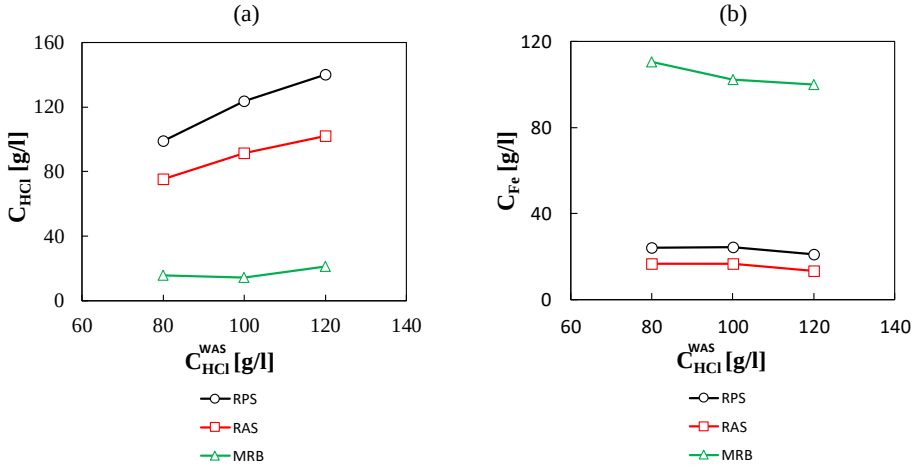

Figure 4-10 HCl concentrations (a) and Iron concentrations (b) in the *RPS*, *RAS* and *MRB* as a function of $\boldsymbol{C_{HCl}^{WAS}}$.

The hydrochloric acid recovery performance from the pickling waste is given by the DD Recovery Ratio and the MD Concentration Ratio, shown in Figure 4-11.

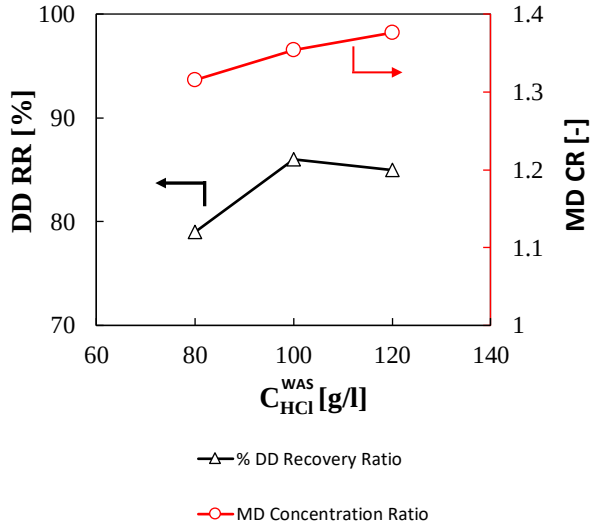

Figure 4-11 DD Recovery Ratio and MD Concentration Ratio as function of $\boldsymbol{C_{HCl}^{WAS}}$.

The integrated system allows an average DD Recovery Ratio higher than 80%. Moreover, high acid concentrations of the *RPS* (MD outlet) are obtained because of the high Concentration Ratio values of the MD unit (i.e. 1.35 on average). Thereby, the *Recovered Pickling Solution* can be effectively recirculated and re-used in the pickling bath.

Concerning the reactive precipitation unit, the inlet and outlet streams flow rates are shown in Table 4-4.

Table 4-4 Oxidizing reactant, Alkaline reactant and Iron Hydroxide streams flow rates as function of $\boldsymbol{C_{HCl}^{WAS}}$.

C_{HCl}^{WAS}(g/l)	80	100	120
Oxidizing reactant (kg/h)	3.41	3.44	3.46
Alkaline reactant (kg/h)	3.83	4.63	4.08
Iron Hydroxide (kg/h)	3.11	3.16	3.13

The flow rates of the *Oxidizing reactant* solution and of the Iron Hydroxide are poorly dependent on the C_{HCl}^{WAS}, while an increasing-decreasing trend was found for the *Alkaline*

reactant solution. The average *Oxidizing* and *Alkaline* reactants flow rates are 3.4 and 4.2 kg/h, respectively. Consequently, an Iron Hydroxide stream of 3.2 kg/h is obtained with high purity (i.e. >99.0%). Such product results in an economic benefit for the company since it represents a marketable product with significant added value.

Likewise, the liquid outlet stream is re-used in the fluxing step of the hot-dip galvanizing plant. This fact ensures the resources circularity strategy and the total elimination of the waste.

Finally, it is worth to underline the two main highlights of what presented in Chapter 4:

1. whatever it is the initial acid concentration optimal stationary conditions are maintained in the entire process through the continuous regeneration of the waste solution by removing iron and zinc released in the bath and recycling almost all the free acid to the pickling tank.
2. no waste streams are generated. As inlet streams we have considered an acid *Make Up*, and *Oxidizing* and *Alkaline reactants*, and as outlets the *Metal Sludge*, iron hydroxide which can be sell as product, the *Outlet Reactive Precipitator* which is again a by-product of the galvanizing plant, and the *Permeate*, low acidic water, that can be integrated in the process itself as *Draw Solution* for the DD operation.

4.5 **Preliminary design of the main processes**

In the present paragraph, following the experimental activities and modelling results of the DD process and the integrated system simulator, the preliminary design activities of the core processes are reported. As a result of the parametric analysis presented in paragraph 4.4, the configuration with a waste acid concentration of 100 g/l and a process treatment capacity (F^{WAS}) of about 20 l/h was selected as nominal condition for the pilot plant system.

The DD modelling tool, detailed in section 2.4, was employed in order to provide design features of the relevant unit. Waste acid solution (A1) and draw solution (A4) flowrate and concentration presented in Table 4-3 were assumed as DD inlet streams. The module geometry, i.e. length 0.8 m, width 0.2 and channel thickness 270 μm, has been fixed equal to the large scale module (refer to Section 2.2.3), while the number of AEM was varied. Simulation results are reported in Table 4-5.

Table 4-5 DD pilot module preliminary design.

N° AEM	Total Area	τ	RR_{HCl}	$Leak_{FeCl2}$	$Leak_{FeCl2}$
-	[m^2]	[min]	-		-
21	3.3	1.3	80,1%	17,8%	64,0
40	6.4	2.6	89,7%	31,7%	79,1
62	10	4.1	87,3%	36,5%	72,0

Thus, a number of AEM between 20 and 40 was suggested in order to obtain high acid recovery and moderate metals leakage. In fact, the acid recovery only slightly increases with residence time until the iron leakage becomes so large that any further increase of the residence time would result in the reduction of the acid recovery. Unfortunately, due to some standardisation constraints, the pilot DD module delivered by the technology supplier (Deukum GmbH) did not reflect the above indications as better detailed in paragraph 5.2.2.1.

Similarly, specifications of the inlet MD stream (A5 in Table 4-3) were considered for the relevant design. Process simulator output in terms of total MD area is 7 m^2. However, the detailed design of the unit, with the thermostatic line and cooling requirement, has been performed by the Fraunhofer ISE project partners and is presented in Chapter 5, paragraph 5.2.2.2.

As regard the reactive precipitator, modelled as a continuous stirred tank reactor (CSTR), design specifications, based on the experimental activities presented in Section 3.2 along with the integrated model results (i.e. flow rates and concentrations of the A2, A9 and A10 streams), are presented in Table 4-6.

The shell and tube heat exchanger for the reactor cooling (paragraph 3.2.2) was commissioned to the Calorplast Company, located in Germany.

Table 4-6 CSTR design: technical specifications.

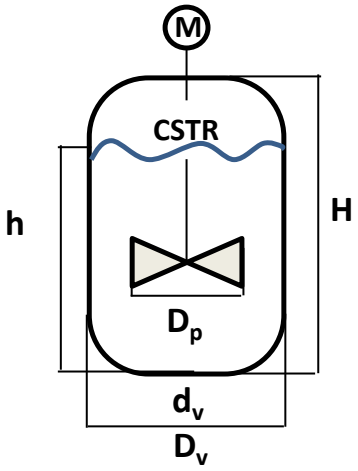

Reactor height (H)	0.4 m
Maximum liquid level (h)	0.3 m
External reactor diameter (D_v)	0.3 m
Internal reactor diameter (d_v)	0.29 m
Paddle diameter (D_p)	0.2 m
Maximum capacity	26 l
Nominal capacity	23 l
Cooling demand	1.5 kW
Residence time	46 min

4.6 **Conclusions**

A novel membrane-integrated waste acid recovery process from pickling solutions based on circular economy is proposed and investigated. In order to do so, a process simulator was developed. The proposed integrated process guarantees a pickling continuous operation under optimal conditions, thus avoiding the standard periodic steps of withdrawing and refilling pickling baths, being one of the major environmental and economic drawbacks of the process.

The parametric analysis carried out showed the effect of increasing the inlet hydrochloric acid concentration in the *Waste Acid Solution* on the main process streams. Main operative parameters were monitored, including HCl and Fe concentrations, performance indicators and membrane area requirements. A high acid recovery (higher than 79%) was obtained in the DD, while keeping a low iron leakage. Moreover, the acid solution concentration step was effectively achieved in the MD unit, where the feed solution is concentrated in HCl of 35%. The process simulator was able to assess the feasibility of the continuous operation of the integrated system that allows pickling to be performed under optimal conditions, thus reducing the pickling time and enhancing the overall system efficiency.

In addition, it provides predictive information of all the currents upstream and downstream of each process unit of the integrated system as the main operating conditions vary. Thus, it has revealed a strategic tool for the process operating design of the demonstrator unit.

5. DEMO SYSTEM

Chapter Outline

Part of this chapter has been accepted for publication in:

"An integrated approach for the HCl and metals recovery from waste pickling solutions: pilot plant and design operations" R. Gueccia, D. Winter, S. Randazzo, A. Cipollina, J. Koschikowski G. Micale, accepted for publication in Chemical Engineering Research and Design

5.1 Introduction

Extended scientific research, in more than 40 years of studies and applications on this topic, has focused mainly on the treatment of the pickling waste at the end of its life. Although several alternative methods of recovering exhausted solutions have been proposed and summarized in Section 1.2, few applications of demonstrator plants are reported in the literature. Balakrishnan et al. [44] investigated three different technologies at the demonstrator scale: diffusion dialysis, acid retardation and nanofiltration. Behind the several issues encountered in the industrial application, the waste solution was very low acid concentrated, since disposal solutions were considered, and the treatment benefit were focused on the acid recovery, thus only minimizing the waste production, which will in any case undergo through a further neutralization step.

A well-known and established technology for the acid regeneration is the spray roasting [21], [24] process, as presented in paragraph 1.2.1. The ANDRITZ Group has proposed their own recovery technology based on spray roasting and fluid bed processes [22] with several applications located worldwide. However, this is a thermal technology whit high energy consumption so far. In addition, they suffer for the presence of zinc in solution, due to the formation of low melting compounds at the high process working temperature, thus a zinc removal steps have to be integrated.

Chapter 5 presents the activities of the demonstrator pilot-scale plant constructed by the project partner Fraunhofer ISE and jointly designed based on results of the extended experimental campaign and modeling activities presented so far. The pilot was installed at the Tecnozinco hot-dip galvanizing plant (Carini, PA, Italy) and tested by myself in collaboration with local operators.

The integrated process feasibility has been studied and proposed through the application of the process simulator [123] presented in Chapter 4. The treatment chain consists of a highly automatized system composed by the three main core processes along with pre-treatment section, cooling and heating network integration.

DD module has the same geometry and characteristics of the large DD module presented in Section 2.2.3, with an increased membrane area.

Taking into account the harsh environment created due to the acids, the MD module applied in the present study is a feed gap air gap membrane distillation (FGAGMD) [124]; here the aggressive media is only in contact with the feed and permeate channels, which are

hydraulically separated from the channels that supply heating and cooling. Consequently, normal water can be used as heat transfer fluid, significantly reducing the potential risk and costs dedicated to the thermal sub-system.

A polypropylene CSTR was designed with a recirculation-cooling loop through an external shell and tube heat exchanger.

A full integration of each part of the demonstrator system with the industrial site was achieved.

Although the construction of the pilot plant and the design and implementation of the control system were performed by Fraunhofer ISE staff, a full description is here reported for the sake of clarity, along with the designed and testing activities carried out within the present PhD.

5.2 **Demonstrator**

The process operating conditions and preliminary design of the demonstrator units were based on the output of the simulation campaign [123] presented in Chapter 4. In particular, the configuration at 100 g/l of waste acid solution concentration resulting from the parametric analysis showed in paragraph 4.4 was selected as nominal operating condition of the demonstrator system. Thus, a treatment capacity of around 20 l/h was considered in sizing the treatment chain, resulting in project suggestions reported in paragraph 4.5. However, membrane units were actual designed according to technologies providers.

The pilot plant was constructed and assembled in all its parts by Fraunhofer ISE project partner, at its premises in Freiburg, Germany, and it was subsequently installed and operated in real environment at Tecnozinco SrL in Carini (Sicily, Italy). The plant for the treatment of waste acid solutions was designed for testing the innovative approach for the recovery of hydrochloric acid and iron, recycling the remaining zinc metal solution, thus reducing the wastewater disposal and guaranteeing continuous optimal conditions of the pickling process. The plant consists of three different core sections: the recovery of free acid, the concentration of recovered acid, the recovery of iron salts and zinc solution. The illustration of the demonstrator is presented in the simplified process flow diagram (PFD) shown in Figure 5-1, for which the meaning of the abbreviations is explained throughout the relevant text and reported in Table 5-1.

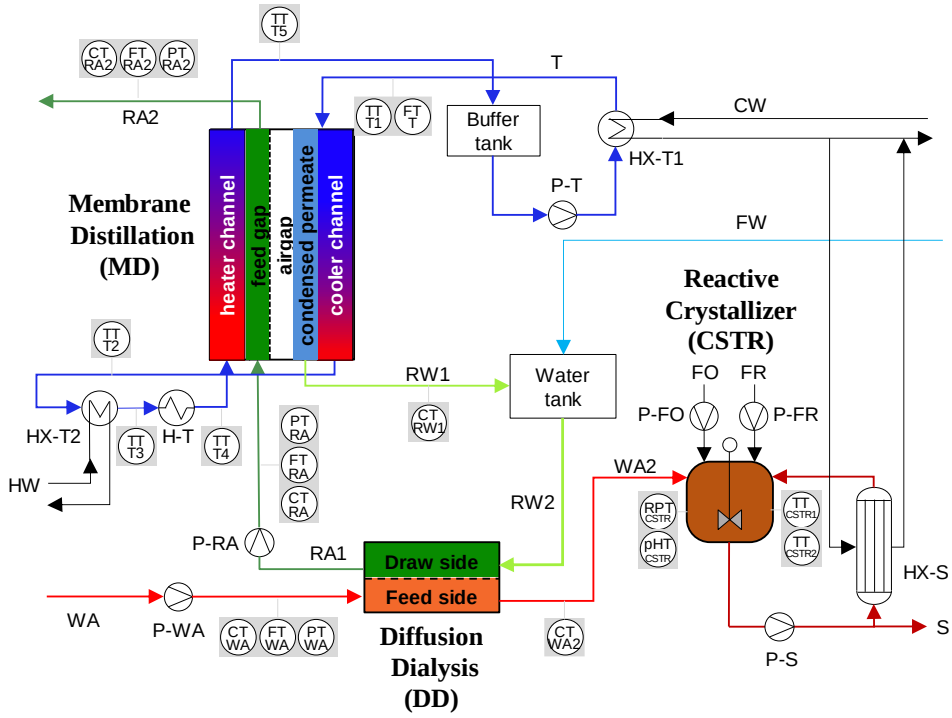

Figure 5-1 Simplified process flow diagram of the demonstrator plant.

Table 5-1 Abbreviations used in the PFD in Figure 5-1 and throughout this work.

Stream Abbrev	Legend	Stream Abbrev	Legend	Sensor Abbrev	Legend	Hydr. Abbrev	Legend
WA	Waste Acid	T	Thermost.	FT	Flow Trans.	P	Pump
RA	Recovered Acid	S	Slurry	TT	Temp. Trans.	HX	Heat Exchanger
RW	Recover Water	FW	Fresh Water	CT	Conduct. Trans	H	Electric Heater
FO	Fresh Oxidant	HW	Hot Water	PT	Pressure Trans.		
FR	Fresh Reactant	CW	Cooling Water	RPT	Redox Trans.		
				pHT	pH Trans.		

The self-priming electrically-controlled membrane pump P-WA (KNF Neuberger GmbH, Freiburg, Germany) primes the pre-treated waste acid solution (WA, labelled WAS in Chapter 4) thorough the DD module. The feed side of the DD module is flushed vertically against gravity from the bottom to the top. In the opposite side, a draw solution, which is a mixture of slightly acidic recovered water (RW2, labelled DS in Chapter 4) and softened fresh water (FW), is sucked from the P-RA pump (KNF Neuberger GmbH, Freiburg, Germany), flowing from top to bottom thus realizing a countercurrent arrangement in the DD unit. The free acid permeates through the anion exchange membranes from the feed to the draw solution thanks to the concentration gradient, while the membrane predominantly rejects the metal ions. As a consequence, the feed solution loses its acid concentration and increases the metals ions concentration when exiting the DD module (WA2, labelled MRB in Chapter 4), while the diffusate solution exits the module with an increased acid concentration (RA1, labelled RAS in Chapter 4) and some metal ions, which have overcome the membrane rejection capacity.

The recovered acid stream RA1 is pumped from P-RA into the feed channel of the MD module, in which water is extracted by the thermally driven evaporation process, thus a concentrated acid stream (RA2, labelled RPS in Chapter 4) is obtained. The driving force for the process is related to the temperature difference across the membrane, which is guaranteed by a heat-transfer fluid flowing in the thermostatic line (T), consisting in softened tap water recirculating in a closed loop by a controlled centrifugal pump P-T (Iwaki Europe GmbH, Willich, Germany).

The thermostatic line allows to cool-down one side of the MD module and heat-up the other one, being itself heated/cooled by the two service heat exchangers, HX-T1 and HX-T2 (Kelvion, Bochum, Germany), respectively. An electrical heater H-T (Siekerkotte, Herford, Germany) is also included in the hydraulic circuit as “emergency” heater to be used when waste heat is not available. Due to the water extraction in the MD module, the acidic stream is concentrated leaving the MD-module on the top side, from which it can be recirculated to the pickling bath following an adjustment with make-up hydrochloric acid (at 34% w/w). By varying temperature and flow rates in the MD-module. Finally, the water vapour extracted condenses on the cold surface of the air gap channel of the module and is cycled back as recovered water (RW1, labelled *Perm* in Chapter 4) into polypropylene (PP) product water tank (Horst Fischer GmbH, Freiburg, Germany). Due to the partially volatile behaviour of HCl, a relevant acid drag over into the extracted product water is also observed.

The metals rich brine (WAS2, labelled MRB in Chapter 4) exiting from the DD process is fed into the crystallizer (CSTR). The iron II in solution ($FeCl_2$) is oxidized to iron III ($FeCl_3$) by the addition of hydrogen peroxide (FO, labelled *ox* in Chapter 4) via dosing pump P-FO (KNF Neuberger GmbH, Freiburg, Germany), operated with an accurate control of the redox potential in the tank. Simultaneously, the reactive precipitation of $Fe(OH)_3$ is induced by the addition of ammonium hydroxide solution (FR, labelled *alk* in Chapter 4) via dosing pump P-FR (KNF Neuberger GmbH, Freiburg, Germany)), producing a $Fe(OH)_3$ slurry in the CSTR tank, by controlling the solution pH. Since the oxidation of $FeCl_2$ is exothermal, the slurry is recirculated through polyethylene (PE) tube bundle heat exchanger HX-S (Calorplast, Krefeld, Germany) via a pneumatic membrane pump P-S (Jessberger GmbH, Ottobrunn, Germany), allowing the continuous cooling of the crystallizer. Zinc ions remain in solution together with ammonium chlorides, due to their higher precipitation pH value (in the form of zinc hydroxide). Solids are separated from the slurry via filtration, and the filtered solution can be reused in the pickling process within the fluxing bath, where a zinc/ammonium chloride solution is used. Conversely, the separated solid particles of $Fe(OH)_3$ are dried and sold to the market.

The plant energy sustainability is achieved also by using the waste heat as primary energy source for the MD process. The plant is connected hydraulically to the local heating water network (HW), which is fed from available waste heat originating from the hot zinc bath.

The cooling requirements for the MD process as well as for the exothermic reactions in the CSTR, are guaranteed via the cooling water (CW) loop, which discard excess heat via a PP-lined aluminium coil placed inside the scrubber unit of the industrial plant.

For the acid piping, fluoropolymers PFA material from EM-Technik (Maxdorf, Germany) was chosen.

The total footprint of the demonstrator plant is 2.4x1.4 m^2 (with a height of 2.1 m). The resulting weight is 1.5 tons when empty, while when full of liquid up to 1.8 tons.

The overall system design relies on a mobile compact design. The system engineering has been done based from Fraunhofer partner on CAD modeling using AutoDesk Inventor. The following graph in Figure 5-2 gives an overview on the system design and packaging, including the labelling of the main components.

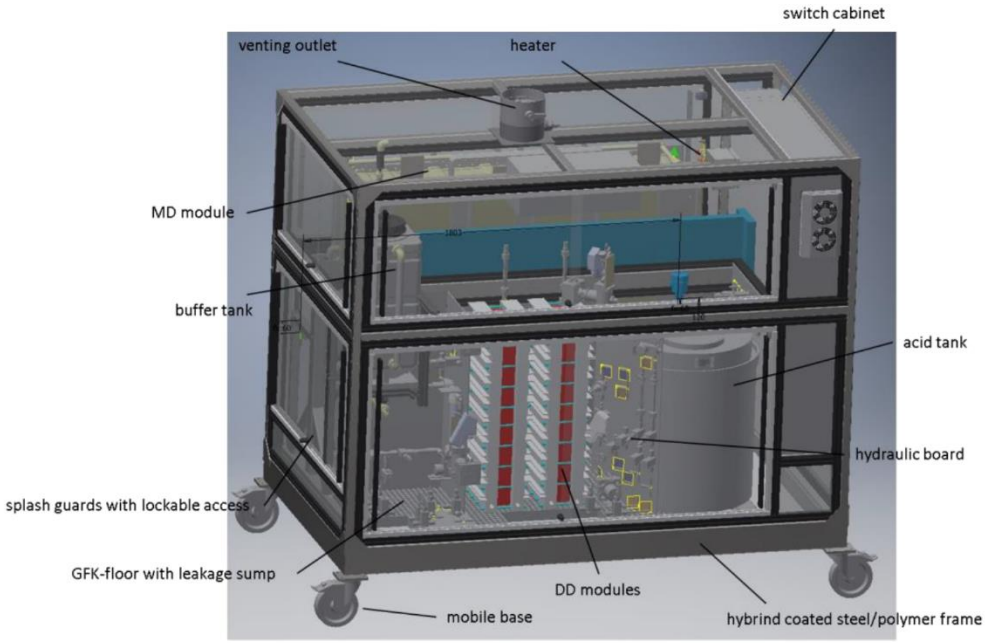

Figure 5-2 CAD drawing of a complete demonstrator system.

In Figure 5-3, two pictures of the demonstrator in the industrial environment are shown.

Figure 5-3 Demonstrator unit installed on the first floor at Tecnozinco hot-dip galvanizing plant (Carini (PA), Italy).

Every sections of the pilot plant and all auxiliary part necessary for the pilot operation are described in the next paragraphs.

5.2.1 *Pre-Treatment Section*

A pre-treatment step is required for the Tecnozinco pickling liquor. The objectives are:

- Filtration of particles until a size of 5 μm
- Removal of oil (0.4 -1 g/l)
- Removal of surfactants (0.3 – 0.5 g/l)

In fact, in Tecnozinco plant surfactants and oils are in the solution dragged from the degreasing tank with the manufactured steel transport. Furthermore, a corrosion inhibitor mix containing surfactants is introduced directly in the pickling tank.

The surfactants dissolved in solution are non-ionic surfactants, specifically alcohols and amines ethoxylated characterized by long chains C9-C30. It was demonstrated that surfactants strongly attack the membranes. DD lab test-rig experiments were carried out to observe surfactants transport trough the membranes. It was observed that surfactants do not pass through the anionic exchange membrane, even though they severally damage the membrane at extended exposure.

As oil and surfactants are joined forming micelles [125], a breaking micelles step is necessary.

Thus, the pre-treatment step is a combination of a heated oil separator and an activated carbon filter (see Figure 5-4).

Figure 5-4 Pre-treatment section: (on the left) heated oil separator and (on the right) activated carbon filter.

The desolator is heated up to 50°C to facilitate the micelles breaking and the oil phase stratification, which therefore thickens in the upper area where it is removed through weirs systems. Thus, the de-oiled solution is directly fed in the tank containing activated carbon filters for the surfactants removal [126].

Filtration is accomplished through a cartridge filter chain connected to the waste acid line, one placed in the external part of the pilot (100 μm), the other two included in the pilot system of 35 μm and 5 μm filters, respectively.

5.2.2 *Core Processes*

The main processes were widely described and discussed in the previously chapters. Here detailed features of the unit employed in the demonstrator unit are presented.

5.2.2.1 Diffusion Dialysis pilot unit

The DD was designed and manufactured by DEUKUM GmbH (Frickenhausen, Germany). Detailed DD module characteristics are reported in Table 5-2.

Table 5-2 Technical data of the Deukum DD pilot modules.

Process	Technical specifications	
DD (DEUKUM)	Membrane	Fumasep FAD PET-75
	N° membranes	94
	Channel length	0.8 m
	Channel width	0.2 m
	Channel thickness	270 μm
	Total membrane area	15 m^2
	Residence time	7 min

Figure 5-5 shows the DD unit position in the demonstrator plant.

The module has a plate and frame configuration, with alternating layers of membranes and spacers. The stack is framed by an end plate on either side that are equipped with inlet and outlet manifolds. In total 94 Fumasep type FAD PET-75 anion exchange membranes from Fumatech GmbH are separated by spacers to form a stack with a total membrane area of 15 m^2. For the AEM properties refers to Table 2-2. The nominal flow for the module is 20 l/h. Taking into account the channel dimensions this leads to a flow velocity of 2 mm/s.

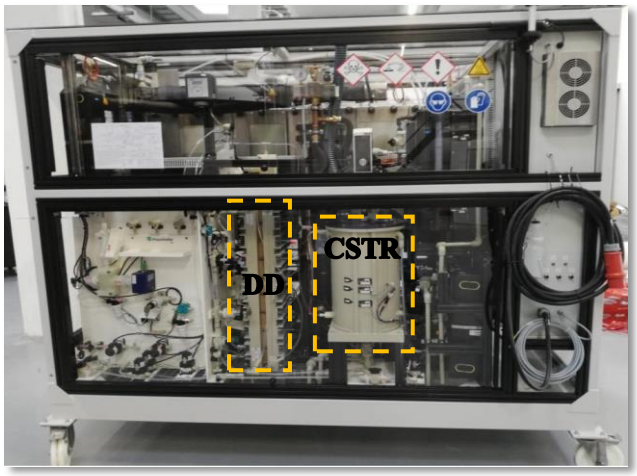

Figure 5-5 Front view of the demonstrator plant. DD and CSTR units are marked with a yellow rectangle.

5.2.2.2 Membrane Distillation pilot unit

The MD module has a plate and frame configuration with a feed gap/air gap configuration (FGAGMD [124]. Technical specification of the MD module (Solar Spring GmbH, Freiburg, Germany) are reported in Table 5-3.

Table 5-3 Technical data of the Solar Spring MD pilot modules.

Process	Technical specifications	
MD	Membrane	L-020A-S (Gore)
	N° parallel stages	2
	Thickness of polymer film	100 μm
	Channel length	4.32 m
	Channel width	0.72 m
	Feed/Distillate channel thickness	0.002 m
	Heater/Cooler channel thickness	0.004 m
	Heating/Cooling demand	6 kW
	Thermostat flow rate	300 - 500 l/h
	Feed flow rate	< 50 l/h
	Total membrane area	6.22 m^2
	Residence time	45 min

The MD module consists of two parallel FGAG stages with channels 0.72 m wide and 4.32 m long. This leads to a total membrane area of 6.22 m^2.

A design drawing of the MD unit module is reported in Figure 5-6.

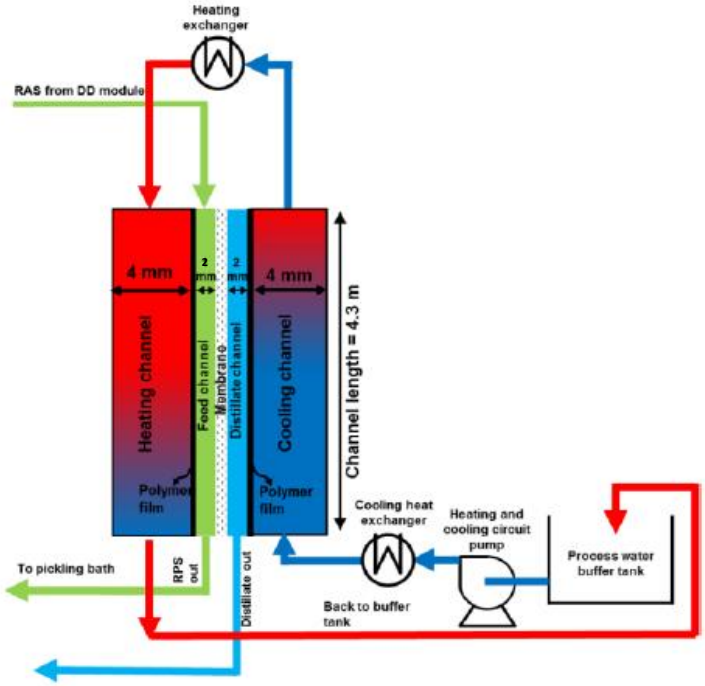

Figure 5-6 Design drawing of the MD module.

In this particular configuration, the heating and feed solution transport are separated. The feed solution channel sits between this heating channel and the membrane and is separated by an impermeable film. When the feed solution enters the module and is not already hot, it takes up heat quickly through the thin film, since the flow of the feed is much smaller and slower than that of the heating channel. Additionally, separating the feed solution from the heating gives the opportunity of having a separate thermostat circle (see Figure 5-6). In this way, heat exchangers and other sensible components are separated from potentially aggressive or dangerous feed solutions. It is worth noting that thanks to the proposed MD module design, the continuous supply of heat from the heater channel allows to enhance the amount of vapour generated per single passage of feed solution, thus overtaking the typical limitation of

Permeate Gap MD modules, i.e. the low value of recovery due to the small amount of sensible heat available with the feed stream to generate the passage of vapour.

A ePTFE commercial membrane product from W. L. Gore & Associates was chosen. It is a flat sheet membrane "M-020A" laminated "L" on a polypropylene scrim backing "S". The technical specifications, in terms of d nominal pore size, δ thickness and ε volumetric porosity, in Table 5-4 were provided by Gore.

Table 5-4 Specifications of MD membrane materials [66].

membrane backing type		d_m [μm]	δ_m [μm]	ε_m [%]
M-020A	none	0.20	70	80
laminate backing type		d_m [μm]	δ^a [μm]	ε_m [%]
L-020A-S	scrim	0.20	350	80

[m]membrane
[a]membrane and backing

In Figure 5-7 a picture of the back view of the demonstrator plant is reported in which the pilot MD unit highlighted.

Figure 5-7 Back view of the demonstrator plant. MD unit is marked with a yellow rectangle.

5.2.2.3 Precipitate reactor pilot unit

Features of the pilot reactor are reported in Table 5-5, while a picture of the integrated unit in the demonstrator system is shown in Figure 5-8.

Table 5-5 Technical data of the CSTR pilot unit.

Process	Technical specifications	
CSTR	Material	PP
	Reactor height	0.4 m
	Maximum liquid level	0.35 m
	Reactor diameter	0.3 m
	Paddle diameter	0.2 m
	Capacity	25 l
	Cooling demand	1.5 kW
	Impeller rotation speed	400 rpm
	Residence time	45 min

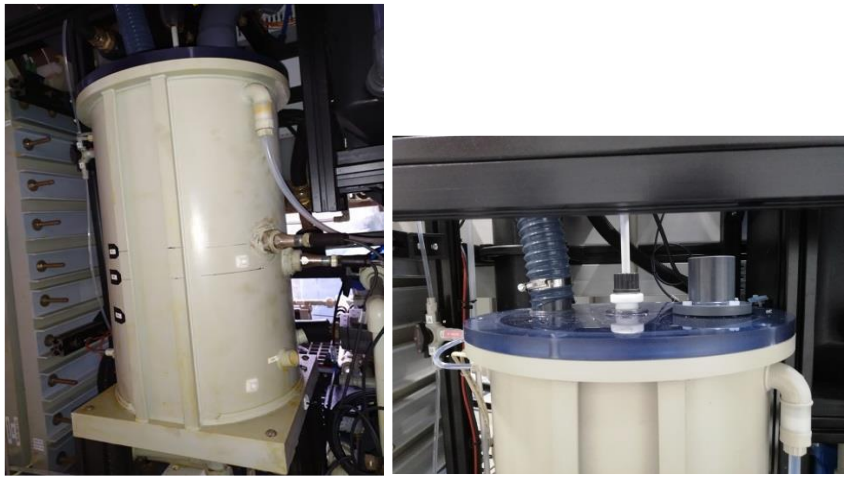

Figure 5-8 Polypropylene CSTR unit equipped with frequency sweep level sensors (on the left) and cover with ventilation access (on the right).

The reactor is connected to venting system of the unit, which was purposely design to avoid the accumulation of harmful gases/vapours (e.g. ammonia, HCl) or the formation of harmful condensates from the vapours in the plant. The venting system includes the venting

of the main plant volume via the central venting hub as well as the separate venting of the CSTR (see picture on the right of Figure 5-8).

The original tank reactor was equipped with three capacitive proximity binary level switches in order to automatically monitoring the tank level (see Figure 5-5). Only the level switch at highest position (LT-CSTR1) and lowest position (LT-CSTR3) fulfil a high level and low level monitoring that initiates a “Software Shutdown” if triggered. The signal of the remaining level switch (LT-CSTR2) is used for the tank level monitoring The CSTR partial draining operation is discontinuously and it is carried out with pump P-S into the outlet OUT-S2 (see Figure 5-9). It is initiated when the filling level exceeds LT-CSTR1, emptying procedure stops when filling level drops under LT-CSTR2.

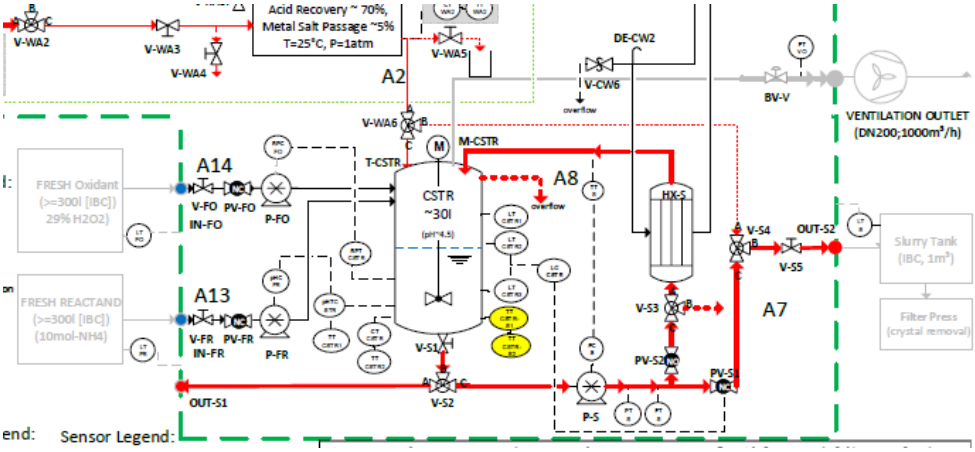

Figure 5-9 Extract of the P&I highlighting the CSTR unit and the cooling circulation.

However, the high viscosity and the sticky nature of the slurry, which sticks on the wall of the CSTR tank, distort the sensor measures by continuously shutting the system down. Different level sensors were hydraulically integrated in the tank (see Figure 5-8). These optimized sensors, based on frequency sweep technologies, are electrically similar, so no change in the software was required. They can be configured to adjust sensitivity and switching type on site, so they are going to work also for any modification of the slurry product specifications.

Cooling Circulation of the CSTR is mandatory to avoid the temperature to rise during the exothermal chemical reactions, thus the circulation of the slurry via heat exchanger HX-S for cooling is always active, if CSTR unit is in operation.

The slurry with a maximum flow rate of 350 kg/h and a maximum temperature of 40 °C is fed into the exchanger on the tube side, while cooling water is fed to the shell side with a maximum flow rate of 800 kg/h and a temperature of 25 ° C. The heat that is subtracted from the slurry is about 1.5 kW. The heat exchanger has 30 pipes with a length of 0.83 m and an external diameter of 1 cm, therefore an exchange area of 0.79 m^2, while the shell has an external diameter of 11 cm.

5.2.3 *Post treatment section*

A filter-press unit is directly connected to the slurry tank for the filtration of the CSTR product. Solid iron hydroxide is separated from the liquid phase. It is a Tecnozinco filter-press unit, already present in the industrial plant (Figure 5-10).

Figure 5-10 Press filter for the iron hydroxide separation.

5.2.4 *Utilities*

5.2.4.1 Hot water and cooling water supply loops

The plant's energy sustainability is achieved by using the waste heat as required energy source for the thermal MD process. The plant is connected to the local heating water network. A hydraulic decoupling by the heat exchanger gives hydraulic independence of the pressure

sensitive thermostat loop (e.g. thin film materials in the MD module) from the fluid loop on the industrial site mainly to avoid the carryover of contamination or critical pressures to any side. The heat supply is controlled by controlling the hot water flow with a motor valve.

Similar strategy is followed for the application of the cooling power in the cold water loop. As concern the water cooling, several options were evaluated. At first, a small open circuit cooling tower was designed. Ceramic Berl-saddle with a diameter of 38 mm was selected as packing material. By considering the specific area and porosity degree of this latter material, and taking into account typical atmospheric condition in Sicily, a tower of 1.5x1.5 m^2 (length x diameter) was designed (Figure 5-11). The small size of the tower would not allow realizing a natural draft so a forced air convection system had to be considered. For this reason, this option was not considered as a valid and economically advantageous one.

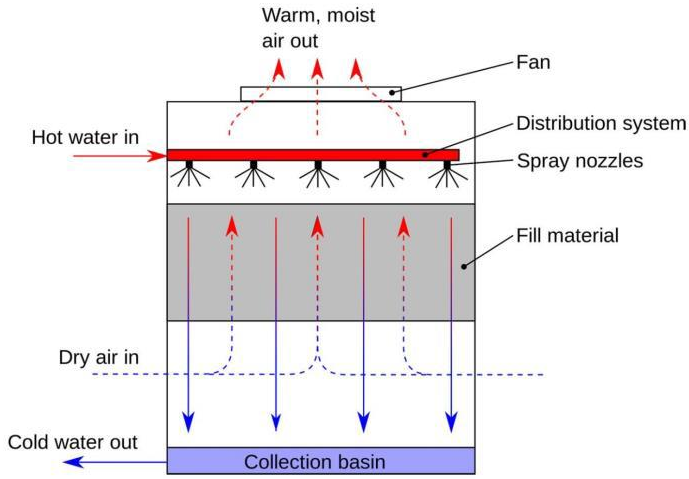

Figure 5-11 Schematic representation of an open circuit cooling tower.

Therefore, the design of evaporating plates to be placed on the industrial site next to the pilot system was carried out. However, the proposed design considers the combination of two 3x3 m^2 plates and a ventilation system. The simulations reported on Figure 5-12 show that reaching the suitable cooling ($T_{water}^{out} = 25°C$), high velocity values of the air have to be considered. This option results of complex installation and economically not advantageous, here too.

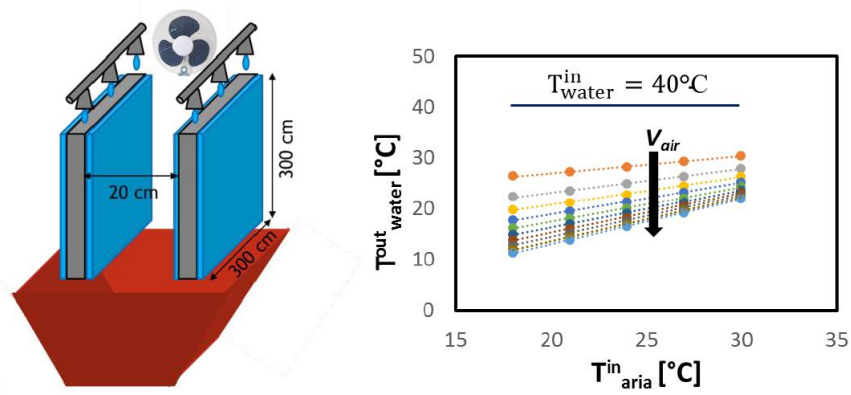

Figure 5-12 Schematic representation of an evaporating plates pair (on the left) and an analysis of the cooled water temperature at different air conditions (temperature and velocity) (on the right).

The final option, eventually selected for implementation, exploits the cooling capacity available in the industrial site and consisting in placing a cooling coil inside the scrubber unit. For the design of the cooling coil, the combination of heat convection (due to air the ventilation) and jet water cooling (which laps the outer surface of the pipes) was taken into account. According to nominal design conditions, it was possible to obtain the required cooling considering a coil length of 200 m and a total exchange area of 12 m^2 (Figure 5-13). This configuration breaks down the overall costs for the cooling operation; it only requires the use of a water circulation pump.

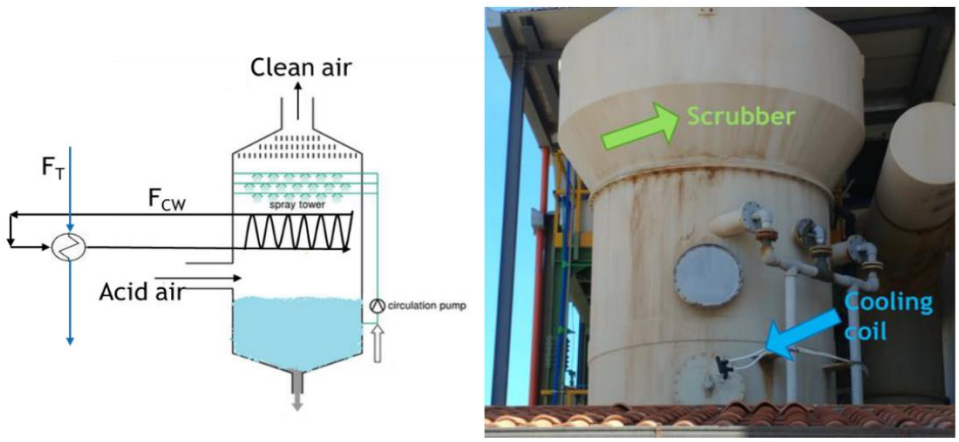

Figure 5-13 Cooling coil placed inside the scrubber unit of the Tecnozinco srl.

5.2.4.2 Fresh water loop

The water consumption as draw solution for the DD diffusate stream (RW2) is higher than the recovered water of the MD-module (RW1), thus the filling level of the tank water T-RW is maintained discontinuously through the fresh water dosing line FW. The fresh water is pre-treated by a water softener to get rid of carbonates.

The water tank is equipped with 4 binary level switches (2 upper, 2 lower). The functionality of the tank management relies on the positioning of the level switches. Filling from the fresh water line IN-FW if the filling level drops lower than LT-RW3; filling procedure stops when filling level reaches LT-RW2 while only the level switch at highest position (LT-RW1) and lowest position (LT-RW4) fulfil a high level and low level monitoring that initiates a “Software Shutdown” if triggered.

5.3 **Data acquisition, Control and Safety Features**

5.3.1 *Data acquisition and monitoring system*

In order to gain a maximum of scientific value, the monitoring was designed to gain information on fluid state and composition on all positions of relevance, which in the main acid streams can be specified as the positions before and after each membrane treatment step on feed and product side. Furthermore, the temperature and pressure sensor values allows the evaluation of the thermal energy demand and the pumping demand. The individual sensor positioning within the system is shown in the detailed in the P&I reported at the end of this Chapter in Figure 5-16, and developed by Fraunhofer ISE project partner.

The samples are mainly used for the analysis of chemical composition (concentrations) and to support sensor values or provide further info where sensors provide controversial results or are not applicable. Hence, they are taken behind sensors or sensor blocks of the corresponding sensor.

The plant has a data recording and storage system that transcribes the values measured by the sensors during the operation into text files. Every 10 seconds the system records values from the sensors and saves them into a separate file for each sensor. These files are stored on a USB stick for later use. Multi-files structure of the different sensors is converted into a single

comprehensive file that contains all data collected during one day of operation (see Figure 5-14).

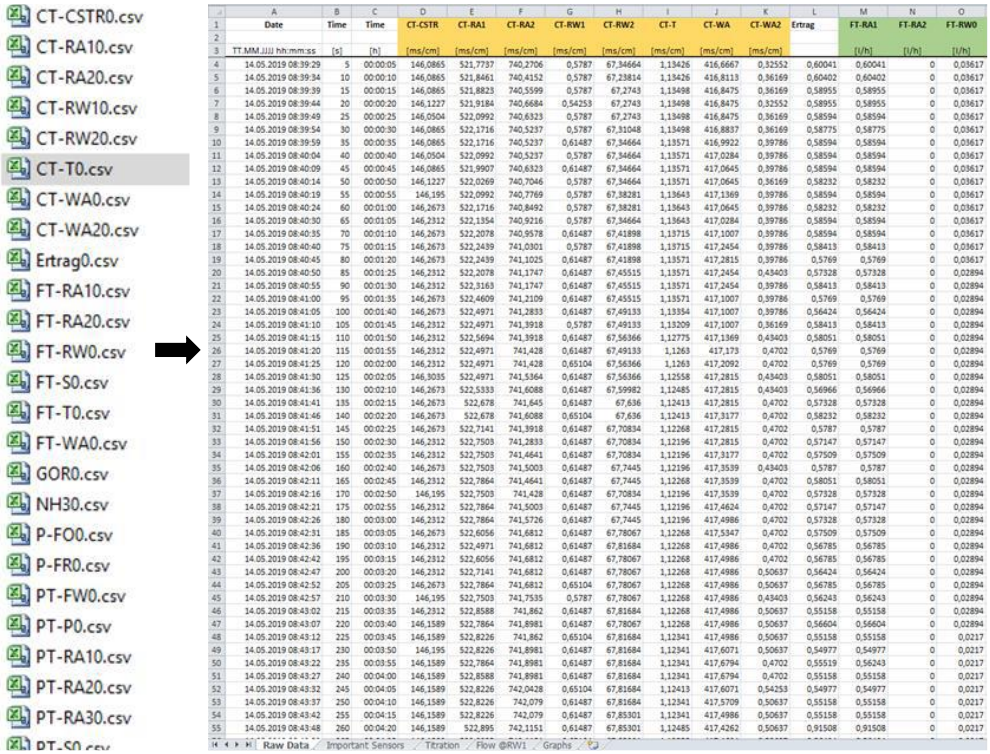

	A	B	C	D	E	F	G	H	I	J	K	L	M	N	O
1	Date	Time	Time	CT-CSTR	CT-RA1	CT-RA2	CT-RW1	CT-RW2	CT-T	CT-WA	CT-WA2	Ertrag	FT-RA1	FT-RA2	FT-RW0
2															
3	TT.MM.JJJJ hh:mm:ss	[s]	[h]	[ms/cm]	[ms/cm]	[ms/cm]	[ms/cm]	[ms/cm]	[ms/cm]	[ms/cm]	[ms/cm]		[l/h]	[l/h]	[l/h]
4	14.05.2019 08:39:29	5	00:00:05	146,0865	521,7737	740,2706	0,5787	67,34664	1,13426	416,6667	0,32552	0,60041	0,60041	0	0,03617
5	14.05.2019 08:39:34	10	00:00:10	146,0865	521,8461	740,4152	0,5787	67,23814	1,13426	416,8113	0,36169	0,60402	0,60402	0	0,03617
6	14.05.2019 08:39:39	15	00:00:15	146,0865	521,8823	740,5599	0,5787	67,2743	1,13498	416,8475	0,36169	0,58955	0,58955	0	0,03617
7	14.05.2019 08:39:44	20	00:00:20	146,1227	521,9184	740,6684	0,54253	67,2743	1,13498	416,8475	0,32552	0,58955	0,58955	0	0,03617
8	14.05.2019 08:39:49	25	00:00:25	146,0504	522,0992	740,6323	0,5787	67,2743	1,13498	416,8475	0,36169	0,58594	0,58594	0	0,03617
9	14.05.2019 08:39:54	30	00:00:30	146,0865	522,1716	740,5237	0,5787	67,31048	1,13498	416,8837	0,36169	0,58775	0,58775	0	0,03617
10	14.05.2019 08:39:59	35	00:00:35	146,0865	522,1716	740,5237	0,61487	67,34664	1,13571	416,9922	0,39786	0,58594	0,58594	0	0,03617
11	14.05.2019 08:40:04	40	00:00:40	146,0504	522,0992	740,5237	0,5787	67,34664	1,13571	417,0284	0,39786	0,58594	0,58594	0	0,03617
12	14.05.2019 08:40:09	45	00:00:45	146,0865	521,9907	740,6323	0,61487	67,34664	1,13571	417,0645	0,39786	0,58594	0,58594	0	0,03617
13	14.05.2019 08:40:14	50	00:00:50	146,1227	522,0269	740,7046	0,5787	67,34664	1,13571	417,0645	0,36169	0,58232	0,58232	0	0,03617
14	14.05.2019 08:40:19	55	00:00:55	146,195	522,0992	740,7769	0,5787	67,38281	1,13643	417,1369	0,39786	0,58594	0,58594	0	0,03617
15	14.05.2019 08:40:24	60	00:01:00	146,2673	522,1716	740,8492	0,5787	67,38281	1,13643	417,0645	0,39786	0,58232	0,58232	0	0,03617
16	14.05.2019 08:40:30	65	00:01:05	146,2312	522,1354	740,9216	0,5787	67,34664	1,13643	417,0284	0,39786	0,58594	0,58594	0	0,03617
17	14.05.2019 08:40:35	70	00:01:10	146,2673	522,2078	740,9578	0,61487	67,41898	1,13715	417,1007	0,39786	0,58594	0,58594	0	0,03617
18	14.05.2019 08:40:40	75	00:01:15	146,2673	522,2439	741,0301	0,5787	67,41898	1,13715	417,2454	0,39786	0,58413	0,58413	0	0,03617
19	14.05.2019 08:40:45	80	00:01:20	146,2673	522,2439	741,1025	0,61487	67,41898	1,13571	417,2815	0,39786	0,5769	0,5769	0	0,03617
20	14.05.2019 08:40:50	85	00:01:25	146,2312	522,2078	741,1747	0,61487	67,45515	1,13571	417,2454	0,43403	0,57328	0,57328	0	0,02894
21	14.05.2019 08:40:55	90	00:01:30	146,2312	522,3163	741,1747	0,61487	67,45515	1,13571	417,2454	0,39786	0,58413	0,58413	0	0,02894
22	14.05.2019 08:41:00	95	00:01:35	146,2673	522,4609	741,2109	0,61487	67,45515	1,13571	417,1007	0,39786	0,5769	0,5769	0	0,02894
23	14.05.2019 08:41:05	100	00:01:40	146,2673	522,4971	741,2833	0,61487	67,49133	1,13354	417,1007	0,39786	0,56424	0,56424	0	0,02894
24	14.05.2019 08:41:10	105	00:01:45	146,2312	522,4971	741,3918	0,5787	67,49133	1,13209	417,1007	0,36169	0,58413	0,58413	0	0,02894
25	14.05.2019 08:41:15	110	00:01:50	146,2312	522,5694	741,3918	0,61487	67,56366	1,12775	417,1369	0,43403	0,58051	0,58051	0	0,02894
26	14.05.2019 08:41:20	115	00:01:55	146,2312	522,4971	741,428	0,61487	67,49133	1,1263	417,173	0,4702	0,5769	0,5769	0	0,02894
27	14.05.2019 08:41:25	120	00:02:00	146,2312	522,4971	741,428	0,65104	67,56366	1,1263	417,2092	0,4702	0,5769	0,5769	0	0,02894
28	14.05.2019 08:41:30	125	00:02:05	146,3035	522,4971	741,5364	0,61487	67,56366	1,12558	417,2815	0,43403	0,58051	0,58051	0	0,02894
29	14.05.2019 08:41:36	130	00:02:10	146,2673	522,5333	741,6088	0,61487	67,59982	1,12485	417,2815	0,43403	0,56966	0,56966	0	0,02894
30	14.05.2019 08:41:41	135	00:02:15	146,2673	522,678	741,645	0,61487	67,636	1,12413	417,2815	0,4702	0,57328	0,57328	0	0,02894
31	14.05.2019 08:41:46	140	00:02:20	146,2673	522,678	741,6088	0,65104	67,636	1,12413	417,3177	0,4702	0,58232	0,58232	0	0,02894
32	14.05.2019 08:41:51	145	00:02:25	146,2673	522,7141	741,3918	0,61487	67,70834	1,12268	417,2815	0,4702	0,5787	0,5787	0	0,02894
33	14.05.2019 08:41:56	150	00:02:30	146,2312	522,7503	741,2833	0,61487	67,70834	1,12196	417,2815	0,4702	0,57147	0,57147	0	0,02894
34	14.05.2019 08:42:01	155	00:02:35	146,2312	522,7503	741,4641	0,61487	67,70834	1,12196	417,3177	0,4702	0,57509	0,57509	0	0,02894
35	14.05.2019 08:42:06	160	00:02:40	146,2673	522,7503	741,5003	0,61487	67,7445	1,12196	417,3539	0,43403	0,5787	0,5787	0	0,02894
36	14.05.2019 08:42:11	165	00:02:45	146,2312	522,7864	741,4641	0,61487	67,7445	1,12268	417,3539	0,4702	0,58051	0,58051	0	0,02894
37	14.05.2019 08:42:16	170	00:02:50	146,195	522,7503	741,428	0,61487	67,70834	1,12196	417,3539	0,4702	0,57328	0,57328	0	0,02894
38	14.05.2019 08:42:21	175	00:02:55	146,2312	522,7864	741,5003	0,61487	67,7445	1,12196	417,4624	0,4702	0,57147	0,57147	0	0,02894
39	14.05.2019 08:42:26	180	00:03:00	146,2312	522,7864	741,5726	0,61487	67,7445	1,12196	417,4986	0,4702	0,57328	0,57328	0	0,02894
40	14.05.2019 08:42:31	185	00:03:05	146,2673	522,6056	741,6812	0,61487	67,78067	1,12268	417,5347	0,4702	0,57509	0,57509	0	0,02894
41	14.05.2019 08:42:36	190	00:03:10	146,2312	522,4971	741,6812	0,61487	67,81684	1,12268	417,4986	0,4702	0,56785	0,56785	0	0,02894
42	14.05.2019 08:42:42	195	00:03:15	146,2312	522,6056	741,6812	0,61487	67,78067	1,12268	417,4986	0,4702	0,56785	0,56785	0	0,02894
43	14.05.2019 08:42:47	200	00:03:20	146,2312	522,7141	741,6812	0,61487	67,78067	1,12268	417,4986	0,50637	0,56424	0,56424	0	0,02894
44	14.05.2019 08:42:52	205	00:03:25	146,2673	522,7864	741,6812	0,65104	67,78067	1,12268	417,4986	0,50637	0,56785	0,56785	0	0,02894
45	14.05.2019 08:42:57	210	00:03:30	146,195	522,7503	741,7535	0,5787	67,78067	1,12268	417,4986	0,43403	0,56243	0,56243	0	0,02894
46	14.05.2019 08:43:02	215	00:03:35	146,2312	522,8588	741,862	0,61487	67,81684	1,12268	417,4986	0,50637	0,55158	0,55158	0	0,02894
47	14.05.2019 08:43:07	220	00:03:40	146,1589	522,7864	741,8981	0,61487	67,78067	1,12268	417,4986	0,50637	0,56604	0,56604	0	0,02894
48	14.05.2019 08:43:12	225	00:03:45	146,1589	522,8226	741,862	0,65104	67,81684	1,12341	417,4986	0,50637	0,55158	0,55158	0	0,0217
49	14.05.2019 08:43:17	230	00:03:50	146,195	522,8226	741,8981	0,61487	67,81684	1,12341	417,6071	0,50637	0,54977	0,54977	0	0,0217
50	14.05.2019 08:43:22	235	00:03:55	146,1589	522,7864	741,8981	0,61487	67,81684	1,12341	417,6794	0,4702	0,55519	0,56243	0	0,0217
51	14.05.2019 08:43:27	240	00:04:00	146,1589	522,8588	741,8981	0,61487	67,81684	1,12341	417,6794	0,4702	0,55158	0,55158	0	0,0217
52	14.05.2019 08:43:32	245	00:04:05	146,1589	522,8226	742,0428	0,65104	67,81684	1,12413	417,6071	0,54253	0,54977	0,54977	0	0,0217
53	14.05.2019 08:43:37	250	00:04:10	146,1589	522,8226	742,079	0,61487	67,81684	1,12341	417,5709	0,50637	0,55158	0,55158	0	0,0217
54	14.05.2019 08:43:42	255	00:04:15	146,1589	522,8226	742,079	0,61487	67,85301	1,12341	417,4986	0,50637	0,55158	0,55158	0	0,0217
55	14.05.2019 08:43:48	260	00:04:20	146,1589	522,895	742,1151	0,61487	67,85301	1,12485	417,4262	0,50637	0,91508	0,91508	0	0,0217

Figure 5-14 Fully automated conversion of the PLC multi file data structure into a structured single file.

5.3.2 *Control system*

The system controls need to provide defined and safe state of operation for every individual flow stream. To do so, actors are required to actively manipulate the state of operation on request. In order to end up with a comprehensive system control strategy also allowing the actuation of safety measures, it was decided that all actors are to be controlled by a central control system. The design and implementation of the control system was performed by Fraunhofer ISE staff, although supported by myself as concern the DD and reactor CSTR control design.

For the implementation of the central process control, an industrial standard PLC “programmable logic controller” was chosen in order to achieve a maximum level of process reliability and robustness. In addition, the potential communication with other PLC systems on the industrial sites is possible. A Siemens “S7 SIMATIC ET 200SP” was chosen, since these components represent the most common international standard for high grade control systems and may also be maintained on site by local stuff. The system represents a modular design and is configured with respective PLC-integrated loops.

The controlled actors may have either a digital or an analogue function. The control of the digital actors (e.g. membrane valves, stirrer) is simply realized by send a low or high voltage signal from the control system digital output ports. The control of the analogue controlled actors (e.g. variable speed pumps, motor valves, resistance heater) needs to rely on a control algorithm, which is implemented on the software. In this last case, a basic PID control is applied to derive the analogue signals on the analogue output ports of the control system. This PID controllers compare a user defined desired state (set point) which the actual value, read from the respective sensor, and calculates the signal values based on the error according to the well-known PID algorithm, taking into account a proportional, an integral and a differential part of the error.

The system is accessible via a touchscreen SIMATIC SIEMENS human-machine interface (HMI), located on the front panel of the demonstrator. The HMI is a graphical interface that provides information from the PLC to the operator (e.g. the actual state of operation and sensor and actor values, error messages, warnings etc.) and allows an operator to control and modify the state of the plant. Figure 5-15 exemplarily shows the process overview and sensors pages. System components like MD, DD and CSTR can be clicked on to open their respective page with settings and sensors values. Through the buttons on the bottom the user can jump to different pages like sensors overview, configuration page or a troubleshooting function.

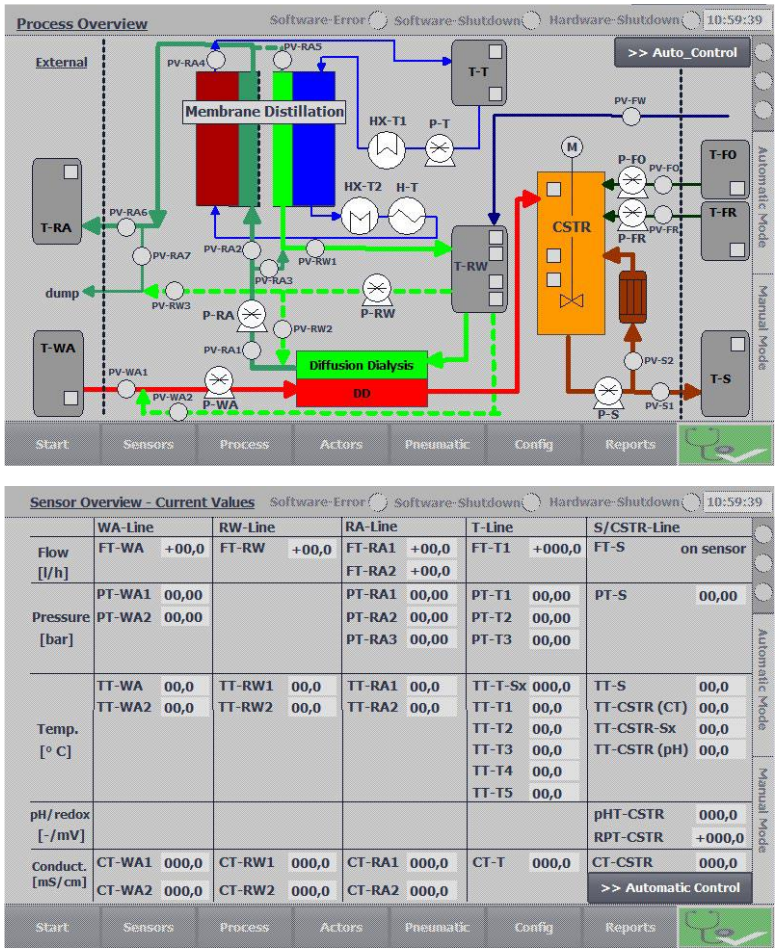

Figure 5-15 HMI Process overview page (on the top) and sensors page (on the bottom).

5.3.3 *Safety strategies*

In order to achieve a PLC independent and safety architecture, a hard-wired safety circuit is implemented, which is designed with self-checking, redundant, certified components in order to achieve a high level of functional safety. Thus, in addition to the "software shutdown" a "hardware shutdown" is implemented as well.

A safe "hardware shutdown" is initiated by four different mechanisms:

- manual actuation of the emergency shut-down button

- exceeding of the limiting temperature in the electrical heater H-T (MD thermostatic line)
- exceeding of the limiting temperature in the CSTR.

Finally, the complete P&I of the demonstrator is reported in Figure 5-16, showing all the parts included in the demonstrator area, the hydraulic interconnections, the positioning and the complete number of sensors, as well as the samples withdrawing access points.

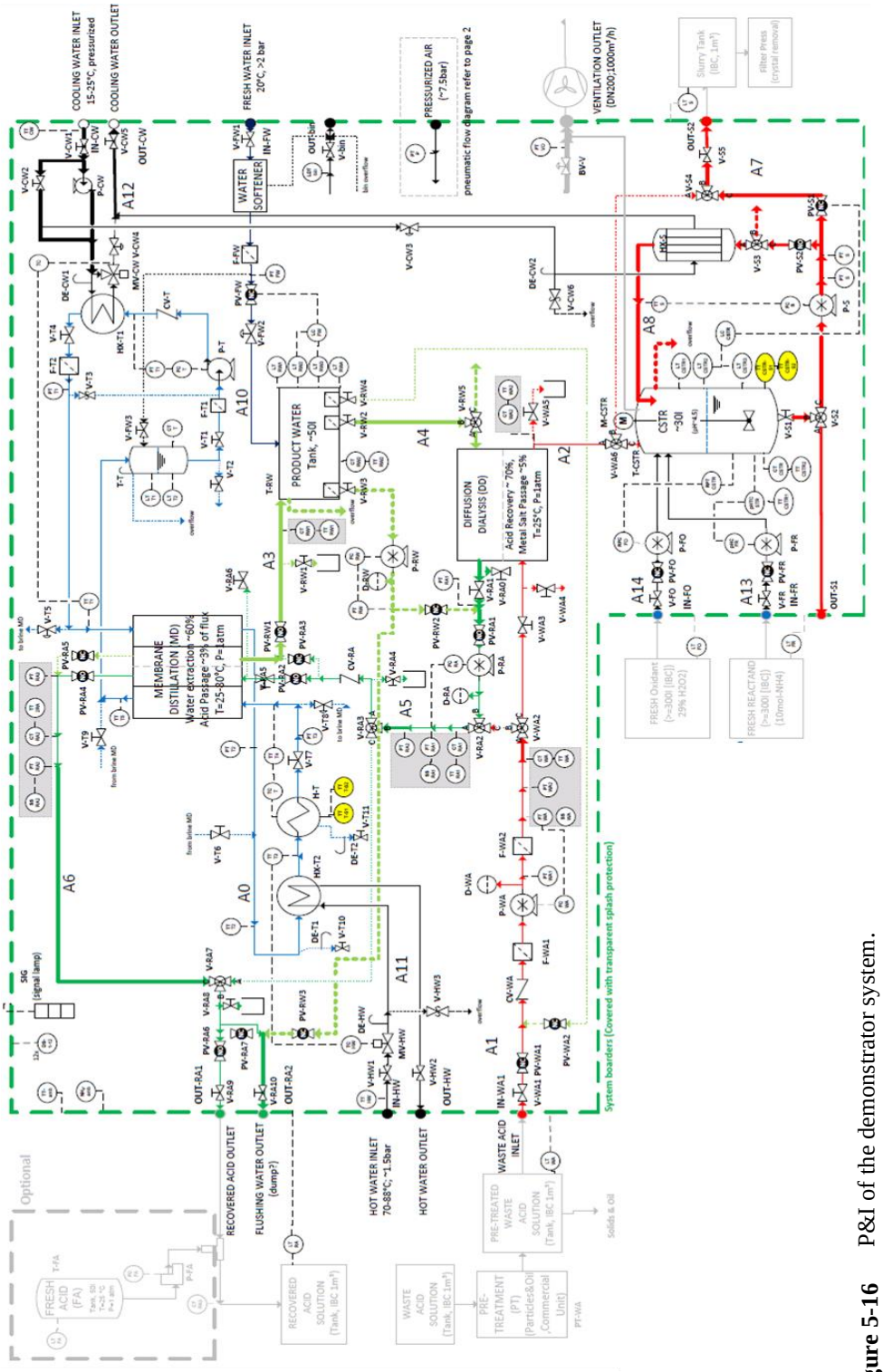

Figure 5-16 P&I of the demonstrator system.

6. PLANT OPERATION

Chapter Outline

Part of this chapter has been accepted for publication in:

"An integrated approach for the HCl and metals recovery from waste pickling solutions: pilot plant and design operations" R. Gueccia, D. Winter, S. Randazzo, A. Cipollina, J. Koschikowski G. Micale, accepted for publication in Chemical Engineering Research and Design

In the present Chapter, the challenge is proofing the continuous regeneration of the pickling bath and the optimal bath composition control by means of the testing and operation of the demonstrator pilot-scale plant installed and operated at the Tecnozinco) hot-dip galvanizing plant (Carini, PA, Italy.

It is worth noting that, in addition to the environmental friendly and low energy consumption aspects, the typical size of galvanizing plants fits perfectly with the size of Diffusion Dialysis and Membrane Distillation units so far available in the market, contrarily to other larger chemical plants, where membrane units scale-up is often unviable. Moreover, the flexibility and size-modularity [61] of membrane units represent another key advantage for adapting size and operating conditions to any specific galvanising plant requirements. Thus, the present pilot demonstrator study could be a very useful example for possible industrialisation analysis.

6.1 Operating procedure and performances parameters

Tests on the demonstrator system were conducted with a stepwise approach, by performing preliminary experiments with synthetic solution of HCl and then operating the system with real pickling liquors. The prepared solution underwent a simple filtration step with cartridge (10 µm) before being fed to the pilot process line. In a second stage, also pickling solutions from the real industrial baths were used after being treated through the demulsifier / oil separator and a subsequent activated carbon filter for the removal of surfactants and residual organics.

Results were processed and presented in terms of key performance indicators, as follows.

For the DD process, the acid recovery ratio (RR_{DD}) and metals leakage ($Metals\ Leakage_{DD}$) were monitored, each one already defined in Section 2.2.3 (Eqs. 2-5 and 2-6) and specified for the particular case as follow:

$$RR_{DD}(\%) = \frac{F_{RA1} \cdot c_{HCl,RA1} - F_{RW2} \cdot c_{HCl,RW2}}{F_{WA} \cdot c_{HCl,WA}} \times 100 \qquad 6\text{-}1$$

$$Metals\ \ Leakage_{DD}(\%) = \frac{F_{RA1} \cdot c_{(Fe;Zn),RA1} - F_{RW2} \cdot c_{(Fe;Zn),RW2}}{F_{WA} \cdot c_{(Fe;Zn),WA}} \times 100 \qquad 6\text{-}2$$

where F is the volumetric flow rate, c the bulk concentration of the acid and metals components; RA1, RW2 and WA subscripts stand for recovered acid from DD, recovered water; and waste acid, respectively.

MD performances are assessed through the Gain Output Ratio (GOR), the acid drag over ($Acid\ drag\ over_{MD}$), the permeate flux (*RW1 flux*) and the conversion ratio (*CR*).

GOR, identifying the thermal efficiency of the evaporative process, is defined as:

$$GOR = \frac{F_{RW1} \cdot \rho_{water} \cdot \Delta h_v \cdot 1000}{\dot{Q}_{heat}} \quad 6\text{-}3$$

where RW1 subscript stands for water vapor extracted from MD, Δh_v(=2257 kJ/kg) [127] is the enthalpy of evaporation, ρ_{water}=997 kg m^{-3} and $\dot{Q}_{heat}$ is the heating power, calculated as:

$$\dot{Q}_{heat} = F_T \cdot cp \cdot (T_{T4} - T_{T2}) \quad 6\text{-}4$$

with cp (=4.19 kJ/kg/K) [128] being the specific heat, $(T_{T4} - T_{T2})$ the temperature difference between condenser outlet and evaporator inlet and T subscript the thermostatic fluid.

The GOR can be read also as a measure of the thermal integration of the system as it shows the ratio between the energy required for the permeate evaporation and the energy supplied externally ideally in the form of saturated condensing vapor.

The acid drag over ($Acid\ drag\ over_{MD}$), the permeate flux ($RW1\ flux$) and the conversion ratio (*ConversionRatio*) are defined as:

$$Acid\ drag\ over_{MD}(\%) = \frac{F_{RW1} \cdot c_{HCl,RW1}}{F_{RA1} \cdot c_{HCl,RA1}} \times 100 \quad 6\text{-}5$$

$$RW1\ flux = \frac{F_{RW1}}{A_{MD}} \quad 6\text{-}6$$

$$ConversionRatio\ (\%) = \frac{F_{RW1}}{F_{RA1}} \times 100 \quad 6\text{-}7$$

where A_{MD} is the effective MD membrane area.

Finally, CSTR performance was assessed by the measure of solid $Fe(OH)_3$ purity:

$$Fe(OH)_3\ purity(\%) = \frac{mass_{Fe}^{analysis}}{mass_{Fe}^{theor}} \times 100 \qquad 6\text{-}8$$

where $mass_{Fe}^{analysis}$ is the fraction of Fe, detected in the solid sample (after filtration, drying and dissolution in stoichiometric quantities plus 10% excess of HCl solution at 1 M) by spectrophotometric analysis; $mass_{Fe}^{theor}$ is the theoretical amount of iron in the sample, assuming that the latter contains only iron hydroxide.

6.2 **On-site experimental campaign**

The plant may be operated in different technological configurations, by enabling simultaneously or not DD, MD and RP at will.

Moreover, both manual and automatic operational mode are implemented in the PLC software. The manual operational mode allows the operator to specifically control and operate individual actors to operate the plant at specific non pre-programmed procedures.

The automatic operational mode is designed for an automated operation of the plant, requiring no or minimal actions by the operator. During automatic operation, the operator cannot manually influence the plants actors control, the corresponding actors control bottoms on the HMI interface are deactivated. Only selected operational parameters (e.g. desired set-points for automatic control) can be adjusted by the operator during operation.

Operations reported in the following paragraphs were performed with the system in automatic operational mode. In Table 6-1, for the sake of clarity, all the relevant investigated operating conditions for the tests performed with the demonstrator plant and discussed in details in Section 6.2.1 to 6.2.3, are summarized.

Table 6-1 Summary of all tests performed for the demonstrator in the industrial environment along with the operating parameters varied for sensitivity analysis.

Test type	Variable operating parameters	WA-FT [l/h]	RA-FT [l/h]	T-FT [l/h]	T-TT [°C]	WA inlet concentration		
						c_{HCl} [g/l]	c_{Fe} [g/l]	c_{Zn} [g/l]
Test with HCl solution (synthetic)	WA and RA flow rate	15 25 20	19 15 21	400	60	106	-	-
	T flow rate and temperature	20	19	300 400 500 300 400 500	60 70			
Test with HCl and Fe solution (real)	WA and RA flow rate	15 20 25	15 19 21	300	60	96	81	-
Test with HCl, Fe and Zn solution (real)	Fe concentration	20	19	300	60	101	44 117	12

6.2.1 *Preliminary tests with synthetic HCl solutions*

The demonstrator was first commissioned in “safe” operational mode with synthetic solutions containing only clean HCl. In such conditions, only DD and MD units were in operation. Results reproducibility was verified by performing 5 tests under the same operating conditions (WA and RA1 flow rate: 20 l/h and 19 l/h, respectively, and WA inlet average HCl concentration: 106 g/l) for which similar concentration values of the RA1 (Std. Dev ~ 1.1 g/l) and RA2 (Std. Dev ~ 2.6 g/l) samples were obtained. Furthermore, these first tests were in line with the results carried out on the laboratory scale unit.

Two different sets of experiments were performed with HCl by changing either the waste or the recovered acid flow rate, while keeping fixed all other parameters. An average acid concentration of 106 g/l was kept for all the tests with hydrochloric acid.

As shown in Figure 6-1(a), RA/WA concentration ratio increases when WA flow rate is increased from 15 to 20 l/h, leading to an increase of the amount of acid entering the DD. However, it remains virtually constant from 20 to 25 l/h. As a direct consequence, the HCl concentration in the recovered acid solution exiting from MD unit (RA2) is enhanced with the WA from 15 to 20 l/h, while for the 25 l/h tests, the higher flow rate, together with the non-enhanced concentration in the DD, results in a lower acid concentration in the RA2 stream.

RA1 flow rate variation was also tested, by increasing the flow rate from 15 to 21 l/h. With the designed pump configuration P-RA, installed in the suction side of the DD module, the designed value of 25 l/h was not possible to be achieved due to gas suction of the pump. As shown in Figure 6-1(b), a RA1 flow rate increase leads to lower concentrations of acid in the RA1, and consequently in the RA2, due to a greater dilution.

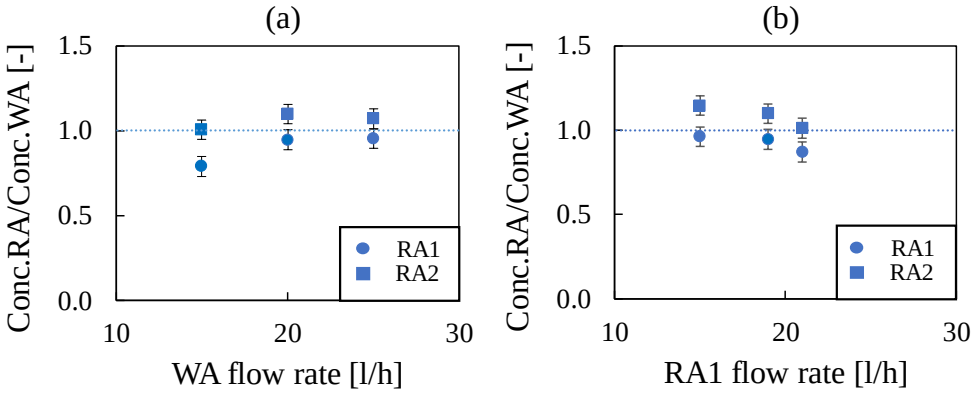

Figure 6-1 HCl concentration ratio between the recovered acid from DD (RA1, round symbols) or from the MD (RA2, square symbols) and the inlet waste acid, versus (a) WA flow rate (RA1 flow rate = 19 l/h) and (b) RA1 flow rate (WA flow rate = 20 l/h). Dotted horizontal line: concentration ratio equal to 1. WA inlet HCl concentration: 106 ± 5 g/l. Thermostatic fluid flow rate and hot / cold temperatures: 400 l/h, 60°C and 25°C. Tests with synthetic HCl solutions.

Contrarily to the higher concentration values observed, the acid recovery in DD decreases from 93% to 68%, when increasing the WA flow rate, and the HCl drag over detected through the MD membrane apparently slight increases from 6% to 8% as shown in Figure 6-2 (a), although considering the experimental error no significant variation is detected.

Opposite results were obtained for the increase of the recovered acid (RA1) flow rate: an increasing trend in the RR values is observed in Figure 6-2(b), from 65% to 85%, with a decreasing acid drag over, from 13% to 5%.

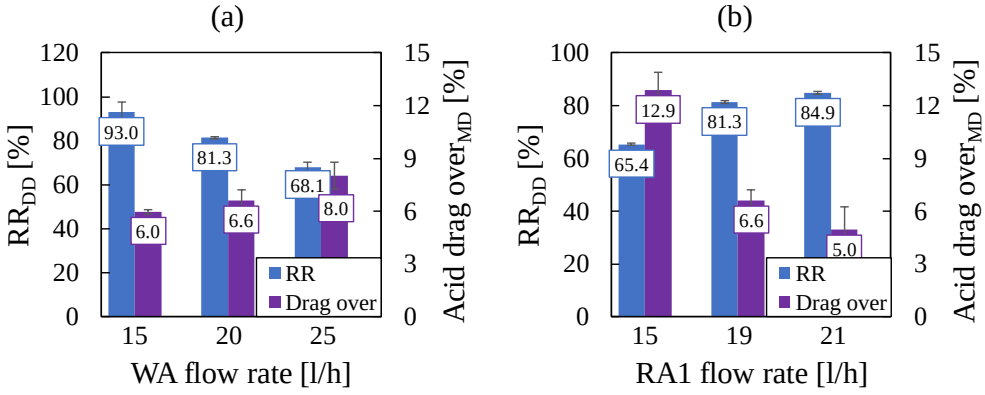

Figure 6-2 DD recovery ratio and MD acid drag over *versus* (a) WA flow rate (RA1 flow rate = 19 l/h) and (b) RA1 flow rate (WA flow rate = 20 l/h). WA inlet average HCl concentration: 106 ± 5 g/l. Thermostatic fluid flow rate and hot / cold temperatures: 400 l/h, 60°C and 25°C. Tests with synthetic HCl solutions.

The MD performance was explored by investigating the best operating conditions for the thermostatic fluid, in terms of hot side inlet temperature and flow rate.

As expected, the permeate flux (RW1 flux) increases with the increase of the thermal power, as well as the conversation ratio, due to the increase of hot side inlet temperature and flow rate (see Figure 6-3(a)).

Consequently, an acid drag over through the MD membrane was observed and, as for the RW1 flux, it increases as the thermostatic flow rate increases at both the studied temperatures and this result is more evident at the higher temperature of 70°C. In fact, as shown in Figure 6-3(b), drag over values up to 18% were observed at this temperature, because HCl vapour pressure curve is steeper with temperature compared to water vapour pressure one.

The thermal performance, in terms of Gain Output Ratio (GOR), is also presented for both the sets of experiments in Figure 6-3 (c). For both temperatures the GOR, and thus the thermal efficiency of the MD unit, declines when increasing the thermostatic fluid flow rate, with a positive effect of temperature on it. In fact, values ranging from 0.29 to 0.40 and from 0.39 to 0.57 were obtained, at inlet T-fluid temperatures of 60 °C and 70 °C, respectively. Indeed, when increasing the flow rate of the thermostatic line, the heat to be provided from the external

supply increases if the T_{T2} and T_{T4} temperature values are kept constant, but also the amount of heat transferred in the MD channels is increased. The increase in thermal power supply exceed the benefit in terms of internal heat transfer and enhanced vapour flux, thus leading to a reduction in the GOR. Thus, the most energy efficient conditions are at the lowest flow rate of 300 l/h and a temperature of 70 °C.

However, the enhanced internal heat transfer and higher hot channels temperatures, generate a larger passage of HCl, which is considered as a detrimental acid leakage. Finally, a temperature of 60°C and a flow rate of 300 l/h were selected as standard operating conditions in all tests performed with the real solutions, as a best tradeoff between the highest GOR and the lowest MD acid drag over.

Notwithstanding the thermal integration implemented inside the MD module, GOR values were all below 1 (i.e. less effective than a simple evaporation unit). This is due to MD design, oriented more to the achievement of high fluxes rather than high thermal efficiency, thanks to the fact that the thermal energy used for the MD operation is on site industrial waste heat, which is a commonly accepted approach when the thermal energy is provided by waste-heat [129].

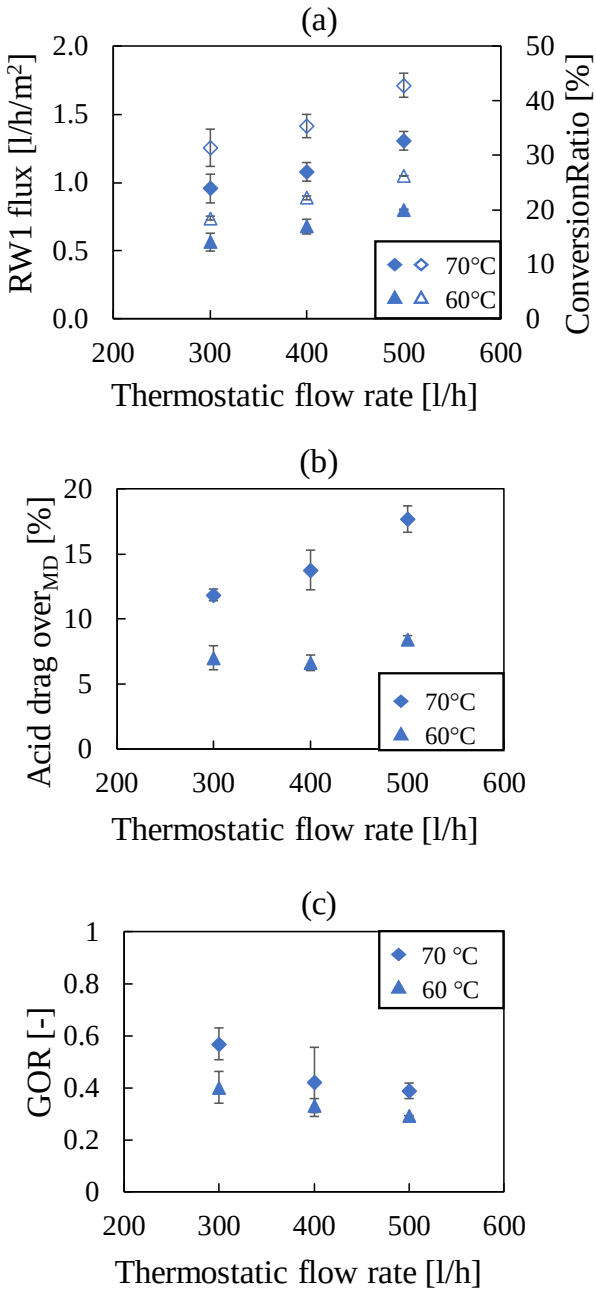

Figure 6-3 (a) RW1 flux and CR, (b) MD acid drag over and (c) GOR values *versus* thermostatic fluid flow rate at variable inlet temperature: 60 °C (triangle symbols), 70 °C (rhombic symbols). WA flow rate: 20 l/h; RA1 flow rate: 19 l/h. WA inlet average HCl concentration: 106 ± 5 g/l. Thermostatic cold temperature: 25 °C. Tests with synthetic HCl solutions.

6.2.2 *Tests performed with HCl and $FeCl_2$ solutions*

The first experiments with $FeCl_2$ and HCl solutions were performed using a purposely generated pickling solution, which resulted free of zinc ions. Results obtained were significantly affected by the well-known "salt effect" [100], [106], [122]. With this respect, it is of interest noting how the HCl concentration in RA1 can even reach higher values than the WA inlet concentration (Figure 6-4(a)), as observed for the highest WA flow rate (concentration ratio higher than 1), and this finding can be certainly attributed to the salt effect. Similarly, higher acid recoveries than those obtained without iron salts in solution were gained due to the presence of additional chlorides, which enhances the HCl diffusion through the DD membranes. This result can be observed in Figure 6-4 (b), where the RR for experiments performed with an acid concentration of 96 g/l and 81 g/l of iron ions are reported as a function of WA flow rate. The lower value at 15 l/h of WA flow rate is due to the lower RA1 flow rate, which is 15 l/h for the test reported in in Figure 6-4, which results in an average lower driving force because the RA1 concentration quickly increases. The highest value of RR, slightly below 90%, was observed for a WA flow rate of 20 l/h, marking an important difference with the value of 81% obtained for the sole HCl solution in the same working condition.

As regards the passage of iron through the DD membranes, an interesting result was observed when the WA flow rate is increased. In fact, despite the increase in the amount of entering iron with the WA flow rate, a slightly lower concentration in the RA1 stream was obtained (Figure 6-4 (a)) and, although this behavior could be attribute to the increase in RA1 flow rate and therefore to a dilution factor, a significant reduction of the iron leakage through the membrane was obtained as shown in Figure 6-4 (b)). A tradeoff between the RR and the iron leakage has to be implemented here too, thus WA and RA flow rates of 20 and 19 l/h, respectively, were adopted as standard working conditions in all subsequent tests.

Conversely, a decline in the MD operation was observed for tests with iron dissolved in solution, as iron salts reduce the water vapor pressure and, therefore, the water permeation through the membrane, leading also to a greater relative acid drag over. Quantitative results for the MD units are reported only for the final tests and presented in the following paragraph (Section 6.2.3 Figure 6-5(c)).

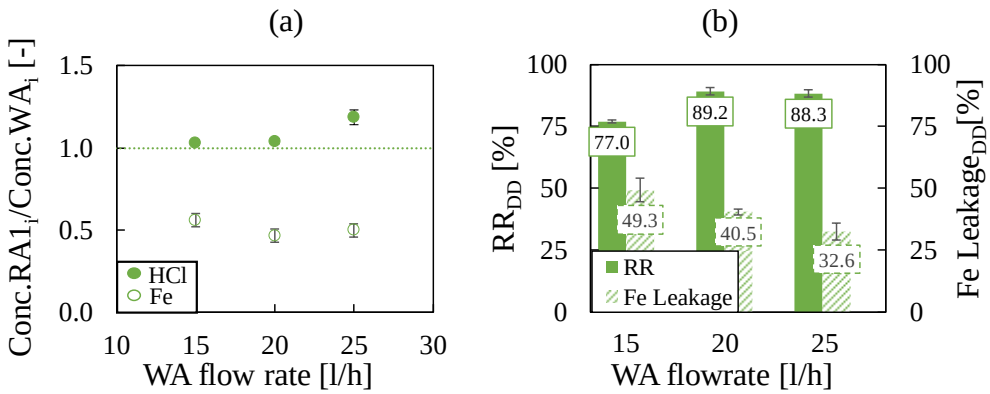

Figure 6-4 (a) HCl (solid symbols) and iron (empty symbols) concentration ratio between the recovered acid from DD and the inlet waste acid, and (b) DD recovery ratio (solid bar) and iron leakage (striped bar) *versus* WA flow rate (RA1 flow rate: 15, 19 and 21 l/h corresponding to the WA flow rate of 15, 20 and 25 l l/h, respectively[1]). Dotted horizontal line: concentration ratio equal to 1. WA inlet HCl and Fe concentration:96 ± 2 g/l and 81± 3 g/l, respectively. Tests with real solutions.

6.2.3 *Tests performed with HCl, $FeCl_2$ and $ZnCl_2$ solutions*

Finally, the presence of all the three main components of real pickling solutions was considered and two different WA cases were investigated, differing in Fe concentration, namely of 44 and 117 g/l, while keeping HCl and Zn concentration at fixed values (see Table 6-1).

The transport mechanism of zinc is somehow similar to the acid one as zinc forms negatively-charged chloro-complexes that can easily permeate through the DD membrane. For this reason, zinc is a "competitor" for acid permeation. As a result, the recovered acid was lower compared to what gained in the HCl+$FeCl_2$ tests for both cases with different iron concentrations (see Figure 6-5(a)). However, at the highest iron concentration (Fe concentration 117 g/l) a high acid recovery is ensured (above 82%), which is comparable with the test with HCl only, thus highlighting the importance of the salt effect in reaching high acid recovery, even in the presence of zinc.

[1] Same flow rates for WA and RA1 were originally planned, but RA1 flow rates could not always reaches the target due to some operational limitations in the RA1 pump.

On the other side, the iron chlorides in solution also result in a higher zinc leakage as their concentration increases (Figure 6-5 (b)). However, the low concentration of zinc in solution allows to manage the closed-loop operation of the whole system, keeping the required small concentration of zinc in the RA2 in order to avoid the accumulation of this component in the pickling tank [123]. In such conditions, iron leakage seems to not be influenced by the presence of zinc chlorides, as a leakage comparable (in the range of 40 and 50%) is detected in all the tests with iron in solution.

Metals leakage is higher than expected, mainly regards to the iron leakage. In fact, results previously obtained in the laboratory large dialyzer, with same configuration and operating conditions indicated an iron leakage of about 30% and a leakage of 60% for zinc (see Table 2-4 in Chapter 2) [122], while values up to 50% and 65%, respectively, are observed here. This could be attributed to the position of the P-RA pump at the suction side of the DD, which resulted in a higher differential pressure along the two sides of the DD unit and, therefore, in a hydraulic leakage from the feed to the draw channels. Moreover, the residence time in the pilot configuration is higher (laboratory dialyzer residence time is around 4 min compared to the 7 minutes of the pilot) thus providing additional time for the metals to diffuse from the concentrate to the dilute side, while marginal benefits are provided to the acid recovery, given the already high values achieved, which can hardly be increased by a longer residence time. Thus, an optimized geometry would require a significantly lower membrane area, which could reduce the metals leakage without affecting the recovery of acid (see Paragraph 6.4).

The MD performances suffer significantly, as the salts concentration increases in the RA1 solution, likely due two main facts: increase of the molar HCl flux through the MD membranes, on one side, and reduction of the water vapor permeation, on the other. In fact, contrarily to the ideal Raoult's law, which would predict a vapor pressure reduction for both volatile components, it is observed that when a salt is dissolved in a mixture of water and acid, the presence of salt enhances the acid vapour pressure, while it reduces water one [73], [130]. This is known as "salting out" effect, which typically results in a higher acid drag over through the microporous MD membranes as shown in Figure 6-5 (c).

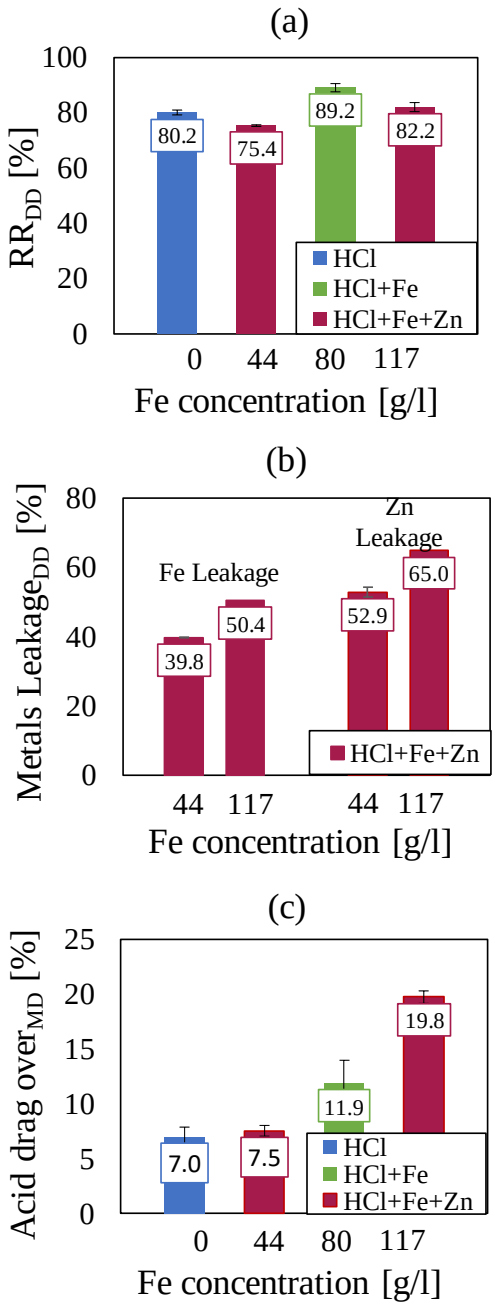

Figure 6-5 (a) DD recovery ratio, (b) DD metals leakage and (c) MD acid drag over *versus* iron concentration. WA inlet HCl and Zn concentration: 101 ± 1 g/l and 12 ± 1 g/l (for the two tests with HCl+Fe+Zn). WA flow rate: 20 l/h; RA1 flow rate: 19 l/h. Thermostatic fluid flow rate and hot / cold temperatures: 300 l/h, 60°C and 28°C. Tests with real solutions.

A polypropylene cooled CSTR unit was used for these latter tests to separate and selectively recover the two metal components. Previous laboratory tests (Chapter 3) had shown that a selective precipitation is possible by controlling the solution pH, since Fe (III) hydroxide precipitation pH is in the range of 2-3, while zinc insoluble salts (e.g. $Zn(OH)_2$) precipitate above the range 6-7. Therefore, to accomplish the iron separation in the CSTR section, hydrogen peroxide and ammonia hydroxide were fed in order to oxidize Fe (II) to Fe (III) and to precipitate iron hydroxide, respectively. All the tests were performed by keeping a constant pH=4 in the CSTR and a redox potential set-point at 300mV (in practice, ranging from 250 to 400 mV), which ensures a complete iron oxidation. Interestingly, a purity of 99% was obtained for the iron hydroxide solid separated after filtration.

6.3 **Long time pilot system performance**

Results of the long-time automatic mode operations for the three different main sections are reported in the following graphs to prove the stability and long-run performance of the demonstrator.

In Figure 6-6, double plots are shown to visualize the conductivities and flow rates in the DD unit for a whole day of operation (7 hours). Typical conductivity profiles during DD backflush steps are detectable. DD backflush cycle typically operates every 2 hours and lasts 2 minutes. The system has the ability to respond quickly to externally generated variations, as can be seen after every backflush or after the flow rate variation purposely operated at 4.3 hours, when the waste acid flow rate increases from 20 to 25 l/h.

The sub-atmospheric pressure in the DD diffusate channel leads to the formation of gas bubbles exiting with the diffusate and entering the pump and, then, the MD module. Consequently, flow sensors, which are very sensitive to gas bubbles, gave values with strong fluctuations (see FT-RA1 points in Figure 6-6 and Figure 6-7).

The RW2 is stored in a water tank where the fresh water FW inlet stream is discontinuously dosing, since the water consumption as draw solution for the DD diffusate stream is higher than the water production from the MD-module, thus resulting in a lower conductivity values compared to RW1 (see Figure 6-7).

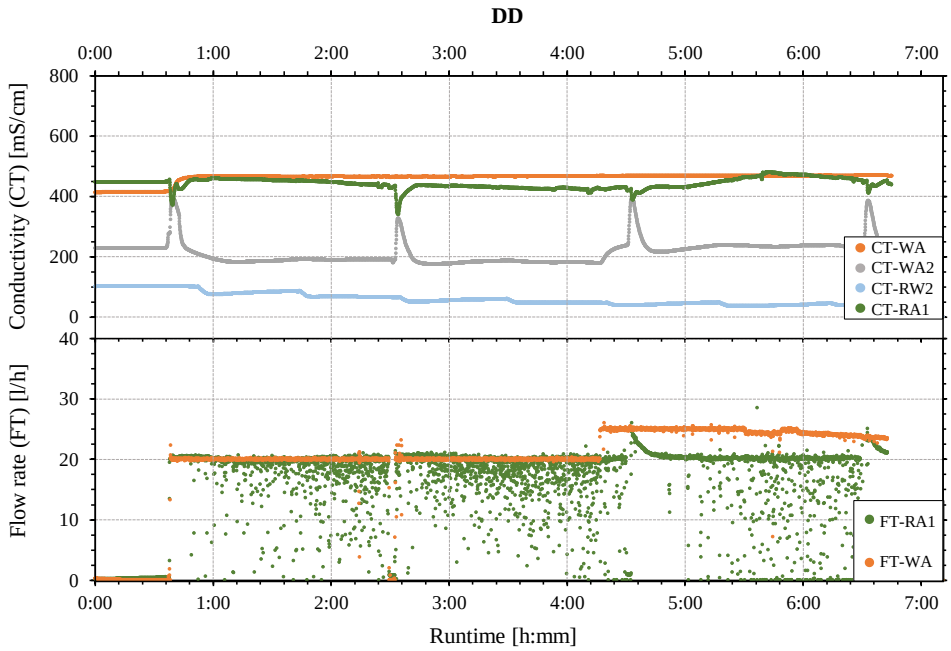

Figure 6-6 Long-run DD operation. Conductivities values (top) and flow rates (bottom) *versus* operation time. Tests with real HCl solution. WA inlet HCl, Fe and Zn concentration: 101 g/l, 44 g/l, 12 g/l, respectively.

A further demonstration of the system stability is shown in Figure 6-7, where variations of flow rate and temperatures in the MD thermostatic line are reported.

An emergency shut-down is also noticeable in Figure 6-7 (after 4 hours of operation), with streams flow rate suddenly going to zero and a slight ramp down in the temperature profiles, while operations are restored in about 1 hour following the shut-down.

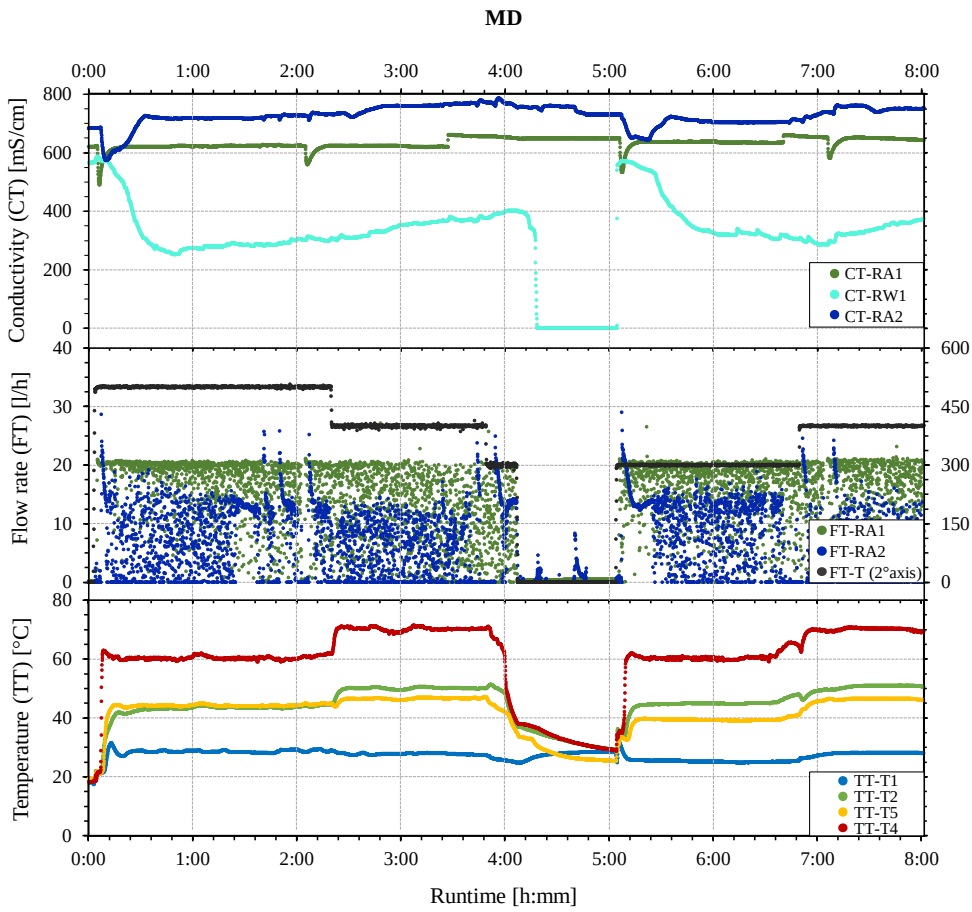

Figure 6-7 Long-run MD operation. Conductivities values (top), flow rates (middle) and temperatures (bottom) *versus* operation time. Tests with synthetic HCl solution. WA inlet HCl concentration: 101 g/l.

Finally, an example of control system action in the CSTR is reported in Figure 6-8. The set points of pH and redox potential are of 4 and 300 mV, respectively. The oxidant and reactants flow rates are automatically adjusted in order to keep controlled variables to their set point. In addition, the slurry temperature in the precipitation unit is controlled by adjusting the cooling water flow rate in the heat exchanger (temperature does not exceed the maximum set value of 35°C).

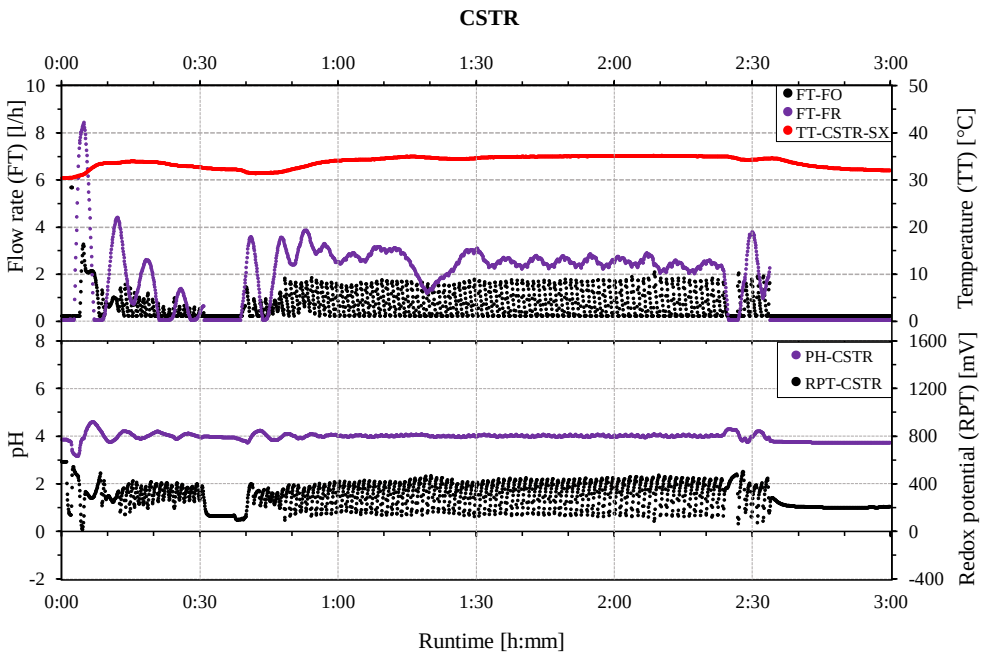

Figure 6-8 Long-run CSTR operation. Flow rates (top) and pH and redox potential values (bottom) *versus* operation time. Tests with real HCl solutions. WA inlet HCl, Fe and Zn concentration: 101 g/l, 117 g/l, 12 g/l, respectively.

6.4 **Operational weakness and new proposal**

The results of the operational trials at Tecnozinco showed that DD is essential for the acid recovery, despite the significant iron and zinc leakages.

Metal leakages had already been taken into consideration in the original integrated plant design, thanks to the wide preliminary laboratory investigations allowing for characterising the systems behaviour. However, metals flux values through the membranes observed in the real pilot tests appears to be higher than expected. Thus, a proposed optimized configuration is a DD module operated with reduced membranes area or higher nominal flow rates. In fact, lower residence times will reduce metals leakages through the DD membranes while maintaining a fairly high acid recovery.

In support of what stated, since both options cannot be implemented on the current pilot system, due to the limitation in the flow rate range and impossibility to open the DD stack

locally for a modification, an experimental campaign was carried out at laboratory scale with the large DD stack presented in Section 2.2.3, which has the same spacers and membranes characteristics of the pilot module, but which was accessible for the membrane surface modification.

Three different tests were performed at different residence time, as reported in Figure 6-9. As it possible to see from the figure below, high leakages of iron, up to 50%, are observed for test carried out with the same DD pilot scale residence time (residence ratio equal to 1). When the residence time ratio is decreased to 0.42, no acid recovery ratio and iron leakage variations are observed, while for the residence ratio of 0.22 a significant iron leakage drop is detected without variation on the acid recovery ratio.

These results are perfectly in agreement with what simulated from the DD model and presented in section 4.5, where it was highlighted the optimal design, which was eventually different from the actual design.

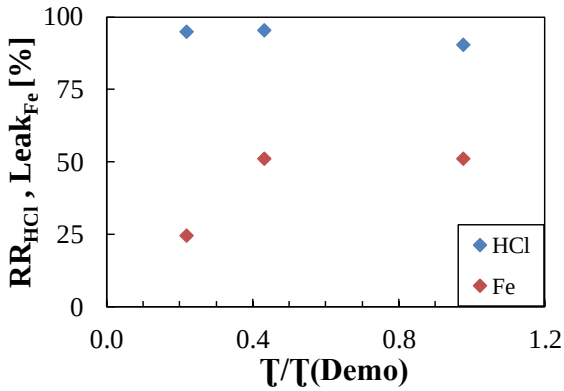

Figure 6-9 Experimental campaign on the DD laboratory large unit over different time residence ratio. HCl recovery ratio (◆) and Fe leakage (◆) are report.

A further modification of the pilot configuration concerns the pump P-RA position. The position of the pump is between the DD and the MD modules, designed in a way that the pressure level in the DD-module (diffusate side) is independent from the pressure losses in the MD module feed channel. In this way, the DD module was operated on the suction side of the pump and the MD module on the pressure side of the pump (see Figure 6-10). Thus, sub-atmospheric pressures were present in the DD diffusate channel. These sub-atmospheric pressures lead to a significant pressure difference between the two DD compartments, as the

feed channel side of the DD module was operated on the pressure side of the waste acid pump (P-WA), which causes high internal leakage from the feed to the diffusate channels, negative aspect mainly in terms of metals leakage. Furthermore, the sub-atmospheric pressure leads to the formation of gas bubbles that exit the diffusate outlet of the DD module, entering the pump and MD module respectively. Consequently, flow control (flow sensors are sensitive with respect to gas bubbles) was reacting to the bad flow signal with strong fluctuations, as shown in Figure 6-6 and Figure 6-7.

Thus in order to eliminate high pressure difference between the two channels of the DD unit and gas bubbles releasing, an enhanced configuration would interest the relocation of the pump P-RA to the inlet side of the DD modules (see Figure 6-10 on the right).

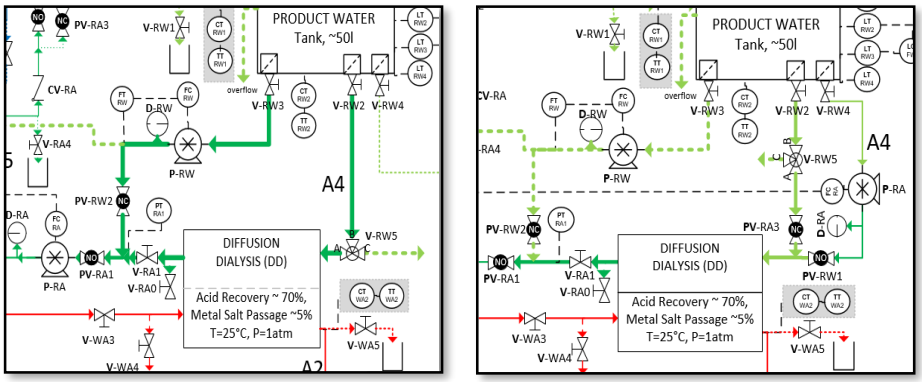

Figure 6-10 P-RA original configuration (on the left) and new proposed configuration (on the right).

Moreover, the MD unit revealed a loss of HCl with its condensate when very high metals concentrations are present in RA1 stream. Thus reducing the DD iron leakage will be beneficial for the MD performance, as well.

6.5 **Inspection of degradation state**

Demonstrator plant adopted in this work operated discontinuously, following the daily operators job turns of maximum 8 hours. Thus long-term data (weeks to months) are not available making hard to carry out an appropriate comparison and membrane performance variation assessment.

It is worth noting that results presented in this chapter were collected along 8 months of demonstrator operation.

A critical comparison can be carried out for the DD unit. The DD membrane unit suffered the membrane plugging phenomena, as it can be seen from Figure 6-11 in which a pressure trend at the inlet of the waste acid channel is reported over the months of pilot operation. These results show that after one month of plant shutdown the membrane plugging occurred, due to some iron (III) precipitation. The unit was flushed with hydrochloric acid solution before and after the plugging occurred and the problem was not overcome.

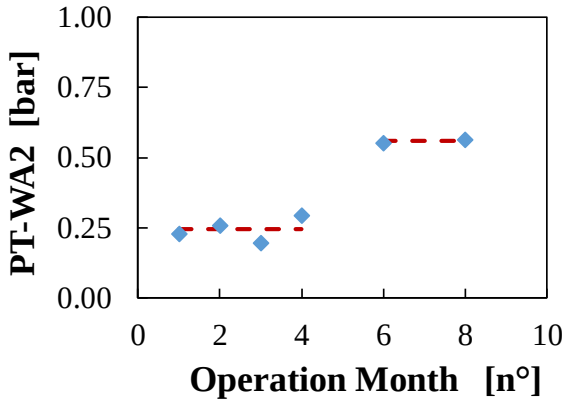

Figure 6-11 Demo A pressure trend at the inlet of WA channel over months' number operation.

In the regard of the MD unit, a performance drop was observed when real solution was tested, at the very early plant operations. To test the degradation of the Membrane Distillation membrane, a standard leakage test with a sodium chloride solution of known conductivity (or concentration) was used as feed liquid and standard operation conditions were used. The MD module consists of 3 stages in series with distillate being collected at each stage which is mixed in-line before to be sent to the product water tank. During the testing, each distillate was separately collected in order to determine the degradation status of the membrane in each of the 3 stages.

The feed solution had a conductivity of 10 mS/cm which translates to ~6.5 g NaCl/kg of solution. The Hot in-Cold out temperature was maintained at 70-25 °C and the flow rates in thermostat and feed loop were 300 l/h and 20 l/h respectively. The following results were observed (see Figure 6-12):

Stage 2 shows the most degradation followed by stage 1. Stage 3 membrane was found to be not degraded. The time to degradation of the membrane was earlier than expected; hence some of the reasons for this degradation were deduced as follows:

1. The membrane was kept in contact with the acid feed liquid during overnight shutdown. During this phase, osmotic forces may have overcome the hydrophobicity of the membrane leading to leakage spots on the membrane. The data shows that when the unit is started each morning, in the first half hour, the distillate quality has higher HCl concentration than what is observed during a normal steady state operation.

2. Mechanical damage might have occurred internally to the MD module leading to leakage of acid and Iron into the distillate channel. From MD technology provider experience, a mechanical damage leads to much higher acid flows into all circuits that are in contact with the MD module. This has not been observed so far. The thermostat loop is acid-free. Furthermore, after a mechanical damage, the quality degrades over time, which has not been the case.

No further deterioration was detected over time, and the percentage metals leakage through the MD membranes remained the same with a value lower than 2%.

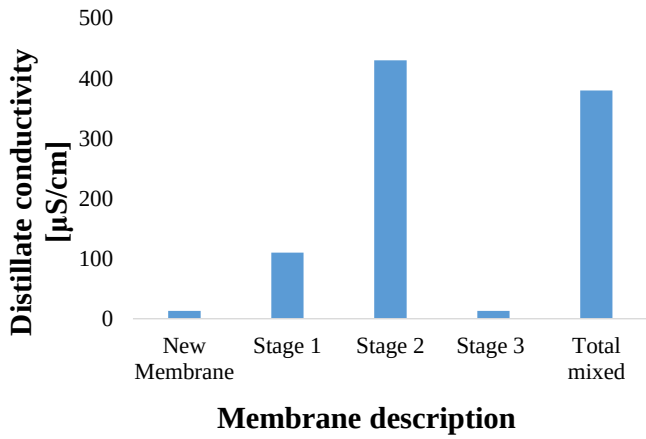

Figure 6-12 Results from testing the degradation state of the Membrane Distillation membranes.

6.6 **Conclusions**

Design, construction and operational results of a pilot plant for the treatment and valorisation of pickling solutions are presented.

The pilot plant was commissioned and operated in a real industrial environment using first synthetic HCl solutions and then real pickling liquors at the premises of a large hot-dip galvanizing plant (Tecnozinco SrL, Carini, Italy), where full integration with industrial waste-heat sources has been realised for the overall process energy sustainability.

The highest acid recovery, nearly 90%, was observed for the HCl+ $FeCl_2$ solution, also achieved thanks to the "iron salt effect", which enhances Cl^- ions permeation. Conversely, lower acid recoveries (~80%) were observed when zinc is in solution, acting as a competitor for the acid permeation because of the anionic zinc chloro-complexes. High values of iron leakage through the DD unit were observed (up to 50%), as a consequence of long residence times in the DD module and some hydraulic leakages caused by the suction position of the P-RA pump. Quantitative separation of iron and zinc was demonstrated in the CSTR unit, generating 99% iron hydroxide product and a $ZnCl_2/NH_4Cl$ solution to be re-used in the fluxing baths.

Finally, an important drop in MD performance was observed with real pickling liquors, where the high volatility of HCl is further enhanced by the "salting out" effect of iron salts depressing water vapour pressure.

Overall, operational results have shown that acid can be successfully recovered and re-concentrated, iron salt recovered in the form of marketable hydroxides and fluxing solution eventually obtained from the outlet of the iron crystalliser. Both acid and fluxing solution can be recirculated into the plant, thus eliminating any waste stream to be disposed.

High level of system reliability and robustness was achieved by the implementation of an industrial-type central process control system. Results of the long-time automatic mode operations have proven the operational stability and performance of the demonstrator.

Further developments were envisaged to improve DD membrane selectivity against Fe and Zn and module integrity to minimise leakages. Moreover, an optimized configuration should aim at reduced residence time in the DD unit and a relocation of the P-RA pump at the channel inlet to improve the hydraulic performance of the unit, thus further reducing the metals leakage in DD diffusate, and improving the MD performance.

SECTION 3: PROCESS OPTIMIZATION AND PROFITABILITY ANALYSIS

ABSTRACT

Economic considerations regarding the integration of the technology in the industrial environment and optimization analysis and strategies are presented in the following section.

The economic analysis was performed aiming to demonstrate the feasibility of the developed technology. The investment and operating costs as well as the avoided costs and the benefits for the company operating the plant were analyzed through an extensive cost tracking and a face-to-face contact with manufacturers and sector leaders.

A mathematical model was implemented on the gPROMS modeling platform, able to simulate steady state operations and run optimization analysis on the process performance. The impact of key operating parameters, as the set-point bath concentration, and design parameters, such as DD and MD membranes area, were investigated and the optimal arrangement was identified for both cases. Finally, operating variables and design parameters were optimized simultaneously in a nonlinear framework solution as a tradeoff between profitability and environmental impact.

Of interest, the technology integration into the traditional pickling industry could provide a solution both for costs reduction and for the ecological impact of the metallurgical industry.

7. ENGINEERING ECONOMIC ANALYSIS

Chapter Outline

7.1 Introduction

Pickling waste liquors are a crucial problem for company economics and, even more, for its related environmental issues. AIZ “Italian galvanizing association” very recently carried out a survey in the framework of the ReWaCEM European project (www.rewacem.eu) thus allowing the knowledge on acid consumption and spent liquor production data on pickling in Italy. A fresh acid consumption range of 10-30 kg/$ton_{galv.steel}$ and a spent liquor production of 15-45 kg/$ton_{galv.steel}$ were reported [131]. These data are consistent all over Europe according to surveys conducted by the EGGA “European General Galvanizers Association” community.

The IPPC (Integrated Pollution Prevention and Control) policy pushes for the adoption of innovative integrated and eco-friendly systems for recovery of acids and metals compounds, by applying the circular economy concept, with the simultaneous goal of (i) reducing the environmental impact and (ii) making the production steps more efficient.

Disclosed herein, economic considerations regarding the integration of the process in the industrial environment are presented, firstly for a hot-dip galvanizing company in Italy (Tecnozinco S.r.l. case study) and, then, considering the medium-size throughput treatment plants, as well. Economic outcomes for the single unit applications are available in the scientific literature. Diffusion Dialysis is counted in the BAT recommendations [62] as it has widely proved its clean nature [51], [102]. Despite of the evidence in cost-effective wise reported in literature, which is only marginally attractive [132], [133], issues related to the stand-alone application (e.g. large volume of streams products [133]) can be overcome on an integrated approach view. More promising results are expected for the MD application, especially when it can be supplied with waste heat [76] as it is in our case.

The huge potential of considering an onsite treatment process in the galvanizing industry is that it will enhance doubly the environmental impact in (i) the reduction/elimination of the disposal waste to treat and (ii) waste transportation as well.

In the present chapter, it will be proved that the integration of the treatment/recycling process will be a cost-effective solution, as already have been stated for different recovery process in the same field [134]. The integration of the process in the industrial plant does not require any particular modification of the industrial plant. Moreover, the flexibility and size-modularity of membrane units let to adapt size and operating conditions to any specific galvanising plant requests.

A standard profitability analysis was carried out by following a well knowing procedure proposed by Turton et al.[135], to evaluate the economic profitability due to the introduction of the proposed innovative integrated system in the hot-dip galvanizing industry.

Pilot plant capacity was designed in order to be able to treat only one of the seven pickling baths of the Tecnozinco S.r.l. plant. Therefore, for a consistent economic analysis, in the calculation the capacity of the treatment-integrated process was scaled-up to the full Tecnozinco capacity. As Tecnozinco S.r.l. company is a small industry in the hot-dip galvanizing sector, more realistically, also higher capacity plants were investigated in order to consider the case of a more significant economical return as it is for a larger portion of companies in the industrial scale.

7.2 Capital and operating cost assessment

7.2.1 *Capital investment*

The fixed capital investment (FCI) estimation was assessed through an extensive cost tracking carried out during the realization of the pilot unit and with the help of single parts manufacturers. Results of the analysis for the demo plant and for the up-scaled sizes (with "scale variable" the waste acid volume flow rate to be treated in the integrated process F^{WAS}) are reported in Table 7-1. These costs are the sum of costs for parts and modules, which account for the Total Material Costs, and transportation, logistics, documentations, assembly, commissioning and training and development. The latter category was estimated based on the number of person-months (PM) required, by considering the relevant salaries reported in Table 7-2. Typical Italian engineer salaries are reported [136], which are quite similar for other European countries as well. The technologies providers fee was assumed 25% of the subtotal. The sum of all these cost items provide the FCI, as it is a waste treatment process to be integrated in an already existing plant, therefore auxiliary facilities costs for site development are not considered.

As results, the demo project investment cost for a commercial system, not tailored to experimental use is 142,000 € (ref. to Pilot size in Table 7-1). The FCI result for the pilot scale is reported as it constitutes the reliable data from which the FCI analysis for the different

treatment capacities was based on. However, the pilot scale will no longer be considered for economic and optimization considerations in the following work.

Table 7-1. FCI analysis at different treatment capacity.

	Treatment Capacity			
Cost Items [€]	Pilot size 0.03 m^3/h	Future same size I 0.1 m^3/h	Future up-scaled size II 1 m^3/h	Future up-scaled size III 10 m^3/h
Mechanical	6300	6300	7600	16000
Hydraulic	8600	16500	33000	82500
Actors	4200	5400	6500	27000
Sensors	13900	12500	12500	12500
Electrical	12600	16000	16000	16000
Total Material Costs (excl. Modules)	**45600**	**56700**	**75600**	**154000**
MD Module	10000	13500	36000	84000
DD Module	8000	9800	58400	418000
Membrane Module cost	18000	23300	94400	502000
Total Material Costs (incl. Modules)	**63600**	**80000**	**170000**	**656000**
Transportation	2000	2000	4000	6000
Logistics, Ordering, Desk	5200 (1.4xPM)*	5200 (1.4xPM)*	6200 (1.7xPM)*	12600 (3.4xPM)*
Documentation	2600 (0.7xPM)*	2600 (0.7xPM)*	3000 (0.8xPM)*	6200 (1.7xPM)*
Assembly	24000 (8.3xPM)**	24000 (8.3xPM)**	48000 (8.3xPM)x2**	240000 (8.3xPM)x10**
Commissioning and Training	8100 (1.4xPM)***	8100 (1.4xPM)***	9900 (1.7xPM)***	19600 (3.4xPM)***
Development	8100 (1.4xPM)***	8100 (1.4xPM)***	9900 (1.7xPM)***	19600 (3.4xPM)***
Subtotal	113600	128000	251000	960000
Technology Provider Fee (=25% of subtotal)	28400	32000	62700	240000
FCI (total)	**142000**	**160000**	**313700**	**1200000**
Lump Factor $= \frac{\text{FCI}}{\text{Membrane Modules Cost}}$	7.9	6.9	3.3	2.4

*Engineer

**2.8Engineer+5.5Assembler

***Senior Engineer

Table 7-2 Estimated salaries [136] used for cost items determination in Table 7-1.

Salary Engineer	44,000 €
Salary Senior Engineer	70,000 €
Salary Assembler	30,000 €

A specific membrane module cost was derived from data provided by DD and MD module manufactures and values of 470 €/m^2 and 310 €/m^2 for the DD and the MD modules were obtained, respectively. The FCI can be conceived as the product of a "lump factor" and the cost of the membrane technologies (Eq. 7-1), thus resulting in a power law of the treatment capacity (Eq. 7-2). This equation will be used later on in the optimization section (Chapter 8).

$$FCI = lump\ factor \cdot \sum_{u=DD,MD} (specific\ membrane\ module\ cost_u \times A_u) \quad 7\text{-}1$$

$$lump\ factor = 4 \cdot F^{WAS^{-0.225}} \quad 7\text{-}2$$

where A_u is the total membrane area of either DD or MD modules.

For a validation of the capital cost-plant capacity curve thus obtained, a comparison with the well-known "six tenths rule" [137] was performed (see Figure 7-1). The curve obtained in the present work is more conservative and predicts higher investment cost for the low size capacity plants. In fact, obtained results are comparable in the wide range of capacity estimated (1 m^3/h -10 m^3/h), while a higher discrepancy is observed in the low size range (0.1 m^3/h to 1 m^3/h). It is worth noting that treatment plants with a capacity higher or equal to 10 m3/h treatment capacity plants are not expected to be constructed and operated, as the investigated range covers all hot-dip galvanizing industry typical capacity (in Italy the highest capacity is nowadays 50,000 ton/y of steel processed, which would mean about 1 m3/h of waste solution to be treated; the Tecnozinco plant capacity is one order of magnitude lower).

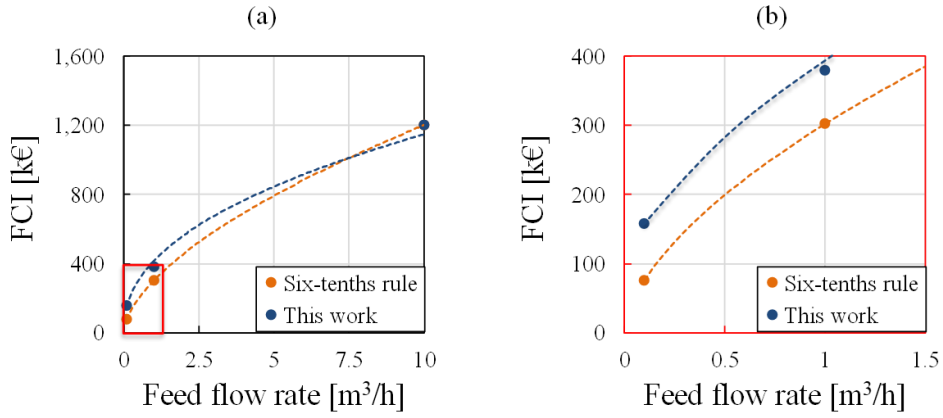

Figure 7-1 FCI vs feed flow rate for the capital cost-plant capacity curve obtained in the present work (blue curve) and the six-tenths rule curve (orange curve). (a) capacity range between 0-10 m^3/h; (b) capacity range between 0-1.5 m^3/h.

7.2.2 *Operating cost estimation*

The yearly operating expenditure ($OPEX_k$) estimation was based on the value of FCI, the cost of operating labor (C_{OL}), the cost of raw material (C_{RM}), the cost of waste treatment (C_{WT}) and the cost of utilities (C_{UT}) following the indications of Turton et al. [138] (see Eq. 7-3).

$$OPEX_k = 0.18 \cdot \mathrm{FCI} + 2.73 \cdot C_{OL} + 1.23 \cdot (C_{RM} + C_{WT} + C_{UT}) \qquad 7\text{-}3$$

The value so calculated takes into account all the costs related to the total manufacturing costs: (i) Direct Costs, (ii) Fixed Manufacturing Costs and (iii) General Manufacturing Expenses. In this OPEX definition, the depreciation is not taken into account, which was considered in the expenses later on. Inputs for the calculation of the different OPEX items were collected and reported in Table 7-3.

Table 7-3. OPEX inputs.

OPEX items	Cost position	Unitary cost	Selected values
Raw Material (inputs for C_{RM} calc.)	HCl Make-Up	30[139]-125 €/ton	125 €/ton
	Alkaline reactant	0.1[140]-0.55 €/l	0.55 €/l
	Oxidizing reactant	0.135[141]-0.38 €/kg	0.38 €/kg
Waste treatment (inputs for C_{WT} calc.)	-	-	-
Utilities (inputs for C_{UT} cal.)	Process Water	-	0.95 €/m^3
	Electricity	-	0.2 €/kWh
Operating Labour C_{OL}		-	11000 €/y

C_{RM} concerns HCl make-up and reactants for the reactive crystallizer. The HCl industrial price is very swinging as, in the relevant sector, it is a by-product of other processes and its price depends on several factors, as the abundance in the specific geographical area or in the particular period, the incidence of transport costs. The chosen and reported price is mainly based on Tecnozinco know-how. Moreover, the HCl make up amount to consider is the difference between the actual design value and the TecnoZinco nominal consumption, as only this aliquot would result in an extra cost for the company. For the NH_4OH and H_2O_2 reactants, Tecnozinco purchasing costs were considered as well. It is worth noting that all the selected purchasing costs are the highest in the relevant range reported in Table 4, thus assessing the worst scenario for the operating cost analysis.

C_{WT} is considered zero for the present technology.

C_{UT} plant utilities consist of process water re-filling and electricity. Thermal energy is provided in the form of waste heat. Therefore, thermal energy cost is assumed to be zero. Electricity is mainly consumed by pumps, controls and switch cabinet cooling.

C_{OL} since the pilot plant principally operates automatic, it was considered only a quarter of an engineer position for maintenance and operation. With an assumed engineering salary of 44.000 €/y this leads to 11.000 €/y.

7.3 **Profitability analysis**

For the yearly revenues (R_k) estimation, different aspects have to be taken into account.

Along with the direct revenues related to the selling or re-cycling of products, a saving for the reduced waste acid production and corresponding disposal, and for the enhanced production for the optimal pickling performance of the baths have to be counted.

In particular, the $S_{Product}$ item are the solid iron hydroxide, which is the direct saleable product, and the fluxing solution, which is the recyclable product. This latter is considered a revenue contribution as it is an avoided expense for the company.

To account for the avoided disposal cost ($C_{Disposal}$) a saving flow rate was estimated as the flow rate corresponding at a Fe concentration disposal of 185 g/l as reported in Eq. 7-4.

$$w_{saving} = \frac{w_{Fe}^{WAS} \rho^{WAS}}{C_{Fe}^{Disposal}} \qquad 7\text{-}4$$

where w_{Fe}^{WAS} is the mass flow rate of iron extracted from the pickling bath and thus processed in the pilot system, ρ^{WAS} is the waste acid solution density and the $C_{Fe}^{Disposal}$ is the highest mass concentration of Iron at which the solution has to be disposed of.

Another revenue contribution comes from the increased production (*Added value of the Enhanced Prod.*). Pickling performances are dependent from several factors: temperature of the bath, acid and iron concentration, inhibitor choice and concentration [12]. A suitable combination of all these factors leads to the determination of optimal operating conditions for the pickling process. Under these conditions, the time required for the dissolution of the oxide layers covering the steel product is minimal and therefore the efficiency of the pickling bath is maximized. The implementation of the proposed process will affect mainly the composition of the bath in terms of acid and iron II concentration. In particular, literature values from Kleingarn [11] were extrapolated and processed in order to derive a minimum pickling time curve with the hydrochloric acid concentration, reported in Figure 7-2(a). The minimum time is the pickling time corresponding to the optimal compositions of acid and iron. Figure 7-2(b), on the contrary, shows the *Enhanced Prod. Factor* obtained by comparing a nominal operating condition of the Tecnozinco pickling baths, averaged over the data of a year of operation (HCl concentration: 1.7 M; Fe (II) concentration: 137 g/l; average pickling time 8.3

min, red dot in Figure 7-2(a)) with data obtained in Figure 7-2(a). It is a correction factor for the processed steel mass flow rate and expresses the variation of the pickling time, transformed into an increase/decrease of the processed material capacity of the plant, with the bath composition. Indeed, as the Tecnozinco nominal reference operating condition is almost an optimal condition of the Kleingran curve, for the reference concentration the *Enhanced Prod. Factor* does not express any variation in terms of productivity. However, if we move in a higher HCl operating concentration an increased production will result, as well as a reduction factor it will be obtained if the acid working concentration is below the nominal case (refer to Figure 7-2(b)). As defined, it is related to the particular plant operation, and it has to be tuned for the specific company considered. However, a typical composition for the relevant industrial sector could be used in order to generalize the *Enhanced Prod. Factor*.

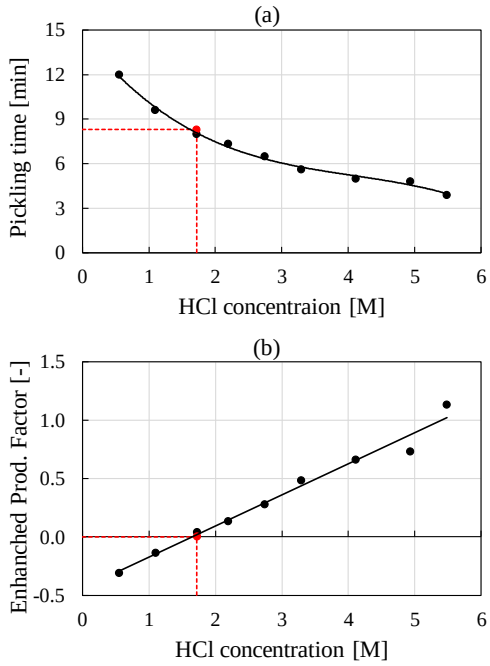

Figure 7-2. (a) Minimum pickling time and (b) enhanced production factor vs hydrochloric acid concentration.

Thus, the increased production *Enhanced Prod* is expressed as follows:

$$Enhanced\ Prod = Enhanced\ Prod.Factor \cdot w_{steel} \qquad 7\text{-}5$$

where $EnhancedProd\ Factor$ is:

$$EnhancedProd\ Factor = 0.267 \cdot c_{HCl}^{WAS} - 0.44 \quad 7\text{-}6$$

Therefore, the yearly revenues were estimated as follow(Eq. 7-7):

$$R_k = S_{Product} + C_{Disposal} + Added\ value\ of\ the\ Enhanced\ Prod. \quad 7\text{-}7$$

where the "$Added\ value\ of\ the\ Enhanced\ Prod.$" is the gain due to the *Enhanced Prod* manufactured steel flow rate.

Table 7-4 summarizes the inputs used for the revenues estimation together with the unitary cost for the selling or saving cost. The iron (III) hydroxide market price depends on the particular application case: values vary from 12 €/kg [142] for the wastewater treatment [117] to 8.5 €/kg[143] for the painting industry, to 0.6 €/kg as reported in "Xiamen Ditai Chemicals Co., Ltd" webpage[144]. The Molbase Chemical E-commerce platform[145] reports an average price of 17$/kg based on more than 50 suppliers of the iron hydroxide product. Thus, a value of 2 €/kg was selected to be very conservative and to take also into account further possible treatment processes necessary to make it marketable. The selected costs for the Fluxing solution saving and the Added value of the Enhanced Prod. have been carefully discussed and agreed with the industrial partner, thus making analysis more reliable.

Table 7-4. Unitary costs for Revenues calculation.

Revenues inputs	Unitary cost	Selected values
Iron (III) hydroxide	0.6-14€/kg[142]–[145]	2€/kg
Fluxing solution	0.06 €/kg	0.06 €/kg
Waste acid disposal saving	40-160€/ton[20], [131]	145€/ton
Added value of the Enhanced Prod.	0.045€/kg	0.045€/kg

Disposal costs faced by Tecnozinco S.r.L. include transportation to a far waste treatment plant in northern Italy (nearly 800km). The disposal cost amounts to about 80 €/ton, which is

in agreement with values reported from Stocks et al. [20], while the additional average cost for transportation is around 65 €/ton.

As already declared in the section 7.1, the profitability analysis was carried out by following the procedure described by Turton [135]. The simple straight-line depreciation method was applied, as reported in Eq. 7-8. This was chosen because it determines minor savings compared to other depreciation methodologies therefore resulting in a more conservative economic estimate. The total capital for depreciation was assumed equal to the fixed capital investment since a salvage value zero has been taken as common custom for chemical plants and either to be more conservative.

$$d_k = \frac{FCI}{y_{PlantLife}} \tag{7-8}$$

where d_k is the yearly depreciation in year *k*, *FCI* is the fixed capital investment equal to the capital investment and $y_{PlantLife}$ is the total year considered for the profitability analysis of the plant. In particular, the project duration was assumed of 5 years, which is comparable with membranes lifetime, even though this is a conservative choice for the economic analysis. The land was assumed zero as the integrated process footprint is little compare to the industrial plant one, while the working capital was neglected as the feed material is the industrial plant waste stream and the reactants employed in the process are already present in the industrial site.

The yearly plant expenses (E_k) are evaluated as sum of the annual manufacturing cost ($OPEX_k$) and yearly depreciation (d_k) (Eq. 7-9):

$$E_k = OPEX_k + d_k \tag{7-9}$$

A fixed taxation rate (*t*) of 33% of profits (corporate taxation rate in Italy) was assumed, where the profit is the difference between annual revenues (R_k) and expenses (E_k). These two variables have significance after the plant start-up, which was assumed it takes place in 6 months. Thus, the net cash flow (CF) for the first half year is the FCI, afterwards is the net profit after tax (*Net Tax Profit*$_k$) plus the yearly depreciation expressed in Eq. 7-10:

$$CF_k = Net\ tax\ Profit_k + d_k = (R_k - E_k) * (1 - t) + d_k \tag{7-10}$$

To account for the time value of money the discounted cash flow (DCF) was calculated. The DCF of year *k* was calculated by offsetting the cash flow years by interest rate *t* according to Eq. 7-11, *t* was assumed 4 %.

$$DCF_k = \frac{CF_k}{(1+t)^k} \qquad 7\text{-}11$$

All the inputs for the profitability analysis relevant to the TecnoZinco case study (ref. Future Size I in Table 7-1) are summarized in Table 7-5 and the resulting cumulative discounted cash flow (CDCF) diagram for the Tecnozinco plant is shown in Figure 7-3.

Table 7-5. Profitability analysis inputs and index for the TecnoZinco case study (ref. Future Size I in Table 7-1).

Profitability analysis inputs		**Unit**
Plant Capacity (F_{WAS})	130	l/h
Process Steel	2030	kg/h
DD total area (A_{DD})	25	m^2
MD total area (A_{MD})	43.5	m^2
FCI	160	k€
$OPEX_k$	125	k€/y
Revenues	180	k€/y
Project duration (n)	5	y
Taxation rate (t)	33%	-
Interest rate (i)	4%	-

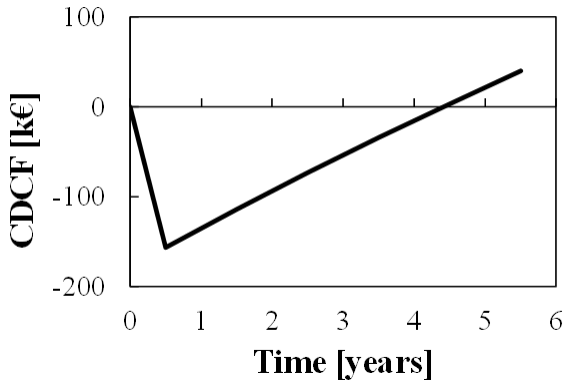

Figure 7-3. Cumulative discounted cash flow versus time.

Specifically, a simplified profitability analysis was performed estimating three main indexes: (i) Net Present Value (NPV), which is the cumulative discounted cash position at the end of a project; (ii) Discounted Payback Period (DPBP), which is the time required, after star up, to recover the capital investment; (iii) Discounted Cash Flow Rate of Return (DCFROR), which is the rate of interest corresponding at zero net present value.
Determined through calculation but also visible in the graph is a DPBP of 4 years. After an assumed 5 years of project duration, the net present value (NPV) is 40.000 € and the DCFROR is 12.6%. The NPV shows the project is profitable. Furthermore, it is really worth noting the economic analysis does not take into account the valuable benefit resulting from the reduction of the plant ecological burden. Notably, it is expected that according to the economy of scale, increasing capacity will reduce the ratio of investment cost to treatment capacity.

7.4 **Conclusions**

In the present chapter, a detailed economic analysis was presented for the hybrid system to be integrated in the hot dip galvanizing process chain as waste liquor treatment/recycling technology. Economic considerations were performed aiming to demonstrate the feasibility of the developed technology. The capital expenditure costs (FCI) were collected through an extensive cost tracking performed during the realization of the pilot scale prototype. Calculations for upscaling scenarios with a capacity from 0.1 m^3/h to 10 m^3/h were added, thus covering all hot-dip galvanizing industry typical capacities. A standard profitability analysis was carried out by following the well knowing procedure described by Turton et al.

Engineering economic analysis results showed that a values of 40.000€ for the NPV can be reached making the project profitable.

The integration of the proposed process in the industrial plant is quite easy, as it does not require any particular modification of the site. Moreover, it is here found to have a huge potential for the relevant sector industry as it provides a solution for the simultaneous reduction of costs and environmental impact, thus moving the pickling process towards a higher level of sustainability.

8. PROCESS OPTIMIZATION

Chapter Outline

8.1 Introduction

At this point of investigation and once all the information has been gathered through laboratory and pilot operations, as well as from economy analysis assessing, the problem of how optimize the process is impending. An optimization analysis is required to create more insight in the proposed technology and increase the attraction from relevant industry, showing when the technology integration into the traditional pickling industry could provide a significant beneficial solution. The process variables optimization relies on solving mass balance equations using a process simulator. gPROMS process simulator has been selected for the steady-state optimization purpose. The model equations are based on the process flow diagram of the pilot plant and the integrated mathematical model developed and made available on the Excel platform (see Chapter 4) [123]. Main rearrangements on the integrated process model concerns the plant scaling equations. Generalization issues were considered, in order to make the analysis not only suitable for the specific case of the Tecnzinco plant.
The impact of key operating and design variables was investigated and optimized configurations are presented in the following chapter.
The importance of apply an optimization analysis if on one side is necessary to investigate the best operating and design conditions, in the other side it aims to explore the possible weakness of the technology. First of all, a limitation on the acid consumption was imposed in order to have a consumption value comparable to the current industrial usage, then considerations on the reduction of fresh water demand were implemented through a multi-objective approach, aiming at identify the most profitable scenarios along with minimizing the plant water consumption. Among the different multi-objective techniques studied [146]–[148], the ε-constraints method has been selected, as we deal with a problem with two objective functions. Thus, the multi-objective approach has been converted in a single objective formulation by parameterizing the second objective function.

8.2 Process modeling on gPROMS

In Table 8-1 are summarized all the main equations implemented on gPROMS. The model construction has been implemented by including gradually the different model units (e.g. Pickling, Diffusion Dialysis, Membrane Distillation, Reactive precipitator) and linking all the

sections through a “Integrated Process” model section together with the Density model and the Economic section. A screenshot of the models section in gPROMS is reported in Figure 8-1.

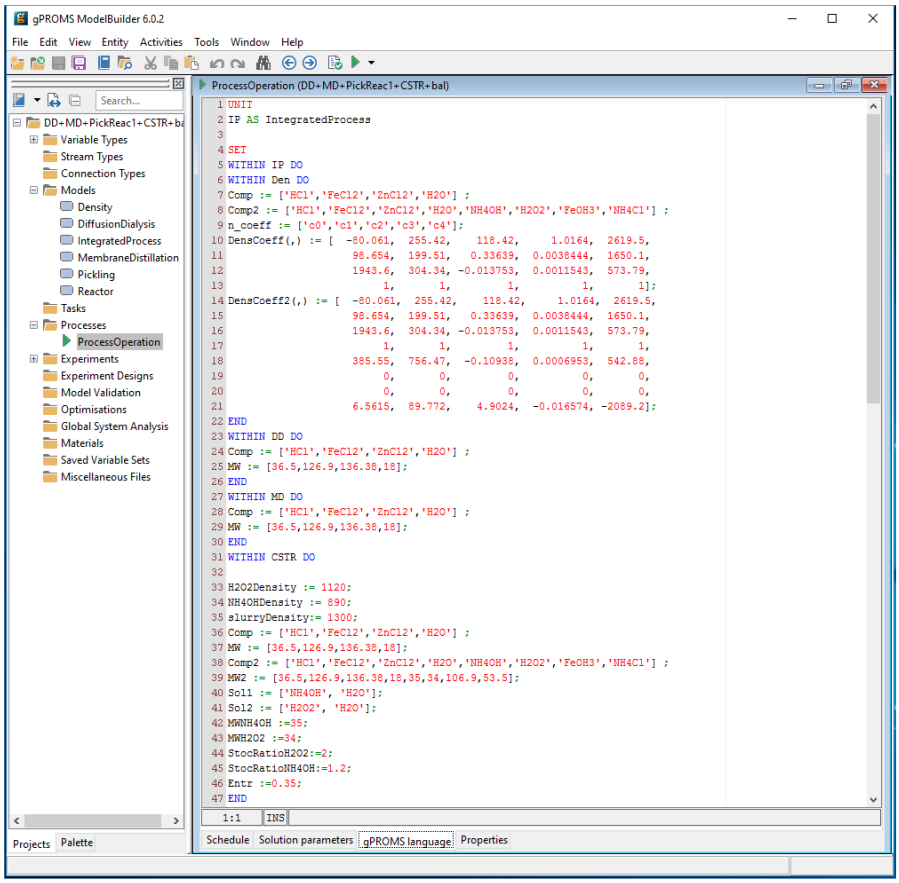

Figure 8-1 gPROMS framework highlighting the different model units.

Main equations concern the *Pickling* section are the evaluation of the kinetic constants for the different components in the pickling bath (*i*) throughout acid consumption data collected from historical statistics of the company. For each inlet and outlet streams (*s*) of the pickling bath volumetric flow rate, concentration and component mass flow rates variables are defined and mass balance equations implemented, as for all the streams in the different sections. Correlation between acid and iron concentration, waste acid volumetric flow rate and mass flow rate of the processed steel is assessed through the Fe component mass balance equation

on the pickling bath and considering the optimal pickling relation between acid and iron in the pickling liquor.

In the *Diffusion Dialysis* model section, fluxes correlations across the anionic exchange membranes were implemented considering the different permeability values assessed through the DD lab tests and considering the global mass balance equation for the DD streams. The membrane area is a design variable for the scale-up purpose. Performance key parameters (e.g. acid recovery and metals leakage) were defined.

For the *Membrane Distillation* section, fluxes correlation dependent on the inlet acid concentration and flow rate executed. The unit scale-up was conceived as different modules in parallel, imposing a maximum capacity per repetitive unit.

In the precipitator *Reactor*, reactions are defined with their own conversion rate. Reactants mass flow rate were evaluated correspondently, and mass balance equations are implemented for the output products evaluation. Reactor design scale up, differently from the membrane units, has minor impact on the investment cost, therefore the cost trend is included in the lamp factor correlation and not displayed as a function of the unit size.

A *Density* model section with Laliberté et al. equations [108] has been implemented too.

The *Integrated Process* includes all the connectivity equations between the different units and the mass balance equation for the DD drawing solution which is the results of process water integration with MD permeate stream.

At last, the *Economic* section, with NPV, DCFROR and DPBP variables was added to perform cost optimization.

Table 8-1. Integrated Model equations.

Pickling	
$Cons/Prod_{i_p,p} = \frac{\upsilon_{i_p,p}}{\upsilon_{HCl,p}} Cons/Prod_{HCl,p} \cdot \frac{MM_{i_p}}{MM_{HCl}} \quad \forall\, i_p \neq \mathrm{HCl}$	p pickling reactions
$\sum_p Cons/Prod_{i_p,p} = 10^{-3} \cdot K_{i_p} \cdot w_{steel}$	$Fe_2O_3 + Fe + 6HCl = 3FeCl_2 + 3H2O$ $Fe3O4 + Fe + 8HCl = 4FeCl2 + 4H2O$
	i_p pickling components
$Cons/Prod_{HCl,p} = -10^{-3} \cdot K_{HCl} \cdot \chi_p \cdot w_{steel}$	Fe_2O_3, Fe_3O_4, Fe, $FeCl_2$, HCl, $ZnCl_2$, H_2O
	s pickling streams
$w_j^s = c_j^s \cdot F^s \cdot MM_j$	MU, RPS, $entr_{in}$, $entr_{out}$, WAS
$F^s \cdot \rho^s = \sum_s w_j^s$	j components
	HCl, $FeCl_2$, $ZnCl_2$, H_2O
$w_j^{RPS} + w_j^{MU} + w_j^{entr_{in}} + 10^{-3} \cdot K_j \cdot w_{steel} = w_j^{WAS} + w_j^{entr_{out}} + w_j^{evap}$	

$$F^{WAS} \cdot c_{FeCl_2}^{WAS} \cdot MM_{FeCl_2} = 10^{-3} \cdot K_{FeCl_2} \cdot w_{steel} + w_{FeCl_2}^{RPS} + w_{FeCl_2}^{entr,in}$$

$$c_{FeCl_2}^{WAS} = -0.544 \cdot c_{HCl}^{WAS} + 3.581$$

$$HCl_{comsumption} = \frac{F^{MU} \cdot \rho^{MU}}{w_{steel}}$$

Diffusion Dialysis

$$J_j^{DD} = \sum_i \left(P_{j,i} \frac{c_i^{WAS} - c_i^{RAS} + c_i^{MRB} - c_i^{DS}}{2} \right)$$

$\forall\ j \neq H_2O$
i = HCl, $FeCl_2$, $ZnCl_2$

$$J_{H_2O} = P_{H_2O} \cdot \Delta\Pi + \sum_m \beta_i J_j^{DD}$$

$$w_j^{MRB} = w_j^{WAS} - J_j^{DD} \cdot MM_j \cdot A_{DD}^{tot}$$

$$w_j^{MRB} + w_j^{RAS} = w_j^{WAS} + w_j^{DS}$$

$$RR_{HCl} = \frac{w_{HCl}^{RAS} - w_{HCl}^{DS}}{w_{HCl}^{WAS}};\ Leak_{Fe;Zn} = \frac{w_{Fe;Zn}^{RAS} - w_{Fe;Zn}^{DS}}{w_{Fe;Zn}^{WAS}}$$

$$FlowRatio = \frac{F^{DS}}{F^{WAS}}$$

$$n_{AEM} = \frac{A_{DD}^{tot}}{Z \cdot W}$$

Membrane Distillation

$$J_j^{MD} = a_j \left(\frac{F^{RAS} \cdot \rho^{RAS}}{n_{feed}} \right)^2 - b_j \left(\frac{F^{RAS} \cdot \rho^{RAS}}{n_{feed}} \right) + c_j$$

a_j, b_j, c_j = $f(c_{HCl}^{RAS})$

$$J_{FeCl_2}^{MD} = J_{ZnCl_2}^{MD} = 0$$

$$w_j^{Perm} = A_{MD} \cdot J_j^{MD} \cdot n_{feed}$$

$$w_j^{RPS} = w_j^{RAS} - w_j^{Perm}$$

$$A_{MD}^{tot} = A_{MD} \cdot n_{feed}$$

$$ConversionRatio = \frac{w_{HCl}^{RPS}}{w_{HCl}^{RAS}}$$

Reactor

$$\zeta_{r_1} = \upsilon_{HCl}^{r_1} (c_{HCl}^{MRB} - 10^{-pH}) F^{MRB}$$

$$\zeta_{r_2} = \upsilon_{FeCl_2}^{r_2} \cdot c_{FeCl_2}^{MRB} \cdot F^{MRB}$$

$$w_{NH_4OH}^{alk} = -\left(\frac{\upsilon_{NH_4OH}^{r_1}}{\upsilon_{HCl}^{r_1}} \zeta_{r_1} + \frac{\upsilon_{NH_4OH}^{r_2}}{\upsilon_{FeCl_2}^{r_2}} \zeta_{r_2} \right) MM_{NH_4OH} \cdot f_{NH_4OH}^{excess}$$

r_1 and r_2 reactions
r_1: HCl + NH_4OH = NH_4Cl + H_2O
r_2: $FeCl_2$ + 1/2 H_2O_2 + $2NH_4OH$ = $Fe(OH)_{3(s)}$ + $2NH_4Cl$

alk: NH_4OH, H_2O
ox: H_2O_2, H_2O

$$w_{H_2O_2}^{ox} = -\frac{v_{H_2O_2}^{r_2}}{v_{FeCl_2}^{r_2}}\zeta_{r_2} MM_{H_2O_2} \cdot f_{H_2O_2}^{excess}$$

$$\begin{cases} w_{NH_4OH}^{ORP} = \left(1 - \frac{1}{f_{NH_4OH}^{excess}}\right) w_{NH_4OH}^{alk}(1-\alpha) \\ w_{H_2O_2}^{ORP} = \left(1 - \frac{1}{f_{H_2O_2}^{excess}}\right) w_{H_2O_2}^{ox}(1-\alpha) \\ w_{NH_4Cl}^{ORP} = \left(\frac{v_{NH_4Cl}^{r_1}}{v_{HCl}^{r_1}}\zeta_{r_1} + \frac{v_{NH_4Cl}^{r_2}}{v_{FeCl_2}^{r_2}}\zeta_{r_2}\right) MM_{NH_4Cl}(1-\alpha) \\ w_j^{ORP} = \left(w_j^{\mathrm{MRB}} + \left(\frac{v_j^{r_1}}{v_{HCl}^{r_1}}\zeta_{r_1} + \frac{v_j^{r_2}}{v_{FeCl_2}^{r_2}}\zeta_{r_2}\right) MM_j\right)(1-\alpha) \end{cases}$$

$$\begin{cases} w_{i_r}^{MS} = w_{i_r}^{ORP} \cdot \frac{\alpha}{1-\alpha} \quad (liq) \\ w_{Fe(OH)_3}^{MS} = v_{Fe(OH)_3}^{r_2} c_{FeCl_2}^{MRB} F^{MRB} \cdot MM_{Fe(OH)_3} \end{cases}$$

i_r reactor components
i_r =j+NH_4OH, H_2O_2, NH_4Cl

Density

$$\frac{1}{\rho} = v_{mix} = x_{w,H_2O} \cdot v_{H_2O} + \sum_i v_i = x_{w,H_2O} \cdot v_{H_2O} + \sum_i x_{w,i} v_{app,i} \quad [108]$$

Integrated Process

Connectivity equations

$$w_j^{DS} = w_j^{Perm} + w_j^{PW}$$

$$WaterRatio = \frac{F^{PW}}{F^{DS}}$$

Economic

$$NPV = \sum_{y=0.5}^{y_{PlantLife}} DCF_y$$

$$\sum_{y=0.5}^{y_{PlantLife}} \frac{CF_y}{(1+DCFROR)^y} = 0$$

$DPBP$ = *time to recover the FCI after start-up*

Once the model was implemented and it was running, simulations at different conditions are available and they are presented in the following sections.

8.3 Optimization formulation and process scale-up

8.3.1 *Optimization with operating variables*

In Table 8-2 are listed all the operating variables which can affect the overall process performance.

Table 8-2. Operating variables.

Process unit	Variable list
Pickling process	Processed steel
	F_{WAS}
	WAS composition ($c_{HCl,WAS}$)
Diffusion Dialysis DD	F_{DS}/F_{WAS}
	RR, Fe and Zn leakage
Membrane Distillation MD	Thermostatic line temperature and flow rate
	MD permeate production
	Conversion ratio MD
Reactive precipitator CSTR	Reactants flow rate
	Sludge flow rate ($Fe(OH)_3$ and $ZnCl_2$ flow rates)

As explicative example, a sensitivity analysis by varying the HCl concentration is reported in Figure 8-2 Figure 8-2. Profitability inputs reported in Table 7-5 were selected as reference case, so while investigating one variable all the others are kept equal to their value in the reference case. Steady state operations were studied, which impose the choice of one variable between the feed flow rate and the acid concentration of the waste stream if the plant capacity is considered as a given data in the model.

Undoubtedly, the HCl concentration in the pickling bath, and consequently the Fe concentration as predict from the Kleingarn curve [11], strongly affects flow rates, composition and performance parameters of the integrated system. Figure 8-2 shows the main operating variable in the different section of the integrated model by letting the HCl waste acid concentration to range from 2 to 5 M. As shown in Figure 8-2(a), declining performances are detected in the DD recovery ratio (RR), as lower recovery values are observed when inlet acid concentration increases. Moreover, although lower iron concentrations correspond to

higher acid concentrations according to the Kleingran curve, the benefit in reduced metals leakage $Leak_{Fe;Zn}$is not so prominent. ConversionRatio in the MD, defined as the ratio between the amount of acid recovered and the MD inlet acid amount, presents a non-monotonic trend. At low c_{HCl}^{WAS} concentrations the ConversionRatio decreases despite the increasing of acid concentration in the recovered pickling solution, as the recovered amount is lower compared to the inlet acid (in the recovered acid solution). Then, at the higher waste acid concentrations, which means higher acid concentrations in the recovered acid solution, the water vapour pressure decreases, thus reducing the water extraction through the MD unit, causing an increase of the conversion ratio (Figure 8-2(b)). Performance of the integrated process are expressed with the acid consumption, i.e. the make-up acid for processed steel, and the water ratio), which is significant of the plant water demand, which both get rapidly worse increasing the HCl pickling bath concentration as visible in Figure 8-2(c).

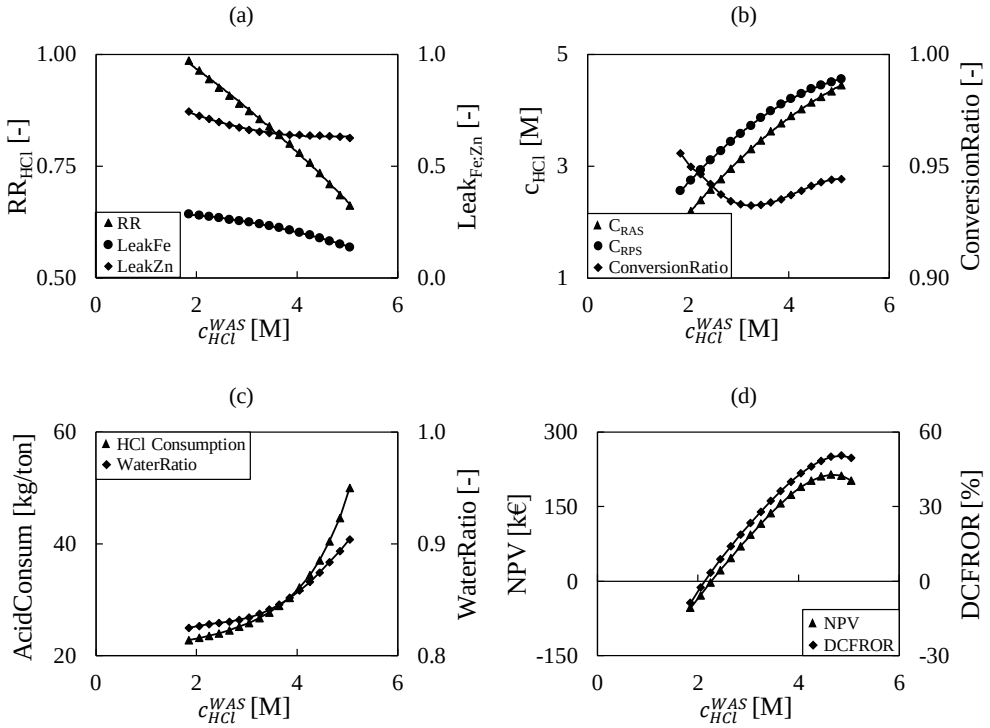

Figure 8-2 Sensitivity analysis with $\boldsymbol{c_{HCl}^{WAS}}$ for the key variables in the DD (a), MD (b), Pickling and Integrated Process (c) and Economic (d) model sections.

The profitability analysis, expressed by the NPV and DCFROR indexes in Figure 8-2(d), predict a maximum at around 4.5 M. However, at this maximum profitability, the consumption of water and acid would be significant higher than the galvanizing companies' standard average consumption.

Based on these sensitivity analysis results, an optimize configuration is gained through the gPROMS process optimization tool simulation. Inputs for the optimization problem are presented in Table 8-3 while results are presented in Table 8-4.

The optimum value, for the Tecnozinco plant, is not so far from the designed variables values (see value obtained in Section 7.3 as benchmark), as the process was designed by choosing the best operating condition performing several sensitivity analyses (see Section 4.4). In addition, the NPV is constrained by the acid consumption which has been chosen comparable to the average acid consumption reported from galvanizing companies, resulting in a limitation for the acid concentration and, consequently, for the net profit. The corresponding *DPBP* is 3.6 years.

Table 8-3 Optimization problem formulation with operating variable.

Optimization			
Given (Scenario)		Plant throughput	w_{steel} = 2030 kg/h
Control variable		Feed flow **(**F^{WAS}) or (c_{HCl}^{WAS})	
Maximize (Obj. function)		NPV	
Constraint	Equality	Steady state operation	
		Acid consumption	25 kg/ton*
	Inequality	Channel velocity	0.1 cm/s < v_{DD}& v_{MD} <3 cm/s
		FlowRatio	0 .5< $\frac{F^{DS}}{F^{WAS}}$<1.5

*AIZ comparable acid consumption data

Table 8-4 Optimization results for the scenario with operating variable as control variables.

Cases	**Variables**	**Designed value**	**Optimized Value**	**Objective function NPV**
Tecnozinco plant	F^{WAS}	130 l/h	135l/h	63,777 €
	c_{HCl}^{WAS}	2.6 M	2.7 M	

8.3.2 *Optimization with operating and design variables*

Profitability of the process strongly depend on the design variables (see Table 8-5), as the capital cost of investment increases with the membrane unit area.

Table 8-5. Design variables.

Process unit	Variable list
Diffusion Dialysis DD	DD total area A_{DD}^{tot}
Membrane Distillation MD	MD total area A_{MD}^{tot}

In a similar way as conveyed for the acid composition sensitivity, in Figure 8-3 a sensitivity analysis is reported by varying the total membrane area of the DD and MD unit. In particular, the DD membrane area is increased for each iteration, while the MD a constant feed flow rate has been fixed for the single unit, thus the total membrane MD area is increasing as the feed flow rate (RA) is increasing as well. An increase of the design variables will benefit, obviously, on the membrane unit performances in terms of recovered acid increasing (RR), even though higher metals leakages occur, as concerned for the DD unit (Figure 8-3(a)); a concentration rate constant is observed in the MD process (Figure 8-3(b)). Thus an overall acid consumption reduction can be obtained in Figure 8-3(c), while the water ratio is increasing because the increasing on the drawing solution flow rate demand is higher than the permeate production from the MD process. Clearly, the NPV (Figure 8-3(d)) of the process will see a falling trend for the higher investment costs.

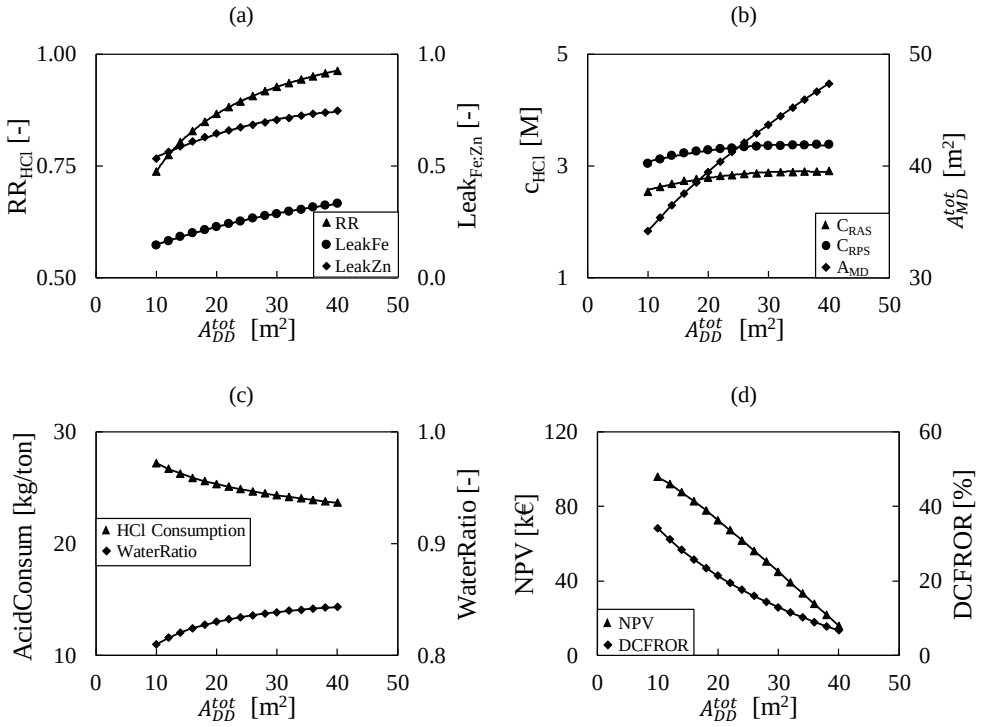

Figure 8-3 Sensitivity analysis with $\boldsymbol{A_{DD}^{tot}}$ for the key variables in the DD (a), MD (b), Pickling and Integrated Process (c) and Economic (d) model sections.

In Table 8-6 is proposed an optimization simulation with both the operating and the design variables.

Table 8-6 Optimization problem formulation with operating and design variables.

Optimization			
Given (Scenario)	Plant throughput	Tecnozinco Future Size II	w_{steel} = 2030 kg/h w_{steel} = 10000 kg/h
Control variables		Feed flow (F^{WAS}) DD membrane area (A_{DD}) MD membrane area (A_{MD})	
Maximize (Obj. function)		NPV	
Constraint	Equality	Steady state operation	
		Acid consumption	25 kg/ton*
	Inequality	Channel velocity	0.1 cm/s < v_{DD}& v_{MD} <3 cm/s
		FlowRatio	0 .5< $\frac{F^{DS}}{F^{WAS}}$<1.5

*AIZ comparable acid consumption data

Optimized values are comparable with results obtained for the operating variable optimization configuration (see Table 8-4): feed flow and acid concentration are quite similar, while the different membrane areas determine the variation in the resulting net profit.

An up-scaled scenario with a processed steel capacity of 10,000 kg/h (ref. Future Size II in Table 7-1 in Chapter 7)) was also analysed as presented in Table 8-7 to cover a larger portion of galvanizing plant size, as the Tecnozinco plant capacity is considered small in the relevant sector. Of course, economy of scale guarantees a higher economical return.

Through upscaling over 913,000 € of NPV is reachable and the discounted payback period decreased from 3.4 to 2.2 years.

Table 8-7 Optimization results for the scenario with operating and design variables as control variables.

Cases	Optimized Value		Objective function NPV (€)
Tecnozinco case study	F^{WAS}	142 l/h	79630
	A_{DD}	30.5 m^2	
	A_{MD}	34.7 m^2	
$\boldsymbol{w_{steel}}$ = 10,000 kg/h	F^{WAS}	842 l/h	913000
	A_{DD}	231 m^2	
	A_{MD}	217 m^2	

8.3.3 *Trade-off solution between profitability and environmental issue*

The profitability aspect was considered so far. A strong limitation was imposed by fixing the acid consumption of the plant, which bounds the acid make up demand. A further critical issue related to the integration of the process in the industrial plant is explored in the present section. The process was proposed in order to avoid exhausted process fluids, and this benefit aspect was taken into account by considering the money saving for the avoided disposal. Another crucial aspect regards the reduction of water use and wastewater production. The DD unit requires drawing solution flow rate comparable to the waste acid flow rate. Almost 90% of the drawing solution is taken from process water. In order to reduce the fresh water consumption, a threshold value has to be considered to have the highest profit along with a low water consumption.

The trade-off value was evaluated considering the multi-objective optimization approach, in order to find out the preferred solutions that maximize the NPV objective function while

minimizing the WaterRatio variable. To this purpose, Pareto Frontier was found by considering the ε-constraints method [148], constructed by using the maximum NPV for a given WaterRatio value, thus converting a multi-objective analysis to a parameterized single-objective one.

Results for this configuration show a strong sensibility of the NPV values with the WaterRatio, as a slight reduction of the water utilization leads to a significant increase of the MD membrane area. Thus NPV is firmly reduced, making this configuration unprofitable for a WaterRatio of about 80% as shown in Figure 8-4(a) (blue line).

In the same figure, a second configuration is also shown. In order to reduce the water demand, a second MD Brine unit has been included in the process. The aim of this second MD unit is to concentrate the fluxing solution while recovering a part of the process water to be used as drawing media in the diffussion dialysis. A schematic representation of the integrated process with the second MD unit is also reported in Figure 8-5. The intregration of this MD Brine leads to an introduction of an additional control variable which is the total membrane area of the unit. For simplicity and comparative purpose, same selling/saving cost for the fluxing solution has been assumed, even though the higher concentration of the solution leads to higher revenues for the plant, thus making the analysis more conservative. The introduction of this second MD gives an wider range of variation, since optimizationg will act on incresing the membrane area of the second MD unit while slightly varying the total DD and MD membrane areas (see Figure 8-4(b)). At any value of WaterRatio the process is profittable Figure 8-4(b) orange line).

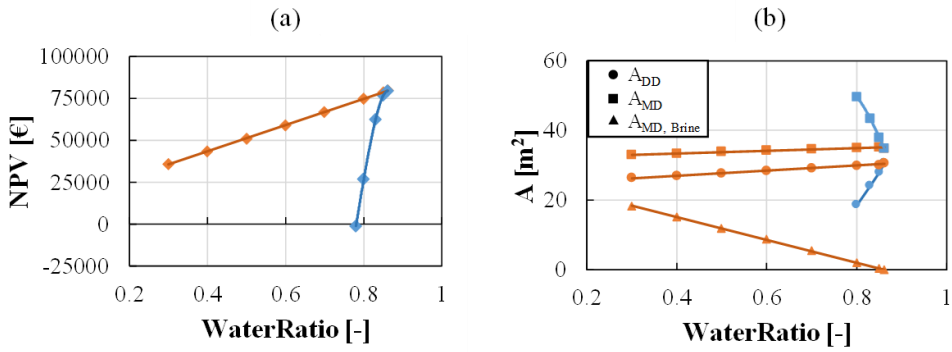

Figure 8-4 (a) Pareto frontier and (b) optimal value of the total membrane area vs WaterRatio variable. Scenario without (blue) and with (orange) the MD unit for outlet brine treatment.

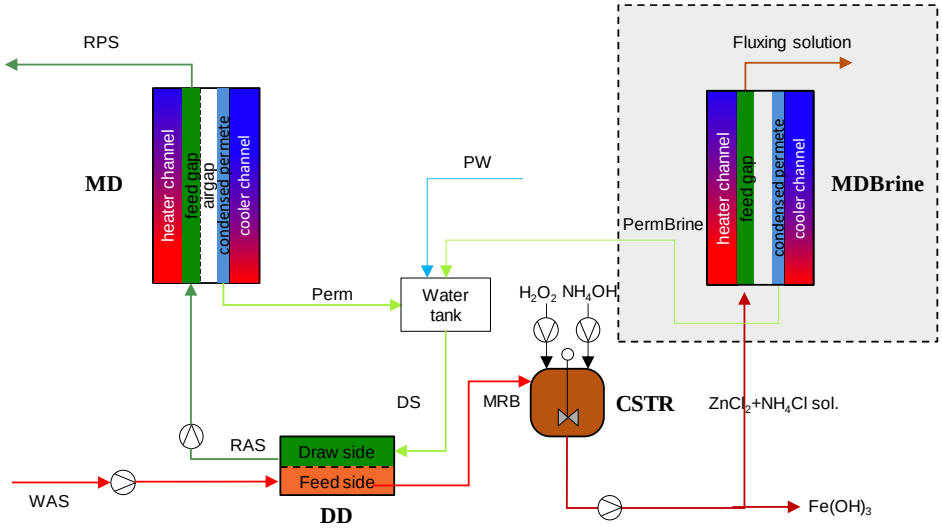

Figure 8-5 Schematic representation of the main units of the integrated process with additional MD brine unit.

8.4 **Conclusions**

The gPROMS software was employed (i) to simulate steady state operations of the process and (ii) to perform optimization analyses. The optimization problem formulation was aimed to maximize the NPV of the process using, firstly, the acid concentration as operating parameter and then the design variables (membrane modules areas) as control variables. The profitability of the plant in both cases is constrained by the acid consumption parameters, as the highest NPV would be always at the highest acid concentration values. Nevertheless, the process is profitable even for the low size capacity of the Tecnozinco plant. An upscaling scenario was also included in order to boost the interest of medium-sized galvanizing enterprises, which are the common sizes for the hot-dip galvanizing plants. According to the economy of scale, this last configuration gives a further optimistic perspective in the future integration of the technology in the industrial scale. Furthermore, the reduction of ecological burden poses a significant valuable benefit in all the scenarios investigated.

At last, a multi-objective optimization has been performed to address the environmental aspect regarding the reduction of water use and wastewater production. Pareto Frontiers were

constructed by considering di ε-constraints method for the standard configuration and for a second scenario including a MD brine unit for fluxing solution concentration.

Comparison of the two scenario shown that there is no a large margin of variation for the standard case, thus the second MD brine unit has to be integrated into the process as trade-off solution between profitability and environmental issue.

FINAL REMARKS AND OUTLOOKS

The aim of this PhD thesis was to provide a proof of the possibility of valorise the industrial pickling waste liquors through the design, development and operation of a membrane hybrid system. To this aim, both modeling and experimental activities were carried out.

The main achievements of the research activities can be summarised as in the following:

i. *Characterisation of the Diffusion Dialysis process for highly concentrated pickling waste solutions.* Modeling and experimental activities were carried out in order to evaluate the impact of using highly concentrated solution within the diffusion dialysis system.

ii. *Development of a metals recovery system.* Experimental activities and conceptual studies were carried out in order to allow the enhancement of the metals present in the pickling waste and, thus, to accomplish the circular approach.

iii. *Development of an integrated process simulator*. Based on modeling and experimental activities for the single process units, a model of the integrated system was developed in order to support the design and operation of the pilot system.

iv. *Commissiong and testing of the integrated system pilot unit.* A demonstrator plant was jointly designed and constructed by Fraunhofer ISE, eventually installed and tested in the industrial environment in order to demonstrate the feasibility in reducing wastewater disposal and guarantying continuous optimal conditions in the relevant industrial processes.

v. *Economic analysis and Process Optimization.* Engineering economic analysis regarding the integration of the technology in the industrial environment was implemented. The optimization problem formulation was presented to investigate the impact of operating and design variables.

For the above five main points, the following concluding remarks are here made.

i. *Characterisation of the Diffusion Dialysis process for highly concentrated pickling waste solutions.*

The first period of this PhD thesis was dedicated explore the diffusion dialysis units. A laboratory batch and a large-scale continuous module, equipped with Fumasep FAD anionic exchange membranes, were used for characterizing the behaviour of the system fed by artificial solution mimicking the real industrial solutions composition. The main effects of operating parameters were highlighted and presented as process performance variations.
The whole process was mathematically described within a time/space distributed-parameters model. The model, implemented in Excel®, describes all the main phenomena involved in the process. The DD model was calibrated and validated against experimental results for a wide range of acid, iron and zinc concentrations, showing in all cases a good agreement with the experiments.

ii. *Development of a metals recovery system.*

Separation of heavy metals from the highly metals concentrated solution leaving the Diffusion dialysis module was studied in order to ensures the resources circularity strategy and the total elimination of the waste. A continuous stirred tank reactor CSTR with an external cooling loop (shell and tube heat exchanger) for the metals separation purpose was selected as a result of the experimental campaign carried out at UNIPA laboratory. Hydrogen peroxide (30% w/w) and ammonium hydroxide (30% w/w) solutions were employed in order to precipitate a nearly pure iron hydroxide solid product (99% purity) and producing a zinc/ammonium chloride solution as by-product for the galvanizing industry itself. Moreover, the laboratory experimental campaign laid the basis for the design of the pilot scale reactive precipitator.

iii. *Development of an integrated process simulator.*

Common industrial practices at Tecnozinco hot-dip galvanizing plant were assimilated in order to have a detailed description and characterization of the industrial process, for the purpose of develop a model as realistic and descriptive as possible of the real operating conditions. As result, a process simulator able to simulate the integrated system operations was developed and implemented in Microsoft® Office Excel spreadsheets with Macros in Visual Basic language. The so constructed model is a hierarchical model including all the sub-models of the plant. The goal was to create a mathematical tool that gives predictive

information on what may be the characteristics of the currents upstream and downstream of each process unit of the integrated system as the main operating conditions vary, with the final aim of supporting the design, construction and operation of a pilot system. The main result of this modeling activity is that whatever it was the initial acid concentration optimal stationary conditions were maintained in the entire process through the continuous regeneration of the waste solution by removing iron and zinc released in the bath and recycling almost all the free acid to the pickling tank.

iv. *Commissiong and testing of the integrated system pilot unit.*

The demonstrator pilot-scale plant of the integrated process was constructed and assembled in all its parts by Fraunhofer ISE staff at its premises in Freiburg, Germany, where I spent more than four months by flanking the assembling activities. The unit has been subsequently installed and operated in real environment at Tecnozinco SrL in Carini (Sicily, Italy). Eighth months of demonstrator operation were proved the operational stability and performance of the demonstrator. Overall, operational results have shown that acid can be successfully recovered and re-concentrated, iron salt recovered in the form of marketable hydroxides and fluxing solution. Both acid and fluxing solution can be recirculated into the plant, thus eliminating any waste stream to be disposed. High level of system reliability and robustness was achieved by the implementation of an industrial-type central process control system.

v. *Economic analysis and Process Optimization.*

Economic considerations regarding the integration of the technology in the industrial environment and optimization analysis and strategies were considered and implemented in the final part of the research activities.

A standard profitability analysis was carried out by following the well knowing procedure and results showed that the project is profitable.

The integrated model was further implemented on the gPROMS modeling platform in order to run optimization analysis on the process performances. The optimization analysis was carried out at the University of London, UCL Engineering Chemical Department, under the supervision of Prof. David Bogle where I spent 4 months. The results of the optimization analysis showed that to take into account both profitability and a possible environmental problem, expressed in terms of mains water consumption, a second MD unit has to be

integrated into the process. In fact, it will be possible concentrate the fluxing solution exiting the reactive precipitator thus producing water to be subtracted from the DD process demand. Of interest, the technology integration into the traditional pickling industry could provide a solution both for costs reduction and for the ecological impact of the metallurgical industry.

NOMENCLATURE

Acronyms

AEM	Anion Exchange Membrane
AGMD	Air Gap Membrane Distillation
AIZ	Italian Galvanizing Association
BAT	Best Available Technologies
C	Cost
CCFD	Cumulative Cash Flow Discounted
CF	Cash Flow
CSTR	Continuous Stirred Tank Reactor
CT	Conductivity Transmitter
CW	Cooling Water
DCF	Discounted Cash Flow
DCFROR	Discounted Cash Flow Rate of Return
DCMD	Direct Contact Membrane Distillation
DD	Diffusion Dialysis
DPBP	Discounted Payback Period
DS	Draw Solution
E	Expenses
ED	Electrodialysis
EGGA	European General Galvanizers Association
EPA	Environmental Protection Agency
EU	European Union

FCI	Fixed Capital Investment
FGAGMD	Feed Gap Air Gap Membrane Distillation
FO	Fresh Oxidant
FR	Fresh Reactant
FS	Fluxing Solution
FT	Flow Transmitter
FW	Fresh Water
GOR	Gain Output Ratio
H	Electric Heater
HMI	Human Machine Interface
HW	Heating Water
HX	Heat Exchanger
IEMs	Ion Exchange Membranes
IN	Initial
IPPC	Integrated Pollution Prevention and Control
LT	Level Transmitter
MD	Membrane Distillation
MRB	Metals Rich Brine
MS	Metal Sludge
MU	Make-up
NPV	Net Present Value
OPEX	Operating Expenses
ORP	Outlet Reactive Precipitator
P	Pump
P&I	Piping and Instrumentation Diagram
PFD	Process Flow Diagram
PFR	Plug Flow Reactor
PLC	Programmable Logic Controller

PM	Person-Months
PT	Pressure Transmitter
PW	Process Water
R	Revenues
RA/RAS	Recovered Acid Solution
ReWaCEM	Resource recovery from industrial Waste water by Cutting Edge Membrane technologies
RO	Reverse Osmosis
RPS	Recovered Pickling Solution
RW	Recovered Water
S	Selling
S	Slurry
SPS	Spent Pickling Solution
T	Thermostatic
theor	theoretical
TT	Temperature Transmitter
WA/WAS	Waste Acid Solution

Symbols

A	$[m^2]$	area
a	[-]	absorption coefficient
c	$\left[\frac{mol}{l}\right]$	molar concentration
C	$\left[\frac{g}{l}\right]$	mass concentration
$Cons/Prod$	$\left[\frac{kg}{h}\right]$	consumption/production
CR	[-]	concentration ratio
D_{eq}	$[m]$	hydraulic diameter

$\mathcal{D}$	$\left[\frac{m^2}{s}\right]$	mass diffusivity
d	[€]	yearly depreciation
F	$\left[\frac{l}{s}\right]$	volumetric flow rate
f	[-]	multiplicative factor
flux	$\left[\frac{l}{h \cdot m^2}\right]$	flux
h	$\left[\frac{W}{m^2 \cdot K}\right]$	heat coefficient
h_v	$\left[\frac{kJ}{kg}\right]$	enthalpy of evaporation
I	$\left[\frac{mol}{kg}\right]$	ionic strength
J_i	$\left[\frac{mol}{m^2 \cdot s}\right]$	molar flux
$J_w; J_{os}; J_{dr}$	$\left[\frac{l}{m^2 \cdot s}\right]$	volumetric flux
i	[-]	Van´t Hoff coefficient
K_{eq}	[-]	equilibrium constant
K	$\left[\frac{kg}{ton}\right]$	kinetic constant
k	$\left[\frac{m}{s}\right]$	mass transport coefficient
m	$\left[\frac{mol}{kg}\right]$	molality
mass	[kg]	mass
MM	$\left[\frac{g}{mol}\right]$	molar mass
n	[-]	discretization number
$n°$	[-]	number of moles
n_{AEM}	[-]	DD membranes number
n_{feed}	[-]	MD feed number
P_i	$\left[\frac{m}{s}\right]$	diffusive permeability
$p_{i,m}$	$\left[\frac{m}{s}\right]$	membrane diffusive permeability

P_{os}	$\left[\frac{l}{bar \cdot m^2 \cdot s}\right]$	osmotic permeability
$\dot{Q}$	[kJ]	heating power
R	$\left[\frac{l \cdot bar}{K \cdot mol}\right]$	gas constant
Re	[-]	Reynolds number
RPT	[mV]	redox potential
RR	[%]	recovery ratio
s	$[m]$	thickness
Sc	[-]	Schmidt number
Sh	[-]	Sherwood number
t	[%]	interest rate
T	[K]	temperature
U	$\left[\frac{m}{s}\right]$	overall mass transfer coefficient
V	$[l]$	volume
v	$\left[\frac{m}{s}\right]$	linear velocity
W	$[m]$	width
w	$\left[\frac{kg}{h}\right]$	mass flow rate of the integrated process streams
w_y	$\left[\frac{ton}{y}\right]$	mass flow rate of the actual Tecnozinco plant streams
y	[y]	year
$y_{PlantLife}$	[y]	Plant life for the profitably analysis
Z	$[m]$	length
z_1	[-]	charge number
α	[-]	amount of solution trapped in the humid cake
β	[-]	hydration number
γ	$\left[\frac{mol}{l}\right]$	activity
Δ	[-]	difference of value
$\Delta H°_{298K}$	$\left[\frac{kcal}{kmol}\right]$	standard enthalpy of reaction
ε	[-]	porosity

ζ	[-]	extent of reaction
η	[%]	recovery efficiency
μ	$[Pa \cdot s]$	dynamic viscosity
v	$\left[\frac{l}{mol}\right]$	molar volume
π	[bar]	osmotic pressure
ρ	$\left[\frac{g}{l}\right]$	density
υ	[-]	stoichiometric coefficient
ϕ	[-]	osmotic coefficient
χ	[-]	conversion

Subscripts and superscripts

alk	alkaline
app	apparent
calc	calculated
ch	channel
d	diffusate
Dist	distillate
DS	draw solution
Dyn	dynamic
dr	drag
eq	equivalent
$entr, in$	entrainment stream, inlet
$entr, out$	entrainment stream, outlet
$evap$	evaporating stream
exp	experimental
f	feed
fin	final

FS	fluxing solution
gas	gaseous emission
i	component i, i.e., HCl, $FeCl_2$ $ZnCl_2$
i_p	pickling components i_p i.e., Fe_2O_3, Fe_3O_4, Fe, $FeCl_2$, HCl, $ZnCl_2$, H_2O
i_r	reactor components i_r, i.e., HCl, $FeCl_2$, $ZnCl_2$, H_2O NH_4OH, H_2O_2, NH_4Cl
in	inlet
int	interface
j	component j, i.e., HCl, $FeCl_2$, $ZnCl_2$, H_2O
k	year
m	membrane
max	maximum
Me	metal
mix	mixture
mod	modeling
MRB	metals rich brine
MS	metal sludge
MU	make-up
n	discretization number
ORP	outlet reactive precipitator
os	osmotic
out	outlet
Ox	Oxidant
$oxides$	oxides and elementary iron
p	pickling reactions
$Perm$	permeate
$prec$	precipitated
PW	process water
r	retentate

r_1, r_2	reactions
RA/RAS	recovered acid solution
$Rinsing$	rinsing solution
RPS	recovered pickling solution
s	pickling streams
sol	aqueous solution
$solv$	solvent
t	time
$tank$	tank
tot	total
u	membrane unit
w	water
WA/WAS	waste acid solution in the integrated process
$waste$	actual waste produced in Tecnozinco plant
I	compartment I
II	compartment II

REFERENCES

[1] D. C. DESELNICU, G. MILITARU, V. DESELNICU, G. ZĂINESCU, and L. ALBU, "Towards a Circular Economy– a Zero Waste Programme for Europe," pp. 563–568, 2018.

[2] Frias et al., "Novel process to recover by-products from the pickling baths of stainless steel," *Project Funded by the European Community under the Industrial & Material Technologies Programme (Brite-Euram III), Project BE-3501, Contract BRPR-CT 97-0407*. pp. 1–3, 1997.

[3] Life Dime, "Spent Pickling Liquor Treatment," 2017. [Online]. Available: https://lifedime.eu/en/spent-pickling-liquor-treatment/.

[4] G. Kong and R. White, "Toward cleaner production of hot dip galvanizing industry in China," *J. Clean. Prod.*, vol. 18, no. 10–11, pp. 1092–1099, 2010.

[5] European Commission (EC), "Report on Critical Raw Materials and the Circular Economy. (PART 1/3)," 2018.

[6] European Commission, "Report on Critical Raw Materials and the Circular Economy. (PART 2/3)," 2018.

[7] European Commission, "Report on Critical Raw Materials and the Circular Economy. (PART 3/3)," 2018.

[8] European Commission (EC), "A new Circular Economy Action Plan For a cleaner and more competitive Europe," 2015.

[9] M. J. L. Gines, G. J. Benitez, T. Perez, E. Merli, M. A. Firpo, and W. Egli, "Study of the picklability of 1.8 mm hot-rolled steel strip in hydrochloric acid," *Lat. Am. Appl. Res.*, vol. 32, no. 4, pp. 281–288, 2002.

[10] Y. Jatuphaksamphan, N. Phinichka, K. Prapakorn, and M. Supradist, "Pickling Kinetics of Tertiary Oxide Scale Formed on Hot-Rolled Steel Strip," *J. Met. Mater. Miner.*, vol. 20, no. 1, pp. 33–39, 2010.

[11] J. P. Kleingarn, "Pickling in hydrochloric acid," in *Intergalva, EGGA European General Galvanizers Association*, 1988, no. 11, p. GF2/1-13.

[12] B. R. Campano, “The Kleingarn Regenerated Spent Acid at Increasing Ferrous (Fe^{+2}) and Ferric (Fe^{+3}) Chloride Content.” HIDADA, Jeddah, Saudi Arabia, pp. 1–18, 2012.

[13] H. M. Freeman, *Standard handbook of hazardous waste treatment and disposal*, 2nd ed. New York, United States: McGraw-Hill Book Company, 1989.

[14] M. Regel-Rosocka, “A review on methods of regeneration of spent pickling solutions from steel processing,” *J. Hazard. Mater.*, vol. 177, no. 1–3, pp. 57–69, 2010.

[15] A. Devi, A. Singhal, R. Gupta, and P. Panzade, “A study on treatment methods of spent pickling liquor generated by pickling process of steel,” *Clean Technol. Environ. Policy*, vol. 16, no. 8, pp. 1515–1527, 2014.

[16] Colorado Department of Public Health, “Hazardous Waste Identification Guidance Document,” no. October, 2008.

[17] W. Kladnig, “New Development of Acid Regeneration in Steel Pickling Plants,” *J. Iron Steel Res. Int.*, vol. 15, no. 4, pp. 1–6, 2008.

[18] J. D. Hernández-Betancur, H. F. Hernández, and L. M. Ocampo-Carmona, “A holistic framework for assessing hot-dip galvanizing process sustainability,” *J. Clean. Prod.*, vol. 206, pp. 755–766, 2019.

[19] J. Fresner *et al.*, “Practical experiences with the implementation of the concept of zero emissions in the surface treatment industry in Austria,” *J. Clean. Prod.*, vol. 15, no. 13–14, pp. 1228–1239, 2007.

[20] C. Stocks, J. Wood, and S. Guy, “Minimisation and recycling of spent acid wastes from galvanizing plants,” *Resour. Conserv. Recycl.*, vol. 44, no. 2, pp. 153–166, 2005.

[21] D. Bascone, A. Cipollina, M. Morreale, S. Randazzo, F. Santoro, and G. Micale, “Simulation of a regeneration plant for spent pickling solutions via spray roasting,” *Desalin. Water Treat.*, vol. 57, no. 48–49, pp. 23405–23419, 2016.

[22] Andritz Metals, “Regeneration systems for hydrochloric waste pickling solutions.” [Online]. Available: https://www.andritz.com/products-en/group/metals/carbon-steel-regeneration/hydrochloric-plant.

[23] M. Ruthner and O. Ruthner, “25 Years of process development in HCl pickling and acid regeneration,” *Iron Steel Eng.*, vol. 56, no. 11, pp. 36–39, 1979.

[24] L. J. F. Harris, “Introduction to spray roasting process for hydrochloric acid regeneration and its application to mineral processing,” *Hydrometall. ’94*, pp. 923–937, 1994.

[25] U. Kerney, “Treatment of spent pickling acids from hot dip galvanizing,” *Resour.*

Conserv. Recycl., vol. 10, no. 1–2, pp. 145–151, 1994.

[26] N. Quaranta *et al.*, "Reuse of red powder of steel plants as fine addition in ceramic bricks manufacture," *WIT Trans. Ecol. Environ.*, vol. 155, pp. 1105–1113, 2011.

[27] A. Agrawal and K. K. Sahu, "An overview of the recovery of acid from spent acidic solutions from steel and electroplating industries," *J. Hazard. Mater.*, vol. 171, no. 1–3, pp. 61–75, 2009.

[28] "Limestone Treatment of rinse waters from hydrochloric acid pickling of steel," 1971.

[29] G. Cusano, M. R. Gonzalo, F. Farrell, R. Remus, S. Roudier, and L. D. Sancho, "Best Available Techniques (BAT) Reference Document for the Ferrous Metals Processing Industry," 2017.

[30] Maria Mäntylä, "Utilisation of regeneration sludge generated in cold rolling of stainless," University of Oulu, 2017.

[31] M. Regel-Rosocka, A. Cieszyńska, and M. Wiśniewski, "Methods of regeneration of spent pickling solutions from steel treatment plants," *Polish J. Chem. Technol.*, vol. 9, no. 2, pp. 42–45, Jan. 2007.

[32] M. Regel, A. M. Sastre, and J. Szymanowski, "Recovery of zinc(II) from HCl spent pickling solutions by solvent extraction," *Environ. Sci. Technol.*, vol. 35, no. 3, pp. 630–635, 2001.

[33] A. Grzeszczyk and M. Regel-Rosocka, "Extraction of zinc(II), iron(II) and iron(III) from chloride media with dibutylbutylphosphonate," *Hydrometallurgy*, vol. 86, no. 1–2, pp. 72–79, 2007.

[34] I. Ortiz, E. Bringas, M. F. San Román, and A. M. Urtiaga, "Selective separation of zinc and iron from spent pickling solutions by membrane-based solvent extraction: Process viability," *Sep. Sci. Technol.*, vol. 39, no. 10, pp. 2441–2455, 2004.

[35] Kawasaki Steel Corporation, "A New Acid and Iron Recovery Process in Stainless Steel Pickling Line," 1986.

[36] E. Marañón, Y. Fernández, F. J. Súarez, F. J. Alonso, and H. Sastre, "Treatment of acid pickling baths by means of anionic resins," *Ind. Eng. Chem. Res.*, vol. 39, no. 9, pp. 3370–3376, 2000.

[37] I. Miesiac, "Removal of zinc(II) and iron(II) from spent hydrochloric acid by means of anionic resins," *Ind. Eng. Chem. Res.*, vol. 44, no. 4, pp. 1004–1011, 2005.

[38] T. I. T. Gábor Csicsovszki, Tamás Kékesi, "Selective recovery of Zn and Fe from spent pickling solutions by the combination of anion exchange and membrane

electrowinning techniques Ga," *Hydrometallurgy*, vol. 77, no. 1–2, pp. 19–28, 2005.

[39] M. F. San Román, I. Ortiz-Gándara, E. Bringas, R. Ibañez, and I. Ortiz, "Membrane selective recovery of HCl, zinc and iron from simulated mining effluents," *Desalination*, vol. 440, no. December 2017, pp. 78–87, 2018.

[40] G. Leonzio, "Recovery of metal sulphates and hydrochloric acid from spent pickling liquors," *J. Clean. Prod.*, vol. 129, pp. 417–426, 2016.

[41] R. M. Machado, M. L. F. Gameiro, J. M. A. Rodrigues, M. R. C. Ismael, M. T. A. Reis, and J. M. R. Carvalho, "Recovery of hydrochloric acid from galvanizing industrial effluents," *Sep. Sci. Technol.*, vol. 52, no. 8, pp. 1333–1340, 2017.

[42] M. F. San Román, I. Ortiz Gándara, R. Ibañez, and I. Ortiz, "Hybrid membrane process for the recovery of major components (zinc, iron and HCl) from spent pickling effluents," *J. Memb. Sci.*, vol. 415–416, pp. 616–623, 2012.

[43] H. Strathmann, "Membrane Separation Processes : Current Relevance and Future Opportunities," *AIChE J.*, vol. 47, no. 5, pp. 1077–1087, 2001.

[44] M. Balakrishnan *et al.*, "Demonstration of acid and water recovery systems: Applicability and operational challenges in Indian metal finishing SMEs," *J. Environ. Manage.*, vol. 217, pp. 207–213, 2018.

[45] Y. Kobuchi, H. Motomura, Y. Noma, and F. Hanada, "Application of ion exchange membranes to the recovery of acids by diffusion dialysis," *J. Memb. Sci.*, vol. 27, no. 2, pp. 173–179, Jun. 1986.

[46] X. Tongwen and Y. Weihua, "Industrial recovery of mixed acid (HF + HNO_3) from the titanium spent leaching solutions by diffusion dialysis with a new series of anion exchange membranes," *J. Memb. Sci.*, vol. 220, no. 1–2, pp. 89–95, 2003.

[47] Z. Palatý and H. Bendová, "Continuous dialysis of mixture of inorganic acids," *Sep. Purif. Technol.*, vol. 172, pp. 277–284, 2017.

[48] J. Luo, C. Wu, T. Xu, and Y. Wu, "Diffusion dialysis-concept, principle and applications," *J. Memb. Sci.*, vol. 366, no. 1–2, pp. 1–16, 2011.

[49] S. Jung Oh, S. H. Moon, and T. Davis, "Effects of metal ions on diffusion dialysis of inorganic acids," *J. Memb. Sci.*, vol. 169, no. 1, pp. 95–105, 2000.

[50] J. Luo, C. Wu, Y. Wu, and T. Xu, "Diffusion dialysis of hydrochloride acid at different temperatures using PPO-SiO_2 hybrid anion exchange membranes," *J. Memb. Sci.*, vol. 347, no. 1–2, pp. 240–249, 2010.

[51] J. Xu, S. Lu, and D. Fu, "Recovery of hydrochloric acid from the waste acid solution

by diffusion dialysis," *J. Hazard. Mater.*, vol. 165, no. 1–3, pp. 832–837, 2009.

[52] H. Bendová and Z. Palatý, "Continuous Separation of an H_2SO_4/$CuSO_4$ Mixture by Diffusion Dialysis," *Chem. Eng. Technol.*, vol. 34, no. 2, pp. 217–224, 2011.

[53] T. W. Xu and W. H. Yang, "Sulfuric acid recovery from titanium white (pigment) waste liquor using diffusion dialysis with a new series of anion exchange membranes - static runs," *J. Memb. Sci.*, vol. 183, no. 2, pp. 193–200, 2001.

[54] W. Li, Y. Zhang, J. Huang, X. Zhu, and Y. Wang, "Separation and recovery of sulfuric acid from acidic vanadium leaching solution by diffusion dialysis," *Sep. Purif. Technol.*, vol. 96, pp. 44–49, 2012.

[55] C. Wei, X. Li, Z. Deng, G. Fan, M. Li, and C. Li, "Recovery of H_2SO_4 from an acid leach solution by diffusion dialysis," *J. Hazard. Mater.*, vol. 176, no. 1–3, pp. 226–230, 2010.

[56] B. D. E. Bailey, "Recycling of Nitric-Hydrofluoric Acid With Diffusion Dialysis," pp. 1–6.

[57] Z. Palatý and H. Bendová, "Dialysis of aqueous solutions of nitric acid and ferric nitrate," *Chem. Eng. Process. Process Intensif.*, vol. 50, no. 2, pp. 160–166, 2011.

[58] M. S. Kang, K. S. Yoo, S. J. Oh, and S. H. Moon, "A lumped parameter model to predict hydrochloric acid recovery in diffusion dialysis," *J. Memb. Sci.*, vol. 188, no. 1, pp. 61–70, 2001.

[59] Z. Palatý and A. Žáková, "Competitive transport of hydrochloric acid and zinc chloride through polymeric anion-exchange membrane," *J. Appl. Polym. Sci.*, vol. 101, no. 3, pp. 1391–1397, Aug. 2006.

[60] F. Aouad, A. Lindheimer, and C. Gavach, "Transport properties of electrodialysis membranes in the presence of Zn^{2+} complexes with Cl^-," *J. Memb. Sci.*, vol. 123, no. 2, pp. 207–223, 1997.

[61] A. Brunetti, "Modularity," in *Encyclopedia of Membranes*, 2015.

[62] European Commission, *Control Reference Document on Best Available Techniques for the Surface Treatment of Metals and Plástics*, no. August. 2006.

[63] A. Alkhudhiri, N. Darwish, and N. Hilal, "Membrane distillation: A comprehensive review," *Desalination*, vol. 287, no. June 2014, pp. 2–18, 2012.

[64] E. Drioli, A. Ali, and F. Macedonio, "Membrane distillation: Recent developments and perspectives," *Desalination*, vol. 356, pp. 56–84, 2015.

[65] M. Tomaszewska, M. Gryta, and A. W. Morawski, "Recovery of hydrochloric acid

from metal pickling solutions by membrane distillation," *Sep. Purif. Technol.*, vol. 22–23, no. December, pp. 591–600, 2001.

[66] D. Winter, *Membrane Distillation - A Thermodynamic, Technological and Economic Analysis (PhD Thesis)*. 2014.

[67] E. Drioli, Y. Wu, and V. Calabro, "Membrane distillataion in the treatment of aqueous solutions," *J. Memb. Sci.*, vol. 33, no. 3, pp. 277–284, 1987.

[68] M. El-Halwagi, N. Elsayed, M. Barrufet, and F. Eljack, "Optimal Design of Thermal Membrane Distillation Systems for the Treatment of Shale Gas Flowback Water," *Int. J. Membr. Sci. Technol.*, vol. 2, no. 2, pp. 1–9, 2015.

[69] P. Wang and T. S. Chung, "Recent advances in membrane distillation processes: Membrane development, configuration design and application exploring," *J. Memb. Sci.*, vol. 474, pp. 39–56, 2015.

[70] C. Fritzmann, J. Löwenberg, T. Wintgens, and T. Melin, "State-of-the-art of reverse osmosis desalination," *Desalination*, vol. 216, no. 1–3, pp. 1–76, 2007.

[71] L. Martínez-Díez and M. I. Vázquez-González, "Temperature and concentration polarization in membrane distillation of aqueous salt solutions," *J. Memb. Sci.*, vol. 156, no. 2, pp. 265–273, 1999.

[72] R. Liu, Y. Qin, X. Li, and L. Liu, "Concentrating aqueous hydrochloric acid by multiple-effect membrane distillation," *Front. Chem. Sci. Eng.*, vol. 6, no. 3, pp. 311–321, 2012.

[73] M. Tomaszewska, M. Gryta, and A. W. Morawski, "The influence of salt in solutions on hydrochloric acid recovery by membrane distillation," *Separation and Purification Technology*, vol. 14, no. 1–3. pp. 183–188, 1998.

[74] M. C. García-Payo, M. A. Izquierdo-Gil, and C. Fernández-Pineda, "Air gap membrane distillation of aqueous alcohol solutions," *J. Memb. Sci.*, vol. 169, no. 1, pp. 61–80, 2000.

[75] G. W. Meindersma, C. M. Guijt, and A. B. de Haan, "Desalination and water recycling by air gap membrane distillation," *Desalination*, vol. 187, no. 1–3, pp. 291–301, 2006.

[76] R. Schwantes, K. Chavan, D. Winter, C. Felsmann, and J. Pfafferott, "Techno-economic comparison of membrane distillation and MVC in a zero liquid discharge application," *Desalination*, vol. 428, no. November 2017, pp. 50–68, 2018.

[77] M. Dejak, "Acid Purification and Recovery Using Resin Sorption Technology," in *15th AESF/EPA pollution prevention and control conference*, 1994, pp. 109–110.

[78] A. N. Mondal *et al.*, "Improved acid recovery performance by novel Poly(DMAEM-co-γ-MPS) anion exchange membrane via diffusion dialysis," *Journal of Membrane Science*, vol. 525. pp. 163–174, 2017.

[79] J. Ran, L. Wu, Y. Ru, M. Hu, L. Din, and T. Xu, "Anion exchange membranes (AEMs) based on poly(2,6-dimethyl-1,4-phenylene oxide) (PPO) and its derivatives," *Polym. Chem.*, vol. 6, no. 32, pp. 5809–5826, 2015.

[80] H. Strathmann, "Ion Exchange Membrane Separation Processes," in *Membrane Science and Technology Series*, 1st ed., vol. 9, Amsterdam, The Netherlands: Elsevier B.V., 2004, pp. 205–212.

[81] F. Sun, C. Wu, Y. Wu, and T. Xu, "Porous BPPO-based membranes modified by multisilicon copolymer for application in diffusion dialysis," *J. Memb. Sci.*, vol. 450, pp. 103–110, 2014.

[82] M. I. Khan *et al.*, "Porous BPPO-based membranes modified by aromatic amine for acid recovery," *Sep. Purif. Technol.*, vol. 157, pp. 27–34, 2016.

[83] J. Jeong, M. S. Kim, B. S. Kim, S. K. Kim, W. B. Kim, and J. C. Lee, "Recovery of H_2SO_4 from waste acid solution by a diffusion dialysis method," *J. Hazard. Mater.*, vol. 124, no. 1–3, pp. 230–235, 2005.

[84] S. H. Lin and M. C. Lo, "Recovery of sulfuric acid from waste aluminum surface processing solution by diffusion dialysis," *J. Hazard. Mater.*, vol. 60, no. 3, pp. 247–257, 1998.

[85] J. Wiśniewski, A. Różańska, and T. Winnicki, "Removal of troublesome anions from water by means of Donnan dialysis," *Desalination*, vol. 182, no. 1–3, pp. 339–346, Nov. 2005.

[86] Z. Palatý, A. Žáková, and P. Doleček, "Modelling the transport of Cl^- ions through the anion-exchange membrane NEOSEPTA-AFN systems HCl/membrane/H_2O and HCl-$FeCl_3$/membrane/H_2O," *J. Memb. Sci.*, vol. 165, no. 2, pp. 237–249, 2000.

[87] A. Elmidaoui, J. Molenat, and C. Gavach, "Competitive diffusion of hydrochloric acid and sodium chloride through an acid dialysis membrane," *J. Memb. Sci.*, vol. 55, no. 1–2, pp. 79–98, 1991.

[88] Z. Palatý and A. Žáková, "Separation of H_2SO_4 + $ZnSO_4$ mixture by diffusion dialysis," *Desalination*, vol. 169, no. 3, pp. 277–285, 2004.

[89] J. Xu, D. Fu, and S. Lu, "The recovery of sulphuric acid from the waste anodic aluminum oxidation solution by diffusion dialysis," *Sep. Purif. Technol.*, vol. 69, no.

2, pp. 168–173, 2009.

[90] K. Wang, Y. Zhang, J. Huang, T. Liu, and J. Wang, “Recovery of sulfuric acid from a stone coal acid leaching solution by diffusion dialysis,” *Hydrometallurgy*, vol. 173, no. July, pp. 9–14, 2017.

[91] Z. Palatý and H. Bendová, “Permeability of a Fumasep-FAD Membrane for Selected Inorganic Acids,” *Chem. Eng. Technol.*, vol. 41, no. 2, pp. 385–391, Feb. 2018.

[92] Z. Palatý and H. Bendová, “Continuous dialysis of hydrochloric acid and sodium chloride mixture,” *Sep. Sci. Technol.*, vol. 52, no. 16, pp. 2611–2621, 2017.

[93] Z. Palatý, “Transport of hydrochloric acid through anion-exchange membrane NEOSEPTA-AFN Application of Nernst–Planck equation,” *J. Memb. Sci.*, vol. 189, no. 2, pp. 205–216, Aug. 2001.

[94] Z. Palatý and A. Žáková, “Transport of some strong incompletely dissociated acids through anion-exchange membrane,” *J. Colloid Interface Sci.*, vol. 268, no. 1, pp. 188–199, 2003.

[95] Z. Palatý and A. Žáková, “Transport of sulfuric acid through anion-exchange membrane NEOSEPTA-AFN,” *J. Memb. Sci.*, vol. 119, no. 2, pp. 183–190, Oct. 1996.

[96] Z. Palatý and H. Bendová, “Separation of HCl + $FeCl_2$ mixture by anion-exchange membrane,” *Sep. Purif. Technol.*, vol. 66, no. 1, pp. 45–50, 2009.

[97] Z. Palatý and A. Žková, “Separation of HCl+$NiCl_2$ mixture by diffusion dialysis,” *Sep. Sci. Technol.*, vol. 42, no. 9, pp. 1965–1983, 2007.

[98] H. Bendová, Z. Palatý, and A. Žáková, “Continuous dialysis of inorganic acids: permeability of Neosepta-AFN membrane,” *Desalination*, vol. 240, no. 1–3, pp. 333–340, 2009.

[99] Z. Palatý and A. Žáková, “Separation of H_2SO_4 + $CuSO_4$ mixture by diffusion dialysis,” *J. Hazard. Mater.*, vol. 114, no. 1–3, pp. 69–74, 2004.

[100] J. Luo, C. Wu, Y. Wu, and T. Xu, “Diffusion dialysis of hydrochloric acid with their salts: Effect of co-existence metal ions,” *Sep. Purif. Technol.*, vol. 118, pp. 716–722, 2013.

[101] T. A. Davis, “II / MEMBRANE SEPARATIONS / Diffusion Dialysis,” *Encyclopedia of Separation Science*. Elsevier Science Ltd., pp. 1693–1701, 2000.

[102] J. Luo, C. Wu, Y. Wu, and T. Xu, “Diffusion dialysis processes of inorganic acids and their salts: The permeability of different acidic anions,” *Sep. Purif. Technol.*, vol.

78, no. 1, pp. 97–102, 2011.

[103] J. R. Black, A. Kavner, and E. A. Schauble, “Calculation of equilibrium stable isotope partition function ratios for aqueous zinc complexes and metallic zinc,” *Geochim. Cosmochim. Acta*, vol. 75, no. 3, pp. 769–783, 2011.

[104] F. Aouad, A. Lindheimer, M. Chaouki, and C. Gavach, “Loss of permselectivity of anion exchange membranes in contact with zinc chloride complexes,” *Desalination*, vol. 121, no. 1, pp. 13–22, 1999.

[105] A. Ruiz-aguirre *et al.*, “Diffusion Dialysis for the treatment of H_2SO_4-$CuSO_4$ solutions from electroplating plants : ions membrane transport characterization and modelling,” *Sep. Purif. Technol.*, 2020.

[106] R. Gueccia, S. Randazzo, D. Chillura Martino, A. Cipollina, and G. Micale, “Experimental investigation and modeling of diffusion dialysis for HCl recovery from waste pickling solution,” *J. Environ. Manage.*, vol. 235, pp. 202–212, 2019.

[107] L. Gurreri, A. Tamburini, A. Cipollina, G. Micale, and M. Ciofalo, “CFD prediction of concentration polarization phenomena in spacer-filled channels for reverse electrodialysis,” *J. Memb. Sci.*, vol. 468, pp. 133–148, 2014.

[108] M. Laliberté and W. E. Cooper, “Model for calculating the density of aqueous electrolyte solutinos,” *J. Chem. Eng. Data*, vol. 49, no. 5, pp. 1141–1151, 2004.

[109] L. Gurreri, A. Tamburini, A. Cipollina, G. Micale, and M. Ciofalo, “Flow and mass transfer in spacer-filled channels for reverse electrodialysis: a CFD parametrical study,” *J. Memb. Sci.*, vol. 497, pp. 300–317, 2016.

[110] D. Lundberg, A. S. Ullström, P. D’Angelo, and I. Persson, “A structural study of the hydrated and the dimethylsulfoxide, N,N′-dimethylpropyleneurea, and N,N-dimethylthioformamide solvated iron(II) and iron(III) ions in solution and solid state,” *Inorganica Chim. Acta*, vol. 360, no. 6, pp. 1809–1818, 2007.

[111] D. Van Gauwbergen, J. Baeyens, and C. Creemers, “Modeling osmotic pressures for aqueous solutions for 2-1 and 2-2 electrolytes,” *Desalination*, vol. 109, no. 1, pp. 57–65, 1997.

[112] K. S. Pitzer and J. J. Kim, “Thermodynamics of Electrolytes. IV. Activity and Osmotic Coefficients for Mixed Electrolytes,” *J. Am. Chem. Soc.*, vol. 96, no. 18, pp. 5701–5707, 1974.

[113] H. Tialowska-mocharla and S. Manohar, “Activity Coefficient Measurements of the System HCI-$ZnCl_2$-H_20 at 25 and 35°C,” *System*, vol. 21, no. 6, pp. 545–546, 1992.

[114] G. M. Marion, D. C. Catling, and J. S. Kargel, “Modeling aqueous ferrous iron chemistry at low temperatures with application to Mars,” *Geochim. Cosmochim. Acta*, vol. 67, no. 22, pp. 4251–4266, 2003.

[115] C. W. Davies, *Ion Association*. London: Butterworths, 1962.

[116] D. R. Lide, *CRC Handbook of physics and chemistry*, 86th Ed. Taylor and Francis, BocaRaton, 2005.

[117] B. Zhao, Y. Zhang, X. Dou, H. Yuan, and M. Yang, “Granular ferric hydroxide adsorbent for phosphate removal: Demonstration preparation and field study,” *Water Sci. Technol.*, vol. 72, no. 12, pp. 2179–2186, 2015.

[118] T. J. Hardwick, “The rate constant of the reaction between ferrous ions and hydrogen peroxide in acid solution,” *Can. J. Chem.*, vol. 35, pp. 428–436, 1957.

[119] L. Markov, V. Blaskov, D. Klissurski, and S. Nikolov, “The thermal decomposition mechanism of iron(III) hydroxide carbonate to α-Fe_2O_3,” *J. Mater. Sci.*, vol. 25, no. 7, pp. 3096–3100, 1990.

[120] B. R. Campano, “The Kleingarn Regenerated Spent Acid at Increasing Ferrous (Fe^{+2}) and Ferric (Fe^{+3}) Chloride Content.” HIDADA, Jeddah, Saudi Arabia, pp. 1–18, 2012.

[121] G. S. Kell, “Density, Thermal Expansivity, and Compressibility of Liquid Water from 0° to 150°C: Correlations and Tables for Atmospheric Pressure and Saturation Reviewed and Expressed on 1968 Temperature Scale,” *J. Chem. Eng. Data*, vol. 20, no. 1, pp. 97–105, 1975.

[122] R. Gueccia, A. R. Aguirre, S. Randazzo, and A. Cipollina, “Diffusion Dialysis for Separation of Hydrochloric Acid , Iron and Zinc Ions from Highly Concentrated Pickling Solutions,” *Membranes (Basel).*, vol. 10, no. 129, pp. 1–17, 2020.

[123] A. Culcasi, R. Gueccia, S. Randazzo, A. Cipollina, and G. Micale, “Design of a novel membrane-integrated waste acid recovery process from pickling solution,” *J. Clean. Prod.*, vol. 236, p. 117623, Nov. 2019.

[124] R. Schwantes *et al.*, “Characterization and assessment of a novel plate and frame md module for single pass wastewater concentration–feed gap air gap membrane distillation,” *Membranes (Basel).*, vol. 9, no. 9, 2019.

[125] G. S. Gohil, R. K. Nagarale, V. K. Shahi, and R. Rangarajan, “Micellar-enhanced electrodialysis: Influence of surfactants on the transport properties of ion-exchange membranes,” *Sep. Purif. Technol.*, vol. 47, no. 1–2, pp. 1–9, 2005.

[126] N. Narkis and B. Ben-David, “Adsorption of non-ionic surfactants on activated

carbon and mineral clay," *Water Res.*, vol. 19, no. 7, pp. 815–824, 1985.

[127] J. N. Israelachvili, "Thermodynamic and Statistical Aspects of Intermolecular Forces," *Intermol. Surf. Forces*, pp. 23–51, 2011.

[128] Perry, *Perry's Chemical Engineers' Handbook*, vol. 91. 2017.

[129] K. S. S. Christie, T. Horseman, and S. Lin, "Energy efficiency of membrane distillation: Simplified analysis, heat recovery, and the use of waste-heat," *Environ. Int.*, vol. 138, no. November 2019, p. 105588, 2020.

[130] A. I. Johnson and W. F. Furter, "Salt effect in vapor-liquid equilibrium, part II," *Can. J. Chem. Eng.*, vol. 38, no. 3, pp. 78–87, 1960.

[131] AIZ associazione italiana zincatura, "ReWaCEM Confidential data," 2019.

[132] Jared Cullivan, Bryan Cullivan, J. Cullivan, B. Cullivan, Jared Cullivan, and Bryan Cullivan, "Economic and chemical comparisons of hydrochloric acid recovery technologies for iron pickling operations," *Wire J. Int.*, pp. 1–12, 2016.

[133] U.S. Department of Defense, "Cost and Performance Report," 1999.

[134] T. Özdemir, C. Öztin, and N. S. Kincal, "Treatment of waste pickling liquors: Process synthesis and economic analysis," *Chem. Eng. Commun.*, vol. 193, no. 5, pp. 548–563, 2006.

[135] R. Turton, R. C. Bailie, W. B. Whiting, J. oseph A. Shaeiwitz, and D. Bhattacharyya, "Profitability Analysis," in *Analysis, Synthesis, and Design of Chemical Processes*, Fourth Ed., PEARSON EDUCATION INTERNATIONAL, 2013, pp. 261–310.

[136] salaryexplorer, "Engineering Average Salaries in Italy 2020." [Online]. Available: http://www.salaryexplorer.com/salary-survey.php?loc=105&loctype=1&job=22&jobtype=1.

[137] R. Turton, R. C. Bailie, W. B. Whiting, J. oseph A. Shaeiwitz, and D. Bhattacharyya, "Estimation of Capital Costs," in *Analysis, Synthesis, and Design of Chemical Processes*, Fourth Ed., PEARSON EDUCATION INTERNATIONAL, 2013, pp. 157–196.

[138] R. Turton, R. C. Bailie, W. B. Whiting, J. oseph A. Shaeiwitz, and D. Bhattacharyya, "Estimating of Manufacturing Costs," in *Analysis, Synthesis, and Design of Chemical Processes*, Fourth Ed., PEARSON EDUCATION INTERNATIONAL, 2013, pp. 197–226.

[139] Echemi, "Hydrochloric Acid Price Analysis." [Online]. Available: https://www.echemi.com/.

[140] Echemi, “Ammonium Hydroxide Price Analysis.” [Online]. Available: https://www.echemi.com/.

[141] Echemi, “Hydrogen Peroxide Price Analysis.” [Online]. Available: https://www.echemi.com/.

[142] Depurstore, “GFH (Idrossido Ferrico Granulare).” [Online]. Available: https://www.depurstore.it/.

[143] azichem, “PROTECH OXICROM.” [Online]. Available: https://www.azichem.it/.

[144] L. Xiamen Ditai Chemicals Co., “Pigmento Inorganico>Idrossido ferrico.” [Online]. Available: https://it.made-in-china.com/co_ditaichem/.

[145] MOLBASE, “1309-33-7 Iron(III) hydroxide.” [Online]. Available: http://www.molbase.com/.

[146] Y. Cui, Z. Geng, Q. Zhu, and Y. Han, “Review: Multi-objective optimization methods and application in energy saving,” *Energy*, vol. 125, pp. 681–704, 2017.

[147] V. Bhaskar, S. K. Gupta, and A. K. Ray, “Applications of multiobjective optimization in chemical engineering,” *Rev. Chem. Eng.*, vol. 16, no. 1, pp. 1–54, 2000.

[148] V. Chankong and Y. Y. Haimes, *Multiobjective Decision Making Theory and Methodology*. Mineola, New York: Dover Publication, Inc, 1983.

LIST OF PUBLICATIONS

ISI Journal publications

"Experimental investigation and modeling of diffusion dialysis for HCl recovery from waste pickling solution" R. Gueccia, S. Randazzo, D. Chillura Martino, A. Cipollina, G. Micale, Journal of Environmental Management 235 (2019) 202–212; doi: 10.1016/j.jenvman.2019.01.028.

"Design of a novel membrane-integrated waste acid recovery process from pickling solution" A. Culcasi, R. Gueccia, S. Randazzo, A. Cipollina, G. Micale, Journal of Cleaner Production 236 (2019) 117623; doi: 10.1016/j.jclepro.2019.117623.

"Donnan dialysis for tap-water softening" R. Gueccia, A.M.M. Alhadidi, A. Cipollina, G. Micale, Desalination and Water Treatment 192 (2020) 19–32 July, doi: 10.5004/dwt.2020.26081.

"Diffusion Dialysis for Separation of Hydrochloric Acid, Iron and Zinc Ions from Highly Concentrated Pickling Solutions" Rosa Gueccia, Alba Ruiz Aguirre, Serena Randazzo, Andrea Cipollina, Giorgio Micale, Membranes 2020, 10, 129; doi:10.3390/membranes10060129.

"Diffusion Dialysis for the treatment of H_2SO4-$CuSO_4$ solutions from electroplating plants: ions membrane transport characterization and modeling" A. Ruiz-Aguirre, J. López; R. Gueccia, S. Randazzo; A. Cipollina; J. L. Cortina; G. Micale, accepted for publication in Separation and Purification Technology.

"An integrated approach for the HCl and metals recovery from waste pickling solutions: pilot plant and design operations" R. Gueccia, D. Winter, S. Randazzo, A. Cipollina, J. Koschikowski G. Micale, accepted for publication in Chemical Engineering Research and Design.

Journal publications in preparation and / or submitted

"Metals recovery from waste pickling solutions by reactive precipitation" Serena Randazzo, Daniele La Corte, Rosa Gueccia, Andrea Cipollina, Giorgio Micale, submitted to Chemical engineering transaction journal.

"Economics and environmental benefits of waste pickling solution valorisation" R. Gueccia, D. Bogle, D. Winter, S.Randazzo, A. Cipollina, G. Micale, J. Koschikowski, in preparation.

"A reliable determination method of concentrated metals ions from pickling solution via portable X-ray fluorescence spectrometry", D. Chillura Martino, S. Randazzo, P. Lo Meo, G. Balistreri, R.Gueccia, A. Cipollina, G. Micale, , in preparation.

Memories presented at national / international congresses

"Recovery of pickling acid solutions by membrane technology: the EU REWACEM project", L. Pernice, S. Randazzo, R. Gueccia, A. Culcasi, A. Cipollina, G. Micale, European General Galvanizers Association, EGGA, 12-15 June 2017, Prague

"Experimental investigation and modelling of diffusion dialysis process for regeneration of acid pickling solutions", S. Randazzo, R. Gueccia, A. Cipollina, A. Tamburini, G. Micale, EuroMed 2017 Desalination for Clean Water and Energy Cooperation around the world, 09-12 May 2017, Tel Aviv, Israel.

"Recovery of hydrochloric acid from pickling solutions of a hot-dip galvanizing plant", R. Gueccia, S. Randazzo, D. Chillura Martino, A. Cipollina, G. Micale, INSPIREWATER "Innovative solutions in the process industry for next generation resource efficient water management", 08 February 2018, Frankfurt. (**poster presentation**).

"Experimental investigation and modelling of diffusion dialysis for the recovery of waste acid solutions", R. Gueccia, S. Randazzo, A. Culcasi, A. Cipollina, G. Micale, Intergalva 17-22 June 2018, Berlin.

"Effective recovery of HCl and metals from pickling solutions by cutting-edge membrane technologies", R. Gueccia, S. Randazzo, D. Chillura Martino, A. Cipollina, G. Micale, EuroMembrane", 09-13 July 2018, Valencia. (**oral presentation**).

“Modeling and Design of Membrane Process Recovery of HCl and Metals from Pickling Solutions ", S. Randazzo, R. Gueccia, A. Cipollina, G. Micale, Desalination for the Environment: Clean Water and Energy”, 03-06 September 2018, Athens.

“Experimental investigation and modelling for sulphuric acid recovery by diffusion dialysis", S. Randazzo, A. Ruiz Aguirre, J. Lopez Rodriguez, R. Gueccia, A. Cipollina, G. Micale, Desalination for the Environment: Clean Water and Energy”, 03-06 September 2018, Athens.

“Modeling and design of a recovery plant of HCl from pickling solutions by membrane technologies", A. Culcasi, R. Gueccia, S. Randazzo, A. Cipollina, G. Micale, Sdewes 30/09-4/10 2018, Palermo. (**oral presentation**)

“Application of diffusion dialysis in separation of sulfuric acid and copper from pickling wastewater", A. Ruiz-Aguirre, J. López, R. Gueccia, S. Randazzo, A. Cipollina, J. L. Cortina, G. Micale, IWA-MTC, 23/27-06 2018, Toulouse, France.

“An integrated approach for HCl and metals recovery from waste pickling solutions: pilot plant design and operations", R. Gueccia, D. Winter, S. Randazzo, A. Cipollina, G. Micale, J. Koschikowski, F. Gross, 3RD IWA RESOURCE RECOVERY CONFERENCE, 08/12-09 2019, Venice, Italy. (**oral presentation**)

“Diffusion dialysis for HCl and heavy metals separation from highly concentrated pickling solutions ", R. Gueccia, A. Ruiz-Aguirre, S. Randazzo, A. Cipollina, G. Micale, 14th Sdewes Conference on Sustainable Development of Energy, Water and Environment Systems, 01/06-10 2019, Dubrovnik, Croatia. (**oral presentation**)

“An integrated approach for HCl and metals recovery from waste pickling solutions: pilot plant design and operations", R. Gueccia, D. Winter, S. Randazzo, A. Cipollina, G. Micale, J. Koschikowski, MELPRO 2020, 08/11-11 2020, virtual conference (**oral presentation**)

“Design, construction and operational results of a pilot plant for the treatment and valorisation of pickling waste solutions”, R. Gueccia, D. Winter, S. Randazzo, A. Cipollina, G. Micale, J. Koschikowski, 38° CONVEGNO NAZIONALE AIM, 18/20-01 2021, Napoli, Italy, virtual conference.

“Metals recovery from waste pickling solutions by reactive precipitation” Serena Randazzo, Daniele La Corte, Rosa Gueccia, Andrea Cipollina, Giorgio Micale, 15th INTERNATIONAL CONFERENCE ON CHEMICAL AND PROCESS ENGINEERING Napoli, Italy, 23-26 May, 2021, abstract submitted.

ACKNOWLEDGEMENTS

In these last few lines, I would like to thank all of those who have supported and have been closed to me in these years making possible the completion of this work.

I thank Professor Micale, for having given me the opportunity of working on such an interesting topic during these wonderful years of PhD full of travels and meetings with amazing people.

My deep gratitude goes to my co-tutor, Professor Cipollina, for his help and his advice. He gave me the opportunity of learning so much. His passion for research, his devotion to work, his wide knowledge have been a pillar of my PhD.

I thank Ing. Serena Randazzo who has supported my work for the last three years.

Further thanks go to the whole “PRANZO” team, which has been a "family" filling even the saddest days with laughs and lovely times.

I would also like to thank the amazing people I met at the Fraunhofer ISE and at UCL, in particular Daniel Winter and Professor David Bogle, for making the time in Freiburg and in London very fruitful, l and the people involved in the ReWaCEM project with whom I have carried out a great job and shared delightful experiences.

Further thanks go to TecnoZinco team for hosting me at their industrial plant and supporting me with all the help that I needed.

I sincerely thank everyone who has accompanied and helped me on my way. Above all my family, my amazing boyfriend and my best friends. For your unconditional love and support, I am more than grateful!

Thank you all!